PhD Thesis

BMP signaling controls postnatal muscle development.

Submitted to

Université Pierre et Marie Curie, Paris, France

Ecole Doctorale ED515 "Complexité du vivant"

and

Freie Universität, Berlin, Germany

Department of Biology, Chemistry and Pharmacy

Presented by **Amalia STANTZOU**

Thesis defense date: 29th September, 2015

Graduate committee:

Dr. Delphine DUPREZ	UPMC representative and reviewer
Prof. Sigmar STRICKER	FU representative and reviewer
Dr Pascal MAIRE	External reviewer
Dr Didier MONTARRAS	External reviewer
Dr Christian HIEPEN	FU postdoctoral research fellow
Prof. Helge AMTHOR	UPMC thesis supervisor
Prof. Markus SCHÜLKE-GERSTENFELD	FU thesis supervisor

Acknowledgements

Firstly, I would like to express my great appreciation to the members of my thesis committee for accepting to evaluate my doctoral work. I am thankful to **Dr. Delphine Duprez** and **Prof. Sigmar Stricker** for respectively representing the Pierre and Marie Curie University (UPMC) and the Free University, and with whom I've had pleasant discussions on the advances of my project especially during the *Myograd* meetings and summer schools in Berlin. I am very grateful to **Dr. Didier Montarras** and **Dr. Pascal Maire** for examining my thesis manuscript. I would also like to thank **Dr. Christian Hiepen** for accepting to be part of the committee.

I would like to express my deepest gratitude to my co-supervisor, **Prof. Helge Amthor**, for his trust and kindness as well as for the invaluable encouragement, guidance, ideas, discussions and availability which altogether made my PhD an enriching experience.

I am also very grateful to my co-supervisor **Prof. Markus Schülke-Gerstenfeld** for his guidance for my research project, for his valuable statistical advice as well as for his comments for this manuscript.

My most sincere thanks also go to **Dr. Frédéric Relaix** for being my tutor and especially for his fruitful collaboration during my PhD. I would like to thank him for all of his support as well as for inviting me to present and attend the lab-meetings of his group that were most helpful for the advancement of my doctoral work.

I would like to express my gratitude to **Dr. Luis Garcia** for his kindness and for providing me the opportunity to join his team and access to all laboratory equipments.

Many thanks go to my former colleague, **Dr. Elija Schirwis**, who initiated my technical instruction in the muscle field as well as in animal experimentation. I will probably never forget that one animal which simply did not want to be part of our experiment. I would also like to thank **Dr. Sonia Relizani** for becoming my friend; needless to say that I enjoyed all the time we spent together in and outside the lab and hope that we always keep in touch. Moreover, I address many thanks to **Faouzi Zarrouki** who joined the lab for his Master thesis and to whom I wish all the best for his PhD project.

It was a real pleasure to work in different laboratories, sharing my PhD experience with so many different people and teams. I sincerely thank all my fellow lab-mates for all their help, generosity and liveliness: i) in the Versailles Saint-Quentin-en-Yvelines University (UVSQ) I address many thanks to **Rachid**, **Aurélie G.**, **Valérie, Aurélie A.**, **Cyriaque**, **Graziella**, **Pierre-Olivier**, **Guillaume**, **Susanne**, **Maëva**, **Gabriella**, **Jakob** and **Marine**; in the UPMC ii) I would like to thank the Relaix team: **Sonia**, **Philippos**, **Shin**, **Vanessa**, **Despoina**, **Frédéric** and **Bernie** who were of great support and help throughout most of my PhD; iii) a special thanks to **Christel, Petra**, **William**, **Valérie** as well as the **Barkats** and **Sassoon team** with whom I shared many fun times in and outside the lab; and finally iv) *Myograd* PhD students and colleagues **Mina** and **Can**.

Statutory declaration

I, Amalia Stantzou, hereby declare that I developed and wrote the present thesis manuscript entitled "BMP signaling controls postnatal muscle development" independently and used no other aids than those cited. In the written paragraphs, I have clearly identified the sources of the passages that are taken word for word or paraphrased from other works. The sources of the figures that I reused from other works have been clearly identified. When necessary, I obtained copyright permissions, in which cases I indicated the license number obtained through the Copyright Clearance Center's RightsLink service below the corresponding figures.

I also hereby declare that I have carried out my scientific work according to the principles of good scientific practice in accordance with the current "Richtlinien der Freien Universität Berlin" (Guidelines of the Free University of Berlin) and "Charte du doctorat de l'Université Pierre et Marie Curie" (the doctorate charter of University Pierre and Marie Curie of Paris). I received assistance in writing of this thesis manuscript in respect of grammar and syntax, which was provided by my thesis co-supervisors Prof. Helge Amthor and Prof. Markus Schülke-Gerstenfeld.

Paris, 06/07/2015

Amalia Stantzou

Table of contents

List of figures and tables

List of abbreviations

A followed by number	Alexa antibody
AAV	Adeno-Associated Virus
AcetylCoa	Acetyl Co Enzyme A
ActR	Activin Receptor
ADP	Adenosine Di-Phosphate
ALK	Activin Like Kinase
ATP	Adenosine Tri-Phosphate
BaCl2	Barium Chloride
bHLH	basic-Helix-Loop-Helix
BMP	Bone Morphogenetic Protein
BMPR	Bone Morphogenetic Protein Receptor
bp	base pairs (unit)
BRE	BMP Responsive Element
BV	Brilliant Violet antibody
Ca^{2+}	Calcium ion
CD	Cluster of Differentiation
CDK	Cyclin-Dependent Kinase
CK	Creatine Kinase
CMV	Cytomegalovirus
Co-Smad	Common mediator-Smad
Cre	Causes recombination
CtBP	C-terminal Binding Protein
Cy	Cyanine
DAPI	4',6-Diamidino-2-Phenylindole
DMEM	Dulbecco's Modified Eagle Medium
DNA	Deoxyribonucleic Acid
DTA	Diptheria Toxin fragment A
E followed by number	Embryonic day, days post coitum (E0.5 is the morning when plug is found)
EDL	Extensor Digitorum Longus
EGFP	Enhanced Green Fluorescent Protein
ER	Estrogen Receptor

ERK	Extracellular signal-Regulated Kinase
ERT	mutated LBD of the ER that binds Tamoxifen
ERT2	more recent mutated LBD of the ER that binds Tamoxifen
FACS	Fluorescent Activated Cell Sorting
FGF	Fibroblast Growth Factor
FITC	Fluorescein Isothiocyanate
FSC	Forward-Scattered light
FOP	Fibrodisplasia Ossificans Progressiva
FoxO	Forkhead box O
Fzd	Frizzled receptor
GDF	Growth Differentiation Factor
GFP	Green Fluorescent Protein
GTP	Guanosine Tri-Phosphate
HBSS	Hank's Balanced Salt Solution
HCl	Hydrogen Chloride
HDAC	Histone Deacetylase
HEK293	Human Embryonic Kidney 293 cells
HGF	Hepatocyte Growth Factor
HSA	Human α-Skeletal Actin
i.e.	in latin "*id est*", meaning *"in other words"*
ID	Inhibitor of Differentiation or Inhibitor of DNA binding
IGF1	Insulin-like Growth Factor 1
IgG1	Immunoglobulin G1
IL	Interleukin
IRES	Internal Ribosome Entry Site
I-Smad	Inhibitory-Smad
Itga7	Integrin-α7
JNK	Jun NH2-terminal Kinase
LAP	Latency Associated Peptide
LBD	Ligand Binding Domain
Lbx1	Ladybird homeobox factor 1
LLC	Large Latent Complex
LoxP	Locus of X-over P1
LTBP	Latent TFG-β Binding Protein

MAB	Mesoangioblast
MAPK	Mitogen-Activated Protein Kinase
Mdx mice	mice with X chromosome-linked Muscular Dystrophy
MHC	Myosin Heavy Chain
MMP	Matrix Metalloproteinase
MRF	Myogenic Regulatory Factor
mRNA	messenger RNA
Mstn	Myostatin
mTOR	mammalian Target Of Rapamycin
MuRF1	Muscle RING Finger 1
MUSA1	Muscle ubiquitin ligase of the SCF complex in atrophy-1
Myf	Myogenic Factor
MyoD	Myogenic Differentiation
MyoG	Myogenin
NaOH	Sodium Hydroxide
NICD	Notch Intracellular Domain
P followed by number	Postnatal day (P0 being the birth day)
Pax	Paired box protein
PBS	Phosphate Buffered Saline
PCR	Polymerase chain reaction
PE	Phycoerythrin fluorescence dye
Peg3	Paternally expressed gene 3
PFA	Paraformaldehyde
PI3K	Phosphatidylinositol 3-kinase
PICs	PW1+ interstitial cells
PKC	Protein Kinase C
P-Smad	Phosphorylated-Smad
RBPJ	Recombination signal Binding Protein for immunoglobulin kappa J region
RNA	Ribonucleic Acid
R-Smad	Receptor-regulated Smads
RT-PCR	Reverse Transcription-Polymerase Chain Reaction
RT-qPCR	Real Time-quantitative Polymerase Chain Reaction
SBE	Smad-Binding Element

Sca1	Stem Cell Antigen 1
SCF complex	Skp1, Cullins, F-box E3 ubiquitin ligase proteins
Scid mice	Severe combined immune deficient mice
SD	Standard Deviation
SEM	Standard Error of Mean
Shh	Sonic Hedgehog
siRNA	Small interfering RNA
Six	Sine oculis-related homeobox
SLC	Small Latent Complex
Smad	homologue of proteins SMA ("small body size", *C. elegans*) and MAD ("mothers against decapentaplegic", Drosophila)
Smurf	Smad Ubiquitin Regulatory Factor
Sol	Soleus muscle
SP	Side Population
SSC	Side-Scattered light
TA	Tibialis Anterior muscle
TCF	T-Cell Factor
TGF-β	Transforming Growth Factor -β
Wnt	Wingless-type MMTV (mouse mammary tumor virus) integration site family member
WT	Wild-type

Abstract

Growth factors from several families of signaling molecules regulate muscle development and regeneration, and thereby determine correct muscle function. However, the regulatory mechanisms that coordinate the timing of muscle precursor generation, their differentiation and the subsequent formation of correct number and size of muscle fibers are still poorly understood. Bone Morphogenetic Proteins (BMPs), a subfamily of TGF-β growth factors, have been shown to be key signals that regulate embryonic and fetal muscle precursors during prenatal myogenesis, as well as the stem cells of adult muscle, termed 'satellite cells', when activated during muscle regeneration. The main aims of my thesis were to elucidate whether BMP signaling plays a role during postnatal/juvenile satellite cell-dependent muscle growth as well as for maintenance of adult muscle mass. I found that components of BMP signaling pathway are expressed in muscle satellite cells of neonatal, juvenile and adult mice. I used transgenic mouse lines to conditionally overexpress the BMP signaling cascade inhibitor Smad6 in muscle satellite cells and in differentiated skeletal muscle. I show that BMP signaling is required for correct proliferation of muscle satellite cells and their differentiation into myonuclei, thereby ensuring that the growing muscle fibers reach the correct final size. Moreover, I demonstrated that the final number of muscle stem cells is established during the postnatal/juvenile growth phase and this also depends on the BMP signaling cascade. Finally, I provide evidence that BMP signaling is a strong hypertrophic signal for the adult skeletal muscle and its presence is indispensable for muscle tissue maintenance. In summary, my findings demonstrate that BMPs are essential growth factors for postnatal skeletal muscle.

Résumé

Les facteurs de croissance de plusieurs familles de molécules de signalisation régulent le développement et la régénération musculaire, et déterminent ainsi une fonction musculaire normale. Cependant, les mécanismes de régulation qui coordonnent le temps de génération de cellules précurseurs du muscle et leur différentiation, et par conséquent la formation du nombre et de la taille finale des fibres musculaires sont peu compris. Il a été montré qu'une sous-famille des facteurs de croissance TGF-β, dénommée "Bone Morphogenetic Proteins" (BMPs), joue un rôle clef dans la régulation de cellules précurseurs du muscle embryonnaire et fœtal, pendant la myogenèse prénatale, ainsi que dans la régulation de cellules souches musculaires adultes, dénommées "cellules satellites", lorsque celles-ci sont actives dans le contexte de régénération du muscle. Les objectifs principaux de ma thèse étaient d'une part de déterminer si la signalisation BMP joue un rôle pendant la phase de croissance du muscle postnatale/juvénile dépendante des cellules satellites, et d'autre part d'investiguer si cette voie est impliquée dans la maintenance de la masse musculaire squelettique adulte. J'ai ainsi trouvé que les composants de la voie de signalisation BMP sont exprimés dans les cellules satellites du muscle de souris néonatales, juvéniles et adultes. Par ailleurs, j'ai utilisé des lignées de souris transgéniques pour surexprimer l'inhibiteur Smad6 de la cascade de signalisation BMP de manière conditionnelle d'une part dans les cellules satellites et d'autre part dans le muscle squelettique différencié. Par ces expériences, j'ai pu démontrer que la signalisation BMP est requise pour une prolifération correcte des cellules satellites et pour leur différentiation en myonuclei, assurant que les fibres musculaires en croissance atteignent une taille finale normale. Par ailleurs, mes travaux révèlent que le nombre final de cellules souches musculaires est établis pendant la phase de croissance postnatale/juvénile et que celle-ci dépend de la cascade de signalisation BMP. Enfin, je fournis des preuves montrant que la signalisation BMP est un puissant signal hypertrophique dans le muscle squelettique adulte et que sa présence est indispensable pour le maintien du tissu musculaire. En résumé, mes résultats de recherche démontrent que les BMPs sont des facteurs de croissance essentiels pour le muscle squelettique postnatal.

Zusammenfassung

Wachstumsfaktoren verschiedener Familien von Botenstoffen regulieren Entwicklung und Regeneration der Skelettmuskulatur und ermöglichen somit eine korrekte Muskelfunktion. Allerdings sind die zugrundeliegenden Mechanismen nur unzureichend geklärt, die das zeitliche Zusammenspiel der Bildung der Muskelvorläuferzellen, deren Differenzierung und die davon abhängige Anzahl und Größe der Muskelfasern koordinieren. Knochenwachstumsfaktoren, oder im Englischen „bone morphogenetic proteins" (BMPs) genannt, sind eine Untergruppe der sogenannten "transforming growth factors-β"- (TGF-β-) Wachstumsfaktoren. BMPs sind sowohl wichtige Regulatoren embryonaler und fetaler Muskelvorläuferzellen als auch der Stammzellen der adulten Skelettmuskulatur, die auch als „Satellitenzellen" bezeichnet werden. Meine Promotionsarbeit hatte zum Ziel, die Regulation der Satellitenzellen durch BMPs während der postnatalen und juvenilen Wachstumsphase der Skelettmuskulatur zu erforschen. Ein weiteres Ziel war die Erforschung der Funktion der BMPs im differenzierten adulten Muskelgewebe. Ich konnte sowohl in postnatalen, juvenilen als auch in adulten Satellitenzellen die RNA-Synthese von Genen nachweisen, die Komponenten der BMP-Signalkaskade kodieren. Ich habe transgene Mäuse gezüchtet, das Smad6-Protein in Satellitenzellen bilden und somit die BMP-Signalkaskade in den Satellitenzellen unterdrücken. Mittels dieser Tiermodelle konnte ich nachweisen, dass BMPs sowohl die Proliferation der Satellitenzellen als auch ihre Differenzierung in Myonuclei und damit die Bildung einer ausreichenden Anzahl und Größe von Muskelfasern steuern. Während der postnatalen und juvenilen Wachstumsphase wird unter BMP-Signalwirkung außerdem das Reservoir adulter Muskelstammzellen angelegt. Im adulten Organismus bewirken BMPs ein hypertrophes Wachstum der Muskelfasern und sind für die Erhaltung des Muskelgewebes unabdingbar. Zusammenfassend beweisen meine Beobachtungen die essentielle Bedeutung von Wachstumsfakturen der BMP-Familie sowohl für das postnatale Muskelwachstum als auch für die Eutrophie der adulten Skelettmuskulatur.

Introduction
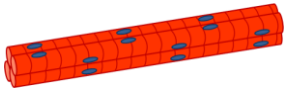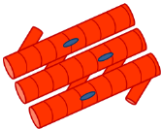
Part I: The skeletal muscle

1- Muscle tissue types

Muscle tissue has the ability to contract or to shorten, thus providing movement of external and internal body parts. In vertebrates there are three types of muscle tissues: skeletal muscle, cardiac muscle and smooth muscle. The function and properties of these three types of muscles are compared in **Table 1**.

Table 1: Comparison of muscle tissue types.

	Skeletal muscle	Cardiac muscle	Smooth muscle
General function	Body posture and locomotion, joint stability, heat generation	Pumping blood through the heart chambers into blood vessels	Maintain flow of fluids and solids along hollow structures
Location	Directly attached to the skeleton by tendons	Heart	iris, erectors of hairs, walls of hollow organs (blood vessels, intestines, stomach, bronchi)
Regulation of contraction	Voluntary, somatic motor neurons	Involuntary, autonomic motor neurons, hormones	Involuntary, autonomic motor neurons, hormones, cytokines
Individual Neuromuscular junction	Yes	No	Yes (in unitary smooth muscle, also called visceral smooth muscle, which is the most abundant form, and has the property of coordinated contraction, opposed to multiunit smooth muscle)
GAP junction	No	Yes	Yes (unitary muscle)
Pacemaker	No	Yes	Yes (unitary muscle)
Stimulus effect	Excitation	Excitation or inhibition	Excitation or inhibition
Cell shape	Long and cylindrical	Branching	Short and fusiform
Nuclei	Multinucleated, periphery located under sarcolemma (cell membrane)	Uni- or binucleated centrally located	Single nucleus, centrally located
Microscopic appearance	Striated (actin and myosin arranged in sarcomeres)	Striated	Not striated (no sarcomeres, arranged in bundles)
Schematic Diagram			

2- Adult skeletal muscle structure

Skeletal muscle tissue is very organized and represents around 40% of the body mass and is composed of muscle fibers, connective tissue cells, adipocytes, vascular cells and nerve.

Each muscle contains hundreds to thousands of muscle cells which are called myocytes, muscle fibers, myofibers or rhabdomyocytes. Muscle fibers are syncytia, containing several hundreds of postmitotic nuclei (myonuclei) positioned in periphery of the cell just under the plasma membrane (sarcolemma). They have a cylindrical form with a diameter between 10 to 100 μm and a length which rarely exceeds 10 cm. The sarcolemma of the myofiber is surrounded by an external basal lamina (Wheater and Burkitt, 1987).

Connective tissue sheaths are found at various structural levels, covering each subdivision of muscle structures. Firstly, each muscle fiber is covered by endomysium, interconnecting adjacent muscle fibers. A group of 20-80 myofibers form a muscle fascicule which is surrounded by perimysium. Finally, several muscle fascicules surrounded by epimysium form a muscle **(Figure 1)**.

The muscle is attached to the skeleton through the tendon. The force generated by myocyte contraction is transmitted through the sarcolemma to the tendon. At the musculotendinous junction, the sarcolemma is folded and increases the interface between the extracellular matrix and the cell surface by 10 to 50 folds. Collagen microfibrils of the tendon are embedded in the cellular invaginations and are in close contact with the sarcolemma. This arrangement allows force transmission from muscle to the bone (Tidball and Daniel, 1986).

Each muscle has blood supply to ensure adequate nutrient delivery and waste removal. The vascular system also ensures supply of cells of the immune system which allow degradation of apoptotic or necrotic cells following muscle injury.

Skeletal muscles are controlled by the peripheral somatic nervous system, with the exception of the diaphragm which is also under autonomic control. Muscles with the same function are innervated by the same nerve. Each muscle fiber possesses a single neuromuscular junction formed by the contact between the motorneurone presynaptic terminal and the postsynaptic sarcolemma. Muscle innervation is crucial for contraction but also for muscle maintenance. Indeed, innervation is an anti-apoptotic stimulus. Following

denervation, muscle suffers from atrophy. Short-term denervation stimulates proliferation of muscle stem cells called satellite cells, but long-term denervation leads to the depletion of satellite cells (de Castro Rodrigues and Schmalbruch, 1995).
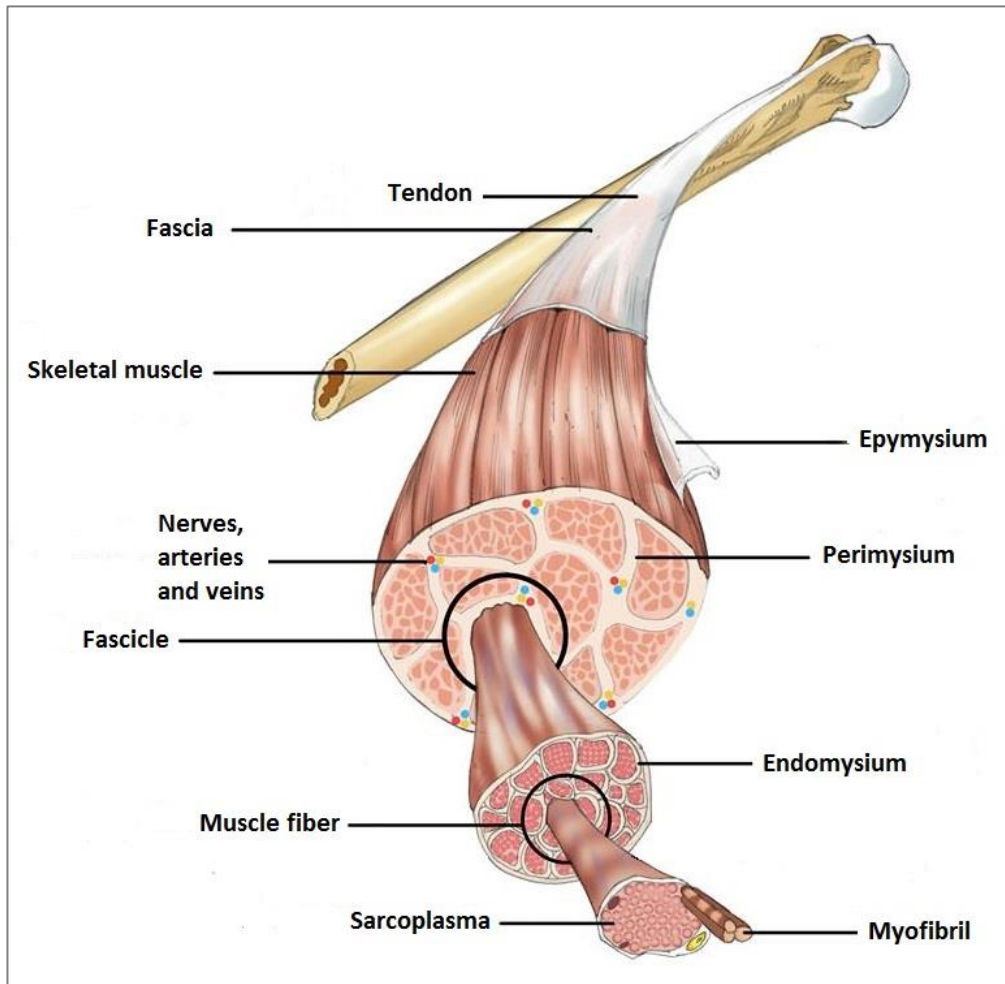
Figure 1 – Skeletal muscle structure. Adapted from the McGraw-Hill Companies.

3- Muscle fiber structure

Muscle fibers contain parallel bundles of contractile units called myofibrils and which compose around 80% of the cellular volume. Myofibrils consist of repeated units called sarcomeres with a diameter of 1 μm and 2-3 μm length. A sarcomere contains overlapping contractile filament proteins (myofilaments): actin (thin) and myosin (thick) filaments connected to Z disks at either end of the sarcomere **(Figure 2)**. The distribution of the myofilaments determines some regions visible in electronic microscopy as transversal striations in the myofiber.
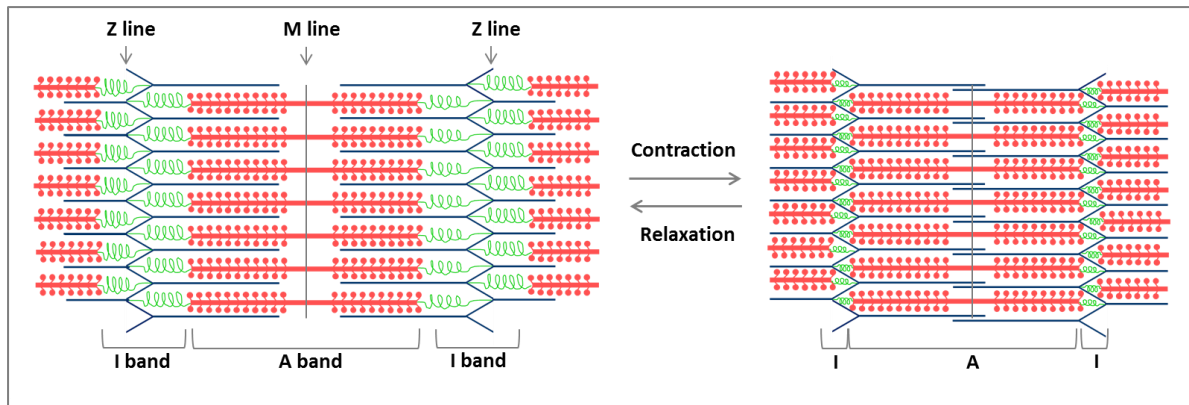
Figure 2 – Scheme of sarcomere contraction and relaxation. The sarcomere is delimited longitudinally by the Z lines and is composed of thin actin filaments (blue) and thick myosin filaments (red). The giant protein called titin (green) extends from the Z-disk through the whole length of hollow myosin filaments to the M-line and is essential for maintaining the sarcomere structure. When visualized by light microscopy myofilaments of skeletal muscle, have a striated appearance due to light isotropic bands (I-band) and dark anisotropic bands (A-band) that respectively correspond to the zone of actin filaments and the zone of overlapping actin and myosin filaments.

4- Skeletal muscle contraction

Contraction of skeletal muscle can either cause shortening (concentric contraction), lengthening (eccentric contraction) or no change (isometric contraction) of muscle length.

Muscles are organs which are able to convert chemical energy into mechanical energy in order to induce muscle tension or contraction. The process starts when an action potential reaches the presynaptic axon terminal of the motoneurone, inducing the release of acetylcholine in the neuromuscular junction. The neurotransmitter will then bind and open the acetylcholine receptor situated on the sarcolemma. Entrance of sodium ions in the muscle fiber will lead to the depolarization of the sarcolemma inducing the formation of a muscle action potential propagating along the sarcolemma invaginations (T-tubules) and opening of dihydropyridine receptor (a voltage dependent L-type calcium channel) on the sarcolemma . Activation of the L-type channel allows local calcium entry and activation of ryanodine receptors (calcium release channels) in the sarcoplasmic reticulum (smooth endoplasmic reticulum of the myofiber which is a calcium reservoir) and their releasing of the stocked calcium ions into the sarcoplasma.

In the presence of calcium and ATP, thick and thin filaments slide past each other leading to shortening the length of the sarcomeres, then the myofibrils and finally the muscle

22

(Figure 2). Indeed, when calcium is present the myosin binding site on actin is unmasked (calcium binds to troponine C, changing the conformation of tropomyosine bound to troponine) allowing actin and myosin to interact. The head of myosin heavy chain conformation changes with ATP hydrolysis and energy transfer. This sliding filament theory was first proposed by Hugh Huxley in 1954 and is depicted in **Figure 3** (Huxley 2004).
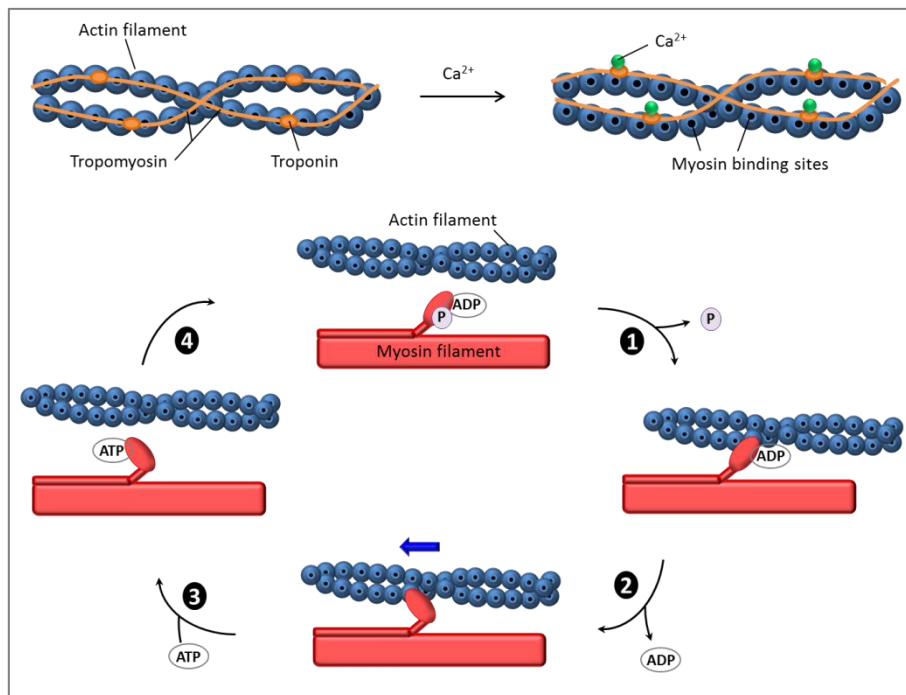
Figure 3- The actin-myosin cross-bridge cycle. When calcium ions are released from the SR, they bind to troponin, which subsequently change conformation and unmask the myosin binding sites present on actin. The cross-bridge cycle can be presented in 4 steps. **(1) Cross-bridge formation**: the activated myosin head binds to actin forming a cross-bridge. Inorganic phosphate is then released and the bond between myosin and actin becomes stronger. **(2)The power stroke**: ADP is released and the activated myosin head pivots by about 5 nm, thus sliding the thin myofilament towards the center of the sarcomere. **(3) Cross-bridge detachment**: ATP binds to the myosin head and the link between actin and myosin head weakens, leading to their detachment. **(4) Reactivation of the myosin head**: ATP is hydrolyzed to ADP and inorganic phosphate. The energy released during hydrolysis reactivates the myosin head, returning it to the *rigor* position (named *rigor* because it is responsible of cadaveric rigidity, *rigor mortis*). As long as calcium ions unmask the myosin binding sites, the cycle is repeated and leads to the shortening of the sarcomere.

5- Skeletal muscle metabolism

As described above, muscular contraction requires energy in the form of ATP. Muscle fibers have a short-term storage of creatine phosphate that can generate ATP when processed by creatine kinase. Muscle fibers also contain glycogen and globules of fatty acids

that can be metabolized to produce ATP. Glycogen can be rapidly converted to glucose, which in turn, through glycolysis, can be catabolized to pyruvate and produce ATP. In absence of oxygen pyruvate is converted to lactate which can be responsible of muscle fatigability. In presence of oxygen, more ATP is produced through mitochondrial oxidation which converts AcetylCoA (obtained from pyruvate oxidation or from fatty acids β-oxidation) to oxaloacetate. The aerobic metabolic pathway is much slower compared to the anaerobic pathway but produces much higher amounts of ATP **(Figure 4)**. Energy for normal mobility or during prolonged physical exercise is provided by the aerobic pathway, whereas the anaerobic pathway is used during short and intense exercise.
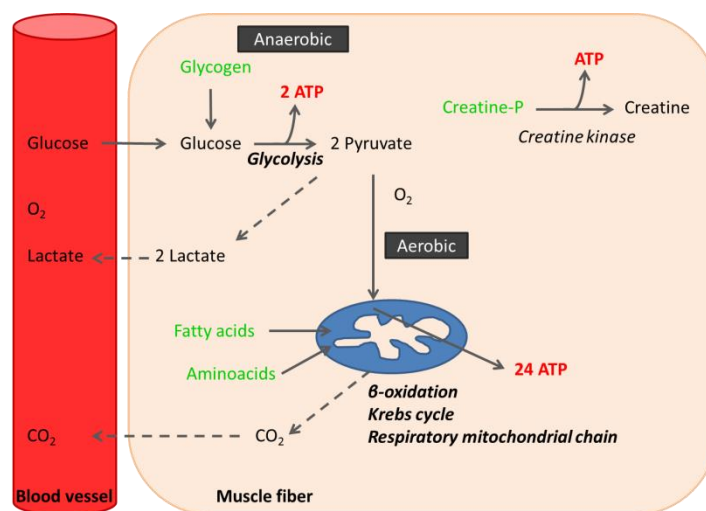
Figure 4 - Muscle ATP source for muscle contraction: phosphagen system and fast anaerobic vs slow aerobic/oxidative metabolisms. The substrates that can be stored in muscle for ATP production are in green. Creatine phosphate, formed from ATP while the muscle is relaxed, forms ATP during muscle contraction. Breakdown of muscle glycogen into glucose and production of 2 pyruvates through anaerobic glycolysis (no oxygen needed) is a fast process. In presence of oxygen the 2 pyruvates are used in the mitochondria to produce 24 more ATP molecules via the Krebs cycle and aerobic cellular respiration, an oxygen-requiring set of reactions. Fatty acids liberated from adipose cells or amino acids from protein breakdown can also be used to produce ATP through aerobic oxidation.

6- Skeletal muscle fiber types

The speed at which a muscle fiber contracts depends on its metabolic and contractile properties. Thus fiber types have been classified in type I or II **(Table 2)** according to: ATPase activity of myosin (Brooke MH and Kaiser KK, 1970), or which isoforms of myosin heavy chain (MHC) they express (Schiaffino et al., 1989) **(Figure 5)**, or according to whether the fiber's metabolism is primarily anaerobic or aerobic (more mitochondria,

myoglobin and capillaries). Moreover, there are also embryonic, fetal and neonatal forms of myosin. The identity of a myofiber is not fixed and fiber types can switch properties under various conditions like ageing (Ciciliot et al., 2013).

Table 2 – Adult fiber type classification

Contraction speed	Fiber type	MHC	Metabolism	ATPase activity	Fatigability
Slow	I	I	Oxydatif (aerobic)	Low	Low
Support long-term moderate activity (mostly in postural muscles) "red" aspect (capillaries, hemoglobin)					
Fast	IIA IIX IIB	IIa IIx IIb	Oxydo-glycolytic Oxydo-glycolytic Glycolytic (anaerobic)	High	Low Intermediate High
Support more powerful but short contractions IIA is "red" whereas IIB has "white" aspect (less capillaries, glycogen storage)					
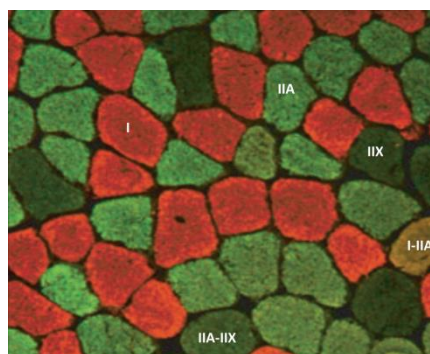
Figure 5 – Muscle fiber types in mouse skeletal muscle. Section of mouse *Soleus* muscle stained with anti-MHC-I (red) and anti-MHC-IIA (green). Unstained fibers correspond to the minor proportion of type IIX fibers, in orange hybrid I-IIA and in intermediate green the IIA-IIX fibers. Image from Schiaffino, 2010 (Copyright clearance center license number 3638431026240).

1- General introduction into myogenesis

The process of generating muscle is called myogenesis and involves the following processes: stem cell and progenitor maintenance, lineage specification and terminal differentiation. Myogenic progenitor cells and committed myoblasts proliferate, differentiate and fuse to each other or to a previous fiber to form muscle.

During myogenesis, a number of cell-extrinsic and cell-intrinsic regulatory mechanisms have been shown to be involved in the spatiotemporal direction of precursor cells for muscle formation. Extrinsic signals are originated from signaling molecules (either secreted or present on adjacent cell surface) binding to their receptors at the cell surface which can then induce intrinsic regulatory mechanisms by modulating interactions of transcription factors, regulatory RNAs or chromatin-remodeling factors (Bentzinger 2012). In amniotes different myogenic processes take place during development: embryonic, fetal, postnatal/juvenile and adult.

2- Embryonic and fetal myogenesis

In the mouse, at embryonic day 8 (E8), a process called metamerisation or somitogenesis, which lays down the segmental body plan of vertebrates, starts to form blocks through the division of the paraxial mesoderm. These blocks, called somites, are formed from head to tail at each side of the neural tube and will rapidly differentiate (Aulehla and Pourquié, 2006). The ventral part of the somite forms the mesenchymal sclerotome which will later give rise to cartilage and bone of the axial skeleton of the embryo (vertebrae and ribs). The dorsal region of the somite remains epithelial and forms the dermomyotome which will be the source of muscle cells throughout the body (with the exception of head muscles which originate in the prechordal and pharyngeal head mesoderm).

Thereafter, at E10.5 cells from the lips of the dermomyotome will delaminate, migrate and generate the first muscle named the primary myotome, located between the sclerotome and the dermomyotome (Cossu et al. 1996) **(Figure 6)**. Different compartments of the dermomyotome will generate distinct muscles. Indeed, dorsal muscles will arise from

the epaxial dermomyotome and myotome, whereas migrating cells, which delaminate (by undergoing an epithelial-to-mesenchymal transition) from the ventrolateral lip of the hypaxial dermomyotome at the level of the limbs, will form muscles of the extremities (limbs), the diaphragm and the hypoglossal chord (tongue) (Vasyutina and Birchmeier, 2006). The dermomyotome also forms other tissues and cell types including connective tissue, dermal fibroblasts, vascular smooth muscle cells, brown fat tissue and endothelial cells. The fate of the multipotent progenitor cells depends on their relative position with respect to adjacent tissues, notably the notochord, neural tube, dorsal ectoderm and myotome which are responsible of extrinsic signals guiding the cells progression in different lineages that are further discussed in II-7-A (Buckingham, 2006).
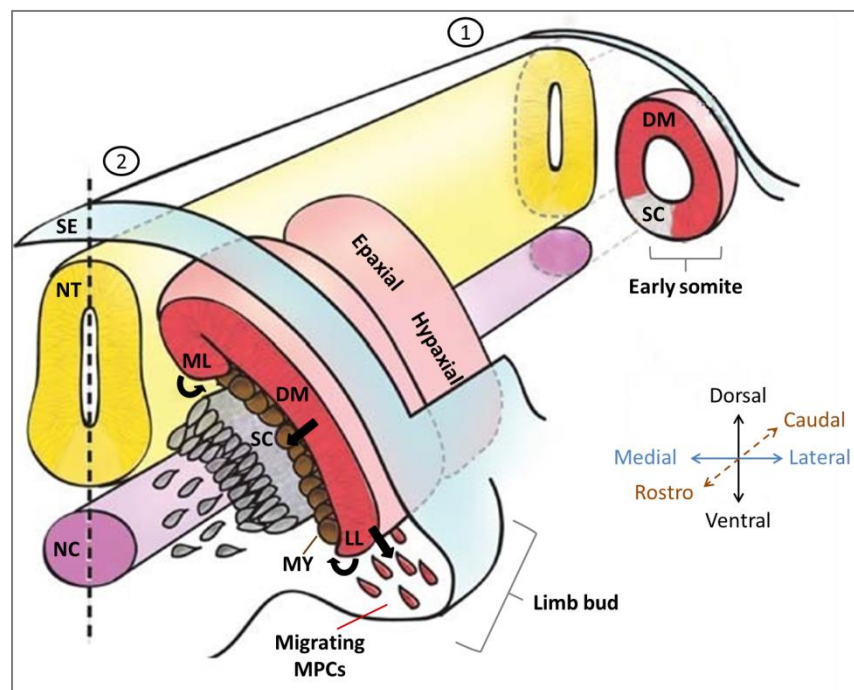
Figure 6 – Illustration of myogenesis along the rostro-caudal axis of the embryo. (1) The early somite, under the surface ectoderm (SE) and next to the neural tube (NT) and notochord (NC), differentiates to form the dermomyotome (DM) and sclerotome (SC). (2) Thereafter muscle precursor cells (MPCs) in the medial lip (ML) and lateral lip (LL) of dermomyotome, but also at a second stage cells from the central part of the dermomyotome, will delaminate to form the first muscle, called the myotome (MY). At the limb level, long distance migrating MPCs will delaminate from the lateral lip towards the limb bud to generate the muscles of the extremities. Different compartments of the dermomyotome (epaxial and hypaxial) will generate distinct muscles. Scheme adapted from Bentzinger et al 2012.

During embryonic myogenesis (in mouse E9.5 - E14.5), also referred to as primary myogenesis, the first muscles appear with primary myotubes formed after fusion of

differentiating myoblasts. Subsequently, during secondary/fetal myogenesis (E14.5 - E17.5), muscle precursor cells either fuse into previously formed primary myotubes or they fuse with each other to create new secondary myotubes (Biressi et al., 2007). The latter have different isoforms of MHC as well as metabolic enzymes (Schiaffino and Reggiani, 1996). Around E17 a basal membrane forms around each myotube rendering them mature muscle fibers. Thereby muscle progenitors are sequestered between the basal membrane and the sarcolemma of the myotube. Due to the unique anatomical position of these progenitors they are termed satellite cells (Mauro, 1961) **(Figure 8)**. These cells (further described in II-4-A) will then be involved in late fetal, juvenile and postnatal myogenesis.
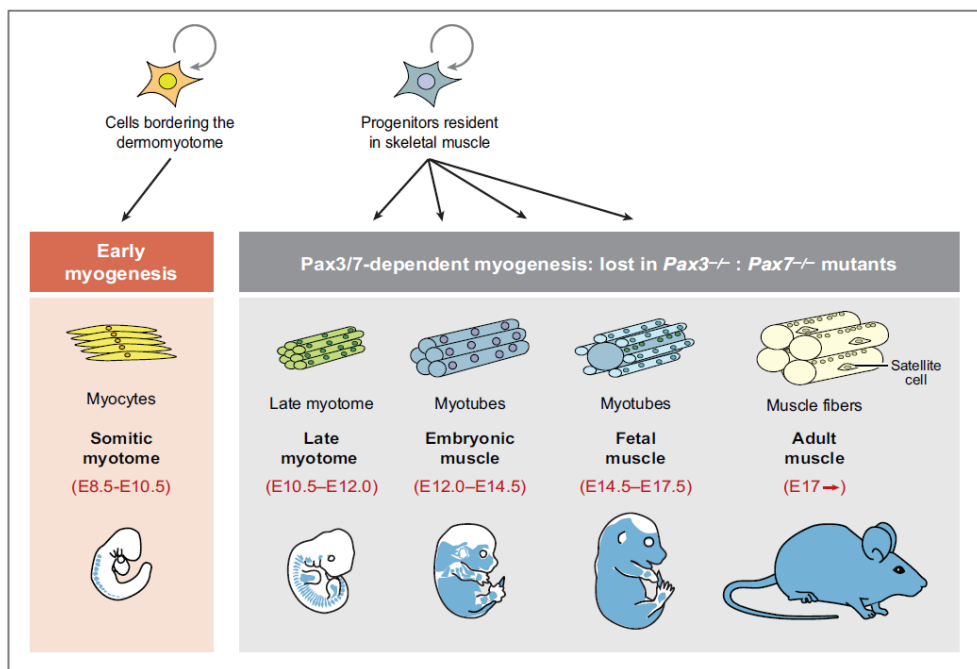
Figure 7 – Scheme of the progenitor cells and their muscle derivatives, together with timing of these events in the mouse. From Buckingham and Relaix, 2007.

3- Myogenic lineage progression

At the limb bud level, the transcription factors sine oculis-related homeobox 1 (Six1) and Six4 have been described as the tip of the genetic regulatory cascade that drive progenitors from the dermomyotome towards the myogenic lineage. Indeed, Six1/4 are required for the expression of several transcription factors involved in embryonic myogenesis (Grifone et al., 2005).

Myogenic progenitor cell specification is first driven by paired domain transcription factors Pax3 and its paralogue Pax7. Pax3 expression begins at E8 in the presomitic

mesoderm, then in the dermomyotome and is progressively restricted to the dorsal and ventral lips of the dermomyotome. At E9, Pax7 expression initiates in the somites and the highest levels of its expression resides in the central dermomyotome (Kassar-Duchossoy et al., 2005). At the limb-level, Pax3, and not Pax7, controls c-met (tyrosine kinase receptor) and Lbx1 (ladybird homeobox factor 1) expression in long-range migrating precursors (Birchmeier and Brohmann, 2000). Pax3 is crucial for embryonic muscle development whereas Pax7 is essential for postnatal and adult myogenesis (Relaix et al., 2005).
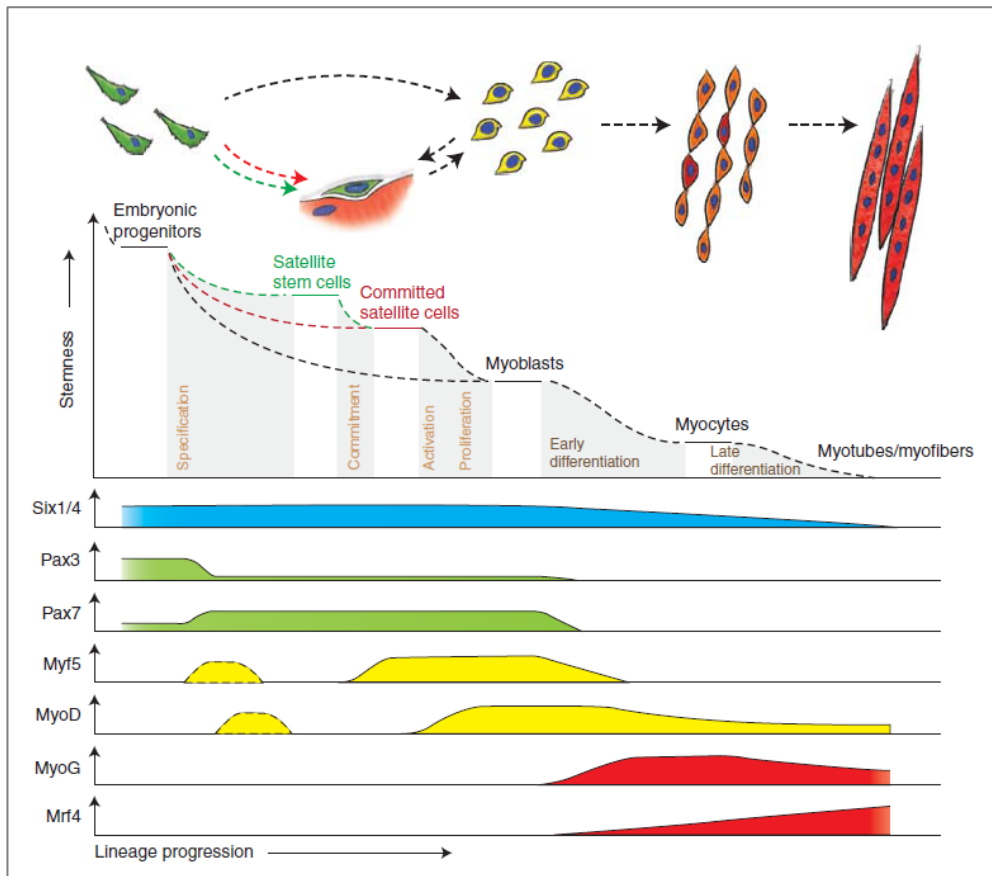
Figure 8 – Hierarchy of transcription factors regulating progression through the myogenic lineage. Six1/4 and Pax3/7 are master regulators of early lineage specification. Myf5 and MyoD are responsible for myogenic commitment of the myoblasts. And finally expression of the terminal differentiation genes, myogenin (MyoG) and Mrf4 is required for the fusion of the myocytes and the formation of myotubes. Embryonic muscle progenitors differentiate in myoblasts whereas adult precursors, termed satellite cells, may either remain quiescent or activate into committed myoblasts. Activated committed satellite cells (myoblasts) can also return to the quiescent state. From Bentzinger et al., 2012.

Progenitor cells are determined as myogenic precursors (termed myoblasts) upon sequential activation of the basic-loop-helix (bHLH) myogenic regulatory factors (MRFs): Myf5, MyoD, Mrf4 (Myf6) and Myogenin (Weintraub et al., 1991; Rudnicki and Jaenisch,

1995). MRFs bind to DNA via their basic domain whereas their helix-loop-helix (HLH) motif allows them to heterodimerise with ubiquitously expressed E proteins that mediate recognition of E boxes found in the promoters of muscle specific genes (Massari and Murre, 2000). At E10.5 determined myoblasts first express Myf5 (Buckingham, 1992), then MyoD (Sassoon et al., 1989). Subsequently, Myogenin is expressed at E11.5 and lastly Mrf4 at E13.5 (Figure 8).

4- Postnatal skeletal muscle stem cells

The primary postnatal skeletal muscle stem cells are satellite cells, supplying myoblasts for growth, muscle homeostasis and repair. However, in experimental conditions, other cell types have also been described to be able to participate in myogenesis.

A) Satellite cells

The muscle satellite cell was first described in 1961 by both Alexander Mauro and Bernard Katz and was named after its anatomical position: between the sarcolemma of the muscle fiber and its surrounding basement membrane (Mauro, 1961; Katz B, 1961) (Figure 9). Already at the cell's discovery its role was stipulated to be a muscle precursor with the following morphological characteristics of an inactive and quiescent cell: small nucleus, large nuclear-to-cytoplasmic ratio, condensed interphase chromatin and few organelles.

Figure 9 – The first satellite cell identified by Mauro in 1961, electron micrograph.

In 1985, Bischoff described a technique to isolate single live muscle fibers from a rat muscle and creating an *in vitro* system in which the basal lamina is maintained and thus allowing the preservation of satellite cell and myofiber association (Bischoff, 1986). This technique delivered decisive proof that satellite cells are in fact muscle precursors. Indeed, when isolated myofibers are cultured, satellite cells activate, proliferate and give rise to myoblasts that differentiate to produce a multinucleated myotube. The progression of this

stem cell in the myogenic lineage is similar to embryonic and fetal muscle precursor's commitment and differentiation **(Figure 10).**
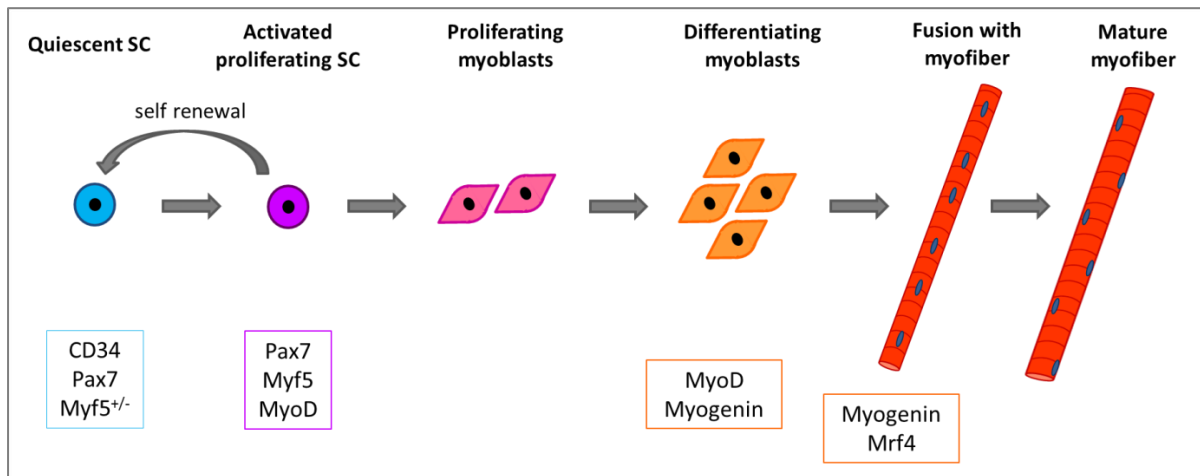
Figure 10 - Progression of myogenic transcription factor program during satellite cell activation, proliferation/self-renewal, differentiation and fusion. Initially satellite cells are mitotically quiescent (G0 phase) and express Pax7 (and/or Pax3) and most of them (90%) also Myf5. Following damage of the basal lamina, satellite cells are activated and enter the cell cycle. Proliferating cells express Pax7 (and/or Pax3), MyoD and Myf5. Following proliferation, activated satellite cells either return to quiescence to maintain the stem cell pool or they continue to proliferate. The resulting myoblasts will further commit to differentiation: they stop proliferating, downregulate Pax7 and Myf5, and express myogenin. Finally, differentiated myocytes align and fuse to a pre-existing myofiber or with each other to form a new multinucleated myofiber. Mrf4 is then required for hypertrophy of the fiber.

Replenishment of the satellite stem cell pool is assured by the ability of these cells to self-renew. Indeed, studies on activated satellite cells on cultured isolated myofibers showed that during proliferation, the cells can undergo symmetric or asymmetric division according to the relative position of the daughter cells **(Figure 11)**. On one hand, the asymmetric division is apico-basal (perpendicular to the myofiber axis) and results in the generation of two distinct daughter cells. The cell closest to the basal lamina will be prevented to undergo differentiation and will be maintained for replenishing the stem cell pool, whereas the apical daughter cell which is in close contact to the sarcolemma will commit to the myogenic lineage. On the other hand, symmetric division of the satellite cell is planar (parallel to the myofiber axis) and gives rise to identical daughter cells, which will either remain "stem-like" or commit to the myogenic lineage (Kuang et al., 2007).

The balance between self-renewal, proliferation and differentiation is crucial to maintain the satellite stem cell pool and to ensure a muscle maintenance and homeostasis.
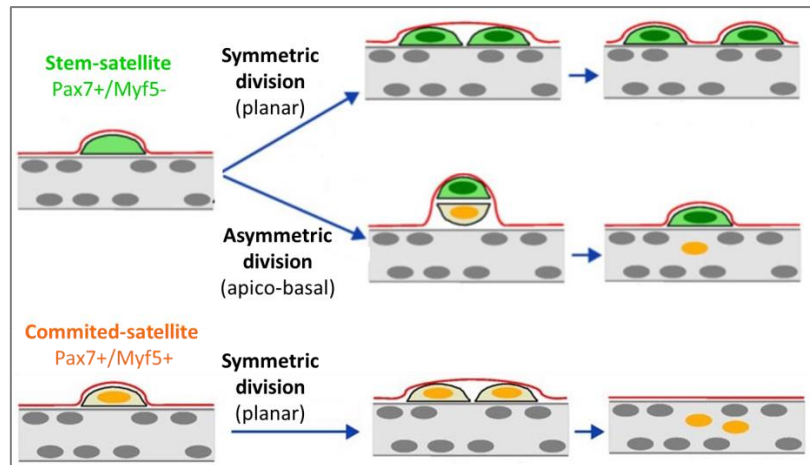
Figure 11 - Satellite cell self-renewal through either asymmetric division (typically in an apical-basal orientation) or symmetric (planar) division. Pax7-only stem-satellite cells undergo symmetric or asymmetric cell division to amplify or maintain, respectively, the stem cell pool. Committed, Pax7$^+$/Myf5$^+$ satellite cells, probably through planar cell division, preferentially undergo terminal differentiation. Adapted from Relaix and Marcelle, 2009 (Copyright clearance center license number 3638440740484)

Satellite cells are a heterogeneous cell population and they express different membrane proteins or transcription factors which can be used as identification markers **(Figure 12).** All satellite cells express Pax7 which is required for their survival. Pax3, however, is only expressed in a subset of satellite cells, including those in the diaphragm, trunk muscles, and around half of the forelimb muscles (Relaix et al., 2006). As previously mentioned, most quiescent satellite cells already express Myf5 and only 10% of the cells, which are considered to have higher stemness, do not express Myf5. A commonly used surface marker is cell surface attachment receptor integrin-α7 (Itga7) (Burkin and Kaufman, 1999). Some markers are also expressed in other cells, such as cluster of differentiation membrane protein CD34, which is present at the surface of satellite cells but is also a marker of endothelial cells (Beauchamp et al., 2000).Therefore, these markers alone do not suffice to identify satellite cells. A solution is using combined immunofluorescence, for example labeling laminin (for the basal lamina) and Pax7 (cell nucleus) or cell adhesion protein M-cadherin (sarcolemma) (Irintchev et al., 1994) **(Figure 13).**

In addition to the single fiber explant technique, another method used for isolating satellite cells, in a larger scale, is using fluorescent-activated cell sorting (FACS), by labeling satellite cell-specific cell surface markers (positive selection) and cell surface markers for non-satellite cell populations (negative selection) (Yin et al., 2013)**.** After testing different FACS fractionation procedures, it has been previously shown that negative

selection of CD45, Ter119, CD31 and Sca1 markers and positive selection of CD34 and α7-integrin markers resulted in isolating cells of which 100% expressed the satellite-cell-specific transcription factor Pax7, but also Myf5, 25% expressed MyoD and 12% Pax3 (Sacco et al., 2008).

Satellite cell markers:

Transcription factors
- Pax7   Myf5
- Pax3   MyoD

Membrane proteins
- Mcad   Notch   Ncam1
- CD34   Fzd7   CXCR4
- cMet   CalcR   Synd3/4
- Itga7   Itgb1   Cav1
- Vcam1   Emerin   Lamin A/C
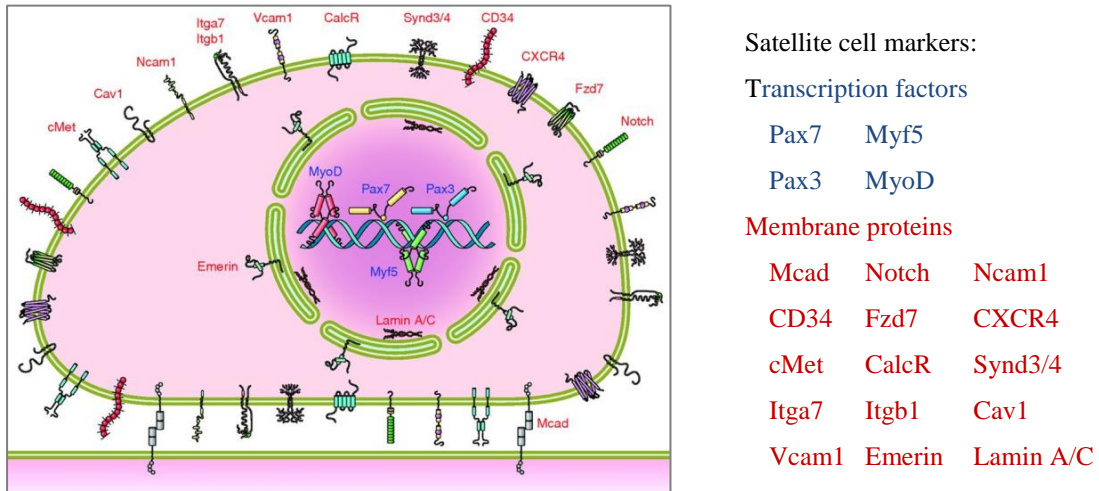
Figure 12 - Markers used to identify satellite cells. Of note, due to heterogeneity in the satellite cell population, these markers are not all expressed together at a specific time but depend on the origin, the stemness and the state of the cell. From Yin et al., 2013.
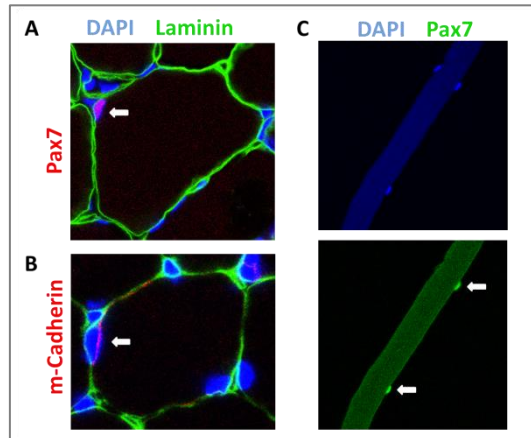
Figure 13 - Immunostaining identifying satellite cells using Pax7 or m-Cadherin antibodies on (A) and (B) mouse *Tibialis Anterior* (*TA*) muscle section or C) on isolated single myofiber from mouse *Extensor Digitorum Longus* (*EDL*) muscle.

Satellite cells also exhibit heterogeneity in respect to their distribution along a myofiber or according to the myofiber type or to the muscle. Indeed, satellite cells are more numerous at the tips of the myofibers (Allouh et al., 2008). Generally, there are 2 to 4 times more satellite cells in slow *Soleus* (*Sol*) muscle compared to fast *Tibialis Anterior* (*TA*) or *Extensor Digitorum Longus* (*EDL*) muscles and within a same muscle there are more cells

on slow type I myofibers than fast types IIa and IIb (Gibson and Schultz, 1982). Studies have also shown that most satellite cells are located in perisynaptic regions (Kelly, 1978) and in close proximity to capillaries (Christov et al., 2007).

B) Non-satellite-cell muscle stem cells

Several studies of engraftment and lineage tracing have shown that besides satellite cells there are several other cells that may participate in muscle growth and regeneration, including side-population cells (SP), CD133+ (or AC133) cells, mesoangioblasts (Mabs), pericytes and PICs (PW1+ interstitial cells). However, it appears that under normal physiological conditions these cells are not able to give rise to new muscle fibers. The characteristics of identified muscle stem cells are listed in **Table 3**.

One of the first non-satellite-cell described was the side population (SP) cells. In the muscle, SP cells are in the interstitium, close to blood vessels and express surface markers Sca1 and ABCG2. During muscle regeneration their primary role is to generate endothelial cells but they also have a minor contribution to regenerated myofibers. Transplanted SP cells in mdx mice (a model for Duchenne muscular dystrophy) resulted in restored dystrophin expression (Gussoni et al., 1999; Asakura et al., 2002; Doyle et al., 2011).

Another subpopulation of hematopoietic cells, CD133+ cells, were isolated from dystrophic patients, transduced *ex vivo* with a lentivirus in order to induce exon skipping of the mutated dystrophin and restore expression of a shorter and functional dystrophin. The genetically corrected CD133+ stem cells were then transplanted in *scid/mdx* mice and resulted in significant recovery of muscle morphology, function and dystrophin expression (Benchaouir et al., 2007).

Moreover, mesoangioblasts (Mabs), stem cells derived from embryonic dorsal aorta, are able to occupy the satellite stem cell niche after transplantation and to somewhat rescue muscles in *α-sarcoglycan*$^{-/-}$ mice (a model for limb girdle muscular dystrophy) (Sampaolesi et al., 2003).

Pericytes are considered to be multipotent stem cells since *in vitro* they are able to differentiate into adipocytes, chondrocytes and osteoblasts (Farrington-Rock et al., 2004; Doherty et al., 1998). Studies have shown that pericytes can also differentiate into skeletal muscle both *in vitro* and *in vivo*. Several engraftment experiments have shown the myogenic

potential of pericytes including their ability to occupy the satellite cell niche and to improve muscle function in *mdx* mice (Dellavalle et al. 2007; Dellavalle et al., 2011).

Furthermore, another population residing in the interstitial space of the muscle is characterized by PW1 (also called Peg3, paternally expressed gene 3) expression and is referred to as PICs (PW1 intersitial cells). Of note, PW1 is also detected in satellite cells. PICs are myogenic *in vitro* and may contribute to postnatal muscle growth and adult muscle regeneration (Mitchell et al., 2010).

Overall, the role of these non-satellite-cell populations in muscle is poorly understood and even though in most cases they do not seem to be of big significance for muscle repair under physiological conditions, the hypothesis that they can be recruited to maintain myofibers and to enhance satellite cells function has not been ruled out. Many laboratories are currently trying to elucidate their role and to improve their participation in regenerating muscle for therapeutical purposes.

Table 3 - Comparative capacities of myogenic precursors. From Pannérec et al., 2012 (Copyright clearance center license number 3638441252696). Abbreviations: i.a, intra-arterial, i.m. intra-muscular.

Cell type	Markers	Proliferation *in vitro*	Systemic delivery	Repopulation of the satellite cell niche	Transplantation efficiency (number or % of positive myofibers, TA)[a]	Improvement of muscle disease
Satellite cells	Pax7, CD34, c-met	High	No	Yes	>500 fibers (i.m)	*mdx* mice
SP	Hoechst exclusion, CD45, Sca1	Low	Yes	Yes	<50 (8%) (i.a.)	*mdx* mice
CD133+ cells	CD133, CD34, Thy1, CD45	Low	Yes	Yes	50–100 fibers (i.a)	*mdx* mice
Mabs	CD34, c-kit, Flk1	High	Yes	??	>20% (i.a)	α-sarco mice, dystrophic dogs
Pericytes	AP, NG-2 proteoglycan	High	Yes	Yes	300–500 i.a, 20 i.m	*mdx* mice
PICs	PW1	Low	Not tested	Yes	60% (i.m)	Not tested

5- Postnatal myogenesis and muscle mass homeostasis

In mammals, postnatal skeletal muscle growth occurs rapidly and continues until adulthood. In rodents, during the first three weeks of its postnatal life, its total body weight can increase up to 8 fold, half of which is the result of skeletal muscle growth (Gokhin et al., 2008). In mice, the total number of myofibers in a mouse is reached between E18 and birth (Ontell et al., 1984). Postnatal muscle growth is achieved by fusion of satellite cells with the myofibers and through protein synthesis leading to the increase of the myofiber volume (both diameter and length) respectively leading to hyperplastic and hypertrophy growth **(Figure 14)**.
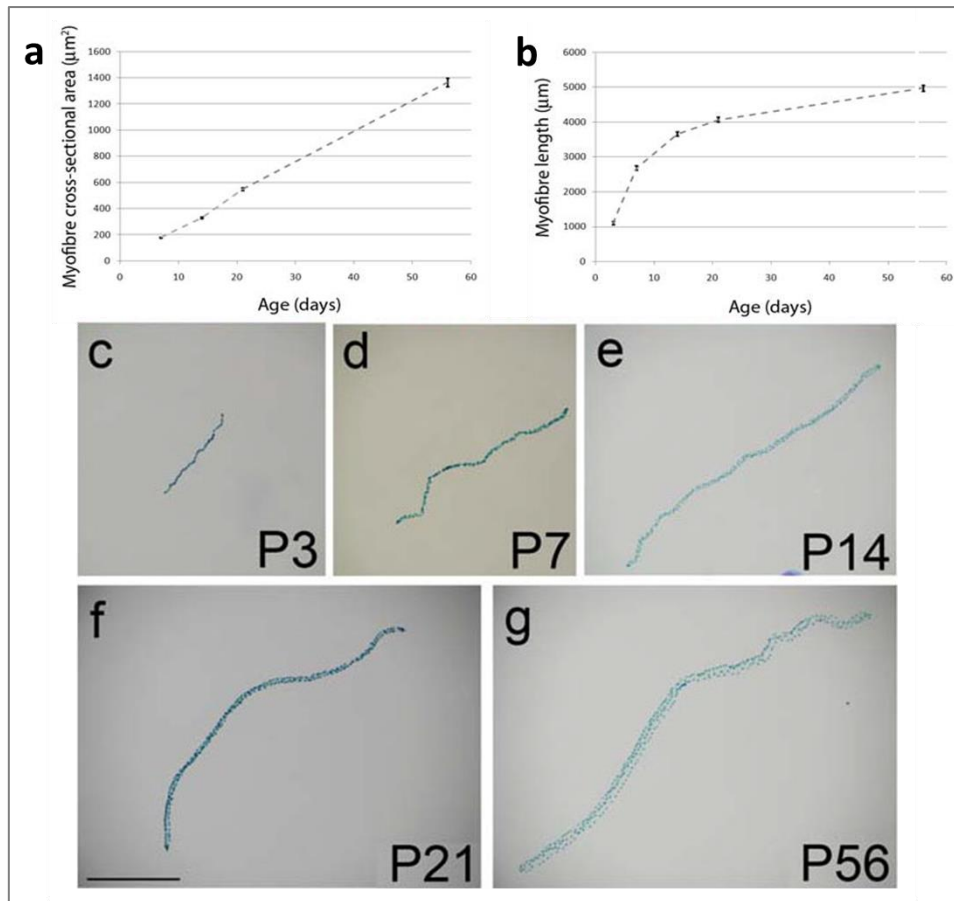
Figure 14 - Postnatal growth of *EDL* myofibers. (a) Measuring myofiber cross-sectional area from mid-belly *EDL* muscle sections showed linear increase with age, (b) which was accompanied by an increase of the length *EDL* myofibers that were isolated from *3F-nLacZ-E* mice (*myosin light chain 3f* locus drives *nLacZ* reporter gene in all fast muscle myonuclei) at postnatal days P3 (c), P7 (d), P14 (e), P21 (f) and in the adult at P56 (g).The isolated myofibers were fixed and incubated in X-Gal solution. Myonuclei, which express β-galactosidase, are subsequently revealed in blue. Scale bar equals 1000 µm. From White et al., 2010.

A) Postnatal myogenesis involving the recruitment of satellite cells.

In early postnatal murine muscles, satellite cells account for 30-35% of the sublaminal nuclei on myofibers. During perinatal/juvenile growth, up to 80% of satellite cells are proliferating and supply new myonuclei to the myofiber. In growing muscle it has been observed that the satellite cell population can be divided in two i) fast dividing population that undergo few divisions before differentiating and ii) slow dividing population that can exit cell cycle (i.e. enter quiescence) or give rise to fast dividing cells (Schultz, 1996). Zammit and colleagues, have recently shown that this process takes place during the first three weeks of a mouse's life and that the adult number of myonuclei and of quiescent

satellite cells (<5%) in a myofiber is reached by P21 **(Figure 15)**. After P21, further muscle growth is achieved solely by hypertrophy (White et al., 2010).
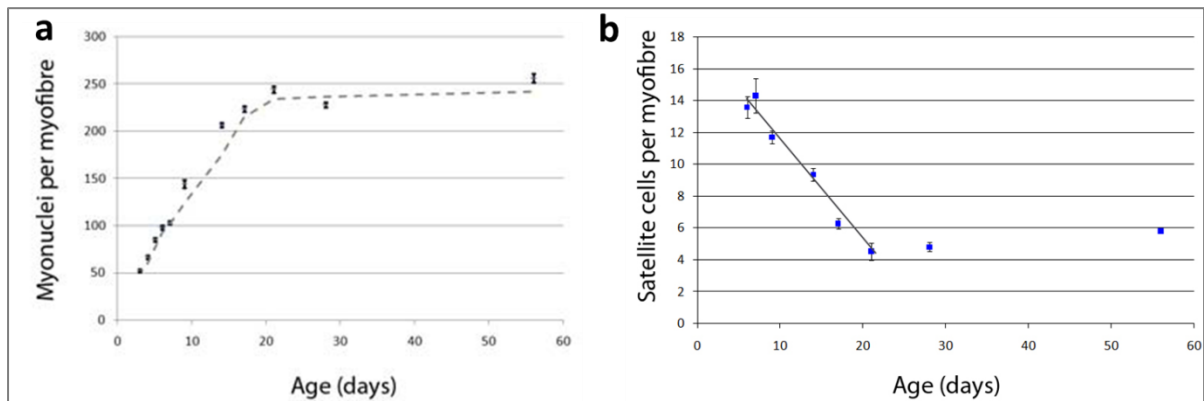
Figure 15 - Satellite cell dependent myonuclear accretion and establishment of the adult satellite stem cell pool is completed by P21. (a) The number of myonuclei on isolated *EDL* myofibers shows a 4-fold increase between P3 and P14 (from ~50 to ~200). The adult complement of myonuclei (~250) is reached by P21. (b)The number of satellite cells per myofiber decrease by 0.66 cells per day to reach the adult level by P21. From White et al., 2010.

The idea that satellite cells are required for muscle hypertrophy was founded by the concept of the myonuclear domain. The theoretical concept was first suggested by (Cheek et al., 1965), supporting that a single myonucleus in a myofiber has "jurisdiction" over a determined amount of the cytoplasm. In other words, the myonuclear domain would correspond to the theoretical volume of cytoplasm within the myofiber regulated by the gene products of one myonucleus (Pavlath et al., 1989; Hall and Ralston, 1989). According to this theory, while cytoplasmic volume increases during hypertrophy the number of recruited satellite cells and thus myonuclei in a fiber also increases, presumably to maintain the myonuclear domain constant (Bruusgaard et al., 2010).

There have been several genetic models utilized to knock-out Pax7 expressing cells (Kuang et al., 2006; Lepper et al., 2009; Mansouri et al., 1996; McCarthy et al., 2011; Oustanina et al., 2004; Seale et al., 2000).

A recent study using a model for specific ablation of satellite cells in adult mice (the conditional *Pax7^{CreER/+};Rosa26^{DTA/+}* strain) concluded that effective myofiber hypertrophy following muscle overload (performed by surgical ablation of synergist muscles, removal of *Gastrocnemius* and *Soleus* muscles places a mechanical overload on the remaining *Plantaris* muscle) can take place without satellite cells, although the typical increase in myofiber

nuclei associated with hypertrophy was absent. This resulted in a significant expansion of the myonuclear domain and an increase in the size of myonuclei was noted, suggesting chromatin reorganization that could result in alteration in gene transcription (McCarthy et al., 2011). This leads to the question whether the absence of satellite cells leads to a change in the gene expression of profile in myonuclei in order to allow the maintenance of a larger myonuclear domain.

Overall, the different studies indicate that Pax7 is required for the maintenance of the myogenic population in the perinatal/juvenile stage, since muscle growth and regeneration are impaired. Indeed, in germline Pax7 null mutants muscle growth is perturbed, with reported muscle weakness displayed by abnormal gait and splayed hindlimbs (Seale et al., 2000), smaller fibers (Kuang et al., 2006; Oustanina et al., 2004; Seale et al., 2000) and less myonuclei (Kuang et al., 2006; Oustanina et al., 2004). Although satellite cells seem to somewhat be dispensable for hypertrophy (McCarthy et al., 2011), it has been established that they are absolutely required up to P21 for normal regeneration of muscle fibers following injury (Lepper et al., 2009). The regenerative capacities of skeletal muscle are further discussed in part II-6.

B) Regulation of muscle mass hypertrophy/atrophy

The increase of muscle size by increase of muscle fiber size is called hypertrophy. Hypertrophy occurs during postnatal development but also in response to exercise and to specific hormones such as androgens (testosterone) or β–adrenergic agonists.

The opposite effect, muscle fiber size decrease, called atrophy, can result from immobilization, starvation, aging, denervation, response to hormones such as corticosteroids, or from pathophysiological conditions (cancer, diabetes).

Muscle mass essentially depends on the balance between the process of protein synthesis (anabolism) and degradation (catabolism) within the muscle fiber. Hypertrophy is characterized by increased protein synthesis, whereas atrophy is due to exceeding protein degradation. Protein turn-over is regulated by different signaling pathways.

Two major signaling pathways that control protein synthesis are the IGF1-Akt-mTOR (insulin-like growth factor 1- serine/threonine kinase Akt – mammalian target of rapamycin) pathway which is a positive regulator and the myostatin-Smad2/3 which is a negative regulator of protein synthesis (Schiaffino et al., 2013) **(Figure 16)**.
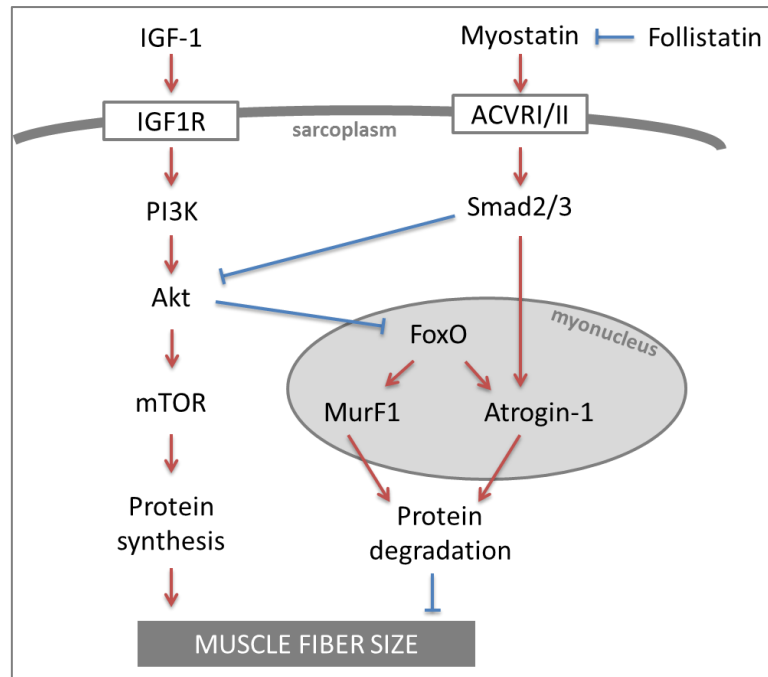
Figure 16 - Signaling pathways involved in regulating muscle hypertrophy and atrophy. Protein synthesis is stimulated by IGF-1 which activates PI3K/Akt/mTOR, and by follistatin which inhibits the negative regulation of myostatin on muscle growth.

IGF1 activates Akt which in turn activates mTOR that stimulates protein synthesis through phosphorylation of its downstream effectors involved in the translational machinery. Akt also blocks the FoxO pathway involved in protein degradation (described below).

Myostatin, a growth factor of the TGFβ family (presented in Part III), upon binding to its receptors, leads to the phosphorylation and activation of Smad2/3 which are involved in inhibition of IGF1/Akt/mTOR pathway and activation of atrogin 1, overall stimulating protein breakdown (Sartori et al., 2014).

The main pathways involved in inducing protein degradation are the proteasomal and autophagic-lysosomal pathways acting through a variety of atrophy related genes also called atrogenes. Forkhead box O (FoxO) transcription factors are able to induce expression of different atrogenes such as specific E3 ubiquitin protein ligases atrogin-1 or MuRF1 (muscle RING finger 1). Atrogin-1 promotes degradation of MyoD and eukaryotic translation initiation factor 3 subunit F (eIF3-f). MurF1 has been reported to control the half-life of many muscle structural proteins, such as myosin heavy and light chains, actin and troponine I. FoxO are inactivated following phosphorylation mediated by Akt (Sandri, 2008; Schiaffino et al., 2013).

6- Postnatal muscle regeneration

At a daily basis, skeletal muscle is subjected to minor lesions that are mostly a result from eccentric muscle contractions. This type of muscle damage does not necessarily induce cell death and inflammation and it has been shown that it can be repaired by recruitment of intracellular vesicles at the damaged site of the sarcolemma and involves dysferlin and caveolin-3 sarcolemmal proteins (Bansal et al., 2003; Steinhardt et al., 1994). This role of dysferlin and caveolin as membrane protectors became clear as their absence causes limb muscular dystrophy.

However in the case of more traumatic damage (caused by either extensive exercise, or exposure to myotoxins, or genetic diseases inducing muscular dystrophies) the regenerating tissue undergoes the following sequential but overlapping steps: necrosis, inflammation, activation, differentiation and fusion of satellite cells, maturation and remodeling of the neo-myofibers (Yin et al., 2013).

The skeletal muscle has this remarkable ability to regenerate robustely and rapidly (by 3 weeks). Indeed, muscle is able to regenerate up to 50 repeated cycles of extensive injury sustained following intra-muscular administration of myotoxin (Sadeh et al., 1985; Luz et al., 2002).

After injury, myofibers undergo necrosis, which can be monitored by increased blood levels of muscle proteins such as creatine kinase. Necrosis is also accompanied by calcium release from the sarcoplasmic reticulum to the sarcoplasm. Subsequently, calcium dependent cysteine-proteases, called calpains, are activated to cleave myofibrillar and cytoskeletal proteins. During necrosis the complement system is activated and leads to inflammatory cell invasion by chemotaxis (Frenette et al., 2000).

The inflammatory response proceeds in the following order: i) muscle resident mast cells are activated and degranulate releasing pro-inflammatory cytokines (tumor necrosis factor TNFα, interleukine-1, histamine), ii) within hours neutrophils and leucocytes infiltrate the myofiber and also release TNFα, iii) by 24 hours macrophages ($CD68^+$/$CD163^-$) are at the site and remove necrotic debris by phygocytosis, iv) 2-4 days after damage those macrophages convert to anti-inflammatory, resident $CD68^-$/$CD163^+$ macrophages. The latter stimulate myoblast proliferation and differentiation (Radley and Grounds, 2006; Ciciliot and Schiaffino, 2010).

In the adult, 2-7% of the nuclei associated with a muscle fiber are satellite cells. The turn-over of myonuclei in a muscle fiber is not frequent, in rodents it is estimated at 1-2% per week (Schmalbruch and Lewis, 2000), and the satellite cell population is primarily quiescent. Following injury, satellite cells are activated upon exposure to signals from a damaged environment. It has been described that satellite cells residing on one myofiber can activate even if the lesion site is at the opposite end of the fiber. Activated satellite cells are able to migrate along the myofiber, or between myofibers, or even between muscles, crossing the basal lamina and connective tissues to reach the regeneration site (Schultz et al., 1985; Watt et al., 1987). Following activation, satellite cells proliferate forming adult myoblasts which in turn will differentiate and fuse to form new myofibers (see II-4-A).

Newly formed myofibers can be distinguished by their small diameter, centrally localized myonuclei and by the expression of embryonic isoforms of myosin heavy chain. At the end of muscle regeneration, the new myofibers increase in size and their nuclei migrate to the periphery close to the sarcolemma.

The question of whether satellite cells are indispensable for muscle regeneration has been addressed by different groups, some of which have approached the question using genetic tools to conditionally ablate satellite cells in the adult muscles. These groups have generated different inducible *Pax7* Cre mouse lines, which are knock-in alleles (Cre/Lox mutagenesis is explained in Materials and Methods). Some lines contain an internal ribosome entry site (IRES) to retain *Pax7* translation (*Pax7^{iCreERT2}*, *Pax7^{CreER}*, respectively (Murphy et al., 2011; Nishijo et al., 2009). Whereas another line contains a "knock-in/knock out" allele since the Cre cassette is placed at the endogenous ATG and disrupts *Pax7* transcription (*Pax7^{CE}*) (Lepper et al., 2009). (Of note, that in the study in Results I, the mouse line used is *Pax7^{CE}*). Three studies (Lepper et al., 2011; McCarthy et al., 2011; Murphy et al., 2011) have crossed the latter described Cre driver mice with mice carrying R26R^{DTA} (Wu et al. 2006) or Rosa26$^{eGFP-DTA}$ (Ivanova et al., 2005) to constitutively express diphtheria toxin fragment A (DTA) after recombination, in *Pax7* expressing cells, of the blocking Stop sequence **(Figure 17)**. Muscle injury was induced by intramuscular injection of either cardiotoxin (snake venom which damages cell membranes and induces necrosis) or barium chloride (BaCl2, which causes depolarization of the sarcolemma and myofiber death by stimulating exocytosis while blocking the efflux of Ca^{2+}). Overall, these studies showed that muscle regeneration is prevented in the absence of satellite cells, thus, demonstrating

that satellite cells are responsible and indispensable for muscle regeneration (Relaix and Zammit, 2012).
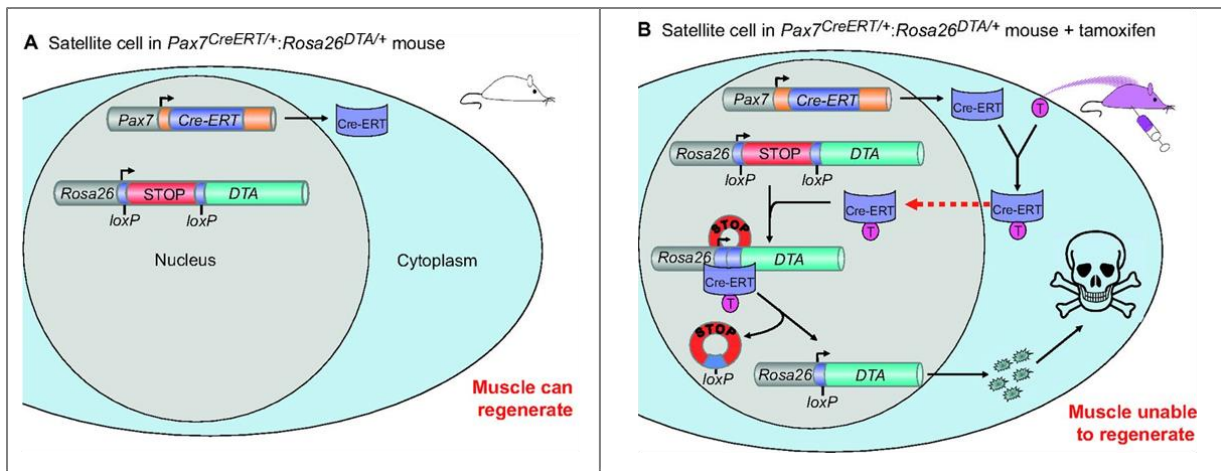
Figure 17 – Satellite cell ablation strategy using Cre-lox recombination. (**A**) $Pax7^{CreERT/+}:Rosa26^{DTA/+}$ mice generate Cre-ERT in all *Pax7*-expressing satellite cells, but it remains in the cytoplasm if tamoxifen is not present. Owing to the stop cassette in the modified *Rosa26* gene, there is no DTA produced without recombination at the locus. In such untreated mice, satellite cells are viable and muscle regenerates effectively after acute injury. (**B**) When tamoxifen (T) is administered systemically to $Pax7^{CreERT/+}:Rosa26^{DTA/+}$ mice, it binds to the cytoplasmic Cre-ERT, enters the nucleus and recombines the engineered *Rosa26* locus between the loxP sites and excises the intervening stop cassette. The *Rosa26* gene is then able to drive expression of DTA, which inhibits protein translation and kills the satellite cell it is expressed in. When satellite cells are genetically ablated in this way, muscle regeneration fails following severe injury. From Relaix and Zammit, 2012.

7- Overview on the different signaling pathways involved in myogenesis

Signaling molecules, which can function as morphogens, control the genetic networks patterning the structure of tissues in the developing embryo through to the adult organism. Depending on concentration and distance from the source secreting the molecules, morphogens qualitatively trigger different cellular behavioral responses (Bentzinger et al., 2012). Moreover embryonic, fetal and adult myogenic cells show differential sensitivity to signaling molecules. It has been suggested that embryonic, fetal and adult progenitors and myoblasts have intrinsic differences which allow them to respond differently to similar environmental signals (Biressi et al., 2007). These signals can be translated into pro- or anti-myogenic commitment factors. The correct combination of all the different signals the cells receive allow in fine a sufficient pool of cells for differentiation and a pool of reserved stem cells throughout development into adult life.

A) Signaling pathways regulating prenatal myogenesis

During somitogenesis, Wnt proteins are secreted from the dorsal tube and the ectoderm (Parr et al., 1993). Upon binding to their cellular Frizzled (Fzd) receptors, Wnts signal either through the canonical activation of the β-catenin/TCF transcriptional complex or through the non- canonical pathway involving PKC (Amerongen and Nusse, 2009). An active Wnt signaling is required for the formation of the dermomyotome and the myotome (Geetha-Loganathan et al., 2008).

In addition, sonic hedgehog (Shh) is secreted from the notochord and the neural tube. This factor binds to patched receptor and triggers the release of smoothened which acts on gene expression through transcription factors. Shh signaling is essential for both the commitment of myogenic precursors of the dermomyotome and for the formation of the sclerotome (Bentzinger et al., 2012).

Moreover, BMP4 (Bone Morphogenetic Protein 4, BMPs are further described in Part III) is expressed in the lateral-plate mesoderm and maintains the myogenic progenitors in an undifferentiated state (Pourquié et al., 1995).

Notch signaling pathway also plays a major role in regulating myogenesis. The transmembrane receptor notch mediates cell to cell communication by binding to delta and jagged ligands on the surface of neighboring cells. Ligand binding results in proteolytic cleavage of the notch intracellular domain (NICD), which can then interact with the RBP-J transcription factor and mediate gene expression regulation. Migrating neural crest cells present delta to dermomyotomal cells. Only the cells that have transiently activated the notch pathway through that contact will undergo myogenesis (Rios et al., 2011). Conditional mutations abrogating notch signaling pathway in muscle precursor (either ablation of ligand Delta1 or RBP-J) resulted in excessive differentiation and loss of muscle precursors (Schuster-Gossler et al., 2007; Vasyutina et al., 2007).

Both notch and BMP signaling seem to promote expansion of muscle precursors and prevent their differentiation.

Furthermore, hepatocyte growth factor (HGF) and its receptor c-met are involved in delamination and long-ranged migration of myogenic precursor cells. Indeed, HGF is secreted by non-somitic mesodermal cells, marking the migratory route to the muscle precursors which present c-met at their surface (Dietrich et al., 1999).

B) Postnatal regulatory signals and the satellite stem cell niche.

Somatic stem cells depend on a specific specialized microenvironment called the stem cell niche, which supports the maintenance of quiescence, activation and self-renewal of the stem cell.

Satellite cells are tightly regulated by cell to cell interactions and cell to matrix contacts, leading to autocrine or paracrine signals, which are influenced by the dynamic microenvironement where they reside. The immediate niche of the satellite cell is composed of the myofiber sarcolemma and the extracellular matrix (collagen IV, laminin, fibronectin, etc.) composing the basal lamina of the myofiber. Beyond the immediate niche, other surrounding entities such as blood vessels, motor neurons, interstitial cells also secrete factors which have the potential to regulate satellite cell function **(Figure 18)**.

Wnt/β-catenin pathway is implicated in satellite cell regulation during muscle regeneration. However, different experimental conditions have led to different conclusions regarding the role of this pathway. One role that has been described is to promote myogenic commitment and terminal differentiation (Brack et al., 2008). Wnts have also shown to regulate proliferation of satellite cells (Otto et al., 2008) and even to play a role in self-renewal by inhibiting differentiation (Perez-Ruiz et al., 2008). These contradicting results can be due to different sources of Wnt ligands (from cultured cells or recombinant protein) which can affect the concentration of these substrates (Yin et al., 2013).

Notch signaling is also crucial for satellite cells. On one hand, it is known that it is essential for the maintenance of satellite cell quiescence (Mourikis et al., 2012). On the other hand, notch is also essential for satellite cell activation and proliferation. Indeed, following myofiber injury, both satellite cells and myofibers upregulate expression of delta ligand, resulting in the appearance of NICD in the satellite cell and activation of the satellite cell, which in turn will proliferate, leading to the expansion of myoblasts (Conboy and Rando, 2002). However, inhibition of notch signaling is required for terminal differentiation and fusion of the myoblast. Inhibition can be mediated by numb, a notch signaling inhibitor by ubiquitination of the NICD, which is asymmetrically partitioned during division. The daughter cell which inherits numb will be lead to differentiation. In parallel, Wnt signaling is present in differentiating myoblasts and it antagonizes notch signaling (Brack et al., 2008).

Hepatocyte growth factor (HGF) is sequestered by heparin sulfate proteoglycans within the basal lamina surrounding the satellite cell. Upon injury, HFG is released from the extracellular matrix and activates satellite cells through binding to c-met receptors at their surface (Miller et al., 2000).

Numerous fibroblast growth factors (FGFs) are expressed in the muscle. FGF signaling mediates myoblast proliferation and inhibits differentiation in myoblasts. FGF-6 is specifically expressed in the muscle and is upregulated during regeneration (Floss et al., 1997).

Insulin-like growth factors (IGFs) are among other cells, secreted by endothelial cells (Christov et al., 2007). Activation of IGF-I tyrosine kinase receptor, induces the expression of MRFs and leads to mitogenic and myogenic responses (Coolican et al., 1997; Musarò and Rosenthal, 1999).

Matrix metalloproteinases (MMPs) are secreted by satellite cells, regenerating fibers or leucocytes and macrophages. MMPs can degrade components of the extracellular matrix (collagen, elastin, fibronectin, laminin, proteoglycans). They are essential during degeneration and regeneration stages for remodeling the extracellular matrix (Kherif et al., 1999; Fukushima et al., 2007).

Skeletal muscle is composed of several compartments that also contribute the environment of the satellite cells. Fibroblasts are the main component of the interstitial muscle tissue. They secrete FGFs and extracellular matrix components such as collagen and laminin. Moreover, motorneurone activity is crucial to muscle maintenance. Indeed, denervation results in muscle atrophy and a decline of satellite cell numbers in the long-term (de Castro Rodrigues and Schmalbruch, 1995; Kuschel et al., 1999). Furthermore, satellite cells reside closely to with capillaries which also secrete a panel of growth factors that regulate the muscle stem cells (IFG, HGF, FGF, platelet-derived growth factors, vascular endothelial growth factor). In addition, immune cells also play a crucial role during regeneration (see II-6). Finally, it is known that androgens have an effect on satellite cell number, myonuclei number and muscle fiber hypertrophy (Joubert and Tobin, 1995; Sinha-Hikim et al., 2003).

In conclusion, the satellite cell niche is very complex and is not yet fully understood. Research in this field is ongoing to further dissect which components control the stemness

and the activity of satellite cells. Understanding the latter might lead to the possibility of designing an *ex-vivo* optimal niche for maintaining satellite cells and the elaboration of "cocktails" of signaling molecules to regulate their faith for cell therapies and regenerative medicine. Our group is interested in dissecting the TGF-β/ BMP signaling pathways in the context of muscle development. These pathways are described further in Parts III and IV.
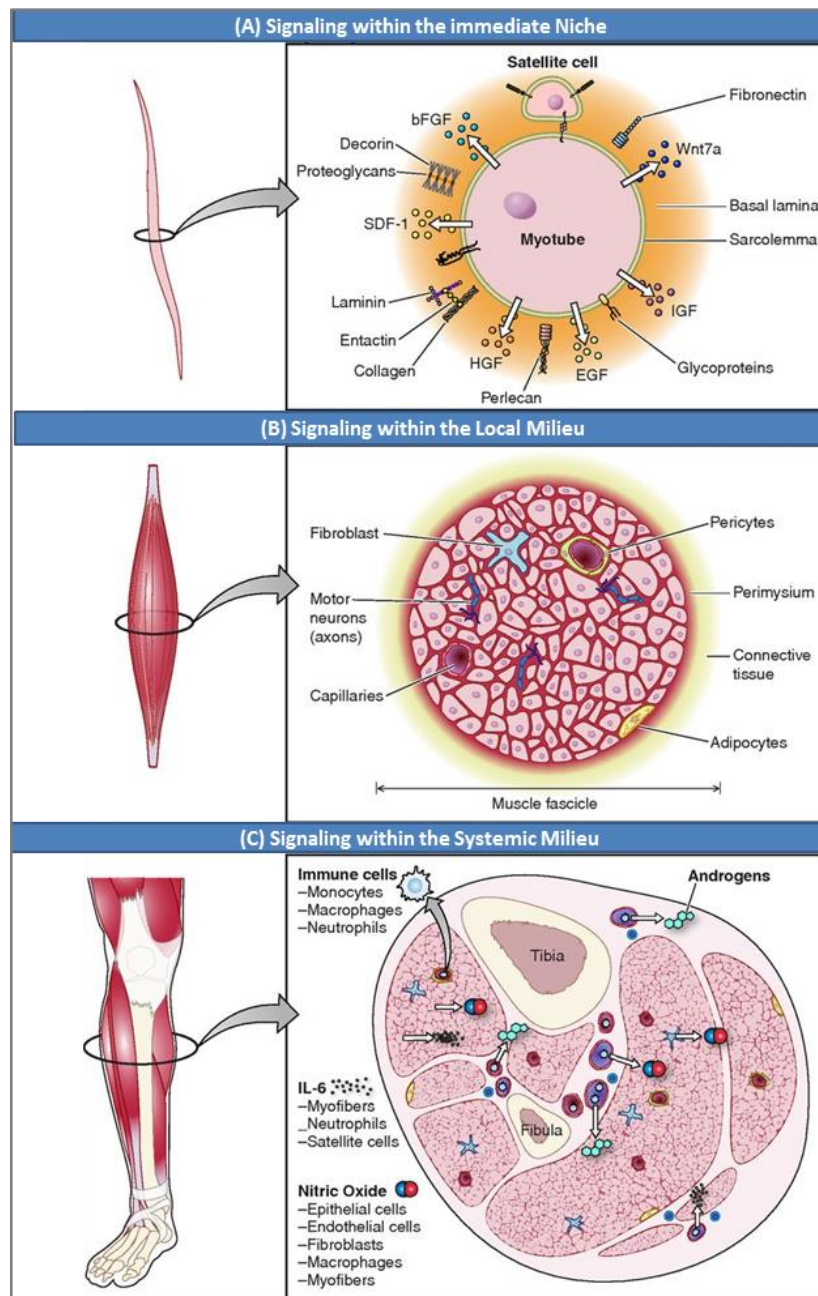
Figure 18 - The satellite cell niche, (A) the immediate niche is composed of the satellite cell, the sarcolemma, the basal lamina/extracellular matrix. Growth factors including HGF, FGF, IGF, Wnts originate from either satellite cells, myofibers, (B) interstitial cells or serum. (C) Satellite cells are exposed to the host's immune system and circulating hormones. From Yin et al., 2013.

1- The TGF-β superfamily

The transforming growth factor β (TGF-β) pathway plays central roles in metazoan organisms from the early stages of embryonic development to the maintenance and regeneration of adult mature tissues. The TGF-β superfamily controls this extended range of biologic processes by regulating the transcription of genes that control cell proliferation, differentiation, death, adhesion, movement, and positioning (Flavell et al., 2010; Moustakas and Heldin, 2009; Wu and Hill, 2009).

The TGF-β family was identified in the early 1980s (de Larco and Todaro, 1978), (Moses et al., 1981; Roberts et al., 1981), and the mechanism of their signal transduction was first described in the 1990s (Kretzschmar et al., 1997; Massagué 1998). Initially, the term "transforming growth factor" was chosen because the discovered factors were secreted by transformed fibroblasts (by the RNA Moloney sarcoma virus) and it was believed at the time that the factors were secreted specifically by cancer cells. The purified factors were able to induce a transformed or malignant phenotype (escape from normal growth controls) on non-neoplastic cultured cells.

Nowadays, in mammals, there are over 33 members identified in the TGF-β superfamily, including TGF-βs themselves, bone morphogenetic proteins (BMPs), growth and differentiation factors (GDFs), activins and nodal **(Figure 19)**. There were multiple and often parallel approaches that led to the discovery of the different secreted proteins, which is the reason why several ligands were given different names. For example BMP14 is also called GDF5, and myostatin is also referred to as GDF8 (Feng and Derynck, 2005).

The main structural differences between the subfamilies are the number and the location of cysteins on the mature peptide. Indeed, the TGF-βs, inhibin-β and activins have nine cysteins, whereas the BMPs, GDFs and inhibin-α have seven cysteins. For both cases one of the cysteins mediates the formation of disulfide bond in ligand dimerization of the ligand. In the exceptional cases of GDF3, GDF9, BMP15, lefty A and lefty B, there are six cysteins and thus it is assumed that they do not form dimers (Feng and Derynck, 2005).
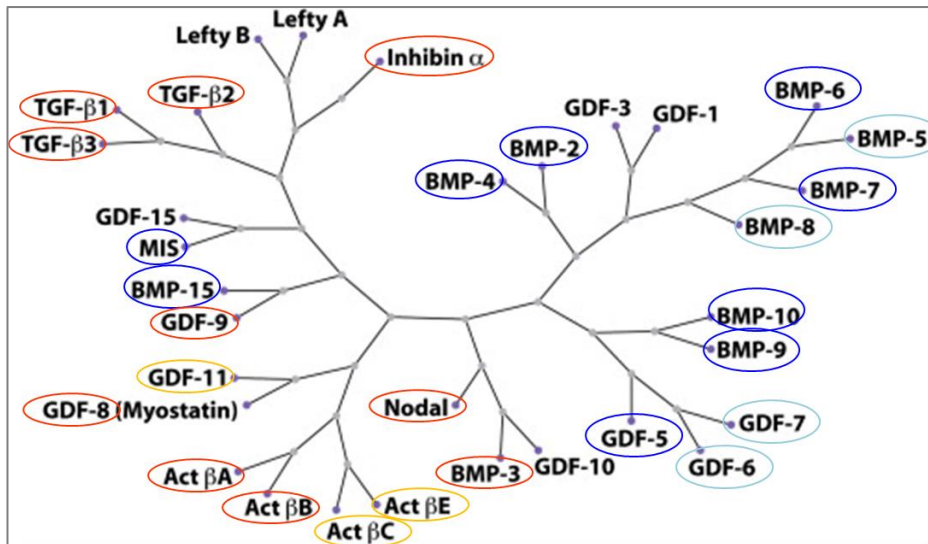
Figure 19 – Phylogenic tree of the TGF-β superfamily proteins in humans. The tree was constructed based on the alignment of the mature C-terminal domains. Adapted from Hinck, 2012 (Copyright clearance center license number 3639540040558) . According to Miyazona K: ligands that activate the TGF-β/activin/nodal/myostatin (GDF8) (Smad2/3) pathway are shown in red, whereas those that signal through the BMP/GDF pathway (Smad1/5/8) are shown in blue. Ligands that may activate TGF-β/activin or BMP pathway, but whose receptors and downstream Smad signaling pathways are not fully determined, are respectively shown in orange and light blue.

TGF-β ligands are synthesized as inactive pre-propeptides that are cleaved in the Golgi apparatus to produce a dimeric mature peptide **(Figure 20)**. Within the cell, the mature peptide is held in a latent/non-active form by non-covalent binding to the remnant ammino-terminal precursor, also termed latency associated peptide (LAP). The latter is also bound to latent TGF-β-binding proteins (LTBPs), which bind a series of extracellular matrix proteins, forming the large latent complex (LLC) within secretory vesicles. Subsequently, TGF-β are secreted as LLC and are held in connective tissues, providing a reservoir of inactive TGF-β (Lafyatis, 2014). Thus, bioavailability of TGF-β depends on the liberation of active cytokine from the LLC. Activation can be achieved by proteases such as elastase (Taipale et al., 1995) and calpain (Abe et al., 1998), or by cleavage by BMP1-like metalloproteinases (Ge and Greenspan, 2006), or interaction of LAP with either thrombospin present in the extracellular matrix (Schultz-Cherry and Murphy-Ullrich, 1993) or with integrins present on the surface of neighboring cell (Munger et al., 1999).

Overall, latency provides a mechanism of temporal and spatial control of the cytokine activity. This mechanism has been essentially studied on TGF-β subfamily and is still poorly understood. Myostatin, BMP7 and GDF11 also exist in a latent form (Lee and

McPherron, 2001; Gregory et al., 2005). The rest of the ligands are also synthetized as dimeric pre-propeptides but are directly cleaved in the cell and subsequently the mature, fully processed dimeric growth factors are secreted (Schmierer and Hill, 2007).
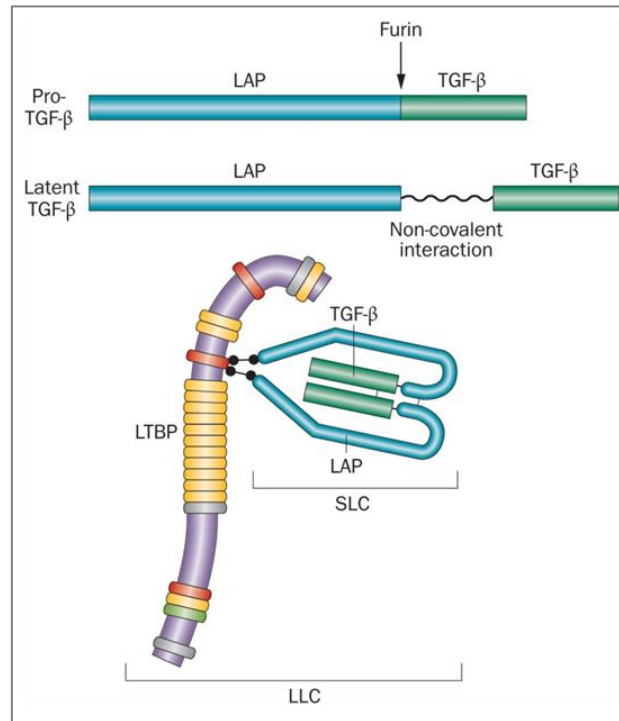
Figure 20 – TGF-β maturation and sequestration. In the cell, the pro- TGF-β is cleaved by a furin protease, producing a non-covalently-bound dimeric complex of LAP (latency associated propeptide) and TGF-β, referred to as the SLC (small latent complex). The latter is bound to LTBPs (latent TGF-β binding protein) forming the LLC (large latent complex), ready for secretion and subsequent incorporation of the matrix. Adapted from (Lafyatis, 2014) (Copyright clearance center license number 3639441120337).

2- TGF-β and BMP canonical (Smad-dependent) signaling pathways

TGF-β ligands signal through a complex of serine/threonine transmembrane receptors which are composed of two different functional classes: type I (in total 7 and are also referred to as Alks, activing receptor-like kinases) and type II (in total 5) receptors. Mature TGF-β ligands can bind selectively to different combinations of receptors (Groppe et al., 2008; Wrana et al., 1992) **(Table 4)**.

In the absence of ligands, the type I and type II receptors exist as homodimers at the cell surface. The type I receptors contain a conserved GS region (Gly/Ser-rich) upstream from the kinase domain. The binding of the ligand induces the formation of a stable heterotetrameric complex composed of two receptors of each type, allowing the

phosphorylation of the GS sequence by the constitutive active type II receptor, which subsequently activates the type I receptor (Feng and Derynck, 2005).

Table 4: Classification of ligands, type I (RI) and II (RII) receptors, and R-Smads between TGF-β subfamilies. Dashed lines separate groups of ligands or receptors based on the division into BMP and TGF-β /activin-like pathways. Ligands, type I receptors and R-Smads are color-coded: blue, BMP-like pathways; red, TGF-β /activin-like pathways. N/A, not applicable. From Moustakas and Heldin, 2009.

Pathway	BMP	GDF	Activin	TGFβ	AMH	Inhibitors
Ligand	BMP2, 4 BMP5, 6, 7 BMP8A, 8B BMP9, 10	GDF5, 6, 7 GDF9b GDF10, 11 GDF15 (MIC1) ------------------ GDF1, 3 GDF8 (MYO) GDF9	Inhibin βA Inhibin βB Nodal	TGFβ1 TGFβ2 TGFβ3	AMH (MIS)	BMP3 Inhibin α Inhibin βC Inhibin βE LEFTYA LEFTYB
RII	BMPRII ActRIIA, ActRIIB	BMPRII ActRIIA, ActRIIB	ActRIIA ActRIIB	TβRII	AMHRII	N/A
RI	BMPRIA (ALK3) BMPRIB (ALK6) ALK2 ALK1	BMPRIA (ALK3) BMPRIB (ALK6) ALK2 ------------------ ActRIB (ALK4) ALK7 TβRI (ALK5)	ActRIB (ALK4) ALK7	TβRI (ALK5) --------------- ALK1 ALK2 BMPRIA (ALK3)	BMPRIA (ALK3) BMPRIB (ALK6) ALK2	N/A
R-Smad	SMAD1, 5, 8	SMAD1, 5, 8 ------------------ SMAD2, 3	SMAD2, 3	SMAD2, 3 ------------------ SMAD1, 5, 8	SMAD1, 5, 8	N/A
Co-Smad	SMAD4	SMAD4	SMAD4	SMAD4	SMAD4	N/A
I-Smad	SMAD6, 7	SMAD6, 7	SMAD7	SMAD7	SMAD6, 7	N/A

The intracellular effectors of the signaling is mediated by phosphorylation of the RSmads by the activated type I receptor. Smads are transcription factors that constantly shuttle between the cytoplasm and the nucleus. There are 8 Smads classified into three categories: i) five R-Smads (receptor-regulated Smads, Smads1,2,3,5 and 8), ii) co-Smad4 (common mediator) and iii) two I-Smads (inhibitory Smads, Smad6 and 7) (Massagué et al., 2005; Feng and Derynck, 2005; Schmierer and Hill, 2007).

R-Smads can be further divided into two classes: i) Smad2 and 3, which are responsible for transducing TGF-β/activin/nodal signals, whereas ii) Smad1, 5 and 8 transduce BMP-like pathways **(Figure 21)**. Selective phosphorylation of R-Smads by the type I receptor creates a binding site for Smad4. Heterotrimers of two phospho-RSmads and one Smad4 molecules form transcriptionally active complexes and accumulate in the nucleus where, in co-operation with a long list of Smad-interacting DNA-binding transcription factors, they can regulate transcription of target genes (Chacko et al., 2004; Qin et al., 2001) form transcriptionally active complexes and accumulate in the nucleus where, in

co-operation with a long list of Smad-interacting DNA-binding transcription factors, they can regulate transcription of target genes.
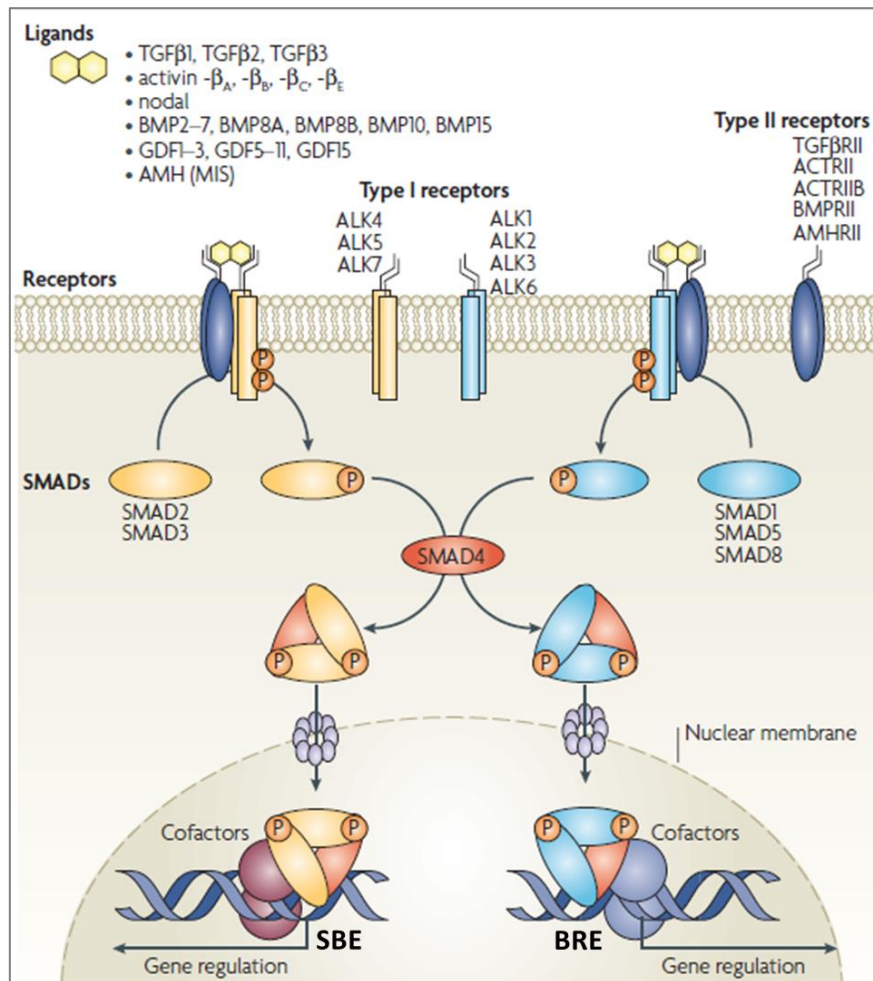
Figure 21 - TGF-β-SMAD signaling pathways. Binding of ligands to type II receptors and recruitment of type I receptors involves high combinatorial complexity. Traditionally, ligands have been split into two groups: Smad2/3 -activating TGFβs, activins and nodal on the one hand, and Smad1/5/8-activating BMPs, GDFs and AMH on the other hand. Note that this concept does not accurately reflect reality (see Table 4). The pathway only splits into two distinct branches downstream of type I receptors: Alk4/5/7 specifically phosphorylate Smad2/3, whereas Alk1/2/3/6 specifically phosphorylate Smad1/5/8. Complex formation of the phosphorylated receptor-regulated Smads with Smad4 causes nuclear accumulation of active Smad complexes, which directly regulate gene transcription in conjunction with transcription factors, chromatin-remodeling complexes and histone-modifying enzymes. Adapted from Schmierer and Hill, 2007(Copyright clearance center license number 3639601411005).

A target DNA sequence for R-Smad3/4 is the Smad-binding element (SBE, 8 bp palindrome sequence 5'-GTCTAGAC-3') (Zawel et al., 1998). R-Smads1/5/8 were found to preferentially bind GC-rich sequences, BMP-responsive elements (BRE), which have been

found in BMP target genes such as *Id1* (inhibitor of differentiation or inhibitor of DNA binding) or *Smad6* (Ishida et al., 2000; López-Rovira et al., 2002). Moreover, in a reporter assay, the BRE identified in the *Id1* promoter was shown to be responsive only to BMP signaling and not to TGF-β/activin (Korchynskyi and Dijke, 2002). Of note, Id1 proteins interact with bHLH transcription factors including MyoD and myogenin **(Figures 8 and 10)** in the muscle, and inhibit their binding to DNA

3- Non-canonical (Smad-independent) TGF- β signaling pathways

The identification of the Smad-mediated intracellular signaling rose a predicament on how can there be such diverse functions of the TGF- β family with such a simple intra-cellular model. Although it is not yet fully understood, increasing evidence points out that the diversity of the functions is in due to the numerous combinations possible of the TGF- β components, including the ligands, receptors, Smads, Smad-interacting transcription factors, but is also due to cross-talks with other signaling pathways and furthermore due to the ability of TGF- β receptors to activate other signaling pathways without the intermediate Smads. These non-Smad pathways, also termed non-canonical TGF-β pathways or Smad-independent pathways, are activated by the TGF- β receptors through either phosphorylation or direct interactions (Zhang 2009; Derynck and Zhang, 2003; Moustakas and Heldin, 2005).

The non-canonical TGF-β pathways include the mitogen-activated protein kinases (MAPKs p38, ERK and JNK) pathways, the small Rho-like GTPases signaling pathways and PI3K/Akt pathways (Suzuki et al., 2007; Bhowmick et al., 2001b ; Bhowmick et al., 2001a). It is not yet understood how the balance between the Smad and the non-Smad signaling is set.

4- Myostatin (GDF8): a negative regulator of skeletal muscle growth

Expression of myostatin is initiated in the myotome of developing embryos and becomes restricted to the cardiac and skeletal muscle in the adult, although it has also been detected in adipose tissue and the mammary gland (McPherron et al., 1997; Sharma et al., 1999). Myostatin is secreted by the myogenic cells in an inactive/latent complex, like TGF-β **(Figure 20)**. After activation, myostatin binds to either ActRIIA or B, leading to the recruitment of ALK4 or 5 which phosphorylate Smads 2 and 3 **(Figure 21)**. A negative

feedback loop occurs through the expression of inhibitory Smad7. Indeed, the latter's promoter contains a SBE and is a target gene of myostatin (Zhu et al., 2004). Moreover, myostatin may compete with other molecules such as BMP7 for binding ActRIIB receptor and thus exert an antagonistic effect (Rebbapragada et al., 2003). Moreover, different proteins can bind to myostatin and inhibit its activity. For example, follistatin which is present in the extracellular matrix in the muscle, can bind to myostatin and impede its binding to the above mentioned TGF-β receptors (Amthor et al., 2004).

Myostatin was first identified as a new member of the TGF-β family by Lee and colleagues in 1997. After generating myostatin deficient mice ($Mstn^{-/-}$), by deleting the mature C-terminal domain by a neo-cassette insertion, they observed that the mice were 30% larger due to increase of skeletal muscle size. Indeed, individual muscles in the myostatin deficient mice were twice the size compared to wild-type mice. The increase of the muscle size was a result of both hyperplasia, i.e. increase of muscle fiber number, and hypertrophy (McPherron et al., 1997). Naturally occurred loss of function mutations of the *Mstn* gene were later identified in other animals including cattle and dogs, one case of a human mutation has also been described (Mosher et al., 2007; McPherron and Lee, 1997; Schuelke et al., 2004) **(Figure 22)**. Furthermore, systemic administration of myostatin in mice leads to the opposite effect of extensive muscle loss, leading to severe muscle atrophy and appearance of cachexia (Zimmers et al., 2002).
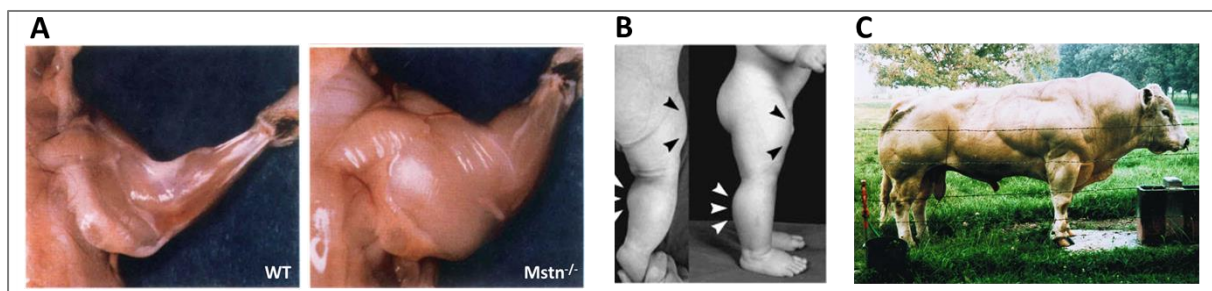
Figure 22 – Increased skeletal muscle mass due to myostatin deficiency. (A) Comparison of skinned mice, WT and Mstn$^{-/-}$ upper limb muscles, from McPherron et al., 1997 (Copyright clearance center license number 3640780360321). (B) Boy with myostatin mutation, from Schuelke et al., 2004. (C) Fullblood Belgian Blue bull deficient in myostatin, from McPherron and Lee, 1997.

A number of studies have shown that myostatin negatively regulates satellite cell activation, proliferation and self-renewal. Indeed, it has been shown that myostatin inhibits myoblast proliferation and satellite cell self-renewal by negatively regulating G1 to S cell cycle progression by upregulating p21 (an inhibitor of cyclin-dependent kinase) and

downregulating Cdk2 (cyclin-dependent kinase 2) protein levels (McCroskery et al., 2003; Thomas et al., 2000). It has also been reported that myostatin treatment of the immortalized mouse myoblast C2C12 cell line (cell line origin: Yaffe and Saxel, 1977) downregulates *MyoD* expression and results in the failure of the myoblasts to differentiate (Langley et al., 2002). Moreover, loss of myostatin enhances muscle regeneration following injury (McCroskery et al., 2005).

However, there is disagreement regarding the role of myostatin in maintaining satellite cell quiescence. Indeed, a study also found that in muscles from Mstn$^{-/-}$ mice had a slightly reduced number of satellite cells and no difference in the rate of satellite cell proliferation compared to *WT* mice (Amthor et al., 2009). Moreover, another study recently suggested that myostatin inhibition induces hypertrophy mainly by acting on myofibers rather than satellite cells (Wang and McPherron, 2012).

Furthermore, myostatin reduces protein synthesis by blocking the activation of the Akt/mTOR pathway **(Figure 16)**, which mediates differentiation in myoblasts and hypertrophy in myofibers (Trendelenburg et al., 2009).

Overall, myostatin controls muscle fiber size by inhibiting protein synthesis, however to which extent myostatin regulates satellite cell proliferation remains unclear.

The gain of muscle mass following myostatin deficiency attracted a lot of attention and lead to the elaboration of different strategies for inhibiting myostatin, some of which made it into clinical trials (Mosler et al., 2014; Patel and Amthor, 2005; Amthor and M.H. Hoogaars, 2012; Schuelke et al., 2004). However bigger muscle does not necessary translate into stronger functional muscle. Indeed, our group has recently proven that myostatin blockade or deficiency results in bigger but more fatigable muscles, with a shift of muscle fiber type towards an anaerobic metabolisim (Relizani et al., 2014; Mouisel et al., 2014).

5- The BMP signaling pathway

A) BMPs: from bone to body morphogenetic proteins

The osteogenic activity of BMPs was first identified in the 1960s but the proteins responsible for bone induction remained unknown until the purification and sequence of bovine BMP-3 (osteogenin) and cloning of human BMP-2 and 4 in the late 1980s (Urist, 1965; Wozney et al. 1988; Wozney, 1992; Luyten et al., 1989).

More than 20 BMPs have since been identified, they display distinct spatiotemporal expression profiles **(Table 5)** and they are involved in distinct morphogenetic processes. It is now common knowledge that these growth factors and cytokines orchestrate tissue architecture throughout the entire body: from embryonic patterning and development through stem cells and their niches, regulating proliferation/differentiation/apoptosis (Hemmati-Brivanlou and Thomsen, 1995; Kobayashi et al., 2005; Zou and Niswander, 1996), to adult tissue homeostasis and regeneration, such as maintenance of joint integrity (Bobacz et al., 2003), fracture repair (Tsuji et al., 2006), vascular remodeling (Huang et al., 2009) and maintenance of iron homeostasis (Andriopoulos Jr et al., 2009).

Table 5: Overview of the BMP ligands, their BMP type I and type II receptors and the detected tissue expression patterns. From Krause et al., 2011 (Copyright clearance center license number 3641330815778).

Ligand	Synonym	Receptors	BMP tissue location
BMP-2	BMP-2A	ALK-3,-6; BMPR-II; Endoglin; TGFP-RIII; Act-RIIA, -RIIB	Intramembranous bone, blood vessels, muscle, cartilage, teeth, liver, heart, sperm, hair follicle
BMP-3	Osteogenin	Alk-4; Act-RIIB	Lung, kidney, intramembranous bone, cartilage, lung, teeth
BMP-4	BMP-2B	ALK-3, -6; Act-RIIA; BMPR-II; TGFP-RIII	Intramembranous bone, muscle, uterus, cartilage, teeth, kidney, gut, salivary gland, liver, pancreas, lung, heart, ovaries, sperm, hair follicle
BMP-5	–	–	Intramembranous bone, cartilage, kidney, ureter, pancreas, lung, heart
BMP-6	Vgr-1	ALK-2, -3, -6; Act-RIIA, -RIIB; BMPR-II	Heart, cartilage, ureter, pancreas, heart, ovaries, epidermis, liver
BMP-7	Op-1	Alk-3, -6; Act-RIIA, -RIIB; BMPR-II	Kidney, intramembranous bone, cartilage, synovium, eye, salivary gland, liver, pancreas, lung, heart, ovaries, sperm, epidermis
BMP-8	Op-2, BMP8b	–	Intramembranous bone, ovaries, sperm
BMP-9	GDF-2	ALK-1, -2; Act-RIIA, -RIIB; BMPR-II; Endoglin	Liver, CNS
BMP-10	–	ALK-1, -3, -6; Act-RIIA, -RIIB; BMPR-II	Heart
BMP-11	GDF-11	Alk-4, -5, -7; Act-RIIA, -RIIB	CNS
BMP-12	GDF-7, CDMP-3	ALK-3, -6; Act-RIIA; BMPR-II	Tendons, CNS, cartilage
BMP-13	GDF-6, CDMP-2	ALK-3, -6; BMPR-II	Tendons, cartilage
BMP-14	GDF-5, CDMP-1	Alk-6; Act-RIIA, -RIIB; BMPRII; TGFP-RIII	Cartilage, synovium, eye
BMP-15	GDF-9B	ALK-6; Act-RIIA; BMPR-II	Ovaries

Subsequently, the authors of the report on the first international BMP workshop (in Berlin 2009) suggested that BMPs deserve nowadays to be called body morphogenetic proteins (Wagner et al., 2010).

BMPs are morphogens and can induce different cellular responses at different concentrations (Dale and Wardle, 1999; Peluso et al., 2011). Therefore, BMP signaling is tightly regulated by various molecules in both extracellular and intracellular compartments.

B) Extracellular regulation of BMP signaling

There are different soluble molecules that have been identified as antagonists of BMP ligands, subsequently modulating extracellular BMP signals. The antagonists can bind directly to BMPs and regulate their diffusion and interaction with their respective receptors. These soluble regulators have both overlapping and distinct specificity, binding to ligands with different affinities.

For instance, follistatin (FST), monomeric glycoprotein, can bind BMP2, BMP4 and BMP7, forming a non-functional ternary complex with BMP and its receptor (Iemura et al., 1998) and inhibits BMP signaling in various contexts, such as during dorsal-ventral patterning of early embryos during which BMP signaling is required for ventral cell fate specification (Fainsod et al., 1997), or to modulate BMP7 activity in embryonic muscle growth (Amthor et al., 2002). Follistatin also binds other members of the TGF-β family. Indeed its highest affinity is for activin, to which it can bind directly (Nakamura et al., 1990) and abolish its interaction with activing receptors (de Winter et al., 1996; Thompson et al., 2005). Follistatin can also bind myostatin with high affinity (Amthor et al., 2004), blocking its association with ActRIIB and interfering with the function of myostatin of muscle growth inhibition

Another BMP antagonist is noggin, which is secreted as a homodimeric glycoprotein, is crucial for blocking BMP during dorso-ventral axis formation (Smith and Harland, 1992). Noggin binds to BMP2, BMP4 and with lower affinities to BMP5, BMP6, BMP7, GDF5 (BMP14), GDF6 (BMP13), subsequently blocking their interaction with the dedicated receptors (Krause et al., 2011). Noggin can also associate with heparin sulfate present at the cell surface in the extracellular matrix, where it can subsequently be stored and promote BMP gradients.

Furthermore, chordin, like noggin, antagonizes BMP function through direct binding to BMP2, BMP4 and BMP7 and regulates multiple developmental events such as the early dorsal patterning in vertebrae (Garcia-Fernàndez et al., 2007) **(Figure 23)**.
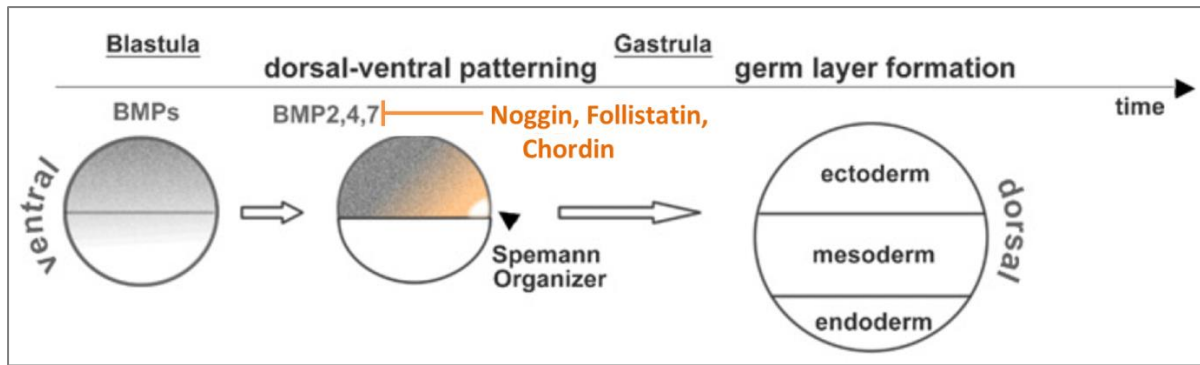
Figure 23 – BMP antagonists regulate dorsal patterning in the embryo. Noggin, follistatin and chordin are secreted by the Spemann organizer in the early Xenopus gastrulae. They inactivate BMP ligands and are thus responsible for forming a dorso-ventral gradient of BMP signaling, allowing the dorsalisation of the mesoderm and promoting neural induction. Adapted from Krause et al., 2011 (Copyright clearance center license number 3641330815778).

Moreover, gremlin (Grem1), which is secreted as a monomeric or homodimeric glycoprotein, can also bind and inhibit BMPs. Indeed, gremlin can associate with BMP2 and BMP4, and has been described to be involved in regulating embryonic limb outgrowth and patterning in the mouse (Khokha et al., 2003).

C) Intracellular regulation of BMP signaling

The inhibitory Smads (I-Smads) comprising Smad6 and Smad7 serve as negative feedback loop mechanisms (Afrakhte et al., 1998). Smad 7 represses both TGF-β and BMP signaling whereas Smad6 preferentially inhibits the BMP pathway. *Smad6* and *Smad7* are both target genes of activated R-Smads. Indeed, activated Smad2/3 upregulate *Smad7* expression (Stopa et al., 2000), and activated Smad1/5 induce *Smad6* expression (Ishida et al., 2000). I-Smads inhibit signaling by either interfering with R-Smad/type I receptor interactions, or R-Smad and Smad4 interactions, or through transcriptional regulation in the nucleus.

Several mechanisms have been described for the inhibitory activity of Smad6 i) it can bind to BMP receptors type I, preferentially Alk3 and Alk6, and inhibit the phosphorylation of Smads1/5/8 (Imamura et al., 1997; Goto et al., 2007), ii) it has also been shown that Smad6 can bind to Smad1 thus interfering with the Smad1-Smad4 complex formation (Hata et al., 1998), iii) Smad6 also recruits the E3 ubiquitin ligase Smurf1 (Smad ubiquitin regulatory factor 1) to the signaling receptor complex and inducing degradation of type I receptors and of Smad1/5/8 via the ubiquitin-proteasome pathway (Murakami et al.,

2003) **(Figure 24),** iv) Smad6 interacts with transcription factors (Bai et al., 2000) and histone deacetylases 1 and 3 (HDAC1 and 3, which remove acetyl group from histones, leading to condensed transcriptionally inactive chromatin) (Bai and Cao, 2002) to inhibit gene transcription. Indeed, there is evidence that Smad6 binds to C-terminal binding protein (CtBP), a transcriptional corepressor, and repress BMP-induced *Id1* transcription (Lin et al., 2003). Furthermore, a recent study has shown that Smad6 negatively regulates the p38/MAPK/JNK non-canonical TGF-β pathway (Jung et al., 2013).

Smad6 appears to be ubiquitously expressed (Konrad et al., 2008). There have been reports of *Smad6* expression in the lungs, heart, blood vessels, the gastrointestinal system, sperm, developing bones, eyes and limbs (Imamura et al., 1997; Alejandre-Alcázar et al., 2008; Galvin et al., 2000a; Vargesson and Laufer, 2009).
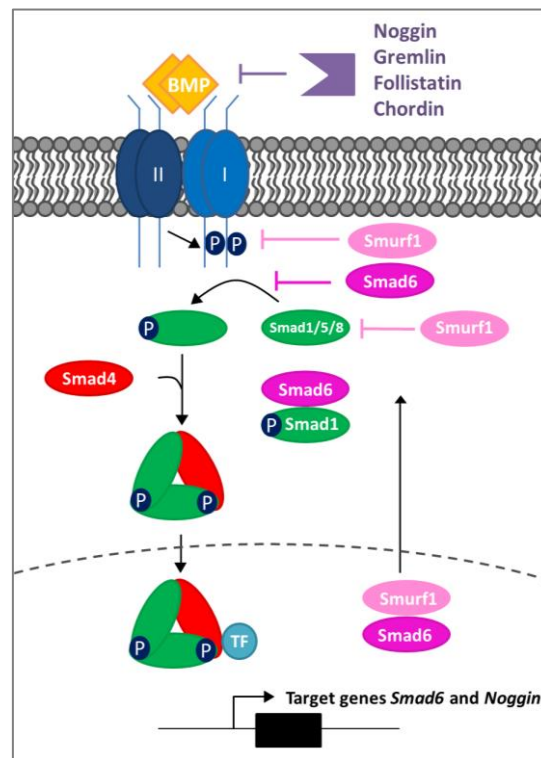
Figure 24: Inhibitory Smad6 mediated regulation of the BMP signaling pathway. Smad6, along with noggin, is a Smad/1/5/8 target gene and acts as an intracellular negative feedback loop by binding to receptor type I and inhibiting Smad1/5/8 phosphorylation, or by recruiting E3 ubiquitin ligase Smurf1, leading to the degradation of Smad1/5/8 or receptor type I through the ubiquitin-proteasome pathway, or by competing with Smad4 for binding with Smad1. Of note, transcriptional regulatory activities of Smad6 are not depicted.

D) BMP mutations and related diseases

Due to the multiple biological functions of the BMP signaling pathway, perturbations of the pathway lead to a variety of developmental and degenerative diseases. A recent review outlines the prominent human pathologies associated with dysregulated BMP signaling and enlists the reported phenotypes of the genetically manipulated knock-out mouse models that have helped elucidate the role of BMPs in development (Wang et al., 2014). Some examples of the effects of the mutations in different tissues are described below. Of note that many BMP signaling components knock-out mice are not viable (embryonically lethal, or die at birth).

BMP signaling and cancer

BMP signaling pathway dysregulations can induce cancer. For instance, mutations in Smad4 and ALK3 (BMPR-1A) leading to the downregulation of the pathway are responsible for juvenile polyposis and can lead to colorectal cancer (Howe et al., 2001; Jee et al., 2013).

Interestingly, Massagué and colleagues have recently provided a web application that compares Smad sequences in different species and displays Smad protein structures and their tumor-associated variants in humans (Macias et al., 2015).

BMP signaling in skeletal system

Brachypodism spontaneous mutations, associated with BMP14 (GDF5) loss of function, result in mice having altered length and number of bones in the limbs (Storm et al., 1994). In humans, GDF-5 deficiency may lead to autosomal dominant brachydactyly type C (Polinkovsky et al., 1997).

Moreover, the short ear phenotype linked with BMP5 mutations in mice also results in skeletal defects with shorter and weaker bones (Kingsley et al., 1992; Mikić et al., 1995).

Furthermore, gain of function mutation in the gene encoding for Alk2 (ActR-1A), rendering the type I receptor constitutively active, or mutation in the noggin gene, causes *fibrodysplasia ossificans progressiva* (FOP). FOP is a congenital disease which causes heterotopic ossification of soft tissues including skeletal muscle (Kaplan et al., 2008; Sémonin et al., 2001).

BMP signaling in cardiovascular systems

Multiple BMP components knock-out mice lead to developmental abnormalities of the heart, including BMP2 (Zhang and Bradley, 1996), BMP4 (Liu et al., 2004), BMP10 (Chen et al., 2004), ALK3 (Gaussin et al., 2002), Smad6 (Galvin et al., 2000b) and Smad7 (Chen et al., 2009).

BMP signaling in skeletal muscle

Other than myostatin/follistatin, there are not many pathways known to regulate postnatal muscle growth. In humans, Smad4 mutations, resulting in a more stable protein, result in the Myhre syndrome, which is associated with generalized muscle hypertrophy. Myhre syndrome is also characterized by pre- and postnatal short stature, brachydactyly, facial dysmorphism, thick skin and restricted joint mobility (Myhre et al., 1981; Le Goff et al., 2012).

Growth factors regulate muscle development and regeneration, subsequently ensuring correct muscle function. A number of signaling systems have been demonstrated to guide muscle stem cells and muscle growth, including notch, Wnts, IGF and myostatin (see II-7 and III-4). However, the regulatory mechanisms that timely coordinate mucle precursor generation and fiber growth, determining adult muscle size and function, are still poorly understood.

BMPs were initially discovered for their ability to induce bone and cartilage formation when injected in the muscle, which is why this family of proteins was named bone morphogenetic proteins (Urist, 1965). The osteogenic effect of BMPs was later studied *in vitro* with the C2C12 cell line and with primary myoblasts. Upon BMP stimulation (in high concentrations), the cells would differentiate into osteoblasts (Katagiri et al., 1994; Asakura et al., 2001). Moreover, the discovery of the ALK2 gain of function mutation in FOP disease (see III-5-D) reinforced the concept that BMPs induce bone formation in muscle tissues.

However, it has been recently shown that despite the osteogenic response to high levels of BMPs of cultured myoblasts, *in vivo* muscle precursors contributed minimally to heterotopic ossification (less than 5%) and the cells that underwent trans-differentiation in the muscle were actually endothelial precursors (Lounev et al., 2009).

There have been relatively few research groups that have investigated the role of BMPs in skeletal muscle development but there has been increasing evidence of that role. The state of the art in the field of muscle development and BMP signaling is hereby described.

1- BMPs and embryonic myogenesis

During somitic myogenesis, concentration gradients of BMPs, produced by the lateral plate mesoderm and the dorsal neurotube, maintain the muscle precursor population while BMP antagonist noggin counter-gradient specifies the onset of myogenesis. Indeed, it has been shown that BMP signaling inhibits the activation of *MyoD* and *Myf5* in *Pax3*^{+} cells, whereas noggin, expressed in the dorsomedial lip of the dermomyotome, allows *Pax3*^{+} cells

to commit into the myogenic lineage (Hirsinger et al., 1997; Pourquié et al., 1996; Reshef et al., 1998; Amthor et al., 1999; Patterson et al., 2010).
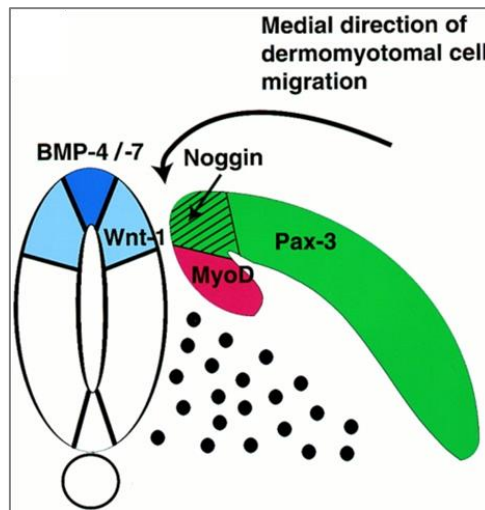
Figure 25 – Diagram of the domains of dermomyotomal gene expression. The somitic expression domains of *Pax3*, *Noggin*, and *MyoD* are indicated within the dermomyotome, the dorsomedial lip of the dermomyotome, and the myotome, respectively. Also diagrammed is the expression domain of *BMP4*, *BMP7*, and *Wnt1* in the neural tube. From Reshef et al., 1998.

Furthermore, it has also been shown that BMPs and noggin, expressed in a spatio-temporal manner forming morphogen gradients in the developing limb bud (BMPs are expressed in the limb margins and the AER (apical ectodermal ridge), whereas noggin is expressed in the core of the limb), are also responsible for regulating development of the muscles in the limbs (Amthor et al., 1998) **(Figure 26)**.
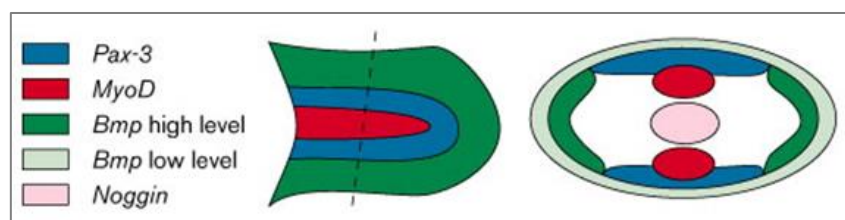
Figure 26 – Diagram summarizing Pax3, MyoD, BMP and Noggin gene expression of a whole-mount wing bud of a chick embryo at stage 25. The right-hand panel shows a section of the whole-mount taken at the position indicated by the dotted line. From Amthor et al., 1998 (Copyright clearance center license number 3642141508653).

Concordantly, in noggin knock-out mice, the onset of myogenesis is not affected but terminal muscle differentiation, myoblast fusion and maturation of the fiber, is impaired and

results in thinner and somewhat disorganized myofibers. Overall, muscle tissue was severely reduced in newborn mice (Tylzanowski et al., 2006).

2- BMPs and fetal myogenesis

It has recently been shown that BMP signaling is involved in regulating fetal skeletal muscle growth. Indeed, ectopic activation of BMP signaling in chick limbs increased the number of fetal muscle progenitors and fibers, while blocking BMP signaling reduced their numbers, ultimately leading to small muscles. Moreover, this study showed that BMP signaling also regulated the number of satellite cells during development. Furthermore, BMP signaling was active (presence of P-Smads1/5/8) in a subpopulation of fetal progenitors and satellite cells at the extremities of muscles, suggesting an appositional growth of muscle anlagen (Wang et al., 2010) **(Figure 27)**.
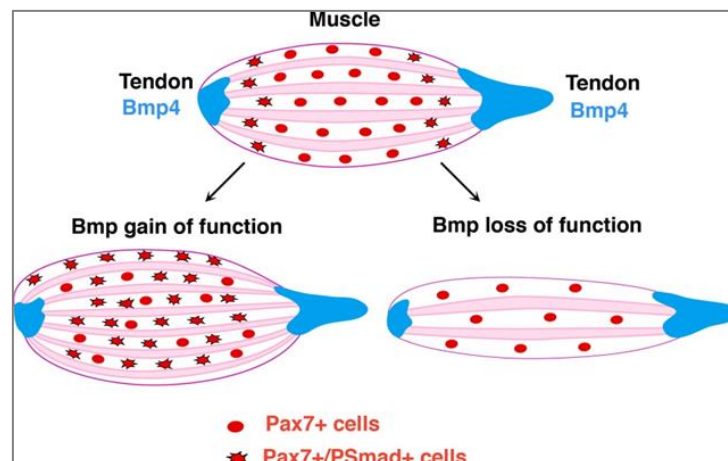
Figure 27- Schematic representation of BMP function during fetal muscle growth. In normal conditions, a Bmp signal produced by the tendons acts on a subpopulation of Pax7$^+$ cells located at the tips of muscle. Activation of Bmp signaling in these muscle progenitors will activate their proliferation and induce their differentiation. This will allow longitudinal muscle growth. Bmp gain-of-function experiments lead to an increase in the number of muscle progenitors and fibers, while Bmp loss-of-function experiments lead to a decrease in the number of muscle progenitors and fibers. From Wang et al., 2010 (Copyright clearance center license number 3642160532870).

3- BMPs and postnatal myogenesis

Ono and colleagues (Ono et al., 2011) recently showed that BMP signaling allows population expansion of activated satellite cells by preventing their premature myogenic differentiation. This study was performed *in vitro* on both isolated myofibers and satellite

cell-derived primary myoblasts. During activation and proliferation, satellite cells expressed BMPR1A (Alk3) and P-Smad1/5/8 indicating intracellular activation of the BMP pathway. Noggin expression in satellite progeny is upregulated as they differentiate **(Figure 28)**.

Exogenous BMP4 treatment sustained satellite cell division and reduced differentiation, whereas inhibition of the BMP signaling pathway, via treatment with noggin, antagonizing the interaction of BMP with its receptors, or by inhibiting Smad phosphorylation with the use of dorsomorphin, or perturbating the cascade by reducing Smad5 and Smad4 with siRNAs, all induced premature differentiation. Manipulation of the BMP signaling pathway also affected Id1 expression levels (a known inhibitor of differentiation, see III-2), showing a possible underlying molecular mechanism of the prevention of differentiation by BMP signaling (Ono et al., 2011).

This role of BMP signaling in balancing proliferation and differentiation of activated satellite cells and their descendants was also described by the study of Friedrichs et al., 2011.

Moroever, both Ono and colleagues as well as Wang and colleagues (Ono et al., 2011; Wang et al., 2010), showed that BMP signaling is present in regenerating muscle *in vivo*. Indeed, in the experimental protocol of Ono and colleagues, three days following cardiotoxin induced injury, 97% of MyoD[+] satellite cell derived myoblasts expressed P-Smad1/5/8. Inhibition of the BMP signaling pathway, by either injecting dorsomorphin or soluble BMPR1A, following injury, regeneration of the muscle was impaired: smaller muscle fibers and increased fibrosis (collagen 1).

Furthermore, injection of noggin into regenerating muscle reduces P-Smad1/5/8, Id1 and Id3 protein levels. In addition, in the Id-mutant mice, the number of proliferating Pax7^{+} cells is reduced following muscle injury. These data suggest that BMP signaling regulates *Id1* and *Id3* in muscle satellite cells thereby maintaining their proliferation before terminal myogenic differentiation (Clever et al., 2010).
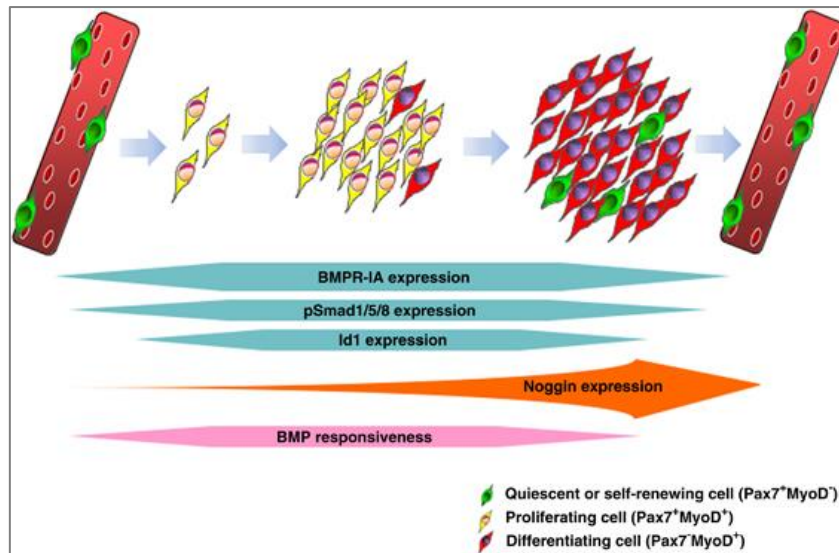
Figure 28- BMP signaling during myogenic progression in satellite cells. During muscle repair and regeneration, quiescent Pax7$^+$ satellite cells are activated to co-express Pax7 and MyoD. Satellite cell-derived myoblasts proliferate extensively before many cells then downregulate Pax7 and differentiate to either repair damaged muscle fibers or fuse together to generate new myofibers. Other satellite cells maintain Pax7 expression but lose MyoD, and self-renew to maintain a viable stem cell compartment. Normal BMP signaling through BMPR-1A and Smad1/5/8 phosphorylation is required during muscle repair/regeneration to allow the satellite cell-derived myoblast population to expand, by preventing precocious differentiation. BMP signaling operates through controlling *Id* levels, a negative regulator of MyoD and myogenic differentiation. As satellite cell progeny differentiate, Noggin is upregulated to antagonize the BMP signal, so facilitating the myogenic differentiation programme. From Ono et al., 2011 (Copyright clearance center license number 3642150388014).

Aims & Objectives

Growth factors regulate muscle development and regeneration, and thereby determine correct muscle function. Different families of signaling molecules have been identified to guide muscle stem cells and muscle growth, such as notch, Wnts and myostatin (see Part II-5-B, Part II-7 and Part III-4). However, the regulatory mechanisms that coordinate the timing of precursor generation and fiber growth and hence determine adult muscle size and function are still poorly understood. Previous studies (see Part IV) have demonstrated that BMPs and their antagonists, such as noggin, regulate embryonic and fetal myogenesis (Amthor et al., 1998; Amthor et al., 2002; Pourquié et al., 1996; Wang et al., 2010), as well as the proliferation, self-renewal and differentiation of adult muscle stem cells (Ono et al., 2011; Friedrichs et al., 2011). However, previous work on the function of BMP signaling in adult satellite cells was largely performed *in vitro* on both isolated myofibers and satellite cell-derived primary myoblasts. The effect of BMP signaling on muscle growth and homeostasis, and muscle stem cell activity *in vivo* remain sofar unknown.

The main aims of my thesis were to further understand the role of BMP signaling during postnatal/juvenile muscle growth as well as during adult muscle mass maintenance. I hypothesized that BMPs and their antagonist proteins establish a signaling network that defines the rate of muscle growth, final muscle size and number of muscle stem cells inherent to the adult skeletal muscle. The signaling properties of BMPs could also be involved in maintaining the muscle mass in homeostasis and thereby defining skeletal muscle function during normal development and disease conditions.

The aims and objectives of my thesis are described below.

> **Aim 1: Investigate whether BMP signaling regulates satellite cell dependent postnatal muscle growth** (Results Part 1. article in preparation for submission).

Objectives:

- To elucidate if BMP signaling is present in both satellite cells and terminally differentiated muscle cells during postnatal muscle growth and to determine the expression dynamics of BMP signaling components during postnatal muscle growth and up to adulthood.

- Establish experimental conditions to inhibit the BMP signaling specifically in postnatal satellite cells and monitor the resulting effects, first *in vitro* and then *in vivo*. Investigate the consequences of this inhibition on postnatal muscle fiber growth and on the establishment of the satellite cell pool.

- Establish experimental conditions to inhibit the BMP signaling in postnatal myofibers and monitor the resulting effects on postnatal muscle fiber growth and on the establishment of the satellite stem cell pool.

> **Aim 2: To investigate whether BMP signaling plays a role in adult muscle mass homeostasis** (Results Part 2, published).

Objectives:

- Determine whether BMP signaling regulate adult muscle mass. Establish experimental conditions to activate BMP signaling in adult skeletal muscle.

- Determine the role of BMP signaling in the context of muscle atrophy (induced following denervation).

Materials & Methods

Materials and Methods

Murine models

Transgenic *Rosa26-LoxP-Stop-LoxP-humanSmad6-IRES-EGFP* mice (on a *C57BL/6J* background), also labeled RS6, were a gift from Thomas Braun (Max Planck Institute for Heart and Lung Research, Bad Nauheim, Germany) and were crossed with different Cre-driver mice.

Pax7$^{CreERT2/+}$ knock-in mice (JAX strain name is B6;129-Pax7tm2.1(cre/ERT2)Fan/J) were bred with wild-type *C57BL/6J* mice . This strain expresses Cre-ERT2 recombinase from the endogenous Pax7 locus. By crosses with the RS6 strain we obtained *Pax7$^{CreERT2/+}$;RS6$^{+/-}$* that were treated with tamoxifen as described later and analyzed at 1 to 4 months old.

Transgenic *HSA-Cre* mice (JAX strain name FVB.Cg-Tg(ACTA1-cre)79Jme/J, on a C57BL/6J background) described by Miniou et al., 1999, have the Cre recombinase gene driven by the human α-skeletal actin (HSA) promoter. By crossing these mice with the RS6 strain we obtained *HSA-Cre$^{+/-}$; RS6$^{+/-}$* that were analyzed at 1 and 2 months old.

Pax3$^{GFP/+}$ mice previously described Relaix et al., 2005 were a gift from Frederic Relaix (Institute of Myology, Paris, France) and used at 2-4 months old as positive controls for FACS-sorting GFP expressing satellite cells.

Myostatin knock-out (KO) mice (*Mstn$^{-/-}$*, JAX strain name is *Mstn^{tm1Sjl}*, on a C57BL/6J background) have a targeted insertion of a neo-cassette in the entire mature C-terminal region (McPherron et al., 1997). Thus, the mutation leads to myostatin deficiency. Mice were bred using a mating system crossing KO males with heterozygote females. Experiments were performed on 3 to 4 month old mice.

GDF5$^{-/-}$ (GDF5 is also known as BMP14, JAX strain name: *Gdf5^{bp-J}*) mice have a spontaneous frameshift mutation leading to truncated non-functional Gdf5. These mice present brachipodism (bp) with alterations in the length and number of bones in the limbs (shorter long bones in the limbs and fusion of phalanges) (Storm et al., 1994). Mice were maintained in a homozygous mating system. Experiments were performed on 3 to 5 month old mice.

The mice were bred in the animal facility of the Medical Faculty of Paris VI and kept according to institutional guidelines. Wild-type *C57BL/6J* mice were purchased from Janvier or Charles River and wild-type *A/J* mice were purchased from Harlan.

Genotyping

Genomic DNA extraction was performed on mouse tissue with 150 μl NaOH 50 mM, incubated at 98 °C for 30 min, and adding 40 μl Tris HCl 1M (pH=8,2). Polymerase chain reaction was executed using Promega PCR Master Mix. The sequences for the primers used are listed below:

Mouse strain	Primer name	Sequence (5'→3')	Amplicon (bp)
Rosa26-Smad6 (RS6)	Rosa-FA	AAAGTCGCTCTGAGTTGTTAT	wt 585 mutant 249
	Rosa-RF	GGAGCGGGAGAAATGGATATG	
	Rosa-SplicAC	CATCAAGGAAACCCTGGACTACTG	
Pax7$^{CreERT2/+}$	Pax7Cre-1	TGATGGACATGTTCAGGGATC	mutant 870
	Pax7Cre-2	CAGCCACCAGCTTGCATGA	
HSA-Cre	HSACre-F	CCTGGAAAATGCTTCTGTCCG	mutant 400
	HSACre-R	CAGGGTGTTATAAGCAATCCC	
Mstn$^{-/-}$	MstnWT-F	GAAGTCAAGGTGACAGACACAC	wt 225 mutant ~ 350
	MstnWT-R	GTGCACAAGATGAGTATGCGG	
	MstnKO-F	GATCGGCCATTGAACAAGATG	
	MstnKO-R	AGCAAGGTGAGATGACAGGAG	

Cre/Lox mutagenesis

The Cre-Lox system is used as a genetic tool to understand gene function in specific cell types and was first developed by Brian Sauer (Sauer, 1987; Sauer and Henderson, 1988). Cre-Lox recombination is a site-specific recombinase system, it involves the targeting of a specific short sequence of DNA called loxP (locus of X-over P1) site and splicing it with the help of an enzyme called Cre (causes recombination) recombinase. The latter DNA sites and recombination enzyme were identified in the P1 bacteriophage.

LoxP is a site on the bacteriophage P1 consisting of 34 bp that does not exist in eukaryotic cells. The site is composed of two sets of palindromic 13 bp flanking an asymmetric 8 bp sequence. The detailed structure of the site is: ATAACTTCGTATA-GCATACAT–TATACGAAGTTAT.

DNA sequence found between two loxP sites is termed the "floxed" region. The product of Cre mediated recombination depends on the orientation of the loxP sites. Indeed, DNA sequence between two loxP sites oriented in the same direction is excised as a circular loop of DNA which is then degraded. When DNA is floxed by two loxP sites that have opposite orientation then the sequence is not excised but is inverted. Moreover, if the loxP sites are located on different chromosomes, the Cre can mediate chromosomal translocation.

When Cre recombinase is placed under a specific promoter it allows a spatial, tissue specific, control of the mutagenesis. Furthermore, the Cre/Lox system was further optimized by adding an additional temporal control step of mutagenesis by using fusion protein Cre-ER^T (Feil et al., 1996). The mutated form of the ligand binding domain (LBD) of the eostrogen nuclear receptor (ER) is able to bind tamoxifen (T, a synthetic ER antagonist) but not oestradiol. Moreover, Cre-ER^T activity depends on tamoxifen binding because in the absence of this ligand, the ER domain of the fusion protein is bound to heat shock proteins such as Hsp90 and is sequestered in the cytosol of the cell. However, when tamoxifen is present, it binds to the mutated LBD domain of the Cre-ER^T, leading to the dissociation of HSPs, the translocation to the nucleus where the Cre can identify the loxP sites. In summary, fusing Cre recombinase to LBD-ER^T results in an inducible tamoxifen-dependent Cre recombinase.

A more recent version of this fusion protein is Cre-ER^{T2}, in which there are additional mutations in the LBD-ER domain rendering the protein around 10 fold more sensitive to tamoxifen induction but also removing leaky activity of the Cre in the absence of ligand which was observed with the previous ER^T (Indra et al., 1999).

In our studies we have crossed the RS6 mouse strain, which has loxP sites flanking a stop sequence upstream of our gene of interest Smad6 inserted into the accessible ROSA26 locs, with different Cre-driver strains (previously described). In the cells where Cre is expressed, and active, the floxed Stop codon is excised allowing the expression of Smad6. When we used the CreER^{T2} strain, tamoxifen was administered to induce Cre activity.

Tamoxifen injection for induction of Cre-ER^{T2} activity

Tamoxifen (Sigma) was prepared in heated corn oil (Sigma) at 37 °C at 20 mg/ml and 5 μl/g were administered by intra-peritoneal injection in pups (P7 and P9) or in the adult mouse (between 2 and 4 months old, 5 daily injections).

Isolating satellite cells by FACS and primary culture

For fluorescent-activated cell sorting, muscles (forelimb, hindlimb, abdominal, pectoral) were processed from P3, P14, P28 mice or adult mice (2-4 months) following sacrifice by cervical dislocation. The dissection of the muscles was performed with care to take off as much fat and connective tissue as possible. The muscles were minced in Hank's Balanced Salt Solution (HBSS) supplemented with 0,2% bovine serum albumin, 1% penicillin-streptomycin in a sterile 6 cm Petri dish on ice. The minced muscles were digested for 1,5 hours at 37°C with 2 µg/ml collagenase A (Roche), 2,4 U/ml dispase I (Roche), 10 ng/ml DNase I (Roche), 0.4 mM $CaCl_2$ and 5 mM $MgCl_2$ in supplemented HBSS. Cells were washed with supplemented HBSS, filtered through 100 µm cell strainer, cells were then pelleted and washing step was repeated with 70 µm and finally 40 µm cell strainers.

For marking extracellular markers, the following primary antibodies were used (10 ng/ml): rat anti-mouse CD45-PE-Cy7 (BD), rat anti-mouse Ter119-PE-Cy7 (BD), rat anti-mouse CD34-BV421 (BD), rat anti-mouse integrin-α7-A700 (R&D Systems), rat anti-mouse Sca1-FITC (BD). Cells were washed once with ice-cold supplemented HBSS, filtered and re-suspended in supplemented HBSS. Flow cytometry analysis and cell sorting were performed on a FACSAriaII (BD) previously calibrated (Fluorescence Minus One and use of compensation beads) at the Lumic-CypS UPMC platform. TER119 (LY76)$^+$ and CD45 (PTPRC, LY5)$^+$ cells were negatively selected, CD34$^+$ and integrin-α7$^+$ cells were positively selected and the remaining cells were gated based on SCA1$^-$ expression.

Purified cell populations were plated on gelatin-coated dishes at low density for clonal analysis (300 cells/well in a 24 well plate). The remaining sorted cells were plated for RNA extraction. Cells were allowed to grow in growth medium: DMEM Glutamax containing 20% fetal bovine serum, 10% horse serum, 1% penicillin–streptomycin, 1% HEPES, 1% sodium pyruvate, 1/4000 bFGF (20 ng/ml Peprotech). Cells were plated at D0, treated or not with either 1 µM of 4-hydroxytamoxifen (Sigma) or 50 ng/ml recombinant mouse Noggin (R&D systems) at D2, D3, D4, and at D5 were either fixed for immunohistochemistry with 4% paraformaldehyde (PFA) or washed and harvested by trypsinisation for RNA extraction. Number of cells in the proliferation assay was quantified by counting at least 180 colonies, from three independent experiments. Quantification of different markers (Ki67, Pax7, MyoD, MyoG, MHC) by immunohistochemistry was done on at least 15 colonies, and from three independent experiments.

Preparation of satellite cell-derived primary myoblasts

The total cells from the muscle tissue, prepared similarly as by the FACS purification procedure, are resuspended in growth medium (see FACS procedure) and pre-plated onto a non-coated 15 cm Petri dish for 4 hours (fibroblasts will adhere to the plate, whereas most myoblasts will remain in suspension). The media, containing the myoblasts in suspension, is then transferred onto gelatin coated 10 cm Petri dishes. Cultures were maintained in growth medium until cells reached 70% confluency, after which cells were harvested by trypsinisation for RNA extraction.

Isolating single fibers from EDL muscle

Mice at P28 were sacrificed by cervical dislocation, thereafter *tibialis anterior* (*TA*) and *extensor digitorum longus* (*EDL*) muscles were surgically isolated. *EDL* muscles were digested in 0.2% collagenase type 1 (Sigma) dissolved in DMEM (Life Technologies). Individual, viable, non-damaged myofibers were isolated by gently passing through Pasteur pipettes with different sized apertures. Myofibers were fixed in 4% PFA dissolved in PBS (Sigma) for 10 min, washed, stained with DAPI and Pax7 (1/50, mouse IgG1, DSHB) and mounted on slides.

Immunohistochemistry

Immunohistochemical analyses were performed using primary antibodies against Pax7 (1/50, mouse IgG1, DSHB), m-cadherin (1/50, mouse IgG1, Nanotools), Laminin (1/400, rabbit, Dako), MyoD (1/100, mouse IgG1, Dako), MyoG (1/100, mouse IgG1, DSHB), panMHC (mouse Ig2a, A4-1025, DSHB), Ki67 (1/100, mouse IgG1, BD), cleaved-caspase 3 (1/300, Cell signaling) and DAPI (1/1000, Sigma), followed by secondary antibodies with various fluorophores (Alexa Fluor 1/400: goat anti mouse IgG1 488 or 594, goat anti rabbit 488 or 594, goat anti mouse IgG2 633). Fluorescence was visualized either by Zeiss Axio Imager with an Orkan camera (Hamamatsu) and AxioVision software or by Nikon Ti microscope equipped with a CoolSNAP HQ2 camera (Roper Scientific), an XY motorized stage (Nikon) using Metamorph Software (Molecular Devices).

Morphometric studies

Cryosections of 12 μm of the *TA* muscles were stained with anti-laminin to delineate the muscle fibers and anti-Pax7 or anti-m-cadherin to mark satellite cells. Fluorescent

photographs were taken with a ×20 objective on a microscope (Zeiss, AxioImage) and saved as TIFF files. These images were projected on a flatscreen coupled with a graphic tablet, which enabled the manual retracing of the muscle fiber outlines and the counting of satellite cells that were found inside it. The fibers of the entire muscle cross section were analyzed.

RNA isolation, RT-PCR and real time quantitative PCR

For frozen muscle tissue total RNA was isolated using Trizol (Invitrogen) extraction combined with RNeasy Mini Kit (Qiagen). For FACS isolated satellite cells or for cultured primary myoblasts total RNA was isolated using RNeasy Micro Kit (Qiagen). In both cases, RNase-Free DNase I Set (Qiagen) was used to eliminate traces of DNA in the RNA extraction. Isolated RNA was quantified using NanoVue Plus GE HealthCare spectrophotometer (Dutscher).

For RNA extracted from muscle tissue, cDNA synthesis was performed using ThermoScript RT-PCR System for First-Strand cDNA Synthesis (Invitrogen) and random hexamer primers. For RNA extracted from FACS isolated satellite cells or cultured primary myoblasts, cDNA synthesis was performed using SuperScript VILO Master Mix (Invitrogen).

Real-time polymerase chain reaction was performed according the SYBR Green protocol (BioRad) in triplicate on the CFX96 Touch Real-Time detection system (BioRad) using iTaq Universal SYBR Green Supermix (BioRad). A 10 min denaturation step at 94°C was followed by 40 cycles of denaturation at 94°C for 10 s and annealing/extension at 60°C for 30 s. Before sample analysis we had determined for each gene the PCR efficiencies with a standard dilution series (10^0-10^7copies/µl), of which subsequently enabled us to calculate the copy numbers from the C_t values. mRNA levels were normalized to 1 million copies of GAPDH mRNA. Fold changes were calculated according to the efficiency corrected $-\Delta\Delta C_t$ method (Pfaffl, 2001). The sequences for the primers used are listed below:

Table of oligonucleotides used for RT-qPCR

Gene	Primer sequence (5'→ 3')	Direction
Oligonucleotide primers used for mice		
Bmp1	TTTGATGGCTACGACAGCAC	Forward
	CTGTGGAGTGTGTCCTGGAA	Reverse
Bmp2	CATCACGAAGAAGCCGTGGA	Forward
	TGAGAAACTCGTCACTGGGG	Reverse
Bmp4	TCCATCACGAAGAACATCTGGA	Forward
	ATACGGTGGAAGCCCTGTTC	Reverse
Bmp5	AGGAATACACAAACAGGGATGC	Forward
	CCAGCAGATTTTACATTGATGC	Reverse
Bmp6	GGGATGGCAGGACTGGATCA	Forward
	ATGGTTTGGGGACGTACTCG	Reverse
Bmp7	AGCTTCGTCAACCTAGTGGAAC	Forward
	CTGGAGCACCTGATAGACTGTG	Reverse
Bmp13	AAGACTTACTCCATTGCCGAGA	Forward
	TCGTCCAGTCCTCTGTCTACAA	Reverse
Bmp14	ATGCTGACAGAAAGGGAGGTAA	Forward
	GCACTGATGTCAAACACGTACC	Reverse
Alk3	TGAGACAGCAGGACCAGTCA	Forward
	GATTCTGCCCTTGAACATGAGA	Reverse
Id1	GGTGGTACTTGGTCTGTCGG	Forward
	CCTTGCTCACTTTGCGGTTC	Reverse
Noggin	GAAGTTACAGATGTGGCTGTGG	Forward
	CACAGACTTGGATGGCTTACAC	Reverse
Gremlin1	AGCAAAAGGGTTTTCCTGAT	Forward
	AGTGGTCAGCATTTCACCCT	Reverse
Follistatin	CCTGCTGCTGCTACTCTG	Forward
	CTCGGTCCATGAGGTGCT	Reverse
p21	GTACTTCCTCTGCCCTGCTG	Forward
	GGGCACTTCAGGGTTTTCTC	Reverse
p57	CTGAAGGACCAGCCTCTCTC	Forward

	AAGAAGTCGTTCGCATTGGC	Reverse
Gapdh	TGACGTGCCGCCTGGAGAAA	Forward
	AGTGTAGCCCAAGATGCCCTTCAG	Reverse
Oligonucleotide primers used for human cDNA insert in RS6 mice		
SMAD6	TACTCTCGGCTGTCTCCTCGC	Forward
	CAGTGGCTCGGCTTGGTGGCG	Reverse

Western blot

Proteins were extracted from frozen triceps muscle using RIPA buffer with a proteinase and phosphatase inhibitor cocktail (Complete tablets, Roche). Proteins were separated through denaturating sodium dodecyl sulphate polyacrylamide gel electrophoresis with the Laemmli system and transferred onto nitrocellulose membranes by the wet method (BioRad). The blots were probed using primary antibodies against GFP (1/5000, Aves Labs), P-Smad1/5/8 (1/500, Cell signaling), Smad4 (1/1000, B-8 sc-7966), P-Smad2 (1:4000, Invitrogen 44-2443G) and actin (1/10000, Sigma). Western blots were analyzed with SuperSignal West Pico Chemiluminescent substrate (Pierce).

AAV production

The constitutive active BMP receptor ALK3 (caALK3) construct (Akiyama et al., 1997) was subcloned into the pCS2$^+$ plasmid vector and then introduced into an AAV-2/1 based vector between the two inverted terminal repeats and under the control of the cytomegalovirus (CMV) promoter using the XhoI and MluI sites. AAV2/1-caALK3 was produced in human embryonic kidney 293 cells by the triple-transfection method using the calcium phosphate precipitation technique with both the pAAV2 propeptide plasmid, the pXX6 plasmid coding for the adenoviral sequences essential for AAV production and the pRepCAp plasmid coding for AAV1. Virus was then purified by two cycles of cesium chloride gradient centrifugation and was concentrated by dialysis. Final viral preparations were kept in PBS at −80 °C. Particle titer (number of viral genomes) was determined by quantitative PCR. A non-functional construction U7-c (AAV-control) was prepared using the same protocol as for AAV-caALK3.

AAV injection

The quantity of AAV used for intramuscular delivery was calculated according to total body weight (x μl = 1.5 × body weight [g]) and was about 30–40 μl. AAV was injected into the muscles of the anterior compartment of the lower leg (*TA* and *EDL* muscles) of 3- to 4-month-old C57Bl/6J mice. AAV-caALK3 was used at 1.3×10^{12} or 1.87×10^{12} viral genomes (vg)/ml, and AAV-control was used at 1.6×10^{12} vg/ml.

Statistical analysis

The wet muscle weights, the mean of myofiber diameter and myonuclei number per myofiber and number of marked cells per myofiber of per 100 fibers were analyzed from at least one leg of three mice assumed as independent. The results were expressed as the median in dotplots or in Whiskers-Tukey box plots. When the "n" number was above three (treated *versus* controls), the significance of statistical differences between the experimental groups was determined by the non-parametric Mann Whitney U-test test for results Part1.

Results

Part I: BMP signaling regulates postnatal satellite cell dependent muscle growth.

The results of this study were obtained through a collaborative work which contributed to the preparation of an article manuscript. The latter is enclosed at the end of this part and contains my results as well as those of my former colleague, a previous PhD student, Dr. Elija Schirwis, who used alternative approaches for this study. I will hereby present the background of this study, followed by my results and finally the manuscript that will be submitted shortly.

1- Introduction

In mice, the generation of myofibers is already completed around birth, meaning that postnatal muscle growth relies on the increase of muscle fiber size (length and diameter) also called hypertrophy (Ontell et al., 1984). The satellite cell dependent phase of postnatal myofiber growth takes place from P0 to P21, after which the number of myonuclei per fiber is established and satellite cells have stopped proliferating and entered quiescence (White et al., 2010).

The molecular mechanisms that guide postnatal muscle growth and control satellite cell proliferation and quiescence are not well understood. Previous studies have shown that BMPs are crucial for embryonic and fetal myogenesis (Pourquié et al., 1996; Amthor et al., 1998; Wang et al., 2010) , and we have recently revealed the role of BMP signaling for adult mass maintenance (Sartori et al., 2013) (Results Part 2). Moreover, *in vitro* studies on isolated single myofibers and satellite cell-derived primary myoblasts have demonstrated that BMP signaling is operating in activated proliferating satellite cells and that the signaling is down-regulated when these cells undergo differentiation (Ono et al., 2011; Friedrichs et al., 2011). We here investigated the contribution of BMP signaling during satellite cell dependent postnatal muscle growth, because during this stage of myogenesis, satellite cells are actively proliferating, thus this juvenile environment can be used as an experimental system to study active satellite cells compared to adult mice where the cells are already quiescent.

2- Results

BMP signaling pathway components are expressed in postnatal and adult skeletal muscle.

We have recently shown that BMP signaling regulates adult skeletal muscle homeostasis (Sartori et al., 2013; Results Part II). I here asked whether the BMP pathway is also active in skeletal muscle during postnatal growth by looking into the expression levels of different components of the pathway in muscles extracted from WT mice (*C57BL/6J*) at different ages: P3 (neonatal), P14 (juvenile) and in adult (8 weeks-old). For pups at P3 and P14, RNA was extracted from total muscles (pooled from forelimbs and hindlimbs). For the adult mice, I chose to analyze three different muscles: *tibialis anterior* (mostly fast muscle), *gastrocnemieus* (mixed muscle) and *soleus* (slow muscle).

I first determined the expression levels of different BMP ligands (*BMP2, 4, 5, 6, 7, 13* and *14*), *BMP1* which is a metalloproteinase, a type I receptor (*ALK3*, also known as *BMPR1A*), a known BMP signaling target gene encoding for inhibitor of differentiation/DNA binding 1, also known as *ID1* (Miyazono and Miyazawa, 2002) and BMP antagonists (*NOG*, *GREM1* and *FST* genes which respectively encode for Noggin, Gremlin and Follistatin). Of note, in Figure 1 and Figure 3 I show qRT-PCR results of gene expression compared to housekeeping gene *Gapdh*, I also used *18S* as a housekeeping gene and the same dynamics of expression of the different components of the BMP signaling were obtained confirming that the results obtained are not due to fluctuations of the reference gene employed.

My findings show that BMP signaling components are indeed expressed in total muscle at all three ages (Figure 1). Regarding BMP ligands, they are overall highly expressed at the neonatal stage and bluntly decrease in juvenile and adult mice. Interestingly, the adult *soleus* muscle has different gene expression levels as compared to the *TA* and *gastrocnemius*, since expression of some ligands, for example *BMP14*, was higher. Moreover, *ALK3* is expressed in neonatal and juvenile muscles and is somewhat decreased in the adult, except for the *soleus* muscle in which high expression levels are maintained. Overall, *ALK3* expression corresponds to the dynamics of expression of ligands. Moreover, I investigated whether the muscle tissue responds to BMP signaling by inspecting the expression level of *ID1*. The latter showed the same dynamics as those found for the BMP

ligands. Furthermore, BMP antagonists had similar expression dynamics: high in neonatal stage and later decreased in juvenile and adult muscles.

However, the limit of this experiment was that I was unable to determine the exact cellular source of gene expression since RNA was extracted from total muscle tissue (containing a majority of muscle fibers, but also other cell types, including satellite cells, fibroblasts and endothelial cells). The second limit of the experiment is that it remained difficult to interpret the fall of BMP signaling pathway components gene expression between neonatal and later stages. The cause of this downregulation could be the result of i) a dilution of the gene expression levels, due to the decrease of the number of mononucleated muscle precursors in comparison to the total differentiated myonuclei during postnatal muscle growth (White et al., 2010), or ii) the result of muscle maturation. Indeed, newborn mouse muscles express mainly developmental isoforms of myosin heavy chain (MHC) and during post-natal muscle growth those isoforms are progressively replaced by adult MHC isoforms. In addition, previous studies have described that the slow *soleus* muscle reaches its mature fiber type phenotype later than other muscles of the hindlimb (Agbulut et al., 2003) and it contains more satellite cells, two to four times the amount found in *tibialis anterior* (Gibson and Schultz, 1982). Moreover, in the embryo and fetus, in both future fast and slow muscles, slow myosin is co-expressed with embryonic myosin (Narusawa et al., 1987). The latter could explain the differences in gene expression levels observed in the adult *soleus* muscle which resembles more to fetal muscle compared to the adult *tibialis anterior* and *gastrocnemius* muscles (Figure 1).

BMP signaling pathway components are expressed in postnatal and adult satellite cells.

Next, I wanted to investigate whether satellite cells, which contribute to postnatal muscle growth up to P21, express BMP signaling components. For this purpose, I isolated satellite cells by FACS from total skeletal muscle harvested from WT mice (C57BL/6J) at different ages: P3, P14 and in the adult (8 weeks old). The gating strategy I used for isolating satellite cells was the following: i) isolate singlets using height (FSC-H, forward-scattered light height) plotted against area (FSC-A), ii) further isolate single cells according to their morphology allowing to further eliminate debris by plotting FSC-A against SSC-A (side-scattered light area), iii) followed by SSC-A versus PE-Cy7 labelling of CD45 and Ter119 to discriminate hematopoietic cells, iv) followed by a positive selection of satellite

cell markers CD34 labelled with the fluorochrome Blue Violet 421-(450/50 off the violet laser) coupled antibody and α7-integrin labelled with A700-coupled antibody (Sacco et al., 2008), and v) finally, I selected the Sca1 negative population, on the ground of negative selection of anti-Sca1-FITC labelled cells, that corresponded to the satellite cells (Mitchell et al., 2005) (Figure 2).

The results of the RT-qPCR show for the first time that BMP signaling components are expressed in postnatal satellite cells (Figure 3). The expression dynamics of the components differs somewhat from the results obtained in total muscle described above. Indeed, BMP ligands were highly expressed in neonatal satellite cells, decreased in juvenile cells, but then increased in adult satellite cells. In particular, *BMP6* expression increased strongly in adult satellite cells. *BMP4* and *BMP13* were also more expressed in adult satellite cells compared to P3 and P14. Moreover, it is of interest to remark that *BMP14* (*GDF5*) was not expressed by satellite cells at any stage. Furthermore, the expression of *ALK3* receptor and *ID1* followed the same dynamic as the majority of the BMP ligands. Interestingly, the BMP antagonists *NOG* and *GREM1* were highly expressed in neonatal satellite cells, decreased in juvenile cells and were completely absent in the adult. However, antagonist *FST* expression also decreased in juvenile satellite cells but had increased levels of expression in the adult.

The decreased levels of expression observed at P14 could be associated to the decreased proliferation of satellite cells and progressive establishment of their quiescence, which is reached by P21(White et al., 2010). Indeed, recent *in vitro* studies demonstrated that BMP signaling was present in activated, proliferating satellite cells and was downregulated in differentiating myoblasts (Ono et al., 2011). However, I here found that BMP signaling components were also strongly expressed in adult, hence quiescent, satellite cells. In fact, a previous study, in which transcriptome analysis was carried out on satellite cells isolated by FACS from *Pax3$^{GFP/+}$* mice, also showed that *BMP6*, *BMP5* and *BMP2* were up-regulated in quiescent adult satellite cells compared to active satellite cells from one week-old mice (Pallafacchina et al., 2010).

From these results, I hypothesized that BMPs, which were expressed in skeletal muscle, and notably in satellite cells, regulate satellite cell activity in a likely autocrine and paracrine manner.

Abrogating the BMP signaling pathway through Smad6 overexpression in *Pax7* expressing cells.

I next investigated the role of BMP signaling in satellite cells using a Cre/Lox system in transgenic mice. Indeed, I crossed *Rosa26-Lox-Stop-Lox-humanSmad6-IRES-EGFP* (*RS6*) mice with *Pax7*^{CreERT2/+} mice in order to overexpress BMP specific inhibitory Smad6 in *Pax7* expressing cells after treatment with tamoxifen (Figure 4a). Of note, RS6 mice were engineered with the insertion of the *Lox-Stop-Lox-humanSmad6-IRES-EGFP* cassette in the endogenous Rosa26 locus which is ubiquitously expressed (these mice were engineered by the group of Prof. Thomas Braun, MPI, Bad Nauheim, Germany, Bücker 2011) *Pax7*^{CreERT2/+} mice were engineered with the insertion of the Cre-ER^{T2} sequence in the endogenous *Pax7* locus, subsequently heterozygous mice with only one functional *Pax7* allele (Lepper et al., 2009). I used a single PCR to genotype the litters, generating the following bands: the Rosa26 locus containing the *huSmad6* cassette was detected at 249 bp, the WT *Rosa26* locus at 585 bp, and the *Pax7* locus containing the *Cre* at 870 bp (Figure 4b).

My first goal was to validate the system, making sure that *human Smad6* is indeed expressed following tamoxifen treatment of *Pax7*^{CreERT2/+};*RS6*^{+/-} mice and that this I-Smad indeed inhibited the BMP signaling pathway.

Firstly, since *Smad6* is ubiquitously expressed, I engineered specific primers detecting the *huSmad6* (containing 3 mismatches if compared to *mouse Smad6* sequence). Adult *Pax7*^{CreERT2/+};*RS6*^{+/-} mice were injected for five consecutive days with tamoxifen. The third day after the last injection, I cultured satellite cell-derived primary myoblasts from forelimb and hindlimb dissected muscles using the pre-plating method. I collected the cells when they reached 70% confluency and extracted their RNA (Figure 4c). After performing a PCR on the synthesized cDNA, I was able to detect the presence of huSmad6 which confirms that the recombination did indeed take place (Figure 4d).

Secondly, I showed that *huSmad6* expression leads to the decrease of *ID1* expression by 30% (when comparing the medians), suggesting an inhibition of the BMP signaling pathway (Figure 4e).

BMP signaling is required for the proliferation satellite cell-derived myoblasts.

My goal here was to identify whether BMP signaling regulates cell function. I first had to establish the FACS-sorting procedure to isolate satellite cells from tamoxifen treated adult $Pax7^{CreERT2/+;}RS6^{+/-}$ mice.

Since *RS6* mice contain an *IRES-EGFP* after the *huSmad6* sequence, I first aimed to isolate the EGFP expressing satellite cells and used *Pax3*$^{GFP/+}$characterized mice as positive controls of my experiment. However, I was unable to identify any EGFP expressing cells in muscles from tamoxifen treated $Pax7^{CreERT2/+;}RS6^{+/-}$ mice (Figure 5). Following immunohistochemichal staining of GFP, I did not identify any GFP staining either (data not shown).

I therefore turned to use the above described antibody based FACS sorting (gating CD45$^-$, Ter119$^-$, CD34$^+$, α7Integrin$^+$, Sca1$^-$ cells), since the expression levels of GFP was negligable and therefore unlikely to cause an artifact. When I proceeded to isolate satellite cells from tamoxifen treated adult $Pax7^{CreERT2/+};RS6^{+/-}$ mice I obtained very few cells (several thousands) in the Sca1$^-$ gate, suggesting that the huSmad6 expressing satellite cells changed their expression levels of *Sca1* (Figure 6). The significance of this observation remains unclear. Since the Sca1 antibody used was coupled to a FITC fluorochrome, another explanation for this effect would be that there is some residual expression of EGFP following recombination and thus creating an artefact. Despite this observation on FACS-sorted satellite cells, I would like to point out that there was no difference in the number of Pax7$^+$ cells *in vivo*, between $Pax7^{CreERT2/+;}RS6^{+/-}$ and $Pax7^{CreERT2/+}$ control mice treated with tamoxifen, as judged by the immunohistochemical quantification on transverse sections from TA muscles (Figure 7).

Since the number of FACS-sorted satellite cells from tamoxifen treated adult Pax7$^{CreERT2/+}$;RS6$^{+/-}$ mice was insufficient for analysis, I turned to evaluate *in vitro* the cell autonomous effect of huSmad6 expression in satellite cells by inducing the recombination *in vitro* with hydroxytamoxifen (4-OHT) treatment. The experimental design I used was the following: i) at D0 (Day 0) satellite cells were isolated by FACS from $Pax7^{CreERT2/+};RS6^{+/-}$ muscles, the cells were cultured in proliferation medium and left to settle down for one day, ii) at D1, D2, D3 cells were treated with 4-OHT (1 μM) or recombinant noggin (50 ng/μl), iii) the cells were analyzed at D5 (Figure 8a).

First, I set out to validate the experimental system by verifying that $Pax7^{CreERT2/+};RS6^{+/-}$ satellite cell-derived 4-OHT treated cells indeed expressed *huSmad6*

(Figure 8b). Of note, there were also low levels of expression of *huSmad6* in non 4-OHT treated cells, which likely represents transcripts of the endogenous murine *Smad6* due to unspecific binding of the primers.

Furthermore, following both 4-OHT and Noggin treatment, expression of *ID1* was significantly reduced (Figure 8c). Of note, downregulation of *ID1* expression levels was similar in 4-OHT and noggin treated cells.

I next evaluated the cellular behavior following such inhibition of the BMP signaling pathway. By overexpressing huSmad6 intracellularly and by supplementing the proliferation media with noggin I was able to compare a cell autonomous inhibition *versus* an extracellular inhibition of the BMP signaling pathway. I designed a proliferation assay experimental protocol, culturing isolated satellite cells at low density which allowed me to evaluate their clonal expansion.

In an experiment using control $Pax7^{CreERT2/+}$ satellite cell derived-cells, the treatment with 4-OHT led to slightly smaller colonies as compared to the control untreated cells meaning that hydroxytamoxifen may have a small effect on the extent of cell proliferation, however noggin treatment resulted in colonies that were less than half the size of the control cells. In the cells of interest, isolated from $Pax7^{CreERT2/+};RS6^{+/-}$ mice, both 4-OHT and noggin treatments resulted in colonies that were less than half the size compared to the untreated cells (Figure 8d).

The latter reduction in cell number could result from different cellular responses to abrogated BMP signaling: i) apoptosis, ii) reduced proliferation, and iii) precocious differentiation.

To determine whether cells underwent apoptosis, I used an antibody detecting cleaved-caspase 3. However no cells were labelled, neither in 4-OHT nor in noggin treated myoblasts from $Pax7^{CreERT2/+};RS6^{+/-}$ mice, suggesting that the reduced generation of cells was not resulting from apoptosis (data not shown).

I used an anti-Ki67 antibody, marking proliferating cells in all phases of the cell cycle (Scholzen and Gerdes, 2000), to investigate the number of cells which had withdrawn from the cell cycle. The quantification clearly showed that 4-OHT or noggin treatment significantly reduced expression of Ki67 compared to the control cultures (Figure 9 and Figure 10a,d), clear evidence for a decreased cell proliferation following BMP abrogation.

Interestingly, expression of cell cycle inhibitors *p21* and *p57*, analyzed by RT-qPCR, were both upregulated in 4-OHT and noggin treated cells compared to controls, which points to the molecular mechanism underlying the decreased proliferation (Figure 10g,h). Of note, RT-qPCR from RNA extracted from noggin treated cells were done on 2 samples (2 mice), I am planning to repeat the experiment for the publication to reproduce these results.

Finally, I next wanted to determine whether abrogation of BMP signaling impinges on the myogenic lineage progression. It is of note, that FACS-sorted cells, independently of the treatment, cease expressing Pax7 after five days in culture (data not shown), whereas the vast majority of the cells still expressed MyoD, and MyoD⁻ cells were rarely seen (Figure 9). Thus, almost all cells had clear myogenic identity, however already lost the satellite cell marker Pax7. Moreover, the quantification of myogenin and myosin heavy chain expressing cells did not reveal any differences between 4-OHT and Noggin treated cultures compared to control cultures (Figure 9 and Figure 10b,c,e,f). Indeed, approximately 65% of nuclei per colony were positive for myogenin, and 40% of the nuclei in a colony were positive for myosin heavy chain (comparing means). This result was surprising as different from the previously described premature differentiation of myoblasts following abrogation of the BMP pathway (Ono et al., 2011; Friedrichs et al., 2011).

BMP signaling is required for postnatal/juvenile muscle growth.

I next investigated the role of BMP signaling on postnatal/juvenile muscle growth *in vivo* by injecting tamoxifen into *Pax7^{CreERT2/+};RS6^{+/-}* pups at P7 and P9 and analyzing the effect on muscle growth when the mice reached one month of age (Figure 11a). I observed a significant reduction of the *TA* and *soleus* wet muscle weights, from the *Pax7^{CreERT2/+};RS6^{+/-}* tamoxifen treated pups as compared to the untreated pups; however the *EDL* muscle weight was insignificantly reduced (Figure 11b). Keeping with such reduced muscle masses, muscle fiber diameters evidenced a shift towards smaller fiber sizes in tamoxifen treated *Pax7^{CreERT2/+};RS6^{+/-}* mice as compared to the different controls (non-tamoxifen treated *Pax7^{CreERT2/+};RS6^{+/-}* mice, tamoxifen treated *RS6^{+/-}* mice and tamoxifen treated *Pax7^{CreERT2/+}* mice) following analysis of mid-belly transverse *TA* cross-sections (Figure 11c,d).

I next determined the cellular composition of myofibers isolated from *EDL* muscles from tamoxifen treated *Pax7^{CreERT2/+};RS6^{+/-}* mice as compared to the different controls (non-tamoxifen treated *Pax7^{CreERT2/+};RS6^{+/-}* mice, tamoxifen treated *RS6^{+/-}* mice and tamoxifen

treated $Pax7^{CreERT2/+}$ mice). I found a 20-26% reduction (if comparing means) in myonuclear number per fiber from tamoxifen treated $Pax7^{CreERT2/+};RS6^{+/-}$ mice as compared to myofibers from the control mice (Figure 11e). Of note, I found also a 7% reduction (if comparing means) in myonuclear numbers in the tamoxifen treated controls ($RS6^{+/-}$ and $Pax7^{CreERT2/+}$ tamoxifen treated mice) as compared to the non-tamoxifen treated $Pax7^{CreERT2/+};RS6^{+/-}$ mice control.

At four weeks of age, the final number of satellite cells, forming the adult reservoir of muscle stem cells, is reached in the *EDL* muscle (White et al., 2010). Surprisingly, when comparing the different genotypes of the control group, I found a 50% reduced number of $Pax7^+$ satellite cells per isolated myofiber from mice harboring only one *Pax7* expressing allele (non-tamoxifen treated $Pax7^{CreERT2/+};RS6^{+/-}$ mice and tamoxifen treated $Pax7^{CreERT2/+}$ mice) as compared to the tamoxifen treated $RS6^{+/-}$ mice, which have two *Pax7* alleles. This implies the presence of a Pax7 haploinsufficiency in the $Pax7^{CreERT2/+}$ mice, suggesting an insufficient amount of Pax7 for the generation of the final adult satellite cell pool. Remarkably, tamoxifen treatment of $Pax7^{CreERT2/+};RS6^{+/-}$ mice further decreased the number of $Pax7^+$ cells by 34-42% as compared to the different controls that harbor only one functional *Pax7* allele (respectively non-tamoxifen treated $Pax7^{CreERT2/+};RS6^{+/-}$ mice and tamoxifen treated $Pax7^{CreERT2/+}$ mice) (Figure 11f).

In addition, I analyzed the result of *Smad6* overexpression in juvenile $RS6^{+/-};Pax7^{CreERT2/+}$ mice when they reached adulthood (at 2 months of age), and observed that muscle growth was still affected, since muscle fibers were smaller (Figure 12b), and the number of Pax7 expressing cells was still reduced (Figure 12c) as compared to the controls: tamoxifen treated $RS6^{+/-}$ mice (72% reduction) and untreated $Pax7^{CreERT2/+}$ mice (47% reduction). Again, the number of the $Pax7^+$ satellite cells in the Pax7 monoallelic controls, *i.e.* $Pax7^{CreERT2/+}$ mice, was reduced by half as compared to the $RS6^{+/-}$ mice. The latter observation reinforces the hypothesis that there is indeed a Pax7 haploinsufficiency in the $Pax7^{CreERT2/+}$ mice.

Therefore, these results show that the adult stem cell pool is generated during the postnatal growth phase, and that BMP signaling is required for its correct size expansion.

Abrogation of BMP signaling in differentiated myonuclei does not impinge on satellite cell number.

The above described experiments do not provide unequivocal evidence that the cell autonomous interference with BMP signaling in *Pax7* expressing satellite cells was causing the drop in satellite cell number. Alternatively, recombinant satellite cells that fused into the myofiber syncitia, thereby forming a mosaique of recombinant Smad6-expressing nuclei and not-recombinant myonuclei, might act indirectly on non-fused satellite cells. Alternatively, one could also hypothesize that reduced number of satellite cells is the simple consequence of the reduced myofiber size.

In order to address these points, I conditionally overexpressed *huSmad6* in differentiated muscle by crossing *RS6* mice with *HSA-Cre* mice. In the latter mice, Cre is expressed under the promoter of human skeletal actin-α (*HSA)* in terminally differentiated striated muscle (Miniou et al., 1999) (Figure 13a).

Muscles from *HSA-Cre$^{+/-}$;RS6$^{+/-}$* mice expressed GFP, as evidenced by Western blotting total protein extract from *Triceps* muscle from one month old mice, whereas no GFP was detected *RS6$^{+/-}$* mice (Figure 13b). In addition, *huSmad6* was also highly expressed in muscles from *HSA-Cre$^{+/-}$;RS6$^{+/-}$* mice (Figure 13c).

In *HSA-Cre$^{+/-}$;RS6$^{+/-}$* mice, body mass increased normally during postnatal growth as compared to *RS6$^{+/-}$* mice (Figure 13d). However, at one and two months of age, *TA* and *EDL* muscles tended to smaller weights as compared to control muscles. *Soleus* muscle weight, however, did not change (Figure 13e and 14a). Unexpectedly, I found that the *TA* myofibers were larger in breadth size in *HSA-Cre$^{+/-}$;RS6$^{+/-}$* mice compared to the control *RS6$^{+/-}$* mice (Figure 13g,h and 14b-c). Such smaller muscle weight combined with larger fibers can only be explained by a reduced total fiber number per muscle. Inspecting H&E (Hematoxylin and Eosin) stained muscle sections from these mice showed normal tissue architecture and did not evidence muscle fiber degeneration or muscle fiber atrophy (no atrophic angular fibers). I counted total fiber numbers per section and found a tendency towards smaller numbers, however there were large inter-individual differences (Figure 13f and 14d). This points to an altered muscle development in these mice during embryonic myogenesis, which remains to be explored.

Importantly, the number of *Pax7* expressing cells remained unchanged between the two genotypes (Figure 13i and Figure 14e). The latter demonstrates that interference with BMP signaling in myofibers did not impair the establishment of the final satellite cell pool. Thus, *huSmad6* overexpressing muscle fibers did not indirectly act on satellite cells.

3- Conclusions

Overall, my results provide evidence that during postnatal/juvenile growth of skeletal muscle:

- Components of the BMP signaling are expressed in both skeletal muscle and satellite cells.

- BMP signaling stimulates proliferation of satellite cells.

- BMP signaling is required for satellite cell dependent myofiber growth.

- BMP signaling determines the size of the adult muscle stem cell reservoir.

I here provide for the first time evidence that a growth factor mediated signaling pathway regulates skeletal muscle growth and determines the size of the adult satellite cell reservoir during postnatal development.

4- Figures and legends of my results

Figure 1 – Gene expression dynamics of BMP signaling pathway components in skeletal muscle from neonatal, juvenile and adult mice.

Diagrams depict the relative mRNA copy numbers per 10^6 *Gapdh* mRNA copies of different *BMP* ligands (*Bmp2*, *4*, *5*, *6*, *7*, *13*, *14*), *Bmp1* metalloproteinase, BMP type I receptor *Alk3* (*Bmpr1a*), BMP target gene *Id1*, BMP antagonists *Nog* (encoding *noggin*), *Grem1* (encoding *gremlin)* and *Fst* (encoding *follistatin)*, in skeletal muscles from wild-type mice at postnatal day 3 (P3) in red and P14 in blue, or in *tibialis anterior*, *gastrocnemius* or *soleus* muscles from 8-week-old adult wild-type mice in different shades of grey (n=3 mice for each age). Values are shown as means ± SEM.

Figure 1

Figure 2 – Isolating muscle satellite cells by FACS using stem cell markers.

(A) Diagrams depict gates used to isolate satellite cells from skeletal muscles from wild-type mice at P3: **i)** selection of singlets FSC-H (Forward Scatter-Height) plotted against FSC-A (Forward Scatter-Area), **ii)** selection of CD45$^-$ Ter119$^-$ cells that are not fluorescent for PE-Cy7, **iii)** selection of CD34$^+$ cells that emit fluorescence at BV421 (450/50 off the violet laser) and of α7-Integrin$^+$ marked with A700, **iv)** gated Sca1$^-$ cells that do not emit FITC fluorescence.

(B) The table shows the number of cells isolated by FACS obtained from skeletal muscles from 3, 14 days old (pooled 6 animals together and repeated the experiment 3 times) or 8 weeks old (pooled 3 animals together and repeated the experiment 3 times) wild-type mice for each experiment and from which RNA was extracted.

Figure 2

A

Population	%Total
All Events	100.0
SINGLETS	86.7
SINGLE CELLS	68.5
CD45 TER119 NEG	52.2
a7INT+CD34+	4.2
SCA1 NEG	3.3
SCA1 POS	0.0
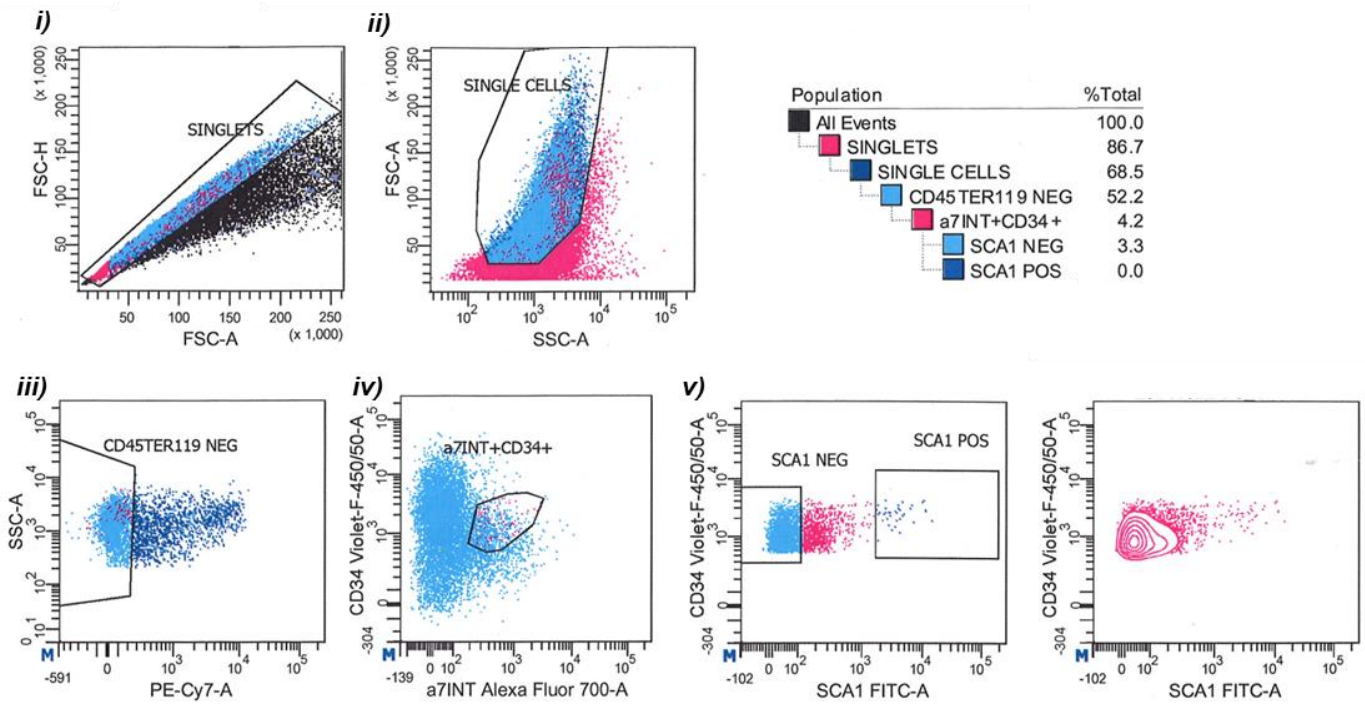
B

Number of cells sorted from digested muscles

	n=1	n=2	n=3
P3	434 000	300 000	250 000
P14	400 000	356 000	232 000
Adult (8 weeks)	105 000	63 000	98 000

99

Figure 3 – Gene expression dynamics of BMP signaling pathway components in isolated satellite cells of neonatal, juvenile and adult mice.

Diagrams depict the relative mRNA copy numbers per 10^6 *Gapdh* mRNA copies of different *BMP* ligands (*Bmp2*, *4*, *5*, *6*, *7*, *13*, *14*), *Bmp1* metalloproteinase, BMP type I receptor *Alk3* (*Bmpr1a*), BMP target gene *Id1*, BMP antagonists *Nog* (encoding *noggin*), *Grem1* (encoding *gremlin)* and *Fst* (encoding *follistatin)* in satellite cells isolated from skeletal muscles of wild-type mice at different ages: P3, P14 or adult (8 weeks-old). Cells were isolated described in Figure 2. Values are shown as means ± SEM.

Figure 3
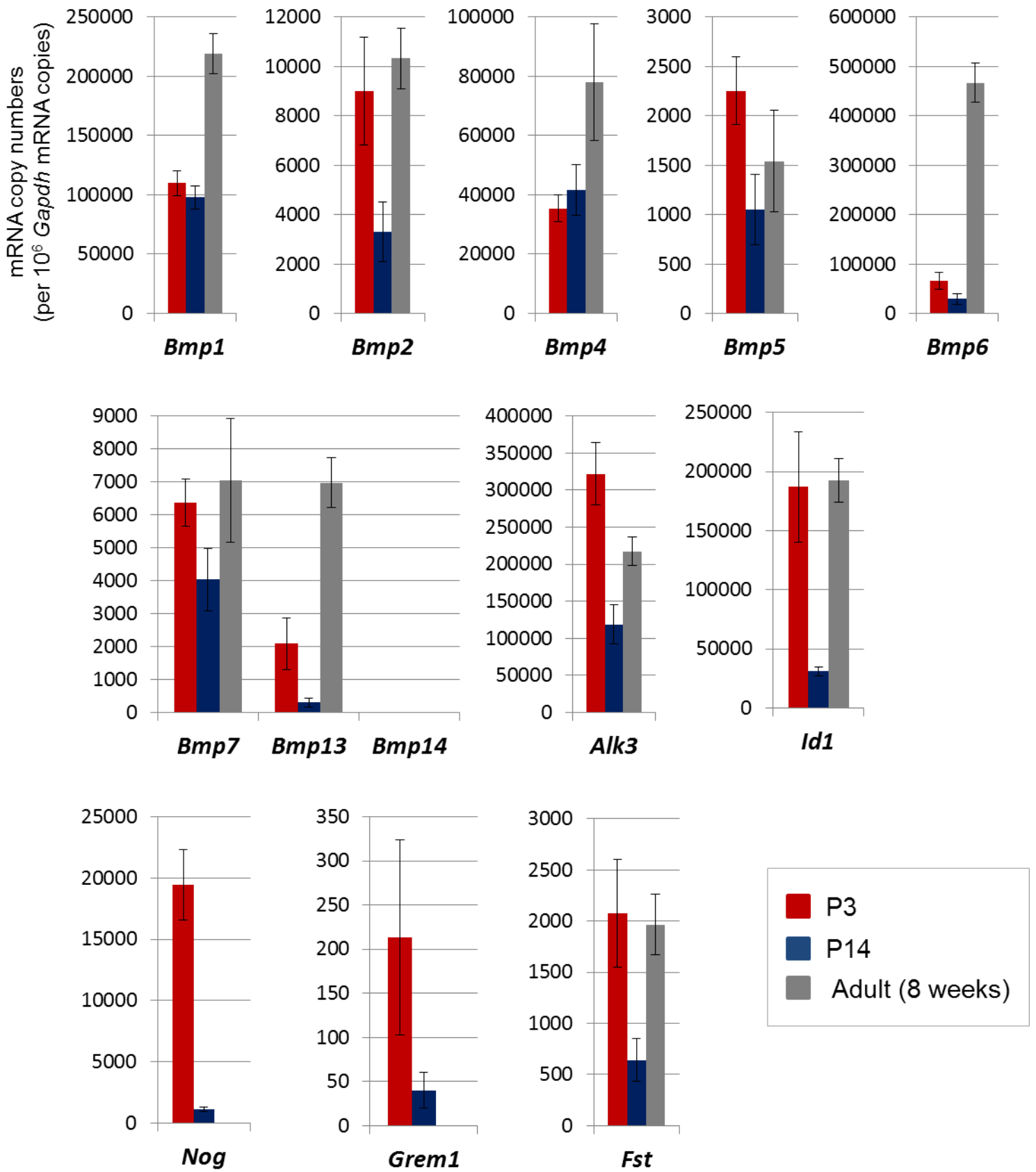
Figure 4 - Cre/Lox system used to abrogate the BMP signaling pathway through inhibitory *Smad6* overexpression in Pax7$^+$ cells.

(A) Scheme of *Rosa26-Lox-Stop-Lox-humanSMAD6-IRES-EGFP* and *Pax7$^{CreERT2/+}$* loci of the used transgenic mice models.

(B) Image of a 1.5% agarose gel supplemented with ethidium bromide showing an example of PCR products for genotyping the litters obtained from crosses of the latter mice: mutant *Rosa26* locus at 249 bp (lanes 3, 4 and 6), WT *Rosa26* locus at 585 bp (lanes 3, 5 and 6), and the *Pax7* locus containing the *Cre* at 870 bp (lanes 5 and 6).

(C) Scheme of the experimental protocol: adult mice were injected with tamoxifen for five consecutive days; adult mice were sacrificed the third day after the last tamoxifen injection; skeletal muscles were collected and processed to isolate satellite-cell derived primary myoblasts with the pre-plating method; cells were cultured in proliferation medium for four days after which the RNA was extracted.

(D) Image of a 1.5% agarose gel supplemented with ethidium bromide showing the presence or absence of *human SMAD6* PCR product (using primers specific for the human sequence). The PCR was performed on cDNA synthesized from RNA extracted from cultured satellite cell-derived primary myoblasts from either tamoxifen treated *Pax7$^{CreERT2/+}$* control mice (lane 2) or tamoxifen treated *Pax7$^{CreERT2/+}$;RS6$^{+/-}$* mice (lane 3). The presence of the band in lane 3 reflects that recombination occurred in these experimental conditions.

(E) Chart showing the relative mRNA copy numbers per 10^6 *18S* rRNA of BMP target gene *Id1* in cultured satellite cell-derived primary myoblasts from tamoxifen injected mice (n=3 mice). Values are shown as dot plots together with the medians.

Figure 4

A

RS6 mice

| Rosa26 | Exon1 | STOP | huSmad6 | IRES-EGFP |

LoxP   LoxP

Pax7^{CreERT2/+} mice

| Pax7 | Cre-ER^{T2} |

B

1 2 3 4 5 6

1 – Ladder 100 bp
2 – Negative control (no gDNA)
3 – RS6 heterozygote
4 – RS6 homozygote
5 – Pax7$^{CreERT2/+}$
6 – Pax7$^{CreERT2/+}$;RS6$^{+/-}$

C

adult ————————————————→ Days

Tamoxifen (ip)   Sacrifice and   RNA extraction
                    culture of satellite
                    cell-derived
                    primary myoblasts

D

1 2 3

1 – Ladder 100 bp
2 – Pax7$^{CreERT2/+}$ + TXF
3 – Pax7$^{CreERT2/+}$;RS6$^{+/-}$ + TXF

E

mRNA copy numbers (per 10^6 18S rRNA copies)

200
150
100
50
0

Id1

▲ Pax7$^{CreERT2/+}$ + TXF
○ Pax7$^{CreERT2/+}$;RS6$^{+/-}$ + TXF

103

Figure 5 – Isolating satellite cells expressing GFP by FACS.

(A) Diagrams depict the gates used to sort Pax3$^+$ satellite cells expressing GFP from *Pax3$^{GFP/+}$* mice, which served as positive controls.

(B) Diagrams depicting the gates used to sort cells expressing GFP from *Pax7$^{CreERT2/+}$;RS6$^{+/-}$* tamoxifen treated mice. In the latter mice, no GFP positive cells were isolated using these gates.

Figure 5

A

Pax3^{GFP/+} mice

B

Pax7^{CreERT2/+};RS6^{+/-} + TXF

105
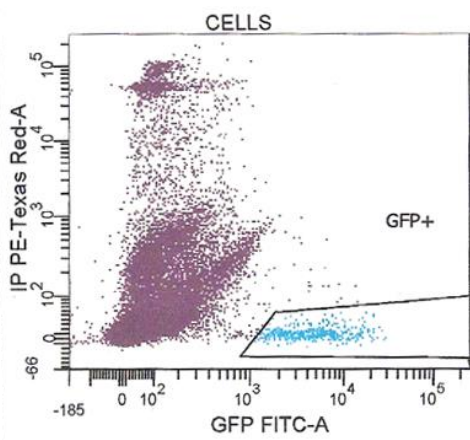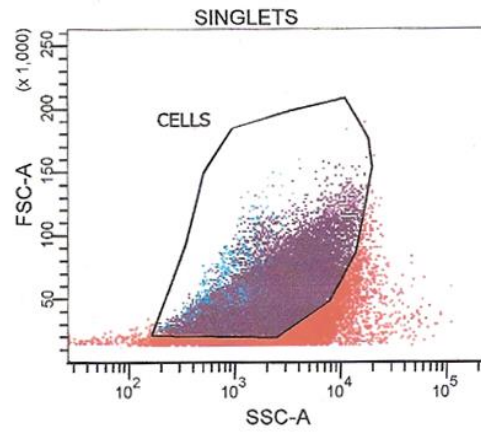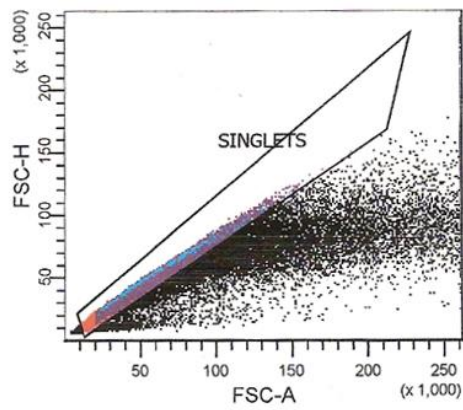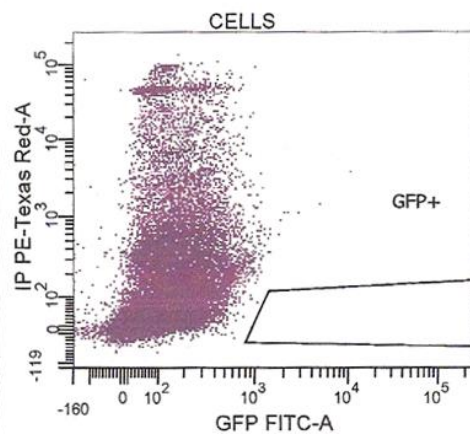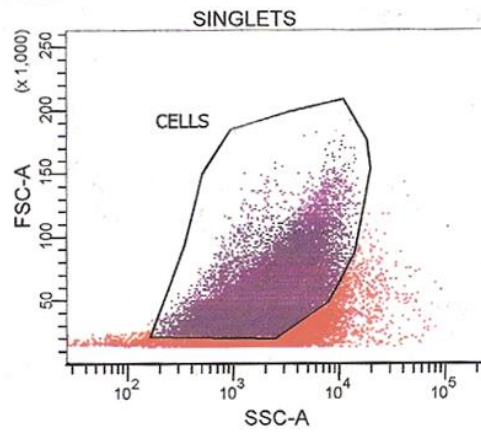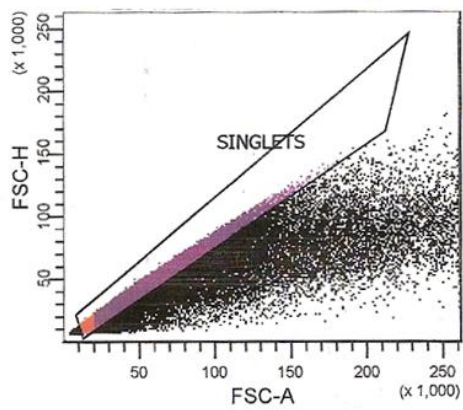
Figure 6 – Isolating satellite cells from skeletal muscles of *Pax7^{CreERT2/+};RS6^{+/-}* mice by FACS.

Diagrams depict the gates used to isolate satellite cells, as described in Figure 2 (using the cell surface markers: CD45$^-$, Ter119$^-$, CD34$^+$, α7-Integrin$^+$ and Sca1$^-$), from **(A)** *Pax7^{CreERT2/+};RS6^{+/-}* untreated adult mice and from **(B)** *Pax7^{CreERT2/+};RS6^{+/-}* adult mice treated for five consecutive days with tamoxifen and sacrificed the third day after the last injection. In the tamoxifen treated mice, the proportion of Sca1 negative cells was reduced compared to the non-tamoxifen treated mice (from 2% to 0.2% of the total cell population, as shown in the tables), resulting in insufficient numbers of sorted cells for *in vitro* assays.

Figure 6

A

Pax7^{CreERT2/+};RS6^{+/-}

Population	%Total
All Events	100.0
SINGLETS	62.4
SINGLE CELLS	48.7
viability	48.6
CD45TER119 NEG	23.0
a7INT+CD34+	4.0
SCA1 NEG	2.0
SCA1 POS	0.9
SCA1 MED	0.7

B

Pax7^{CreERT2/+};RS6^{+/-} + TXF

Population	%Total
All Events	100.0
SINGLETS	63.0
SINGLE CELLS	57.1
viability	57.0
CD45TER119 NEG	20.2
a7INT+CD34+	2.4
SCA1 NEG	0.2
SCA1 POS	0.3
SCA1 MED	1.4

107
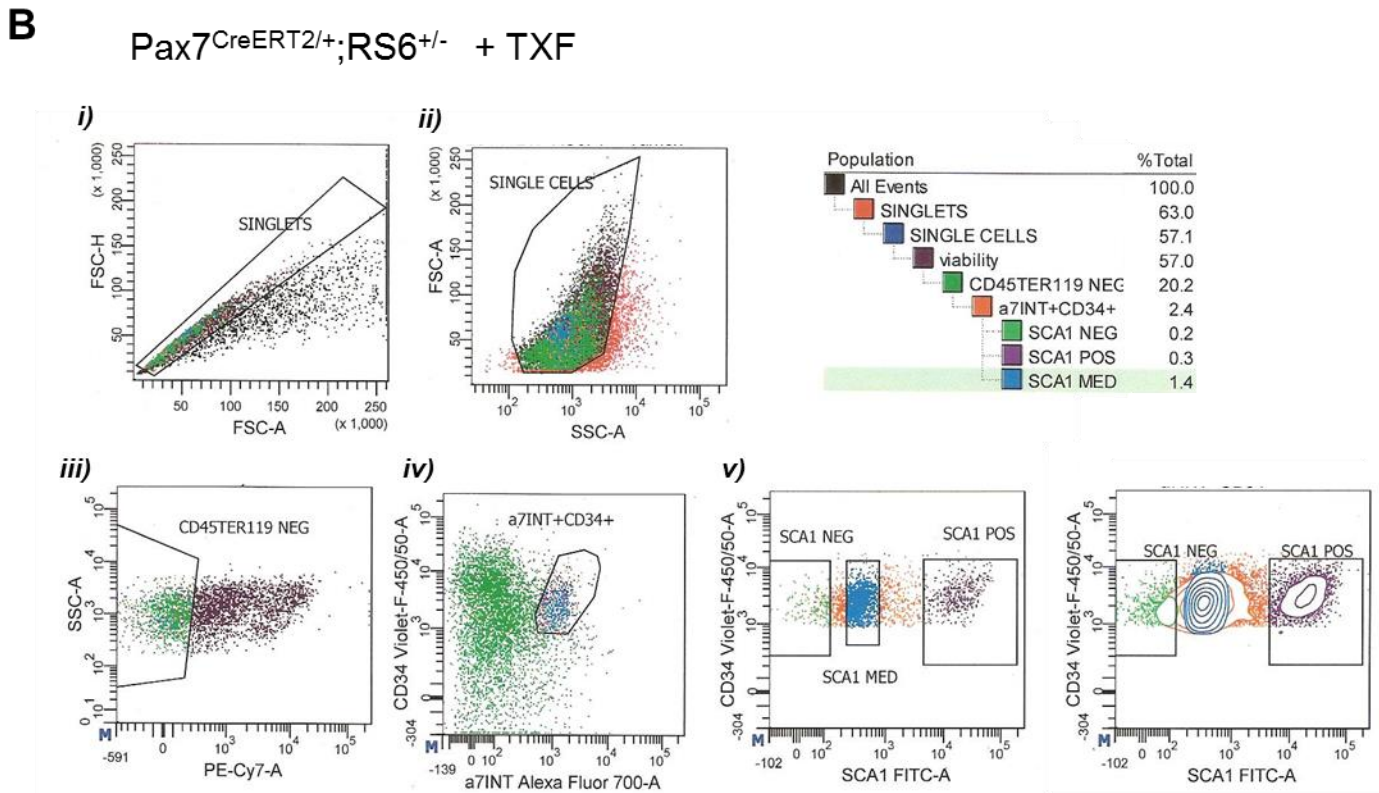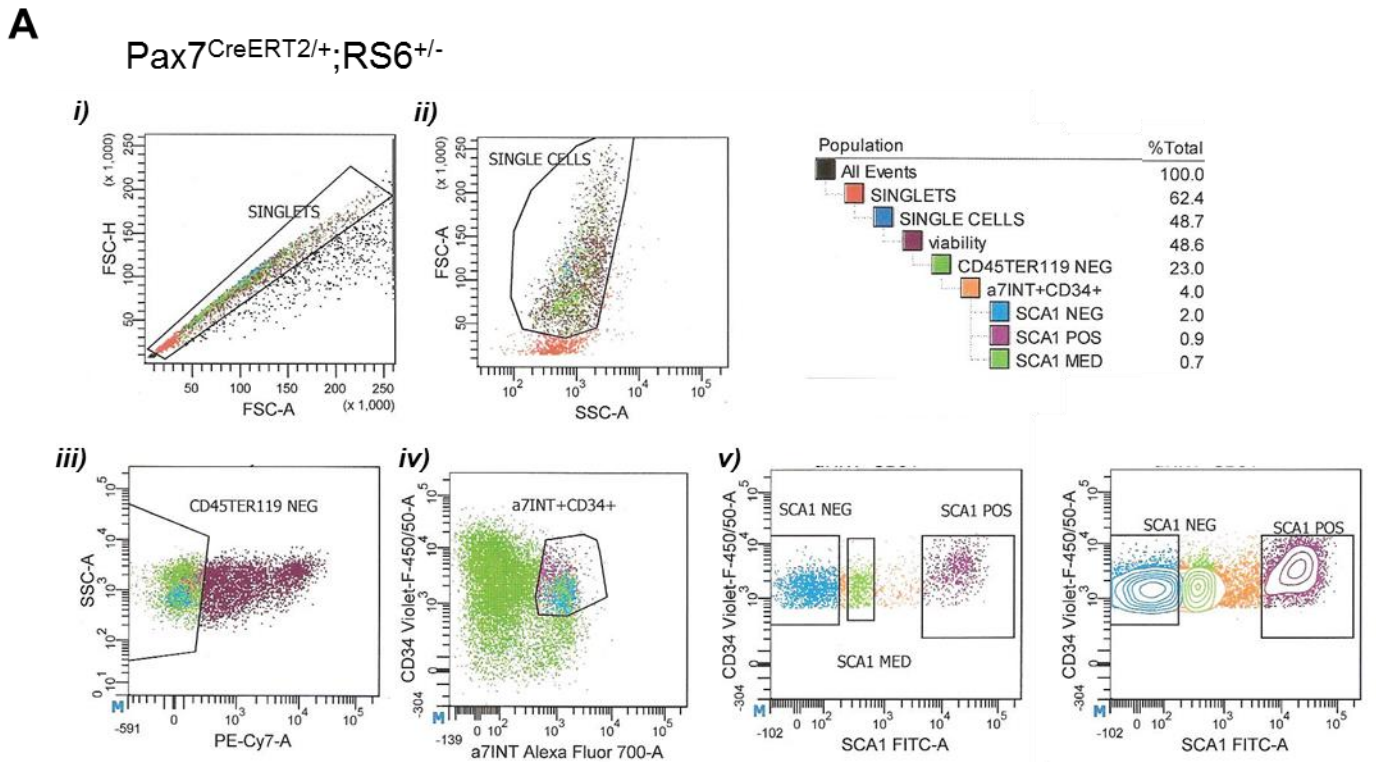
Figure 7 – Effect of *Smad6* overexpression in adult satellite cells *in vivo*.

(A) Scheme of the experimental protocol: $Pax7^{CreERT2/+};RS6^{+/-}$ and control $Pax7^{CreERT2/+}$ adult mice were injected with tamoxifen for five consecutive days; adult mice were sacrificed 24 days after the last tamoxifen injection.

(B) Fluorescence images following immunostaining against Pax7 in red (arrows), against laminin in green and DAPI stained nuclei in blue of mid-belly transverse sections of *TA* from both $Pax7^{CreERT2/+};RS6^{+/-}$ and $Pax7^{CreERT2/+}$ tamoxifen treated mice (scale bar is 20 μm).

C) Chart depicts the number of Pax7$^+$ nuclei quantified per 100 fibers on immunostainings of transverse sections of *TA* muscles from control $RS6^{+/-}$ mice (n=4, black and white squares), control tamoxifen treated $Pax7^{CreERT2/+}$ mice (n=4, black triangles) and tamoxifen treated $Pax7^{CreERT2/+};RS6^{+/-}$ mice (n=3, white circles). Values are shown as dot plots together with the medians.

Figure 7

A

B

Pax7$^{CreERT2/+}$ + TXF   Pax7$^{CreERT2/+}$;RS6$^{+/-}$ + TXF

C

- ▣ RS6$^{+/-}$
- ▲ Pax7$^{CreERT2/+}$ + TXF
- ⊙ Pax7$^{CreERT2/+}$;RS6$^{+/-}$ + TXF
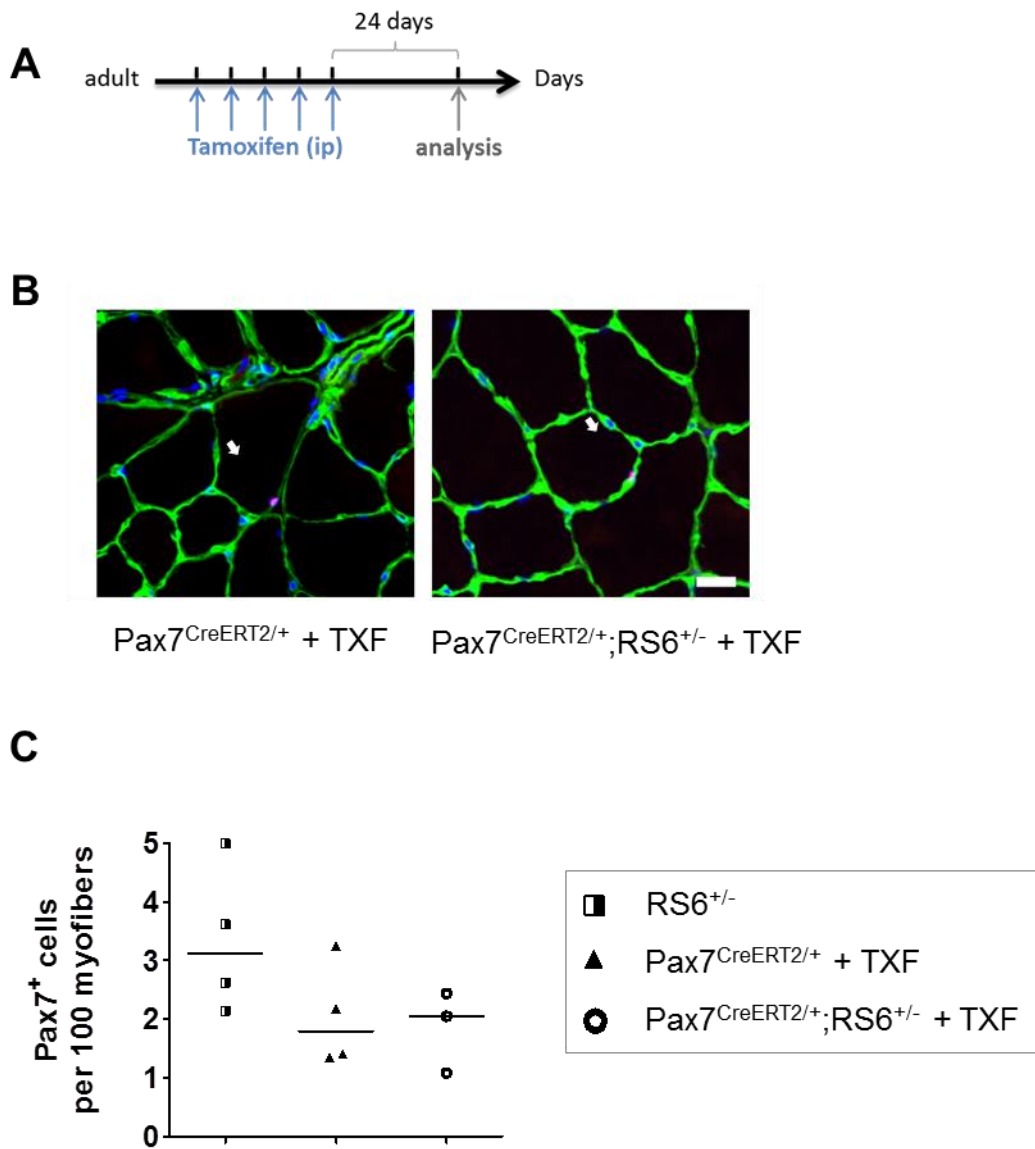
Figure 8 – Abrogation of BMP signaling in cultured FACS isolated satellite cell-derived primary myoblasts.

(A) Scheme of the experimental protocol: At day 0 (D0) satellite cells from $Pax7^{CreERT2/+}$ or $Pax7^{CreERT2/+};RS6^{+/-}$ adult mice were isolated using FACS (as described in Figure 2) and cultured in proliferation media; at D2-4 they were either not treated (control, CT), or treated with 1 μM hydroxytamoxifen (4-OHT) or 50 ng/mL of recombinant mouse noggin protein; at D5 cells were either fixed for immunocytochemistry or collected for RNA extraction.

(B) Chart depicts the relative mRNA copy numbers per 10^6 *Gapdh* mRNA of *human SMAD6* or **(C)** BMP target gene *Id1* from cultured satellite cells isolated from $Pax7^{CreERT2/+};RS6^{+/-}$ mice. Values are shown as dot plots together with the median.

(D) Cells were cultured in low density for a proliferation assay comparing non-treated and treated satellite cells isolated by FACS from skeletal muscles of $Pax7^{CreERT2/+}$ and $Pax7^{CreERT2/+};RS6^{+/-}$ mice. The number of cells per colony was counted from at least three wells per condition and per mouse; at least 50 colonies of cells per condition and per mouse were quantified. Data are shown as Whiskers-Tukey box plots together with the medians. *P* values were calculated using the nonparametric *U*-test.

Figure 8
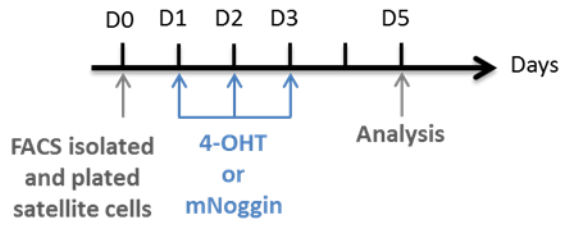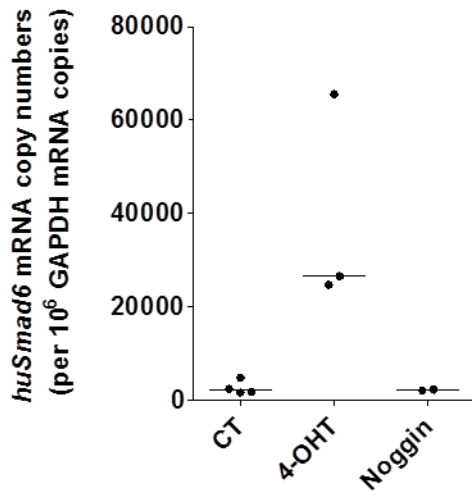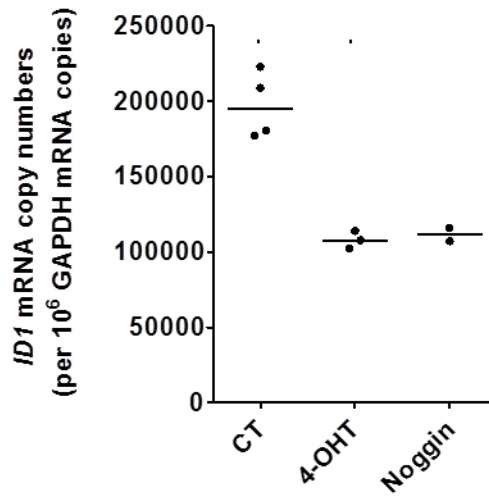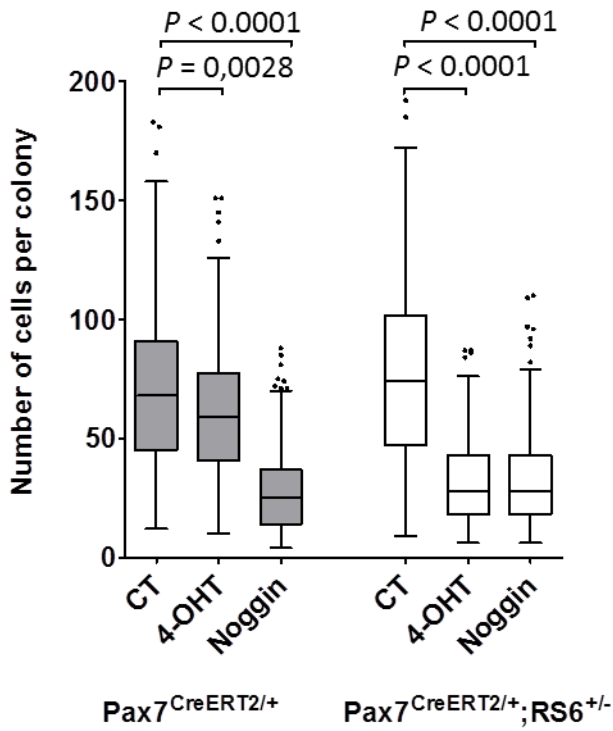
Figure 9 – Cell imaging following abrogation of the BMP signaling pathway in satellite cell-derived primary myoblasts from *Pax7$^{CreERT2/+}$;RS6$^{+/-}$* mice.

Satellite cells were isolated by FACS from skeletal muscles of *Pax7$^{CreERT2/+}$;RS6$^{+/-}$* mice. The cells were cultured in low density for a proliferation assay comparing non-treated cells (control) and treated cells with either hydroxytamoxifen (4-OHT) or noggin as described in Figure 8A. Representative fluorescence images of single colonies in which nuclei stained with DAPI are blue and immunostaining against Ki67, MyoD, myogenin or myosin heavy chain in red (from top to bottom). Scale bar is 100 µm.

Figure 9

Figure 10 – Quantitative analysis following abrogation of BMP signaling in cultured *Pax7^{CreERT2/+};RS6^{+/-}* satellite cell-derived primary myoblasts.

The experimental protocol of the proliferation assay was described in Figure 8A. Cells from *Pax7^{CreERT2/+};RS6^{+/-}* adult mice were either not treated (control, CT) or treated with 1 μM hydroxytamoxifen (4-OHT) or 50 ng/mL of recombinant mouse noggin protein.

The number of positive cells is given as a percentage of the total number of stained cells per colony following immunostaining against **(A)** Ki67, **(B)** myogenin (MyoG) and **(C)** myosin heavy chain (MHC). The quantification was performed on 13 to 20 colonies per culture (n=3 cultures, each derived from cells isolated from one mouse). Data is shown as Whiskers-Tukey box plots together with the medians. *P* values were calculated using the nonparametric *U*-test.

(D-F) Data is also shown as cumulative rank ogives of the numbers of myoblasts expressing the protein of interest in untreated (blue), 4-OHT treated (red) and noggin treated (green) cultures. The number of cells that are positively stained for **(D)** Ki67, **(E)** myogenin (MyoG) and **(F)** myosin heavy chain (MHC) is plotted on the horizontal axis. The vertical axis corresponds to the individual ranks, normalized to the rank total for each experiment to permit comparison of data sets of different sample size.

(G-H) Charts depict the relative mRNA copy numbers per 10^6 *GAPDH* mRNA of **(G)** *p21* and **(H)** *p57* from FACS-isolated and cultured satellite cells isolated from *Pax7^{CreERT2/+};RS6^{+/-}* mice. Cells were either not treated (CT, n=4) or treated with 1 μM 4-OHT (n=3) or 50 ng/mL of recombinant mouse noggin protein (n=2, due to the low "n" number this experiment needs to be repeated, it is included here to show the tendency of the results). Data is shown as dot plots together with the median.

Figure 10
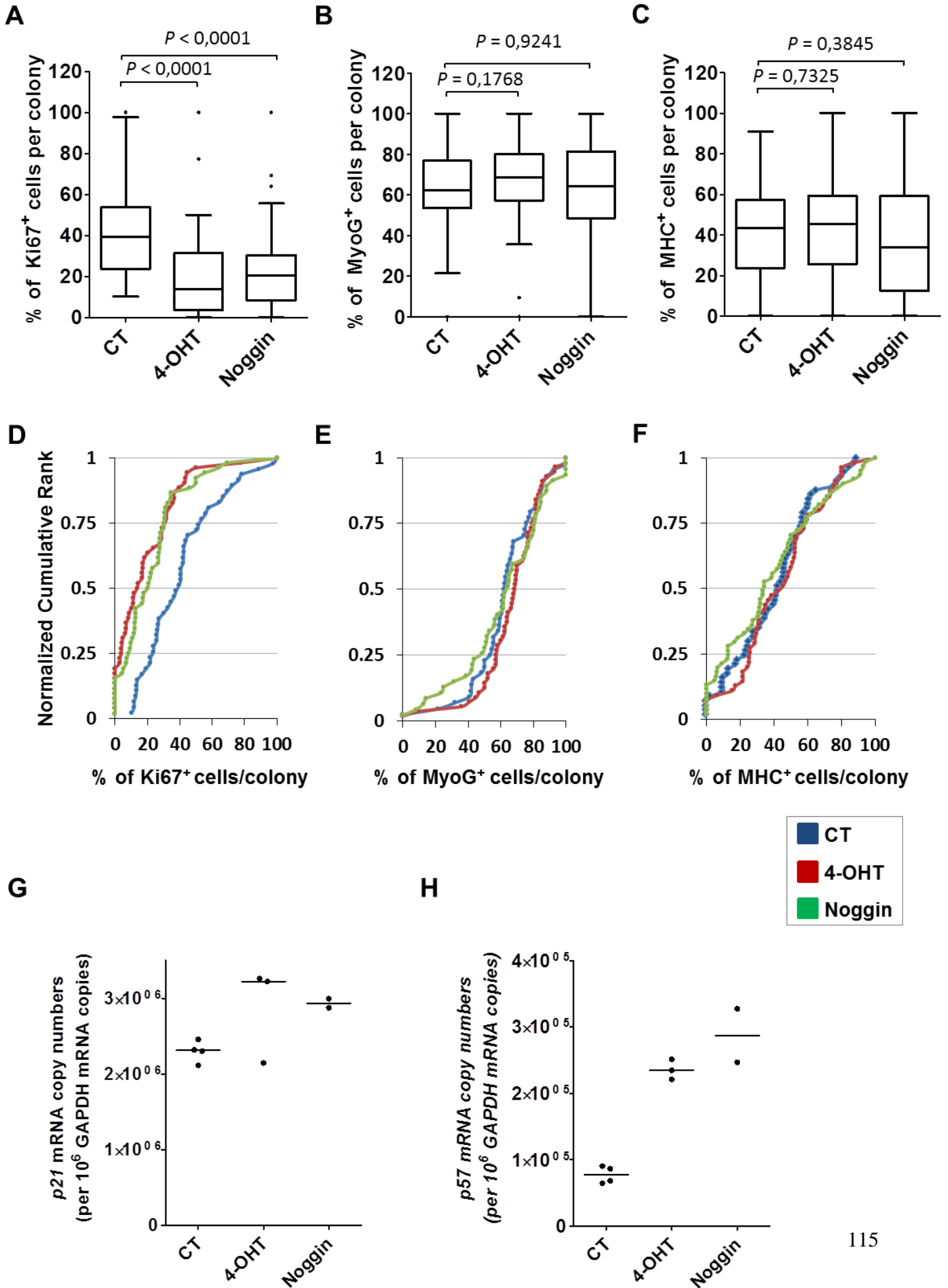
Figure 11 – Consequences of Smad6 mediated abrogation of BMP signaling in neonatal satellite cells for juvenile muscle growth.

(A) Scheme of the experimental protocol: mice were injected with tamoxifen at P7 and P9 and sacrificed at the age of one month.

(B) Charts depict the *TA*, *EDL* and *soleus* wet muscle weights from control untreated *Pax7$^{CreERT2/+}$;RS6$^{+/-}$* mice (n=8 muscles, 4 mice, white circles) and tamoxifen treated *Pax7$^{CreERT2/+}$;RS6$^{+/-}$* mice (n=5 muscles, 3 mice, black circles). Values are shown as dot plots together with the median. *P* values were calculated using the nonparametric *U*-test.

(C) Chart depicts the quantification of the breadth of *TA* muscle fibers, analyzed on mid-belly muscle sections following immunostaining against laminin, from control tamoxifen treated *RS6$^{+/-}$* mice (n=3, grey background and white stripes) and control tamoxifen treated *Pax7$^{CreERT2/+}$* mice (n=5, grey and white squares), control untreated *Pax7$^{CreERT2/+}$;RS6$^{+/-}$* mice (n=3, dark grey), all compared to tamoxifen treated *Pax7$^{CreERT2/+}$;RS6$^{+/-}$* mice (n=4, white). Values are shown as Whiskers-Tukey box plots together with the medians. *P* values were calculated using the nonparametric *U*-test.

(D) The latter data is also presented in a histogram depicting the distribution of the quantified *TA* muscle fiber breadth.

(E) Diagram depicts the number of myonuclei per isolated muscle fiber from *EDL* muscles from control tamoxifen treated *RS6$^{+/-}$* mice (n=51 isolated fibers from 3 mice), control tamoxifen treated *Pax7$^{CreERT2/+}$* mice (n=128 isolated fibers from 5 mice) and control untreated *Pax7$^{CreERT2/+}$;RS6$^{+/-}$* mice (n=60 isolated fibers, from 3 mice), all compared to tamoxifen treated *Pax7$^{CreERT2/+}$;RS6$^{+/-}$* mice (n=66 isolated fibers from 4 mice).

(F) Number of Pax7^{+} satellite cells per isolated muscle fiber from EDL muscles from control tamoxifen treated *RS6$^{+/-}$* mice (n=52 isolated fibers from 3 mice), control tamoxifen treated *Pax7$^{CreERT2/+}$* mice (n=128 isolated fibers, 5 mice) and control untreated *Pax7$^{CreERT2/+}$;RS6$^{+/-}$* mice (n=60 isolated fibers from 3 mice), all compared to tamoxifen treated *Pax7$^{CreERT2/+}$;RS6$^{+/-}$* mice (n=73 isolated fibers from 4 mice). Values are shown as Whiskers-Tukey box plots together with the medians. *P* values were calculated using the nonparametric *U*-test.
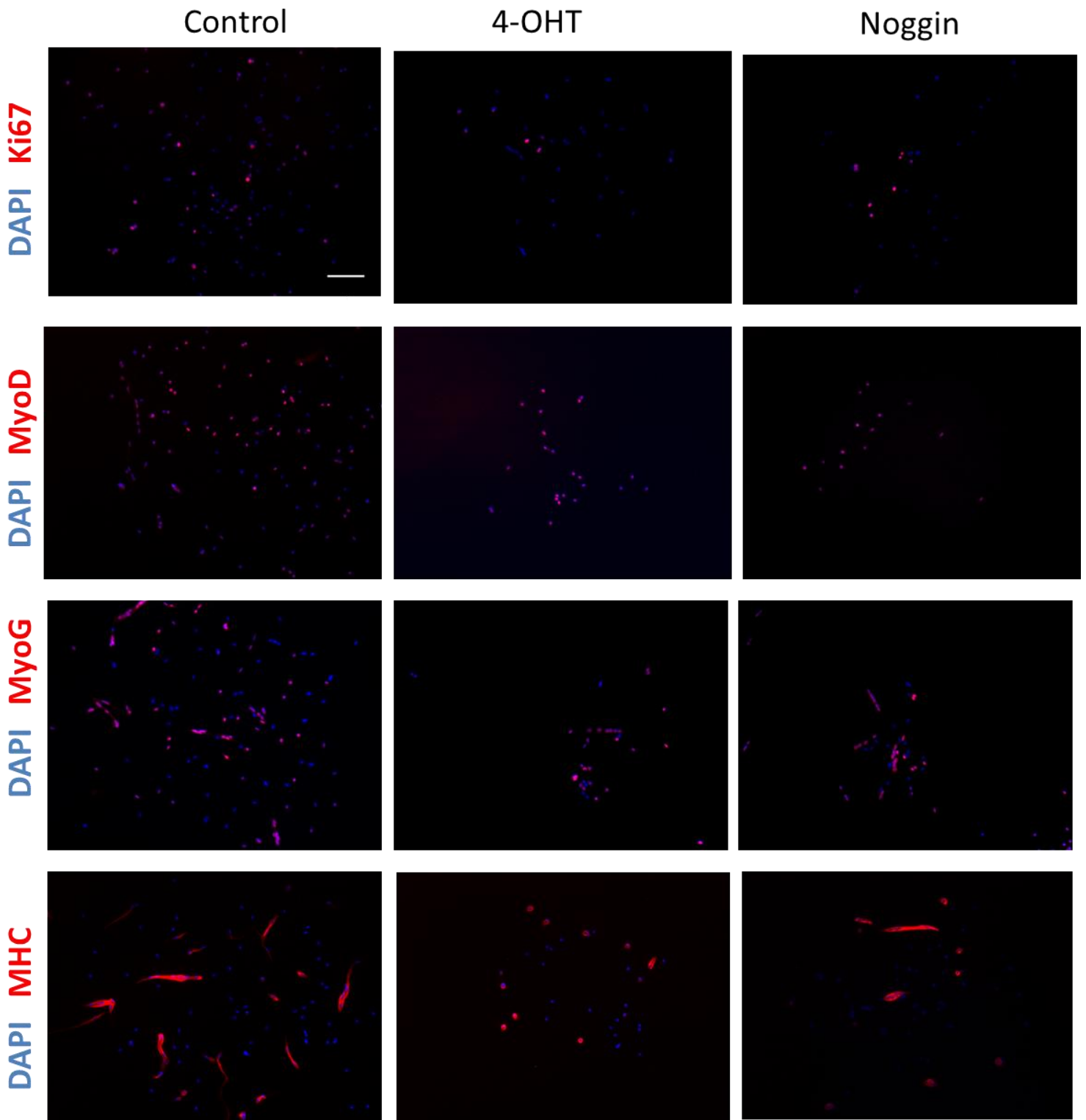
Figure 11

A

P7 P9 P28 Days after birth

Tamoxifen (ip)   analysis

B

P = 0,0055   *P* = 0,2942   *P* = 0,0027

Wet muscle weight (mg)

TA   EDL   Soleus

C

P < 0,0001

Myofiber breadth (µm)

D

Fiber frequency (%)

Fiber breadth (µm)

RS6^+/- + TXF
Pax7^CreERT2/+ + TXF
Pax7^CreERT2/+;RS6^+/-
Pax7^CreERT2/+;RS6^+/- + TXF

E

P < 0,0001

Number of nuclei per isolated single fiber (EDL)

F

P < 0,0001
P = 0,0009
P = 0,0035

Number of Pax7^+ nuclei per isolated single fiber (EDL)

117

Figure 12 – Consequences of Smad6 mediated abrogation of BMP signaling in neonatal satellite cells for muscle growth up to adulthood.

(A) Scheme of the experimental protocol: $Pax7^{CreERT2/+};RS6^{+/-}$ mice and control $RS6^{+/-}$ mice were injected with tamoxifen at P7 and P9, and sacrificed at the age of two months. Additional $Pax7^{CreERT2/+}$ control mice were sacrificed at the age of three months.

(B) Histogram presenting the distribution of *TA* muscle fiber breadth quantified on *TA* mid-belly muscle sections, in which each fiber was delineated with laminin immunostaining, from control tamoxifen treated $RS6^{+/-}$ mice (n=3, grey background and white stripes), control untreated $Pax7^{CreERT2/+}$ mice (n=3, black background and white dots) compared to tamoxifen treated $Pax7^{CreERT2/+};RS6^{+/-}$ mice (n=3, white).
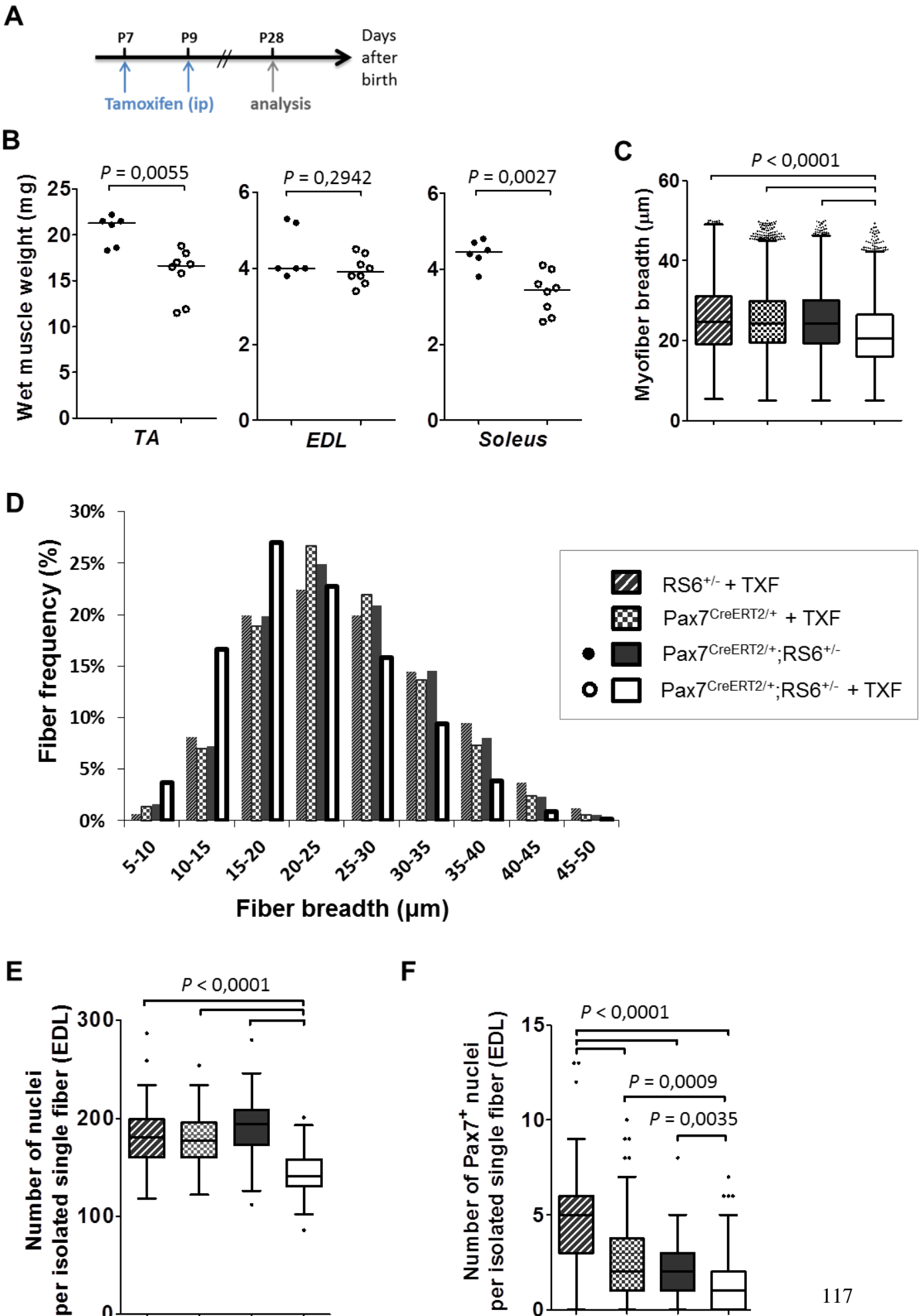
(C) Chart depicts the quantification of the breadth of *TA* muscle fibers, analyzed on mid-belly muscle sections following immunostaining against laminin, from control tamoxifen treated $RS6^{+/-}$ mice (n=3, black triangles), control untreated $Pax7^{CreERT2/+}$ mice (n=3, black diamonds) compared to tamoxifen treated $Pax7^{CreERT2/+};RS6^{+/-}$ mice (n=3, white circles). Values are shown as Whiskers-Tukey box plots together with the medians. *P* values were calculated using the nonparametric *U*-test.

(D) Diagram depicts the number of Pax7$^+$ nuclei quantified per 100 myofibers on *TA* mid-belly transverse muscle sections from control tamoxifen treated $RS6^{+/-}$ mice (n=3,black triangles), control untreated $Pax7^{CreERT2/+}$ mice (n=3, black diamonds) compared to tamoxifen treated $Pax7^{CreERT2/+};RS6^{+/-}$ mice (n=3,white circles).

(E) Fluorescence images of immunostaining against Pax7 in red (highlighted with arrows), nuclei stained with DAPI in blue and immunostaining against laminin in green of mid-belly transverse sections of *TA* muscles from control tamoxifen treated $RS6^{+/-}$ mice and control untreated $Pax7^{CreERT2/+}$ mice compared to tamoxifen treated $Pax7^{CreERT2/+};RS6^{+/-}$ mice. Scale bar is 20 μm. Values are shown as dot plots together with the median.

Figure 12

A

B

C

D

E

RS6$^{+/-}$ + TXF   Pax7$^{CreERT2/+}$ Pax7$^{CreERT2/+}$;RS6$^{+/-}$ + TXF
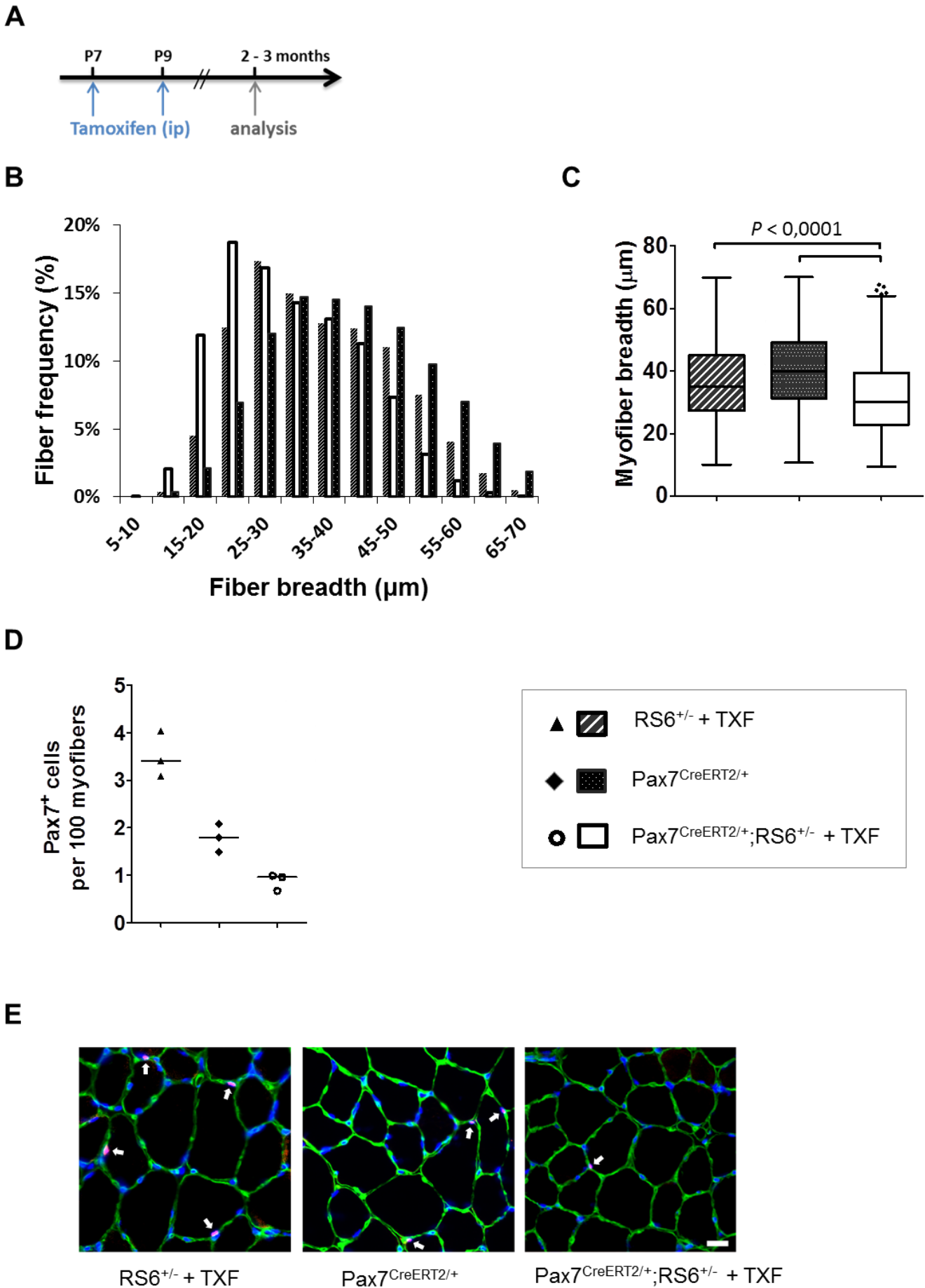
Figure 13 – Effect of *Smad6* overexpression in terminally differentiated muscle in juvenile mice.

(A) Scheme of *Rosa26-Lox-Stop-Lox-humanSMAD6-IRES-EGFP* and *HSA-Cre* loci of the employed transgenic mice models.

(B) Image of immunoblots showing GFP and actin bands, along with the Ponceau staining. Total proteins were extracted from the *triceps* muscle of two *HSA-Cre$^{+/-}$;RS6$^{+/-}$* mince and two *RS6$^{+/-}$* mice that were one month of age.

(C) Chart depicts the relative mRNA copy numbers per 10^6 *Gapdh* mRNA of *human SMAD6*. RNA was extracted from *gastrocnemius* muscle of one month old *RS6$^{+/-}$* mice (n=3, black dots) and *HSA-Cre$^{+/-}$;RS6$^{+/-}$* mice (n=5, white dots).

(D) Diagram illustrates the body weights presented as means during postnatal growth of *HSA-Cre$^{+/-}$;RS6$^{+/-}$* mice (n=5-11 for each time point) and *RS6$^{+/-}$* mice (n=3-5 for each time point). Data are presented as means ± SEM.

(E) Charts depict *TA* and *EDL* wet muscle weights of one month old *HSA-Cre$^{+/-}$;RS6$^{+/-}$* mice (n=8-10 muscles from 5 mice) and *RS6$^{+/-}$* mice (n=6 muscles from 3 mice).

(F) Diagram illustrates the total number of fibers counted on *TA* mid-belly muscle sections from one months old control *RS6$^{+/-}$* mice (n=3) compared to *HSA-Cre$^{+/-}$;RS6$^{+/-}$* mice (n=5).

(G) Chart depicts the quantification of the breadth of *TA* muscle fibers, analyzed on mid-belly muscle sections following immunostaining against laminin, from one months old control *RS6$^{+/-}$* mice (n=3) compared to *HSA-Cre$^{+/-}$;RS6$^{+/-}$* mice (n=5). Values are shown as Whiskers-Tukey box plots together with the medians.

(H) Histogram presenting the distribution of *TA* muscle fiber breadth size.

(I) Chart depicting the number of Pax7^{+} satellite cells per 100 myofibers counted on *TA* mid-belly muscle sections from one months old control *RS6$^{+/-}$* mice (n=3) compared to *HSA-Cre$^{+/-}$;RS6$^{+/-}$* mice (n=5). Unless stated otherwise, values are shown as dot plots together with the medians. *P* values were calculated using the nonparametric *U*-test.

Figure 13
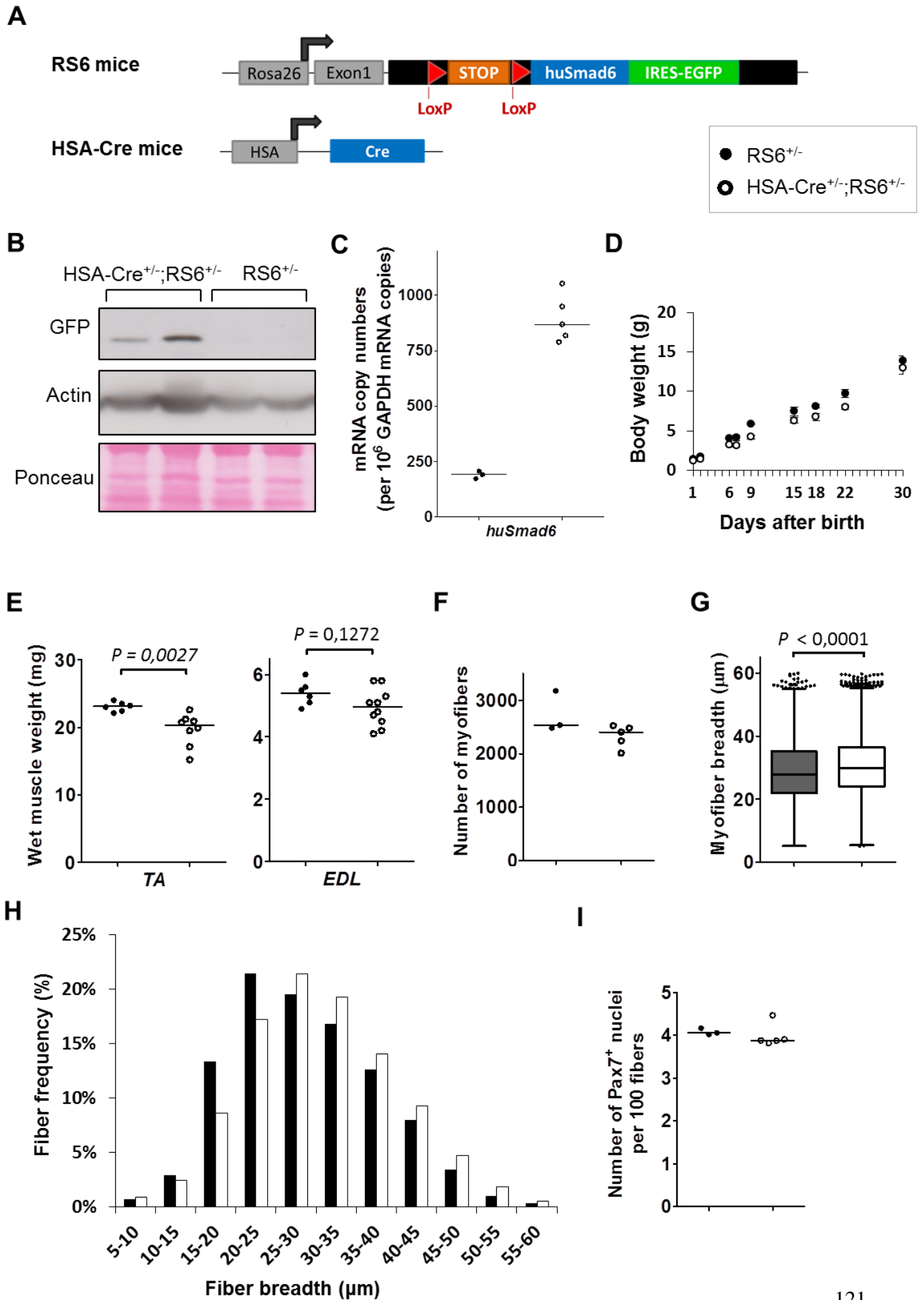
Figure 14 – Effect of *Smad6* overexpression in terminally differentiated muscle in adult mice.

(A) Charts depict *TA*, *EDL* and *Soleus* wet muscle weights of two months old *HSA-Cre$^{+/-}$;RS6$^{+/-}$* mice (n=8 muscles from 4 mice, black dots) and control *RS6$^{+/-}$* mice (n=8 muscles from 4 mice, white dots).

(B) Histogram presenting the distribution of *TA* muscle fiber breadth quantified on *TA* mid-belly muscle sections, in which each fiber was delineated with laminin immunostaining, from two months old control *RS6$^{+/-}$* mice (n=4, black) compared to *HSA-Cre$^{+/-}$;RS6$^{+/-}$* mice (n=4, white).

(C) Chart depicts the quantification of the myofiber breadth quantified on *TA* mid-belly muscle sections two months old control *RS6$^{+/-}$* mice (n=4) compared to *HSA-Cre$^{+/-}$;RS6$^{+/-}$* mice (n=4). Values are shown as Whiskers-Tukey box plots together with the medians.

(D) Diagram illustrates the total number of fibers counted on *TA* mid-belly muscle sections from two months old control *RS6$^{+/-}$* mice (n=4) compared to *HSA-Cre$^{+/-}$;RS6$^{+/-}$* mice (n=5).

(E) Chart depicts the number of Pax7^{+} satellite cells per 100 myofibers counted on *TA* mid-belly muscle sections from two months old control *RS6$^{+/-}$* mice (n=4, black) compared to *HSA-Cre$^{+/-}$;RS6$^{+/-}$* mice (n=4, white). Of note, the data regarding the quantification of Pax7^{+} satellite cells of the control *RS6$^{+/-}$* mice have also been depicted in Figure 7C.

(F) Example of a fluorescence image following immunostaining against Pax7 in red (arrows), DAPI stained nuclei in blue and immunostaining against laminin in green of mid-belly transverse sections of *TA* muscle from control *HSA-Cre$^{+/-}$* mice compared to *HSA-Cre$^{+/-}$;RS6$^{+/-}$* mice. Scale bar is 20 μm. Unless stated otherwise, values are shown as dot plots together with the medians. *P* values were calculated using the nonparametric *U*-test.

Figure 14

A

B

C

D

E

F

RS6$^{+/-}$ HSA-Cre$^{+/-}$;RS6$^{+/-}$
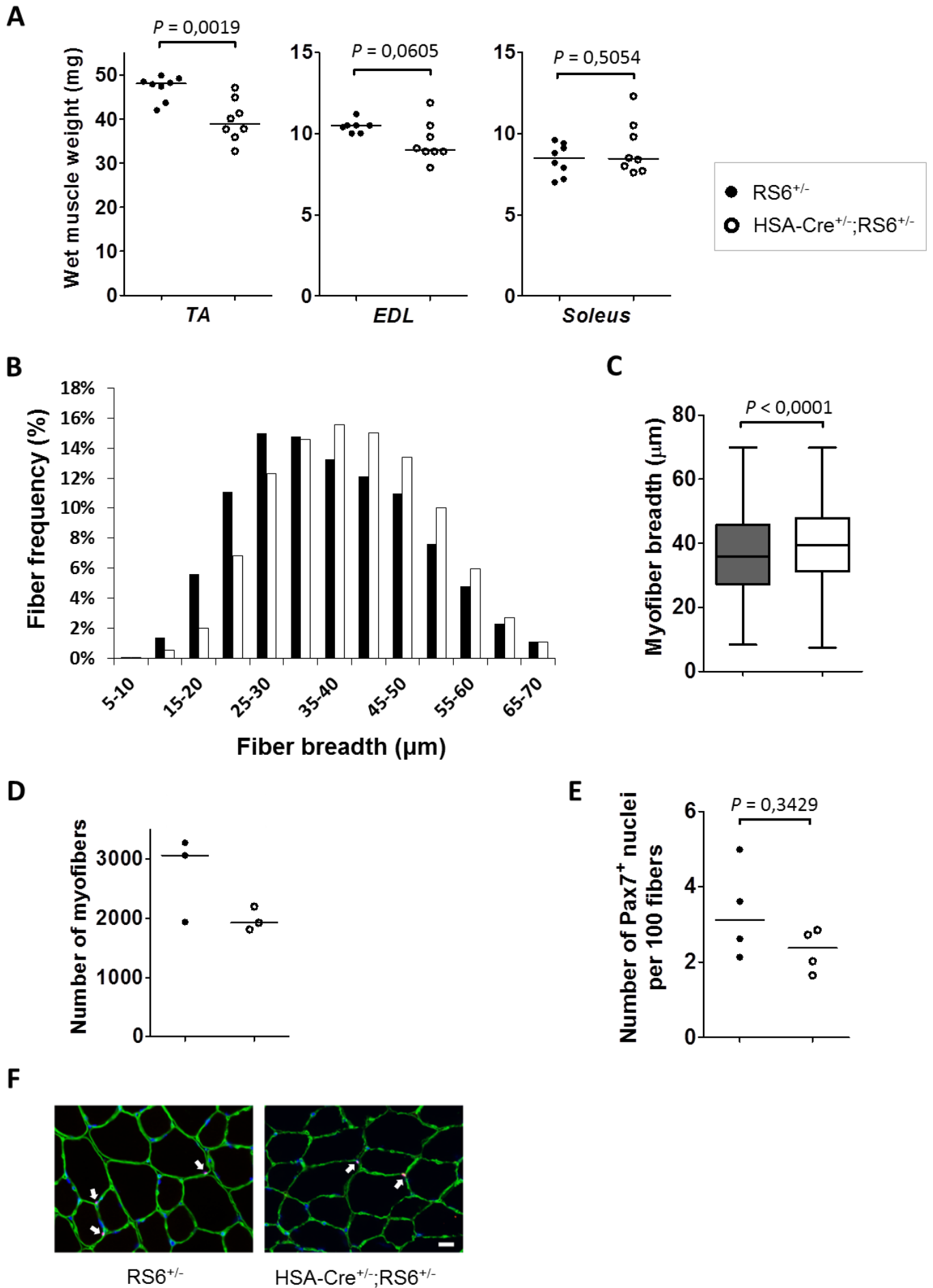
5- Manuscript of the article in preparation for submission

Next, I enclosed the manuscript in preparation for publication in an international peer reviewed scientific journal, which comprises both my herein described results, as well as those from a previous PhD student of our group, Dr Elija Schirwis, who investigated the role of BMP signaling during postnatal growth using a different methodology, e.g. using an AAV expression vector to overexpress the BMP antagonist noggin. Importantly, his results complement my results and therefore strengthen my conclusions, which I will discuss in further detail the General Discussion chapter.

Article 1

Manuscript

BMP signaling controls satellite cell dependent postnatal muscle growth.

Amalia Stantzou[1,2,3,§], Elija Schirwis[3,§], Sandra Bücker[4], Sonia Alonso-Martin[3], Faouzi Zarrouki[1], Etienne Mouisel[3,5], Cyriaque Beley[1], Luis Garcia[1], Carmen Birchmeier[6], Thomas Braun[4], Markus Schülke[2], Fabien Legrand[3,7], Frédéric Relaix[3,8], Helge Amthor[1]

[1]Université de Versailles Saint-Quentin-en-Yvelines, UFR des sciences de la santé, INSERM U1179, LIA BAHN CSM, 78180 Montigny-le-Bretonneux, France; [2]Department of Neuropediatrics & NeuroCure Clinical Research Center, Charité Universitätsmedizin Berlin, 13353 Berlin, Germany; [3]Sorbonne Universités, UPMC Univ Paris 06, INSERM, UMRS974, CNRS FRE3617, Center for Research in Myology, 75013 Paris, France; [4]Department of Cardiac Development and Remodeling, Max-Planck-Institute for Heart and Lung Research, 61231 Bad Nauheim, Germany; [5]Inserm UMR 1048, Université Paul Sabatier, Toulouse, France (present address); [6]Developmental Biology / Signal Transduction Group, Max Delbruck Center for Molecular Medicine, Robert-Rössle-Str. 10, 13125 Berlin, Germany; [7]Institut Cochin, Université Paris-Descartes, Centre National de la Recherche Scientifique (CNRS), UMR 8104, Paris, France ; [8]INSERM, Université Paris Est, Faculté de médecine, IMRB U955-E10, 94000 Creteil, France.

[§]equal contribution

*Correspondence to Helge Amthor (helge.amthor@uvsq.fr)

ABSTRACT

Postnatal growth of skeletal muscle largely depends on the expansion and differentiation of resident stem cells of postnatal skeletal muscle, so-called satellite cells. Here we demonstrate that Bone Morphogenetic Proteins (BMPs), a subfamily of diffusible morphogens of the TGF-β family of signaling molecules, regulate the generation of postnatal muscle satellite cells, thereby defining postnatal muscle growth. Postnatal skeletal muscle and satellite cells expressed BMP-ligands, -transmembrane receptor, -antagonists and up-regulated BMP-dependent intracellular signaling components. Treatment of postnatal mice with noggin, to antagonize BMP ligands, or satellite cell-targeted overexpression of Smad6, to cell-autonomously interfere with BMP signaling, decreased satellite cell proliferation and diminished the myonuclear recruitment during myofiber growth, which severely retarded muscle growth. Moreover, in lack of BMP signaling, such as following overexpression of noggin or Smad6 or in constitutive absence of BMP6 or BMP14, muscle depleted the adult satellite cell pool. Abrogation of BMP signaling in satellite cell-derived primary myoblasts strongly diminished cell proliferation alongside with up-regulated cell cycle inhibitors *p21* and *p57*, suggesting that cells gained quiescence. In conclusion, these results show that BMP signaling during postnatal muscle development is required for satellite cell dependent myofiber growth and the generation of adult muscle stem cell pool.

INTRODUCTION

The basic cellular units of skeletal muscle are myofibers, which are multinuclear syncytia capable of contraction. Myofibers are continuously formed during embryonic, fetal and postnatal/juvenile development from a source of mononuclear muscle progenitors. Multiple molecular events commit these precursors towards a myogenic commitment, in which the expression of the paired box genes Pax3/Pax7 followed by MyoD and other members of the myogenic regulatory factor family play a central role to gain myogenic identity (1). Terminal differentiation starts with expression of muscle specific proteins and this process coincides with multiple fusions of muscle precursors into myotubes and subsequent maturation in myofibers. However, differentiated muscle cells become mitotically quiescent (2). Therefore, continuous muscle growth requires a sufficient large pool of muscle precursors that from early embryonic development intermingle in between differentiated muscle cells (3). By the end of fetal development, muscle precursors typically locate between basal lamina and sarcolemma of muscle fibers and are henceforth called satellite cells (4). In mice, the number of muscle fibers that form a specific muscle is laid down during prenatal development. During the first three weeks of postnatal mouse development, muscle fibers grow by recruiting satellite cells thereby enlarging myonuclear number as well as by expanding the cytoplasmic domain (5). Thereafter, muscle fibers grow mainly by expending the cytoplasmic volume without further addition of myonuclei. Whereas postnatal/juvenile satellite cells cycle to generate progenitors to fuse with muscle fibers, they become quiescent in adult muscle and are only reactivated to regenerate damaged muscle fibers (6). The postnatal/juvenile growth period is accompanied by a steady decline in number of muscle satellite cells until 21 days and remains stable thereafter throughout adulthood (5).

Little is known about which intercellular signaling systems guide postnatal/juvenile muscle growth and the setup of adult satellite cell number. We and others previously determined the crucial role of bone morphogenetic proteins (BMPs) during embryonic, fetal and adult muscle growth (7–13). Reminiscent to other members of the TGF-β signaling molecules, BMPs act on target cells via transmembrane serine/threonine kinases receptors. BMPs bind to type II and type I receptors, thereby forming a ligand-receptor complex and permitting the phosphorylation of the type I receptor via the constitutively active type II receptor (14, 15). The type I receptor in turn phosphorylates the BMP responsive proteins Smads 1/5/8.

Phosphorylated Smad1/5/8 proteins subsequently form complexes with co-Smad4 and translocate to the nucleus to regulate transcriptional activity of target genes such as Ids (16).

Inhibitors of differentiation/DNA-binding proteins (Id1-4) block E-proteins from binding with the myogenic regulatory transcription factor MyoD and inhibit terminal differentiation (17). Interestingly, the BMP signaling up-regulates inhibitory Smad6 which interferes with BMP signaling at receptor level and complex formation of receptor regulated Smad with common mediator Smad4 as part of a negative feed-back-loop (18).

A number of secreted proteins, amongst noggin, can non-covalently bind BMPs and inhibit receptor binding (9, 19). Previous work demonstrated that during embryonic development, concentration gradients of BMP maintain the Pax3 muscle precursor population and counter gradients of noggin specify the onset of myogenesis by down-regulating *Pax3* expression and up-regulating *MyoD* expression (12, 13). Noggin induced precocious loss of *Pax-3* expression resulted in a growth deficit of embryonic muscle anlagen, whereas BMP stimulated embryonic muscle growth. However, BMP was suggested to act concentration dependent on embryonic muscle, with high concentrations inducing apoptosis, sub-apoptotic concentrations stimulating *Pax3* dependent muscle development, and BMP withdrawal inducing myogenic differentiation (7). Interestingly, myotube formation is delayed in *noggin* null mice, pointing to a muscle differentiation defect in lack of noggin (20).

The signaling system BMP/noggin also regulates satellite cell (SC) function. We previously showed that BMP signaling stimulated SC division and inhibited myogenic differentiation, whereas abrogation of BMP signaling induced precocious differentiation (10). Importantly, we could demonstrate that the receptor BMPR1A transmits BMP signaling on muscle precursors. Importantly, injection of noggin into regenerating muscle inhibits BMP signaling and reduces P-Smad1/5/8, Id1 and Id3 proteins levels (21). Moreover, in the Id-mutant mice, the number of proliferating Pax7+ cells is reduced following muscle injury. These data suggest that BMP signaling regulates Id1 and Id3 in muscle satellite cells thereby maintaining their proliferation before terminal myogenic differentiation (21). Furthermore, MyoD binding elements were found in the promoter region of *BMPR1A* and MyoD enhances *BMPRIA* expression, suggesting that BMP signaling may have an important role for myogenic progression (22).

We here investigated the contribution of BMP signaling during satellite cell dependent postnatal muscle growth. We employed noggin as a strategy to interfere with BMP signaling

at ligand level and overexpressed Smad6 to interfere with BMP signaling at cell-autonomous level in satellite cells. We also analysed the impact of BMP signaling in *BMP6* and *BMP14* null mice. We show that in lack of BMP signaling, satellite cell activity, myonuclear recruitment as well as the generation of the adult satellite cell pool is severely inhibited.

MATERIALS AND METHODS

Animals

Transgenic *Rosa26-LoxP-Stop-LoxP-humanSmad6-IRES-EGFP* mice (on a *C57BL/6J* background), also labeled *RS6*, were obtained from the Max Planck Institute for Heart and Lung Research, Bad Nauheim, Germany, and crossed with different Cre-driver mice.

Pax7$^{CreERT2/+}$ knock-in mice (JAX strain name is B6;129-Pax7tm2.1(cre/ERT2)Fan/J) were bred with wild-type *C57BL/6J* mice. This strain expresses Cre-ERT2 recombinase from the endogenous *Pax7* locus. By crosses with the *RS6* strain we obtained *Pax7$^{CreERT2/+}$;RS6$^{+/-}$* offsprings.

Transgenic *HSA-Cre* mice (JAX strain name FVB.Cg-Tg(ACTA1-cre)79Jme/J, on a *C57BL/6J* background) have the *Cre* recombinase gene driven by the human *α-skeletal actin* (*HSA*) promoter (23). By crossing these mice with the *RS6* strain we obtained *HSA-Cre$^{+/-}$; RS6$^{+/-}$* offsprings.

Pax3$^{GFP/+}$ mice (24) were used as positive controls for FACS-isolated GFP expressing satellite cells.

Gdf5$^{-/-}$ (GDF5 is also known as BMP14, JAX strain name: *Gdf5^{bp-J}*) mice have a spontaneous frameshift mutation leading to truncated non-functional Gdf5 (25). Mice were maintained in a homozygous mating system on *A/J* background.

BMP6$^{-/-}$ mice (26) were bred in a heterozygous mating system on *CD1* background.

The mice were bred in the animal facility of the Medical Faculty of Paris VI or Cochin Hospital and kept according to institutional guidelines. Wild-type *C57BL/6J* mice were purchased from Janvier or Charles River and wild-type *A/J* mice were purchased from Harlan.

Animal studies have been approved and were carried out under the laboratory and animal facility licenses A75-13-11 and A91-228-107.

AAV-production

The noggin construct, prepared by PCR amplification of chick cDNA (Suppl. 1), was subcloned into the pCR2.1-TOPO plasmid vector (TOPO Cloning, Invitrogen) and thereafter introduced into an AAV-2-based vector between the 2 inverted terminal repeat and under the control of the cytomegaly virus promoter using the XhoI and EcoRI sites. The AAV2/1-noggin (thereafter called AAV-noggin) was produced in human embryonic kidney 293 cells by the triple-transfection method using the calcium phosphate precipitation technique with both the pAAV2 propeptide plasmid, the pXX6 plasmid coding for the adenoviral sequences essential for AAV production, and the pRepCAp plasmid coding for AAV1. The virus was then purified by 2 cycles of cesium chloride gradient centrifugation and concentrated by dialysis. The final viral preparations were kept in PBS solution at -80°C. The particle titer (number of viral genomes) was determined by a quantitative PCR.

AAV-injection

AAV quantity for intramuscular delivery was calculated dependent on total body weight (x [µl] = 1.5 x body weight [g]), which was 5-30 µl. AAV was injected into the muscles of the anterior compartment of the lower leg of three days old *C57Bl6* mice. We here used PBS and AAV-U7-scramble for control experiments as in previous work we never observed any effect on muscle morphology or histology in control injected animals when injecting PBS or AAV-U7-scramble intramuscularly except of some regenerating fibers along the injection trajectory (27–29). AAV-noggin was used at concentration of 1 x 10E13 viral genome (vg)/ml, AAV-BMP4 at 2 x 10E13 vg/ml, and AAV-control at 5 x 10E12 vg/ml. At four weeks of age, muscle were isolated and prepared for cryosections/histology, western blotting, qPCR or isolation of single muscle fibers.

Tamoxifen injection for induction of Cre-ERT2 activity

Tamoxifen (Sigma) was prepared in heated corn oil (Sigma) at 37 °C at 20 mg/ml and 5 µl/g were administered by intra-peritoneal injection in pups (P7 and P9) or in the adult mouse (between 2 and 4 months old, 5 daily injections).

Isolating satellite cells by FACS and primary culture

For fluorescent-activated cell sorting, muscles (forelimb, hindlimb, abdominal, pectoral) were processed from P3, P14, P28 mice or adult mice (2-4 months) following sacrifice by cervical dislocation. The dissection of the muscles was performed with care to take off as much fat and connective tissue as possible. The muscles were minced in Hank's Balanced Salt Solution (HBSS) supplemented with 0.2% bovine serum albumin, 1% penicillin-streptomycin in a sterile 6 cm Petri dish on ice. The minced muscles were digested for 1.5 h at 37°C with 2 μg/ml collagenase A (Roche), 2.4 U/ml dispase I (Roche), 10 ng/ml DNase I (Roche), 0.4 mM $CaCl_2$ and 5 mM $MgCl_2$ in supplemented HBSS. Cells were washed with supplemented HBSS, filtered through 100 μm cell strainer, cells were then pelleted and washing step was repeated with 70 μm and finally 40 μm cell strainers.

For marking extracellular markers, the following primary antibodies were used (10 ng/ml): rat anti-mouse CD45-PE-Cy7 (BD), rat anti-mouse Ter119-PE-Cy7 (BD), rat anti-mouse CD34-BV421 (BD), rat anti-mouse integrin-α7-A700 (R&D Systems), rat anti-mouse Sca1-FITC (BD). Cells were washed once with ice-cold supplemented HBSS, filtered and re-suspended in supplemented HBSS. Flow cytometry analysis and cell sorting were performed on a FACSAriaII (BD) previously calibrated (Fluorescence Minus One and use of compensation beads) at the Lumic-CypS UPMC platform. TER119 (LY76)$^+$ and CD45 (PTPRC, LY5)$^+$ cells were negatively selected, CD34$^+$ and integrin-α7$^+$ cells were positively selected and the remaining cells were gated based on SCA1$^-$ expression.

Culture of FACS sorted satellite cells

Purified cell populations were plated on gelatin-coated dishes at low density for clonal analysis (300 cells/well in a 24 well plate). The remaining sorted cells were plated for RNA extraction. Cells were allowed to grow in growth medium: DMEM Glutamax containing 20% fetal bovine serum, 10% horse serum, 1% penicillin–streptomycin, 1% HEPES, 1% sodium pyruvate, 1/4000 bFGF (20 ng/ml Peprotech). Cells were plated at D0, treated or not with either 1 μM of 4-hydroxytamoxifen (Sigma) or 50 ng/ml recombinant mouse noggin (R&D systems) at D2, D3, D4, and at D5 were either fixed for immunohistochemistry with 4% paraformaldehyde (PFA) or washed and harvested by trypsinisation for RNA extraction.

Culture of satellite cell-derived primary myoblasts using preplating

The total cells from the muscle tissue, prepared similarly as the FACS purification procedure, are resuspended in growth medium (see FACS procedure) and pre-plated onto a non-coated 15 cm Petri dish for 4 h (fibroblasts will adhere to the plate, whereas most myoblasts will remain in suspension). The media, containing the myoblasts in suspension, is then transferred onto gelatin coated 10 cm Petri dishes. Cultures were maintained in growth medium until cells reached 70% confluency, after which cells were harvested by trypsinisation for RNA extraction.

Immunocytochemistry/Immunohistochemistry

Immunocytochemistry/histological analyses were performed using primary antibodies against Pax7 (1/50, mouse IgG1, DSHB, or hybridoma cell supernatant at 1/2) or (1/100, guinea pig, produced by (30)), P-Smad1/5/8 (1/100, rabbit, Cell Signaling), dystrophin (1/50, mouse IgG2a, NCL-dys1, Novocastra), laminin (1/400, rabbit, Dako), anti-BrdU (1/100, rat, Abcam), m-cadherin (1/50, mouse IgG1, Nanotools), MyoD (1/100, mouse IgG1, Dako), myogenin (1/100, mouse IgG1, DSHB), panMHC (mouse Ig2a, A4-1025, DSHB), Ki67 (1/100, mouse IgG1, BD), cleaved-caspase 3 (1/300, Cell signaling), followed by secondary antibodies with various fluorophores (Alexa Fluor 1/400 goat anti mouse IgG1 488 or 594, goat anti rabbit 488 or 594, goat anti mouse IgG2 633) and DAPI (1/1000 or 1/5000, Sigma).

Fluorescence was visualized either by Zeiss Axio Imager with an Orkan camera (Hamatsu) and AxioVision software or by LSM 700 laser scanning microscope (Carl Zeiss) with ZEN-2009 software or by Nikon Ti microscope equipped with a CoolSNAP HQ2 camera (Roper Scientific), an XY motorized stage (Nikon) using Metamorph Software (Molecular Devices).

Western blot

Proteins were extracted from frozen *triceps brachialis* muscle using RIPA buffer with a proteinase and phosphatase inhibitor cocktail (Complete tablets, Roche). Proteins were separated through denaturing sodium dodecyl sulphate polyacrylamide gel electrophoresis with the Laemmli system and transferred onto nitrocellulose membranes by the wet method (BioRad). The blots were probed using primary antibodies against GFP (1/5000, Aves Labs) and actin (1/10000, Sigma). Western blots were analyzed with SuperSignal West Pico Chemiluminescent substrate (Pierce).

BrdU analysis

Mice were treated with AAV-noggin or AAV-control which were intramuscularly injected into *tibialis anterior* (*TA*) muscle at postnatal day (P) 3. At P14, animals were labeled with BrdU (Invitrogen) by subcutaneous injection with 10 µl per 1 g body weight for 3 consecutive days. Following sacrifice, histological sections of *TA* muscle (0.8 µm) were fixed with 4% paraformaldehyde for 10 min, and permeabilized with methanol (-20°C) for 6 min. Antigens were retrieved by boiling for 30 min at 70-80°C in 0.01 M sodium nitrate (pH 6). This was followed by incubation with HCl (1N) for 20 min at 37°C. Samples were washed in PBS and incubated for 1h in blocking buffer (2% BSA + 2% swine serum). Samples were incubated overnight at 4°C with anti-BrdU (rat, Abcam) in combination with other primary antibodies (see above).

RNA isolation and real-time PCR

For frozen muscle tissue total RNA was isolated using Trizol (Invitrogen) extraction combined with RNeasy Mini Kit (Qiagen). For FACS isolated satellite cells or for cultured primary myoblasts total RNA was isolated using RNeasy Micro Kit (Qiagen). In both cases, RNase-Free DNase I Set (Qiagen) was used to eliminate traces of DNA in the RNA extraction. Isolated RNA was quantified using NanoVue Plus GE HealthCare spectrophotometer (Dutscher). For RNA extracted from muscle tissue, cDNA synthesis was performed using ThermoScript RT-PCR System for First-Strand cDNA Synthesis (Invitrogen) and random hexamer primers. For RNA extracted from FACS-isolated satellite cells or cultured primary myoblasts, cDNA synthesis was performed using SuperScript VILO Master Mix (Invitrogen). Real-time polymerase chain reaction was performed according the SYBR Green protocol (BioRad) in triplicate on the CFX96 Touch Real-Time detection system (BioRad) using iTaq Universal SYBR Green Supermix (BioRad). A 10 min denaturation step at 94oC was followed by 40 cycles of denaturation at 94°C for 10 s and annealing/extension at 60°C for 30 s. Before sample analysis we had determined for each gene the PCR efficiencies with a standard dilution series (10E1-10E7 copies/µl), of which subsequently enabled us to calculate the copy numbers from the Ct values. mRNA levels were normalized to 1 million copies of GAPDH mRNA. Fold changes were calculated according to the efficiency corrected $-\Delta\Delta Ct$ method (31). The sequences for the primers used are listed below:

Gene	Primer sequence (5'→ 3')	Direction
Oligonucleotide primers used for mice		
Bmp1	TTTGATGGCTACGACAGCAC	Forward
	CTGTGGAGTGTGTCCTGGAA	Reverse
Bmp2	CATCACGAAGAAGCCGTGGA	Forward
	TGAGAAACTCGTCACTGGGG	Reverse
Bmp4	TCCATCACGAAGAACATCTGGA	Forward
	ATACGGTGGAAGCCCTGTTC	Reverse
Bmp5	AGGAATACACAAACAGGGATGC	Forward
	CCAGCAGATTTTACATTGATGC	Reverse
Bmp6	GGGATGGCAGGACTGGATCA	Forward
	ATGGTTTGGGGACGTACTCG	Reverse
Bmp7	AGCTTCGTCAACCTAGTGGAAC	Forward
	CTGGAGCACCTGATAGACTGTG	Reverse
Bmp13	AAGACTTACTCCATTGCCGAGA	Forward
	TCGTCCAGTCCTCTGTCTACAA	Reverse
Bmp14	ATGCTGACAGAAAGGGAGGTAA	Forward
	GCACTGATGTCAAACACGTACC	Reverse
Alk3	TGAGACAGCAGGACCAGTCA	Forward
	GATTCTGCCCTTGAACATGAGA	Reverse
Id1	GGTGGTACTTGGTCTGTCGG	Forward
	CCTTGCTCACTTTGCGGTTC	Reverse
Noggin	GAAGTTACAGATGTGGCTGTGG	Forward
	CACAGACTTGGATGGCTTACAC	Reverse
Gremlin1	AGCAAAAGGGTTTTCCTGAT	Forward
	AGTGGTCAGCATTTCACCCT	Reverse
Follistatin	CCTGCTGCTGCTACTCTG	Forward
	CTCGGTCCATGAGGTGCT	Reverse
p21	GTACTTCCTCTGCCCTGCTG	Forward
	GGGCACTTCAGGGTTTTCTC	Reverse
p57	CTGAAGGACCAGCCTCTCTC	Forward
	AAGAAGTCGTTCGCATTGGC	Reverse

Gapdh	TGACGTGCCGCCTGGAGAAA	Forward
	AGTGTAGCCCAAGATGCCCTTCAG	Reverse
Oligonucleotide primers used for human cDNA insert in RS6 mice		
SMAD6	TACTCTCGGCTGTCTCCTCGC	Forward
	CAGTGGCTCGGCTTGGTGGCG	Reverse

Single fiber preparation

Mice were sacrificed at P3 and P28 and *TA* and *extensor digitorum longus* (*EDL*) muscles surgically isolated. Muscles were thereafter digested in 0.2% collagenase Type 1 dissolved in DMEM (Life Technologies). Individual, viable, non-damaged myofibers were isolated by gently passing through Pasteur pipettes with different sized apertures and abundantly washed in PBS, as described in detail elsewhere (Rosenblatt JD, 1995). Then the myofibers were fixed in in 4% paraformaldehyde dissolved in PBS (Sigma) for 10 min, washed, stained with DAPI and Pax7 (1/50, mouse IgG1, DSHB), stained with DAPI and mounted on slides.

Morphometric studies

Cryosections of 12 μm of *TA* muscles were stained with anti-laminin to delineate the muscle fibers and anti-Pax7 or anti-m-cadherin to mark satellite cells. Fluorescent photographs were taken with a x20 objective on a microscope (Zeiss, AxioImage) and saved as TIFF files. These images were projected on a flatscreen coupled with a graphic tablet, which enabled the manual retracing of the muscle fiber outlines and the counting of satellite cells. The fibers of the entire muscle cross section were analyzed.

Statistical analysis

The results are expressed as the mean together with standard error for qPCR data. Other data are presented as the median in dot plots or in Whiskers-Tukey box plots. The probability of statistical differences between the experimental groups was determined by the non-parametric Mann Whitney U-test unless otherwise stated.

RESULTS

BMP signaling is active in postnatal and adult muscle satellite cells.

We first asked whether the BMP signaling pathway is active during the postnatal/juvenile growth phase of skeletal muscle. We found the presence of transcripts of genes encoding BMP ligands, the BMP receptor *ALK3*, the *inhibitor of differentiation/DNA binding 1* (*ID1*) BMP target (16) as well as BMP antagonists *Nog*, *Grem1* and *Fst* (encoding noggin, gremlin1 and follistatin) in RNA extracted from skeletal muscle from 3 days and 14 days old neonatal mice as well as 8 weeks old adult mice (Suppl. Fig. 1). Generally, expression of BMP signaling components declined from postnatal towards adulthood. Of note, expression of analyzed genes remained high in adult *soleus* muscle compared to *gastrocnemius* and *tibialis anterior* (*TA*) muscles.

In order to identify which cells respond to BMP signaling, we monitored the presence of phosphorylated Smad1/5/8 proteins using immunohistochemistry. Surprisingly, we found expression of P-Smad1/5/8 in myonuclei as well as in satellite cells of juvenile and adult muscle (from 2, 4 and 8 weeks old mice respectively) (Fig. 1A; Suppl. Fig. 2). Adult satellite cells, however, expressed P-Smad1/5/8 at lower levels compared to myonuclei.

Having identified active BMP signaling being present in satellite cells, we next studied the expression of BMP signaling pathway components in FACS-isolated muscle satellite cells from 3 days, 14 days and 8 weeks old mice. We found the presence of transcripts of all genes that were also studied in whole muscle extracts except for *BMP14* (Fig. 1B). Interestingly, most BMP ligands as well as *ALK3* and *ID1* declined in expression from P3 to P14 and became re-upregulated in adult satellite cells. From the different BMP ligands that were analyzed, *BMP6* was most strongly expressed and peaked notably in adult satellite cells. Altogether, these results suggest that BMP signaling plays a role during satellite cell dependent postnatal muscle growth.

BMP-antagonist noggin retards postnatal/juvenile satellite cell-dependent muscle growth.

We next challenged the role of BMP signaling on postnatal/juvenile muscle growth *in vivo* and abrogated BMP signaling by overexpressing noggin to antagonize BMP ligands. *Tibialis anterior* (*TA*) and *triceps brachialis* (*TB*) muscles were transfected at P3 with an AAV-noggin, which resulted in high transgene expression (Suppl. Fig. 3A). Noggin

overexpression severely impaired muscle growth compared to saline injected controls as evidenced by the anatomical analysis of skeletal muscle at 4 weeks of age (Fig. 2A). The muscle weight of noggin treated muscles was considerably smaller compared to control limbs (Fig. 2B). Morphometrical analysis of single fibers or transverse sections from *TA* muscles revealed a strong shift of myofiber diameters towards smaller sizes (Fig. 2C; Suppl. Fig. 3B, Suppl. Fig. 4B), whereas fiber length remained of the same size compared to controls (Suppl. Fig. 3C). Postnatal skeletal muscle enlarges by continuously recruiting satellite cells into the growing myofiber syncytium, the total fiber myonuclear number therefore reflecting the cumulative history of previous satellite cell activity. To understand the cellular mechanism behind the noggin induced growth retardation, we thus determined the total myonuclear number on isolated muscle fibers from *TA* muscles prior and after noggin overexpression (Suppl. Fig. 3D). Prior noggin transfection at day P3, muscle fibers contained 74±2 myonuclei, which increased in control treated muscles to 419±11 myonuclei, whereas noggin treated myofibers increased myonuclear number only to 244±5 (mean± S.E.M.), (Fig. 2D). Thus, whereas myonuclear number doubled 2.4 fold between days P3 and P28 in controls, presence of noggin reduced the doubling to 1.6 fold, clear evidence for decreased satellite cell recruitment during postnatal/juvenile myofiber growth.

BMP-antagonist noggin decreases postnatal/juvenile satellite cell activity.

We next studied the effect of noggin on satellite cell proliferation during the postnatal growth phase. We treated mice at P3 with AAV-noggin, administered BrdU at P14 for 3 consecutive days and analyzed muscles at P17 and P21. The population of Pax7$^+$/BrdU$^+$ represents proliferating satellite cells, Pax7$^+$/BrdU$^-$ quiescent satellite cells, whereas the Pax7$^-$/BrdU$^+$ population at sublaminar position represent former satellite cells that became differentiated and hence mitotically inactive once recruited into the myofiber (Fig. 3A). Interestingly, Pax7$^+$/BrdU$^+$, Pax7$^+$/BrdU$^-$ and the Pax7$^-$/BrdU$^+$ cell population were reduced following noggin mediated abrogation of BMP signaling (Fig. 3B, Suppl. Fig. 4A). Decreased satellite cell proliferation was therefore the main cellular mechanism causing delayed myonuclear recruitment and reduced postnatal muscle growth, whereas we found no evidence for satellite cell exhaust by precocious differentiation. Interestingly, the reduced Pax7$^+$/BrdU$^-$ population suggests a decreased satellite cell self-renewal in lack of BMP signaling.

At about 21 days of age, final satellite cell number is established and does not further increase towards adulthood (5). We therefore asked for the consequence of decreased satellite cell proliferation during the postnatal/juvenile stages for the generation of the adult muscle stem cell pool. Remarkably, treatment with noggin at day P3 decreased the reservoir of young adult satellite cells at 4 weeks of age to about half the size found in controls, when counting satellite cells using markers Pax7 and m-cadherin (Fig. 3C,D; Suppl. Fig. 4B). Thus, adult muscle stem cells are generated during the postnatal/juvenile growth phase under the control of BMP signaling.

To test whether AAV-noggin induced myofiber hypotrophy can indirectly alter the number of satellite cells per myofiber, we quantified satellite cells following denervation-induced muscle atrophy. We found no evidence that denervation induced muscle atrophy reduced the number of satellite cells. Instead, satellite cell number was moderately increased (Suppl. Fig. 4C).

Smad6 cell-autonomously inhibits satellite cell-dependent postnatal muscle growth and generation of the adult satellite cell pool.

We next tested the consequence of cell-autonomous abrogation of BMP signaling during postnatal/juvenile muscle growth by overexpressing human-Smad6 (huSmad6), an inhibitory Smad of the intracellular BMP signaling cascade, directed to *Pax7* expressing satellite cells. Such time- and lineage specific expression of the huSmad6 was generated by crossing $Pax7^{CreERT2/+}$ mice with $Rosa26^{Lox-Stop-Lox-humanSmad6-IRES-EGFP}$ ($RS6$) mice and tamoxifen induced activation of the transgene (Suppl. Fig. 5A). The presence of *huSmad6* expression was confirmed in satellite cell-derived myoblasts from tamoxifen treated adult $Pax7^{CreERT2/+};RS6^{+/-}$ mice but not in cells from control mice, evidence for successful Cre-induced recombination (Suppl. Fig. 5B,C). Importantly, satellite cell-derived myoblasts downregulated *ID1* expression following *in vivo* tamoxifen injection of double mutants and more robustly when hydroxytamoxifen-treated *in vitro*, and much confirming the biological activity of human Smad6 to decrease BMP signaling as evidenced for an exemplary BMP target gene (Suppl. Fig. 5D and Fig. 5B).

To explore the role of BMP signaling in activated satellite cells during postnatal muscle growth, we next injected tamoxifen in $Pax7^{CreERT2/+};RS6^{+/-}$ mice at P7 and P9 and analyzed the effect on muscle growth compared to appropriate genetic controls (non-tamoxifen treated $Pax7^{CreERT2/+};RS6^{+/-}$ mice and tamoxifen treated $Pax7^{CreERT2/+}$ mice) when mice

reached one month of age (Fig. 4A). Tamoxifen treatment of $Pax7^{CreERT2/+};RS6^{+/-}$ pups caused 22% smaller *TA* muscles and 22% smaller *soleus* muscles compared to controls, whereas *EDL* muscles did not change (Fig. 4B). Morphometric fiber size analysis of transverse cross sections from *TA* muscles revealed a shift towards smaller fibers in tamoxifen treated double mutants compared to controls, indicating that decreased muscle growth resulted from delay in fiber size increase (Fig. 4C,D). Importantly, this retardation in muscle fiber growth was not compensated during further development and myofibers were still smaller in two months old tamoxifen treated $Pax7^{CreERT2/+};RS6^{+/-}$ compared to controls (Suppl. Fig. 6A-D). Isolated *EDL* myofibers from tamoxifen treated, four weeks old $Pax7^{CreERT2/+};RS6^{+/-}$ mice contained fewer myonuclei than their respective genetic controls, suggesting a decreased satellite cell activity during postnatal growth in cells deficient for BMP signaling (Fig. 4E). Furthermore, the number of Pax-7 expressing satellite cells per single fiber was decreased in tamoxifen treated double mutants compared to controls (Fig. 4F), further evidence that the adult satellite cells are generated during the postnatal growth phase under the control of BMP signaling. Lastly, the adult muscle satellite cell pool remained decreased by 47% when analyzing 8 weeks old *TA* muscles from tamoxifen treated double mutants compared to control mice, thus the information about final satellite cell number is set during postnatal muscle growth and their number does not recover at later stages (Suppl. Fig. 6E).

Myonuclear expressed huSmad6 does not alter satellite cell activity.

Above experiments failed to give unequivocal evidence whether decreased satellite cells activity resulted from Smad6 mediated cell-autonomous inhibition of BMP signaling, as myonuclei formed from fused recombined satellite cells may indirectly alter satellite cell function. We therefore generated $HSA^{Cre/+};RS6^{+/-}$ mice to overexpress Smad6 exclusively in terminally differentiated myofibers (Suppl. Fig. 7A). Muscles from these mice expressed *huSmad6* as well as GFP, suggesting effective recombination of the transgene (Suppl. Fig. 7B,C). Of note, GFP was only revealed by Western blot and not visible on dissected muscles *in toto* or on muscle cross sections. Histological analysis of cross sections of *TA* muscles from 4 and 8 weeks old $HSA^{Cre/+};RS6^{+/-}$ mice revealed normal tissue architecture (Suppl. Fig. 7D,E). Next, Pax7$^+$ satellite cells were quantified on *TA* cross sections from 4 and 8 weeks old $HSA^{Cre/+};RS6^{+/-}$ mice compared to $RS6^{+/-}$ control mice. Importantly, satellite cell number did not change, thus overexpression of Smad6 in differentiated muscle did not act indirectly on satellite cells (Suppl. Fig. 7E-G).

These experiments confirm that BMP signaling in skeletal muscle affects satellite cells by direct signaling.

BMP signaling is required for myoblast activation and proliferation.

We next used cultures to further explore the role of BMP signaling on satellite cell-derived myoblasts muscle precursor cells. The *in vitro* system has for advantage to permit monitoring of the rapid dynamics of BMP signaling on cell behavior. Cultures of FACS-sorted satellite cells from adult forelimb and hindlimb $Pax7^{CreERT2/+};RS6^{+/-}$ muscles were either treated with 1 μM hydroxytamoxifen (4-OHT) to evaluate the cell autonomous effect of *huSmad6* upregulation or with 50 ng/μl recombinant noggin to antagonize BMP ligands present in the culture medium (Suppl. Fig. 10a). 4-OHT treated cells strongly expressed *huSmad6*, but not cells from untreated control cultures or noggin treated cultures (Fig. 5A). Furthermore, 4-OHT as well as noggin downregulated the BMP target gene *ID1* (Fig. 5B). These results demonstrate the efficacy of the 4-OHT induced recombination of $Pax7^{CreERT2/+};RS6^{+/-}$ satellite cells and the value of noggin as a positive control for BMP signaling abrogation.

We then assessed cell proliferation by monitoring clonal cell expansion after seeding cells at low density. After 5 days in culture, cells expressed MyoD and lost expression of Pax7, showing that satellite cells became committed to myoblasts (Suppl. Fig. 8B). Both, treatment with 4-OHT and noggin reduced the generation of satellite cell-derived myoblast progenitors below 50% of control values (Fig. 5C). In a control experiment, 4-OHT revealed some inhibiting effect on cell proliferation on its own when treating FACS-isolated cells from $Pax7^{CreERT2/+}$ mice, however, to a far minor extent when compared to the severe inhibition by noggin or by 4-OHT on $Pax7^{CreERT2/+};RS6^{+/-}$ derived cells (Fig. 5C).

The reduction in cell number could not be explained by induction of apoptosis as cells in neither culture conditions expressed the apoptosis marker cleaved-caspase 3 (data not shown). Further, we found similar proportions of cells expressing myogenin and myosin heavy chain in $Pax7^{CreERT2/+};RS6^{+/-}$ derived cultures treated with 4-OHT and noggin when compared with control cultures, showing that inhibition of BMP signaling did not affect cell lineage progression (Fig. 5D,E; Suppl. Figs. 8B, 9A,B). We finally analyzed expression of the proliferation marker Ki67 and found a 64% decreased proportion of cells in proliferation following treatment with 4-OHT and a 49% decrease following treatment with noggin (Fig. 5F; Suppl. Figs. 8B, 9C). Such decreased proliferation was associated with an increased

transcript levels for cell cycle inhibitors p21 and notably for p57, suggesting an increased cell cycle arrest as the likely molecular mechanism following abrogation of BMP signaling (Fig. 5G,H).

Lack of BMP6 and BMP14 reduces satellite cell number.

We finally approached the question, which BMP ligand could be involved in satellite cell regulation. We first analyzed constitutive *BMP6* knockout mice as *BMP6* was most strongly expressed, notably in adult satellite cells. Interestingly, muscle fibers developed normally in size and number in *BMP6$^{-/-}$* mice, and fibers had also normal myonuclear number, suggesting a normal postnatal muscle development (Fig. 6A; Supp. Fig. 10C). Remarkably, however, we found a 25% reduction in *Pax7^{+}* satellite cell number compared to wild-type controls when i) quantifying cells on cross sections from adult *TA* muscles (Fig. 6A), or ii) quantifying isolated fibers from adult *EDL* muscles (Supp. Fig. 12C).

We recently provided evidence for the important role of BMP14 (also known as growth and differentiation factor-5, GDF5) in muscle mass maintenance. In fact, *BMP14* was strongly upregulated in skeletal muscle following denervation and protects muscle from denervation-induced atrophy (27). Above we showed that BMP14 is not expressed in satellite cells but in skeletal muscle, and hence is a good candidate for BMP-mediated paracrine signaling. *TA* muscles from *Gdf$^{bp-J/bp-J}$* mice (deficient for BMP14) contained a slightly, however not significantly, decreased satellite cell number. Remarkably, satellite cell number dropped significantly further following denervation of *BMP14* deficient muscles, showing that BMP14 protects from satellite cell loss in atrophying muscle.

DISCUSSION

The present study has provided several important new insights concerning the BMP signaling and its contribution to the regulation of satellite cell dependent muscle growth in postnatal/juvenile skeletal muscle.

We here showed *in vitro* as well as *in vivo* that postnatal/juvenile satellite cells express compounds of the BMP signaling pathway and respond to BMP signaling, which is reminiscent to previous observations on the role of BMP during embryonic and fetal chick myoblast development as well as adult murine satellite cell regulation (7–11). Therefore, BMP signaling is an important regulator of muscle stem cell activity during all stages of muscle development.

We deciphered for the first time the function of BMP signaling on satellite cell function during postnatal/juvenile muscle growth *in vivo*. We used noggin, an efficient BMP antagonist (19), as a mean to abrogate BMP signaling during the postnatal/juvenile growth phase. We show that noggin mediated BMP blockade decreased satellite cell proliferation, which supports previous observations on the role of BMP on fetal and adult muscle precursor cells during postnatal/juvenile myofiber growth resulting in a largely diminished myonuclear number. However, our *in vivo* experiments using noggin neither gave ultimate evidence whether BMP signaling was indeed abrogated at cell autonomous level, nor can we exclude secondary effects on satellite cells, such as signaling via differentiated myofibers. We therefore took advantage of the inducible Cre-lox system to overexpress Smad6 in either satellite cells or differentiated muscle. Smad6 mediated cell-autonomous interference with BMP signaling in satellite cells decreased their activity, whereas Smad6 expression in differentiated muscle did not, unequivocal evidence for direct BMP signaling in satellite cells *in vivo*. Neither *in vivo* nor *in vitro* we found evidence of precocious differentiation of myogenic precursors following BMP pathway inhibition, contrasting previous findings in cultures of satellite cells (10). We can only speculate about reasons underlying these discrepancies. Possibly the effect of noggin as well as Smad6 on the BMP target gene *ID1* in our study was too little to alter MyoD transcriptional activity. Recent work demonstrated that myogenic proliferation and differentiation can be decoupled (32). In agreement, we here find increased expression of cell cycle inhibitors, notably *p57*, that are known to increase stem cell quiescence together with decreased proliferation (33), whereas myogenic progression towards myogenin and MHC expression was not altered. This offers a molecular mechanism for the function of BMPs on muscle stem cells, however, the exact signaling pathway remains to be elucidated.

It is now clear that adult muscle satellite cells are of somite origin (3), however, it has been less studied how expansion of the satellite cell pool is controlled to give rise to final cell number at adult stages. Here we show that BMP signaling controls the generation of adult satellite cells during the postnatal/juvenile growth phase. We suggest that BMPs maintain precursor proliferation to generate a sufficient precursor cell pool and cells become quiescent once BMP signaling is tapered during muscle maturation. Interestingly, we found a decrease of BMP signaling pathway components in satellite cells between postnatal day 3 and 14 with subsequent upregulation in adult satellite cells. This approximately corresponds with the acquisition of quiescence at P21, however, it leaves open the question of the

function of BMP in quiescent satellite cells. Previous work demonstrated that BMP4 was sufficient to maintain Pax7 expression in serum-free cultures of non-activated satellite cells, suggesting that BMPs are required to maintain myogenic commitment (34).

The exact source and identity of BMPs that control postnatal/juvenile satellite cell activity remains obscure. We here show the presence of BMP transcripts in whole muscles as well as in satellite cells at different time points of postnatal/juvenile development. *BMP6* was highly expressed in satellite cells compared to other BMPs and satellite cells drop in number in *BMP6*$^{-/-}$ mice. However, the respective role of BMPs synthesized by satellite cells, by mature muscle, blood vessels or derived from extrinsic sources such as growing bone remains to be determined.

Abnormal levels of BMP signaling in skeletal muscle can trigger ectopic bone formation such as in patients suffering from fibrodysplasia ossificans progressive (35). Interestingly, myogenic precursors contribute only minimally to BMP-mediated heterotopic ossification (<5%) *in vivo* (36). Using AAV-mediated overexpression of BMP4, we observed an immense ossification of soft tissues in hind limbs of adult mice upon 4 weeks of treatment (data not shown) similarly as previously reported in the literature (36). Therefore non physiological levels of BMPs can induce an osteogenic program in skeletal muscle, whereas physiological BMP signaling is required for muscle growth and homeostasis.

In conclusion, BMP signaling is an important regulatory system during postnatal/juvenile muscle growth and determines satellite cell dependent myofiber growth and the generation of the adult muscle satellite cell pool.

ACKNOWLEDGEMENTS

REFERENCES

1. Perdiguero E, Sousa-Victor P, Ballestar E, Muñoz-Cánoves P (2009) Epigenetic regulation of myogenesis. *Epigenetics Off J DNA Methylation Soc* 4(8):541–550.

2. Zammit PS, Partridge TA, Yablonka-Reuveni Z (2006) The skeletal muscle satellite cell: the stem cell that came in from the cold. *J Histochem Cytochem Off J Histochem Soc* 54(11):1177–1191.

3. Relaix F, Marcelle C (2009) Muscle stem cells. *Curr Opin Cell Biol* 21(6):748–753.

4. Mauro A (1961) SATELLITE CELL OF SKELETAL MUSCLE FIBERS. *J Biophys Biochem Cytol* 9(2):493–495.

5. White RB, Biérinx A-S, Gnocchi VF, Zammit PS (2010) Dynamics of muscle fibre growth during postnatal mouse development. *BMC Dev Biol* 10(1):21.

6. Beilharz MW, Lareu RR, Garrett KL, Grounds MD, Fletcher S (1992) Quantitation of muscle precursor cell activity in skeletal muscle by Northern analysis of MyoD and myogenin expression: Application to dystrophic (mdx) mouse muscle. *Mol Cell Neurosci* 3(4):326–331.

7. Amthor H, Christ B, Weil M, Patel K (1998) The importance of timing differentiation during limb muscle development. *Curr Biol* 8(11):642–652.

8. Amthor H, Christ B, Patel K (1999) A molecular mechanism enabling continuous embryonic muscle growth - a balance between proliferation and differentiation. *Development* 126(5):1041–1053.

9. Amthor H, et al. (2002) Follistatin Regulates Bone Morphogenetic Protein-7 (BMP-7) Activity to Stimulate Embryonic Muscle Growth. *Dev Biol* 243(1):115–127.

10. Ono Y, et al. (2011) BMP signalling permits population expansion by preventing premature myogenic differentiation in muscle satellite cells. *Cell Death Differ* 18(2):222–234.

11. Wang H, Noulet F, Edom-Vovard F, Le Grand F, Duprez D (2010) Bmp Signaling at the Tips of Skeletal Muscles Regulates the Number of Fetal Muscle Progenitors and Satellite Cells during Development. *Dev Cell* 18(4):643–654.

12. Pourquié O, et al. (1996) Lateral and Axial Signals Involved in Avian Somite Patterning: A Role for BMP4. *Cell* 84(3):461–471.

13. Hirsinger E, et al. (1997) Noggin acts downstream of Wnt and Sonic Hedgehog to antagonize BMP4 in avian somite patterning. *Development* 124(22):4605–4614.

14. Nohe A, et al. (2002) The mode of bone morphogenetic protein (BMP) receptor oligomerization determines different BMP-2 signaling pathways. *J Biol Chem* 277(7):5330–5338.

15. Nohe A, Keating E, Knaus P, Petersen NO (2004) Signal transduction of bone morphogenetic protein receptors. *Cell Signal* 16(3):291–299.

16. Miyazono K, Miyazawa K (2002) Id: a target of BMP signaling. *Sci STKE Signal Transduct Knowl Environ* 2002(151):pe40.

17. Jen Y, Weintraub H, Benezra R (1992) Overexpression of Id protein inhibits the muscle differentiation program: in vivo association of Id with E2A proteins. *Genes Dev* 6(8):1466–1479.

18. Goto K, Kamiya Y, Imamura T, Miyazono K, Miyazawa K (2007) Selective Inhibitory Effects of Smad6 on Bone Morphogenetic Protein Type I Receptors. *J Biol Chem* 282(28):20603–20611.

19. Krause C, Guzman A, Knaus P (2011) Noggin. *Int J Biochem Cell Biol* 43(4):478–481.

20. Tylzanowski P, Mebis L, Luyten FP (2006) The Noggin null mouse phenotype is strain dependent and haploinsufficiency leads to skeletal defects. *Dev Dyn* 235(6):1599–1607.

21. Clever JL, Sakai Y, Wang RA, Schneider DB (2010) Inefficient skeletal muscle repair in inhibitor of differentiation knockout mice suggests a crucial role for BMP signaling during adult muscle regeneration. *Am J Physiol - Cell Physiol* 298(5):C1087–C1099.

22. Liu R, et al. (2009) Myoblast sensitivity and fibroblast insensitivity to osteogenic conversion by BMP-2 correlates with the expression of Bmpr-1a. *BMC Musculoskelet Disord* 10:51.

23. Miniou P, et al. (1999) Gene targeting restricted to mouse striated muscle lineage. *Nucleic Acids Res* 27(19):e27–e30.

24. Relaix F, Rocancourt D, Mansouri A, Buckingham M (2005) A Pax3/Pax7-dependent population of skeletal muscle progenitor cells. *Nature* 435(7044):948–953.

25. Storm EE, et al. (1994) Limb alterations in brachypodism mice due to mutations in a new member of the TGFβ-superfamily. *Nature* 368(6472):639–643.

26. Meynard D, et al. (2009) Lack of the bone morphogenetic protein BMP6 induces massive iron overload. *Nat Genet* 41(4):478–481.

27. Sartori R, et al. (2013) BMP signaling controls muscle mass. *Nat Genet* 45(11):1309–1318.

28. Hoogaars WMH, et al. (2012) Combined effect of AAV-U7-induced dystrophin exon skipping and soluble activin Type IIB receptor in mdx mice. *Hum Gene Ther* 23(12):1269–1279.

29. Goyenvalle A, et al. (2004) Rescue of dystrophic muscle through U7 snRNA-mediated exon skipping. *Science* 306(5702):1796–1799.

30. Bröhl D, et al. (2012) Colonization of the satellite cell niche by skeletal muscle progenitor cells depends on Notch signals. *Dev Cell* 23(3):469–481.

31. Pfaffl MW (2001) A new mathematical model for relative quantification in real-time RT–PCR. *Nucleic Acids Res* 29(9):e45–e45.

32. Zalc A, et al. (2014) Antagonistic regulation of p57kip2 by Hes/Hey downstream of Notch signaling and muscle regulatory factors regulates skeletal muscle growth arrest. *Dev Camb Engl* 141(14):2780–2790.

33. Matsumoto A, et al. (2011) p57 Is Required for Quiescence and Maintenance of Adult Hematopoietic Stem Cells. *Cell Stem Cell* 9(3):262–271.

34. Friedrichs M, et al. (2011) BMP signaling balances proliferation and differentiation of muscle satellite cell descendants. *BMC Cell Biol* 12(1):26.

35. Shore EM, et al. (2006) A recurrent mutation in the BMP type I receptor ACVR1 causes inherited and sporadic fibrodysplasia ossificans progressiva. *Nat Genet* 38(5):525–527.

36. Lounev VY, et al. (2009) Identification of Progenitor Cells That Contribute to Heterotopic Skeletogenesis. *J Bone Jt Surg* 91(3):652–663.

Figure 1 – BMP signaling activity and gene expression dynamics of BMP signaling pathway components in satellite cells during postnatal muscle growth.

(A) Exemplary images of immunohistochemistry on *TA* muscle section from 4 weeks old juvenile mice. The Pax7 (red) positive nucleus shows low P-Smad1/5/8 (green) level (highlighted with arrows), whereas some but not all myonuclei show strong P-Smad1/5/8 levels. Myofibers stained against dystrophin (white). Scale bar is 20 µm.

(B) Diagrams depict the relative mRNA copy numbers per 10^6 *Gapdh* mRNA copies of different *BMP* ligands (*Bmp2*, *4*, *5*, *6*, *7*, *13*, *14*), *Bmp1* metalloproteinase, BMP type I receptor *Alk3* (*Bmpr1a*), BMP target gene *Id1*, BMP antagonists *Nog* (encoding *noggin*), *Grem1* (encoding *gremlin)* and *Fst* (encoding *follistatin)* in satellite cells isolated from skeletal muscles of wild-type mice at different ages: P3, P14 or adult (8 weeks-old). Cells were isolated described in Figure 2. Values are shown as means ± SEM.

Figure 1

A

P-Smad1/5/8   Pax7   Merged

B

mRNA copy numbers (per 10^6 GAPDH mRNA copies)

Bmp1   *Bmp2*   *Bmp4*   *Bmp5*   *Bmp6*

Bmp7 *Bmp13* *Bmp14*   *Alk3*   *Id1*

Nog   *Grem1*   *Fst*

P3
P14
Adult (8 weeks)
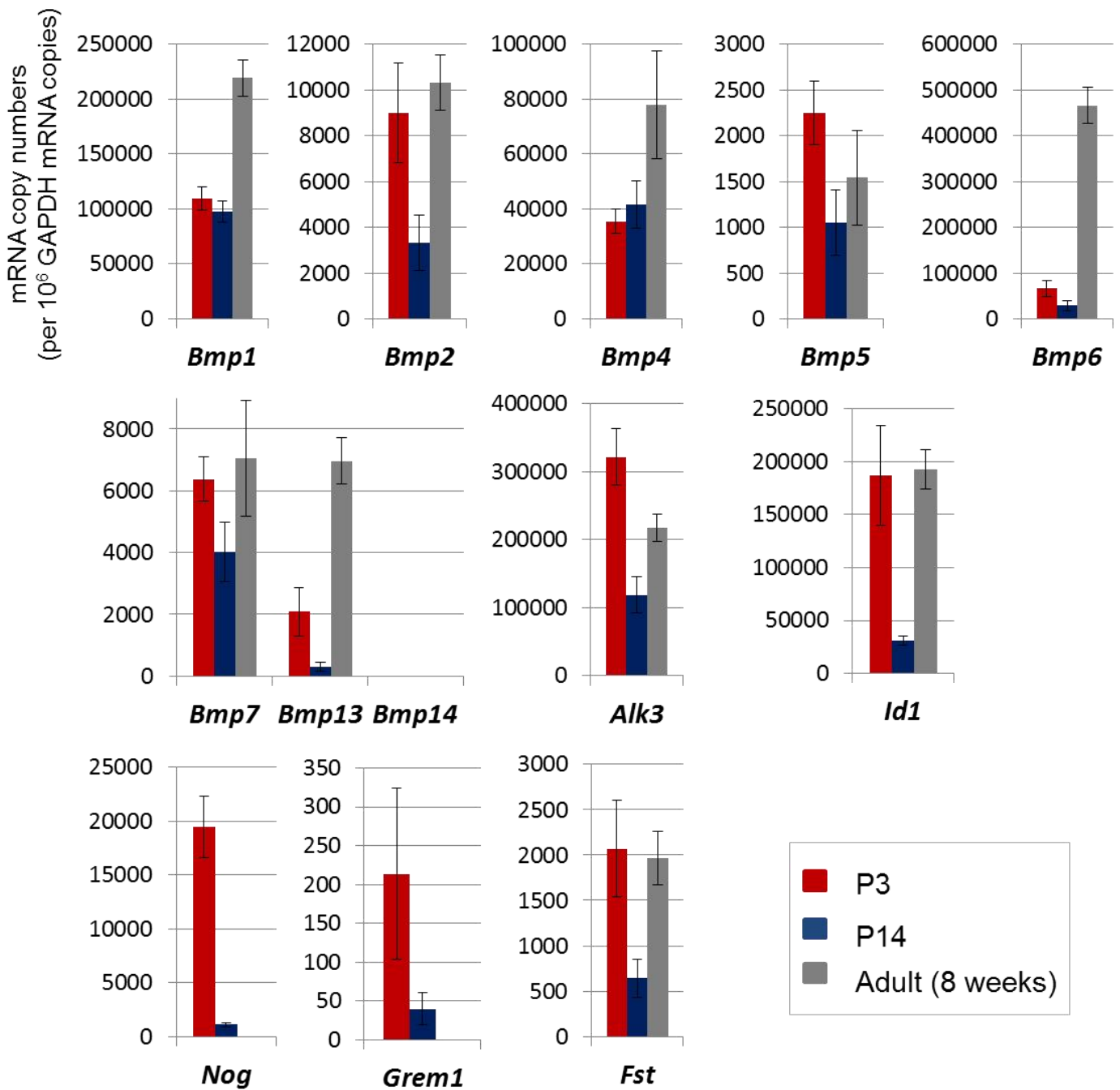
Figure 2 - Consequences of noggin mediated abrogation of BMP signaling for juvenile muscle growth.

Triceps brachii (*TB*) muscle and the anterior compartment of the lower hindlimb were transfected with AAV-noggin at postnatal day 3 (P3). Muscles were analyzed at four weeks of age.

(A) Dorsal view on the forelimb shows massive muscle hypotrophy of the AAV-noggin treated *TB* muscle (left images) compared to the saline injected contralateral side (right image). Exemplary images of n=4 injected mice.

(B) Diagram depicts muscle wet weights of *TB*, *TA* and *extensor digitorum longus* (*EDL*) muscles. Data are shown as dot plots together with the median.

(C) Histogram presents the distribution of myofiber breadth from anti-laminin stained cryosection of 4 weeks old *TA* muscles.

(D) Diagram depicts myonuclear number per single fiber from *TA* muscles, 4 weeks following AAV-noggin (n=120 fibers from 3 mice) or saline (n=68 fibers from 3 mice) injections at P3. Data are shown as Whiskers-Tukey box plot. *P* values were calculated using the nonparametric *U*-test.

Figure 2

A

B

C

D
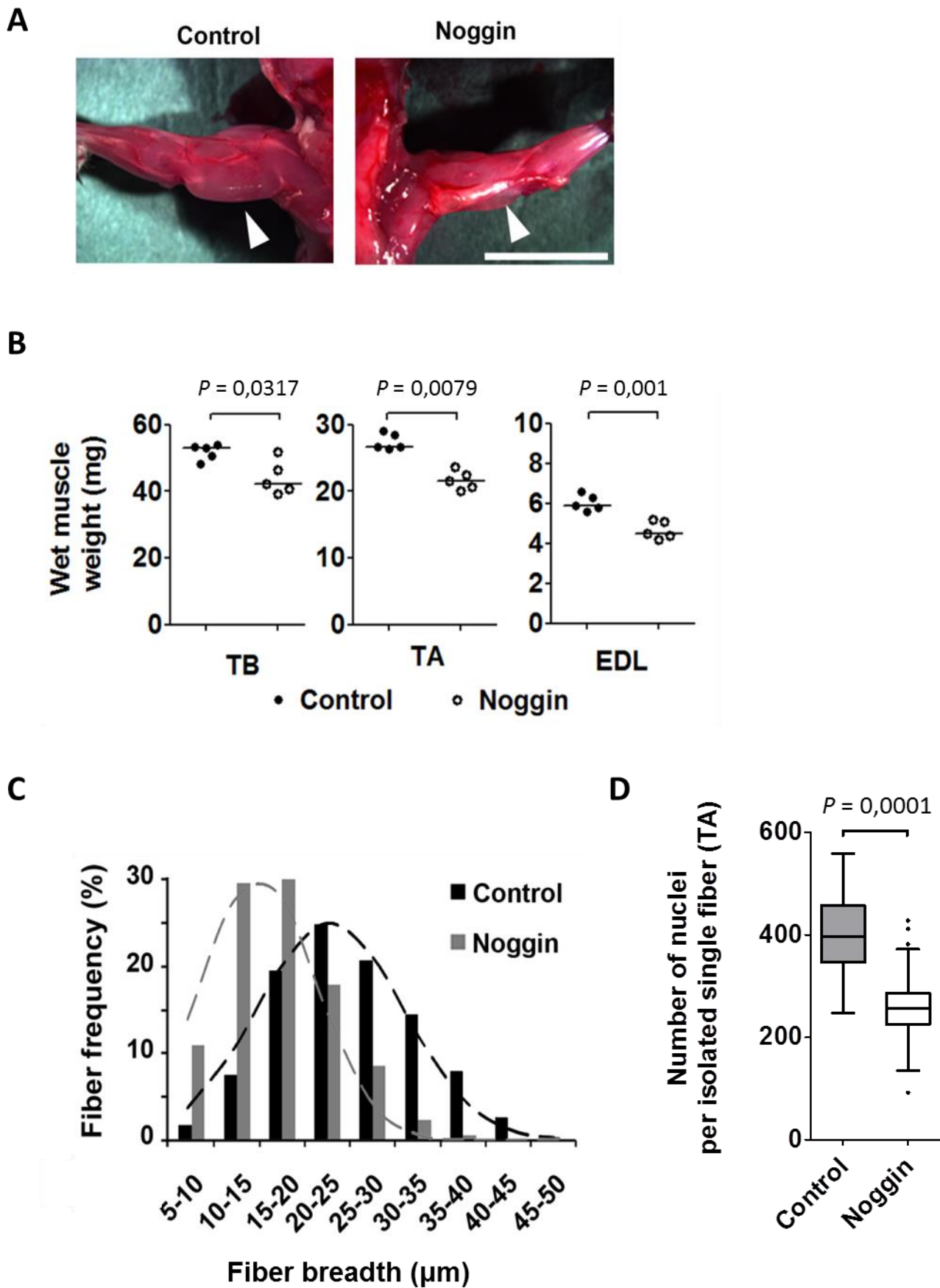
Figure 3 - Effects of noggin mediated abrogation of BMP signaling on juvenile satellite cell activity.

The anterior compartment of the lower hindlimb was transfected with AAV-noggin at P3. Following two weeks, mice were treated for three consecutive days with subcutaneous injection of BrdU for 3 days and sacrificed at P17.

(A) Fluorescence images following immunostaining against Pax7 in red (arrows), against BrDU in red, laminin in white and DAPI stained nuclei in blue of mid-belly transverse sections of *TA*. Pax7$^+$/BrdU$^+$ cells are indicated with straight and tail-less arrows (high and low BrdU incorporation, respectively). Pax7$^+$/BrdU$^-$ satellite cells and BrdU$^+$ sublaminal myonuclei are indexed with inverted and flexed arrows, respectively. Scale bar is 20μm.

(B) Diagram presents number of Pax7$^+$ satellite cells normalized per 100 myofibers (left panel). Diagram in the middle panel depicts the number of Pax7$^+$/BrdU$^+$ satellite cells per 100 myofibers. The ratio of BrdU$^+$ myonuclei per 100 myofibers is presented in the left panel. n=4 for each condition. *P* values were calculated using the nonparametric *U*-test.

 (C) Diagram depicts number of Pax7$^+$ and **(D)** m-cadherin$^+$ satellite cells per 100 myofibers quantified from whole TA muscle sections (n=3-4 for saline injected control and n=3 for AAV-noggin injected muscle). Data are shown as dot plots together with the median. In (C) and (D) *P* values were calculated using the *T*-test.

Figure 3

A
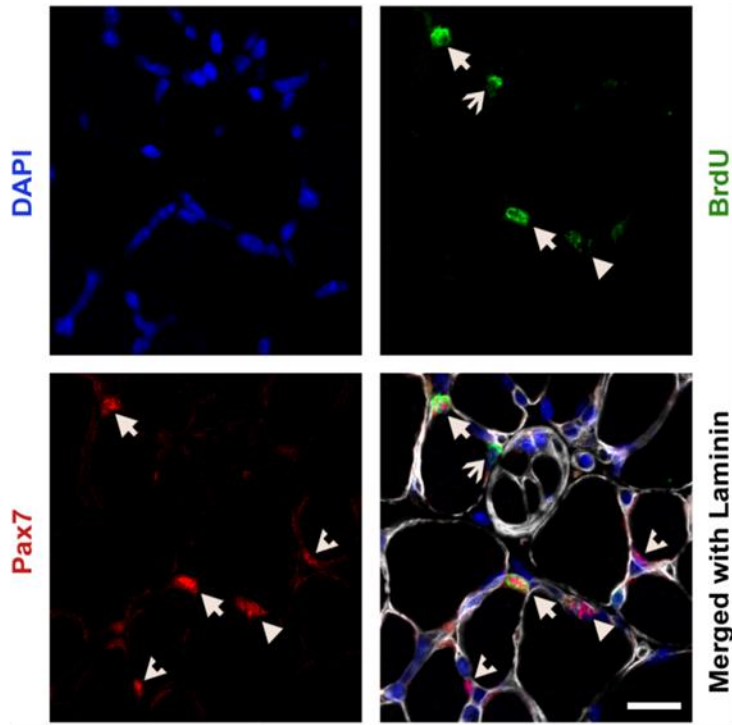
B

C

D

Figure 4 – Consequences of Smad6 mediated abrogation of BMP signaling in neonatal satellite cells for juvenile muscle growth.
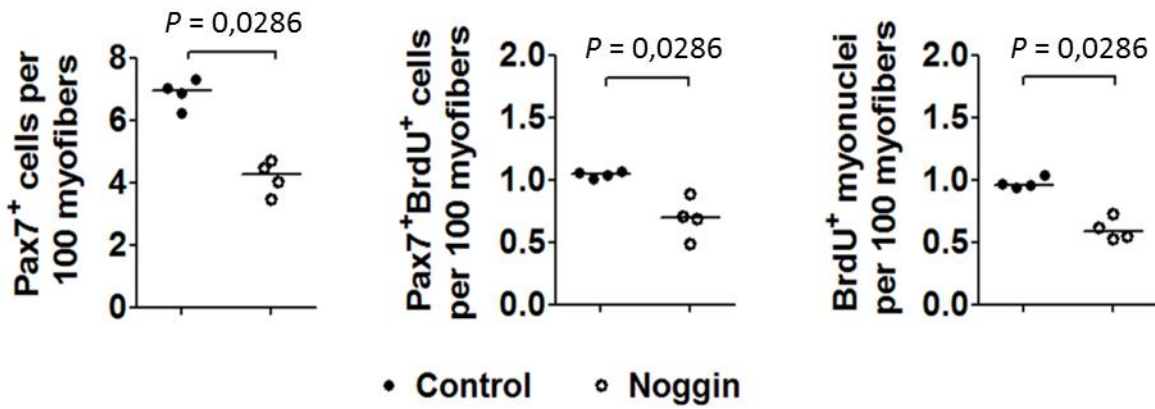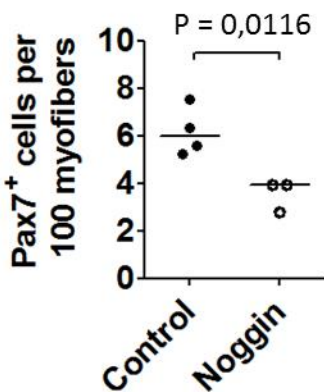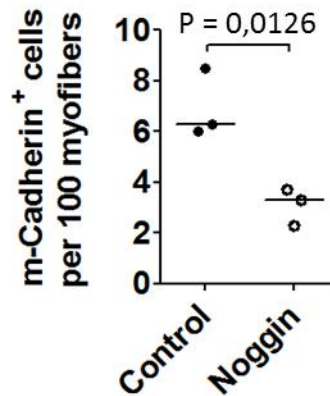
(A) Scheme of the experimental protocol: mice were injected with tamoxifen at P7 and P9 and sacrificed at the age of one month.

(B) Charts depict the *TA*, *EDL* and *soleus* wet muscle weights from control untreated $Pax7^{CreERT2/+};RS6^{+/-}$ mice (n=8 muscles, 4 mice, white circles) and tamoxifen treated $Pax7^{CreERT2/+};RS6^{+/-}$ mice (n=5 muscles, 3 mice, black circles). Values are shown as dot plots together with the median. *P* values were calculated using the nonparametric *U*-test.

(C) Chart depicts the quantification of the breadth of *TA* muscle fibers, analyzed on mid-belly muscle sections following immunostaining against laminin, from control tamoxifen treated $Pax7^{CreERT2/+}$ mice (n=5, grey and white squares), control untreated $Pax7^{CreERT2/+};RS6^{+/-}$ mice (n=3, dark grey), all compared to tamoxifen treated $Pax7^{CreERT2/+};RS6^{+/-}$ mice (n=4, white). Values are shown Whiskers-Tukey box plots together with the medians. *P* values were calculated using the nonparametric *U*-test.

(D) The latter data is also presented in a histogram depicting the distribution of the quantified *TA* muscle fiber breadth.

(E) Diagram depicts the number of myonuclei per isolated muscle fiber from *EDL* muscles from control tamoxifen treated $Pax7^{CreERT2/+}$ mice (n=128 isolated fibers from 5 mice) and control untreated $Pax7^{CreERT2/+};RS6^{+/-}$ mice (n=60 isolated fibers, from 3 mice), all compared to tamoxifen treated $Pax7^{CreERT2/+};RS6^{+/-}$ mice (n=66 isolated fibers from 4 mice).

(F) Number of Pax7$^+$ satellite cells per isolated muscle fiber from *EDL* muscles from control tamoxifen treated $Pax7^{CreERT2/+}$ mice (n=128 isolated fibers, 5 mice) and control untreated $Pax7^{CreERT2/+};RS6^{+/-}$ mice (n=60 isolated fibers from 3 mice), all compared to tamoxifen treated $Pax7^{CreERT2/+};RS6^{+/-}$ mice (n=73 isolated fibers from 4 mice). Values are shown as Whiskers-Tukey box plots together with the medians. *P* values were calculated using the nonparametric *U*-test.

Figure 4

A

P7   P9   P28   Days after birth

Tamoxifen (ip)   analysis

B

C

D

Pax7^CreERT2/+ + TXF

Pax7^CreERT2/+;RS6^+/−

Pax7^CreERT2/+;RS6^+/− + TXF

E

F

155

Figure 5 – Quantitative analysis following abrogation of BMP signaling in cultured *Pax7$^{CreERT2/+}$;RS6$^{+/-}$* satellite cell-derived primary myoblasts.

The experimental protocol was the following: At day 0 (D0) satellite cells from *Pax7$^{CreERT2/+}$* or *Pax7$^{CreERT2/+}$;RS6$^{+/-}$* adult mice were isolated using FACS and cultured in proliferation media; at D2-4 they were either not treated (control, CT), or treated with 1 μM hydroxytamoxifen (4-OHT) or 50 ng/mL of recombinant mouse noggin protein; at D5 cells were either fixed for immunocytochemistry or collected for RNA extraction.

(A) Chart depicts the relative mRNA copy numbers per 10^6 *Gapdh* mRNA of *human SMAD6* or **(B)** BMP target gene *Id1* from cultured satellite cells isolated from *Pax7$^{CreERT2/+}$;RS6$^{+/-}$* mice. Values are shown as dotplots together with the median. *P* values were calculated using the *T*-test.

(C) Cells were cultured in low density for a proliferation assay comparing non-treated and treated satellite cells isolated by FACS from skeletal muscles of *Pax7$^{CreERT2/+}$* and *Pax7$^{CreERT2/+}$;RS6$^{+/-}$* mice. The number of cells per colony was counted from at least three wells per condition and per mouse; at least 50 colonies of cells per condition and per mouse were quantified. Data are shown as Whiskers-Tukey box plots together with the medians. *P* values were calculated using the nonparametric *U*-test.

(D-F) Following cultures of satellite cells isolated from *Pax7$^{CreERT2/+}$;RS6$^{+/-}$* mice, the number of positive cells is given as a percentage of the total number of stained cells per colony following immunostaining against **(D)** myogenin (MyoG), **(E)** myosin heavy chain (MHC) and **(F)** Ki67. The quantification was performed on 13 to 20 colonies per culture (n=3 cultures, each derived from cells isolated from one mouse). Data is shown as Whiskers-Tukey box plots together with the medians. *P* values were calculated using the nonparametric *U*-test.

(G-H) Charts depict the relative mRNA copy numbers per 10^6 *Gapdh* mRNA of **(G)** *p21* and **(H)** *p57* from FACS-isolated and cultured satellite cells isolated from *Pax7$^{CreERT2/+}$;RS6$^{+/-}$* mice. Cells were either not treated (CT, n=4) or treated with 1 μM 4-OHT (n=3) or 50 ng/mL of recombinant mouse noggin protein (n=2). Data is shown as dot plots together with the median. *P* values were calculated using a *T*-test.

Figure 5
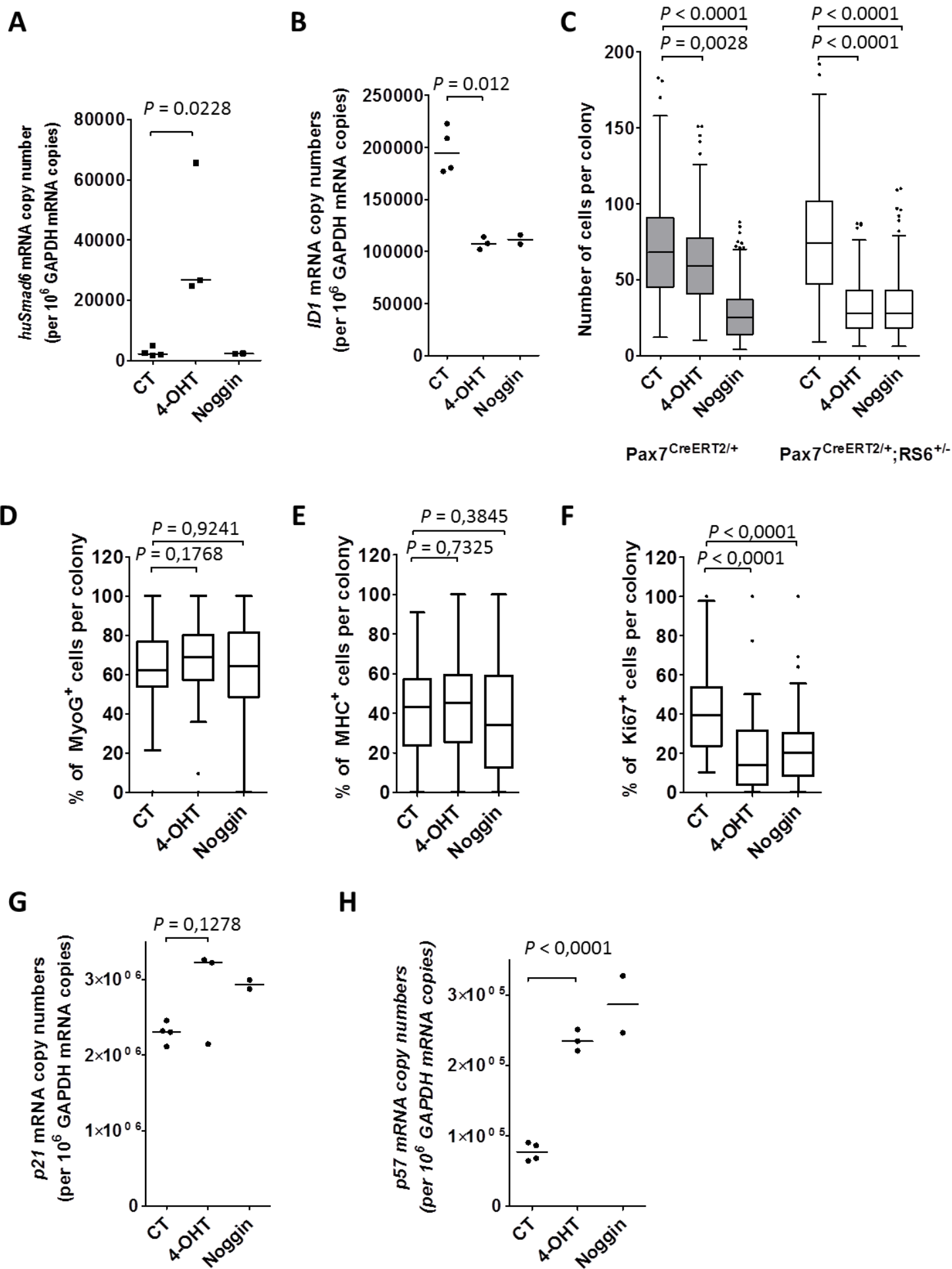
Figure 6 - Absence of BMP6 and BMP14 controls satellite cell pool.

(A) Diagram depicts the number of satellite cells per 100 myofibers. Satellite cells were stained against Pax7 and quantified from whole *TA* muscle sections. BMP6$^{-/-}$ mice have less satellite cells than wild-type mice (n=3). *P* value was calculated using a *T*-test (*P*<0.05).

(B) Diagram depicts the number of Pax7^{+} satellite cells per 100 myofibers of *TA* muscle of innervated (INR) and denervated (DNR) wild-type and *BMP14*$^{-/-}$ mice. Hindlimbs of adult mice (4-5 months of age) were denervated (sciatic nerve neurotomy) for 2 weeks. n=4 for each condition. Data are shown as dot plots together with the median. *P* value was calculated using the nonparametric *U*-test.

Figure 6

A

B
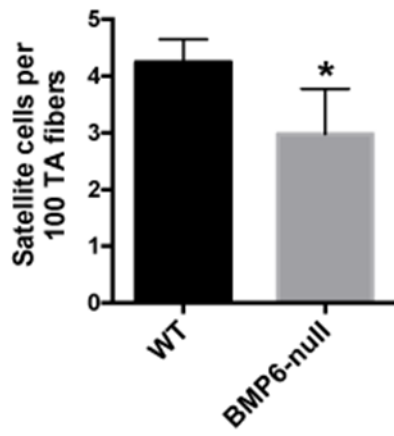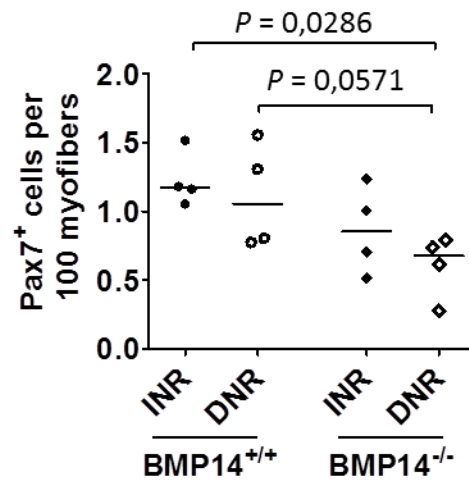
Supplementary Figure 1 – Gene expression dynamics of BMP signaling pathway components in skeletal muscle from neonatal, juvenile and adult mice.

Diagrams depict the relative mRNA copy numbers per 10^6 *Gapdh* mRNA copies of different *BMP* ligands (*Bmp2*, *4*, *5*, *6*, *7*, *13*, *14*), *Bmp1* metalloproteinase, BMP type I receptor *Alk3* (*Bmpr1a*), BMP target gene *Id1*, BMP antagonists *Nog* (encoding *noggin*), *Grem1* (encoding *gremlin)* and *Fst* (encoding *follistatin)*, in skeletal muscles from wild-type mice at postnatal day 3 (P3) in red and P14 in blue, or in *tibialis anterior*, *gastrocnemius* or *soleus* muscles from 8 week-old adult wild-type mice in different shades of grey (n=3 mice for each age). Values are shown as means ± SEM.

Supplementary Figure 1
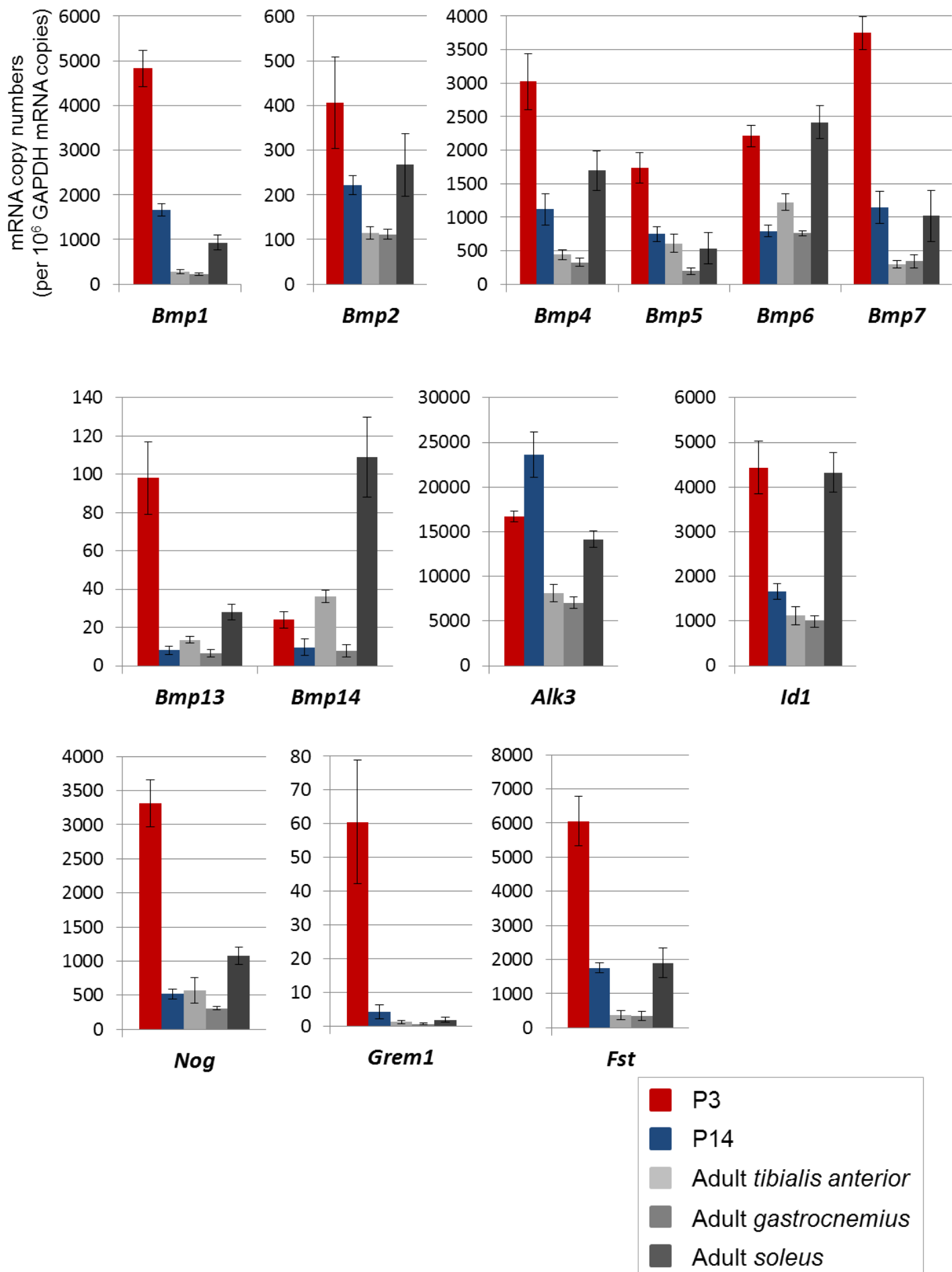
Supplementary Figure 2 – BMP signaling activity in satellite cells in juvenile and adult muscle.

Immunohistochemistry to monitor P-Smad1/5/8 expression (green) and Pax7 expression (red) in muscles from sections of *TA* muscles from 2, 4 and 8 weeks old wild-type mice (n=3). Nuclei are stained with DAPI in blue. Each panel represents nine exemplary images from different regions of the muscle section. Satellite cells express heterogeneous levels of P-Smad1/5/8 at the different ages. Scale bar is 10 μm.

Supplementary Figure 2

P-Smad1/5/8   Pax7   Merged

2 weeks
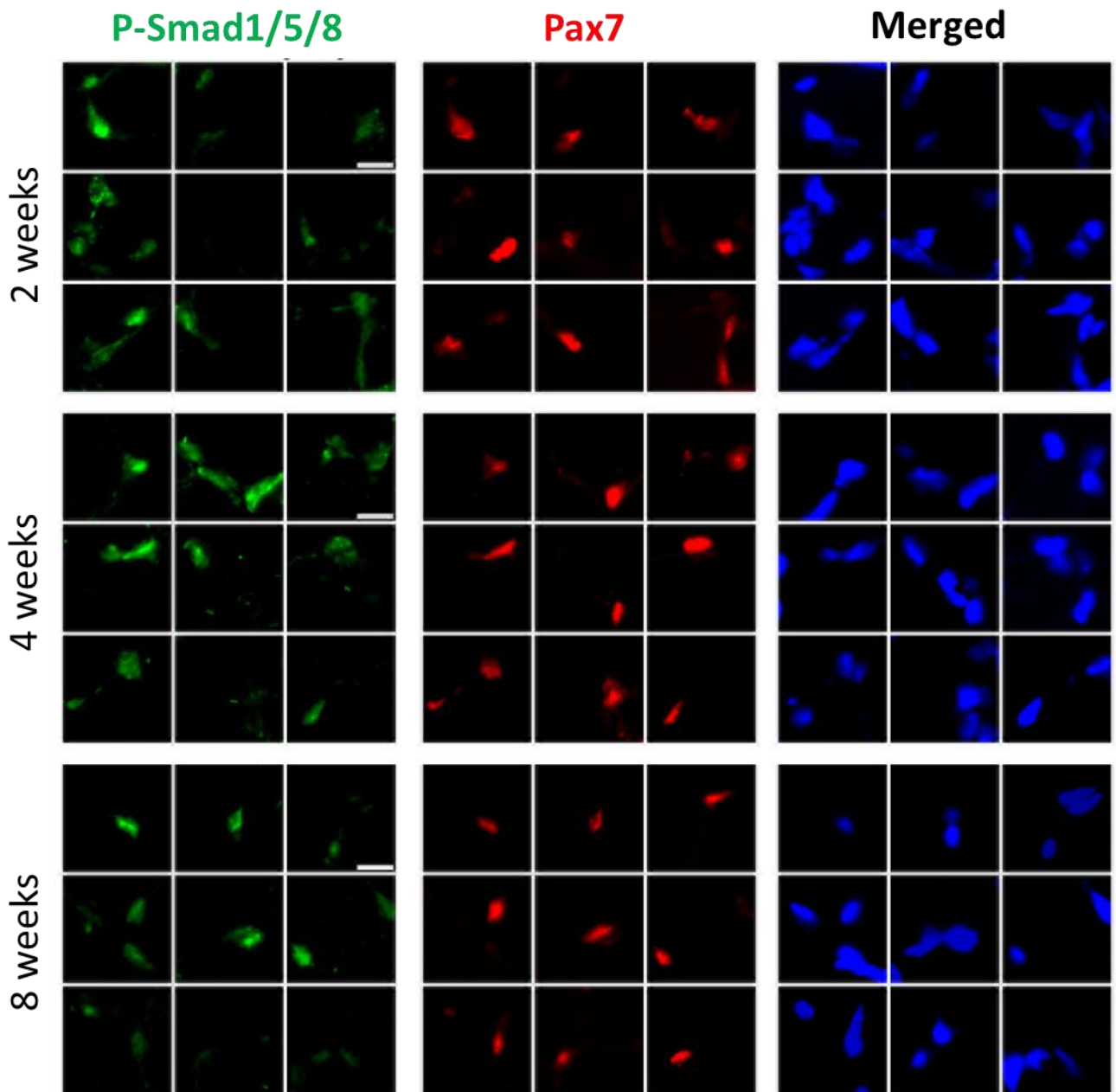
4 weeks

8 weeks

Supplementary Figure 3 – Consequences of noggin mediated abrogation of BMP signaling for juvenile muscle growth.

(A) Diagram presents the gene expression of noggin (chicken origin) in control and AAV-noggin injected adult mice (two weeks of treatment, n=4). Data represent mRNA copies per 10^6 *Gapdh*-mRNA copies and are shown as dot plots together with the median.

(B) Histogram presents the distribution of myofiber breadth of single myofibers from four weeks old *TA* muscles. n=107 and n=128 myofibers were analysed from 3 non-injected control and 5 AAV-treated muscles, respectively.

(C) Diagram shows myofiber length. n=65 and n=103 myofibers from 3 non-injected control and 5 AAV-treated muscles, respectively. Data are shown as Whiskers-Tukey box plots.

(D) Exemplary images of isolated single fibers of *TA* muscle from day P3 old mice (left panel) and four week old mice (right panel). The inlays show a magnified section of the fibers. Fibers were stained with DAPI and mosaic images were acquired using an automated microscope. Fluorescence images were superimposed over transmission light images. Scale bar is 500 μm.

Supplementary Figure 3

A
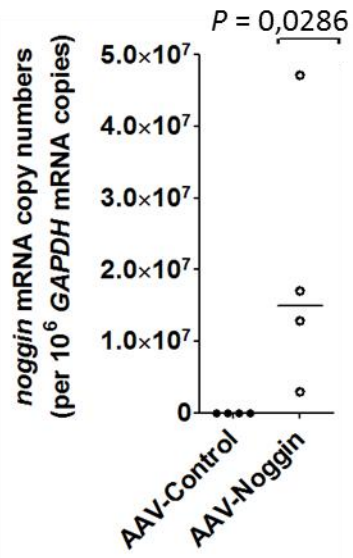
B
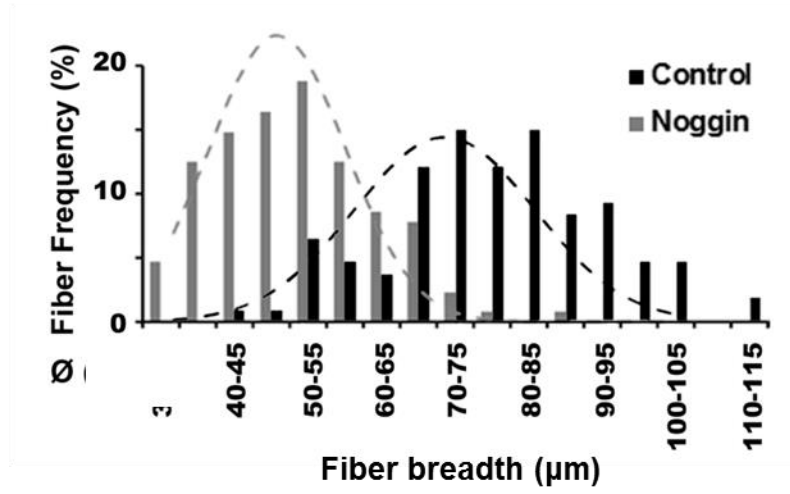
C

D
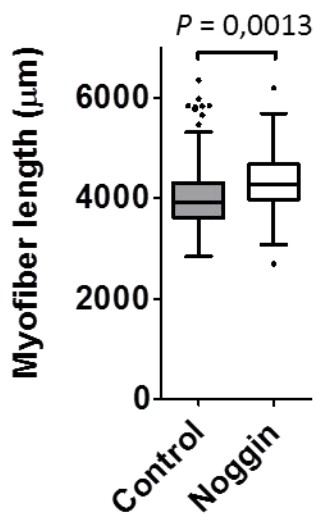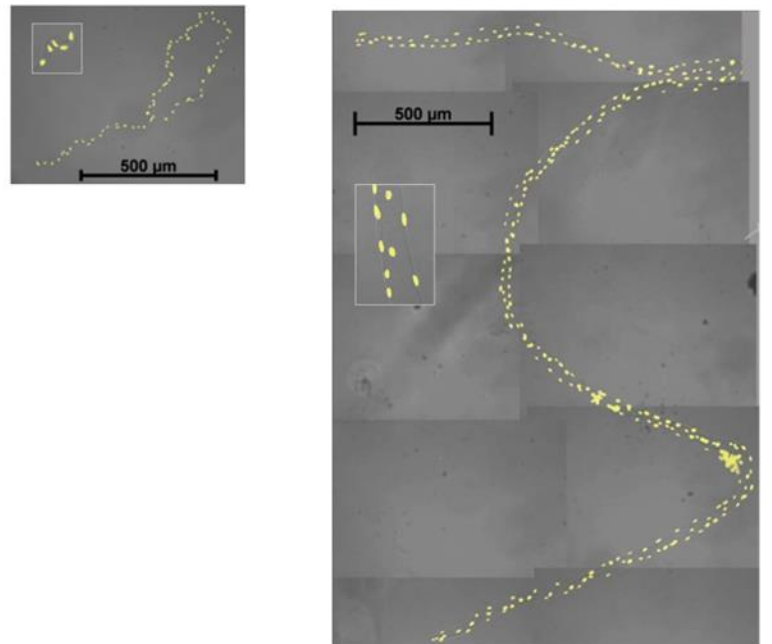
Supplementary Figure 4 – Effects of noggin and of muscle denervation on the satellite stem cell pool.

(A) The anterior compartment of the lower hindlimb was transfected with AAV-noggin at P3. Following two weeks, mice were treated daily with subcutaneous injection of BrdU for seven days and sacrificed at P21. Diagram presents number of Pax7$^+$ satellite cells normalized per 100 myofibers (left panel). Diagram in the middle panel depicts the number of Pax7$^+$/BrdU$^+$ satellite cells per 100 myofibers. The ratio of BrdU$^+$ myonuclei per 100 myofibers is presented in the left panel. n=3 for each condition. Data are shown as dot plots together with the medians. *P* value was calculated using a *T*-test.

(B) Exemplary images of immunohistochemistry to illustrate Pax7$^+$ satellite cells (red), laminin (green) illustrates the size of myofibers and DAPI was used as nuclear stain. Scale bar is 20μm.

(C) Satellite cell number increases non-significantly in denervated atrophic muscle. Hind limbs of 2 weeks old mice were denervated (ablation of nervus femoralis) and were analyzed after 2 weeks. Cryosections of TA muscles were stained against Pax7 and Laminin. n=4 for each condition. Data are shown as dot plots together with the medians. *P* value was calculated using a *T*-test.

Supplementary Figure 4

A
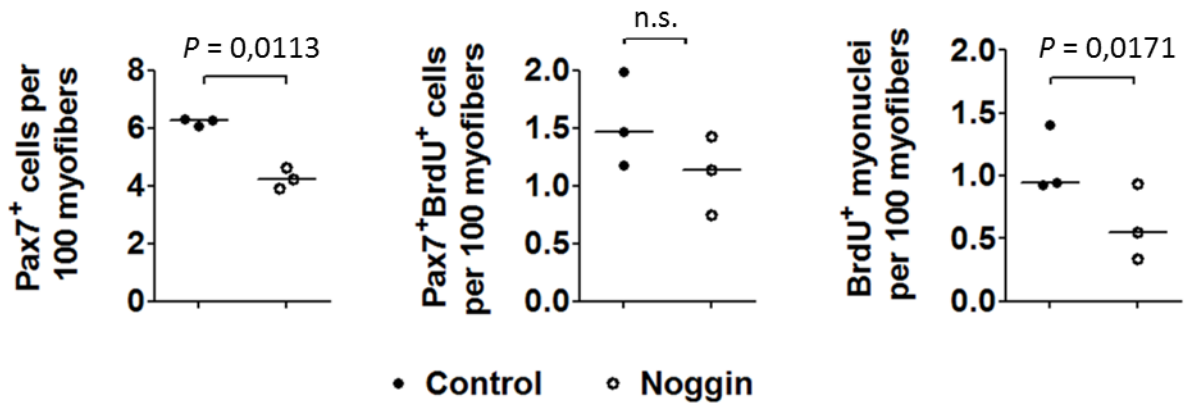
B
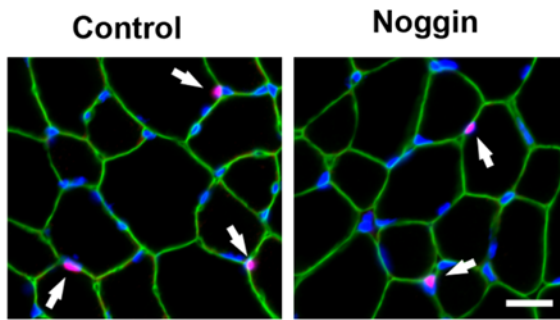
C

Supplementary Figure 5 – Cre/Lox system used to abrogate the BMP signaling pathway through inhibitory Smad6 overexpression in Pax7$^+$ cells.

(A) Scheme of *Rosa26-Lox-Stop-Lox-humanSMAD6-IRES-EGFP* and *Pax7$^{CreERT2/+}$* loci of the used transgenic mice models.

(B) Scheme of the experimental protocol: adult mice were injected with tamoxifen for five consecutive days; adult mice were sacrificed the third day after the last tamoxifen injection; skeletal muscles were collected and processed to isolate satellite-cell derived primary myoblasts with the pre-plating method; cells were cultured in proliferation medium for four days after which the RNA was extracted.

(C) Image of a 1.5% agarose gel supplemented with ethidium bromide showing the presence or absence of *human SMAD6* PCR product (using primers specific for the human sequence). The PCR was performed on cDNA synthesized from RNA extracted from cultured satellite cell-derived primary myoblasts from either tamoxifen treated *Pax7$^{CreERT2/+}$* control mice (lane 2) or tamoxifen treated *Pax7$^{CreERT2/+}$;RS6$^{+/-}$* mice (lane 3). The presence of the band in lane 3 reflects that recombination occurred in these experimental conditions.

(D) Chart showing the relative mRNA copy numbers per 10^6 *18S* rRNA of BMP target gene *Id1* in cultured satellite cell-derived primary myoblasts from tamoxifen injected mice (n=3 mice). Values are shown as dot plots together with the medians.

Supplementary Figure 5

A

RS6 mice

Rosa26 — Exon1 — LoxP — STOP — LoxP — huSmad6 — IRES-EGFP

LoxP   LoxP

Pax7^{CreERT2/+} mice

Pax7 — Cre-ER^{T2}

B

adult → Days

Tamoxifen (ip)

Sacrifice and culture of satellite cell-derived primary myoblasts

RNA extraction

C

1 — Ladder 100 bp
2 — Pax7^{CreERT2/+} + TXF
3 — Pax7^{CreERT2/+};RS6^{+/-} + TXF

D

P = 0,1687

mRNA copy numbers (per 10^6 18S rRNA copies)

Id1

▲ Pax7^{CreERT2/+} + TXF
○ Pax7^{CreERT2/+};RS6^{+/-} + TXF
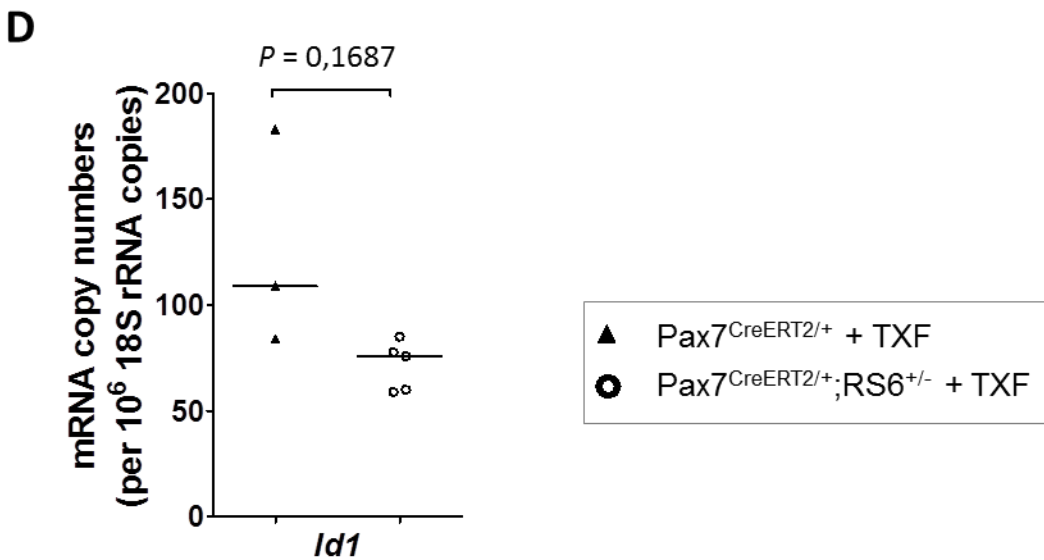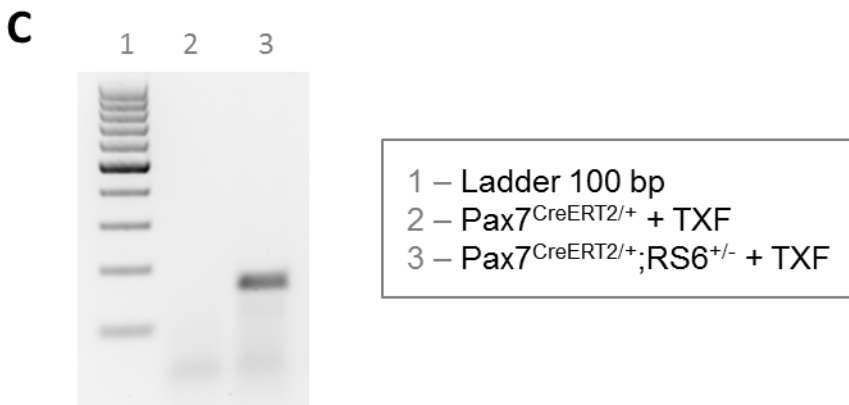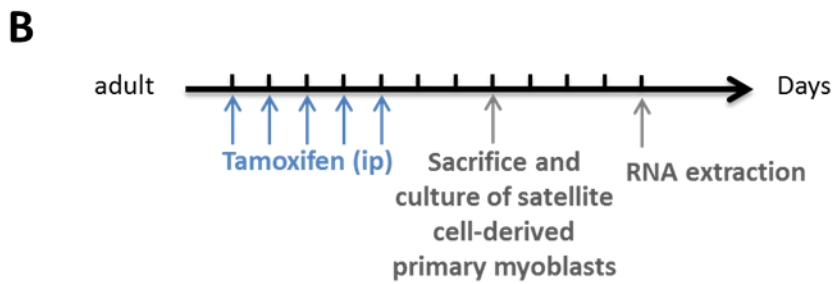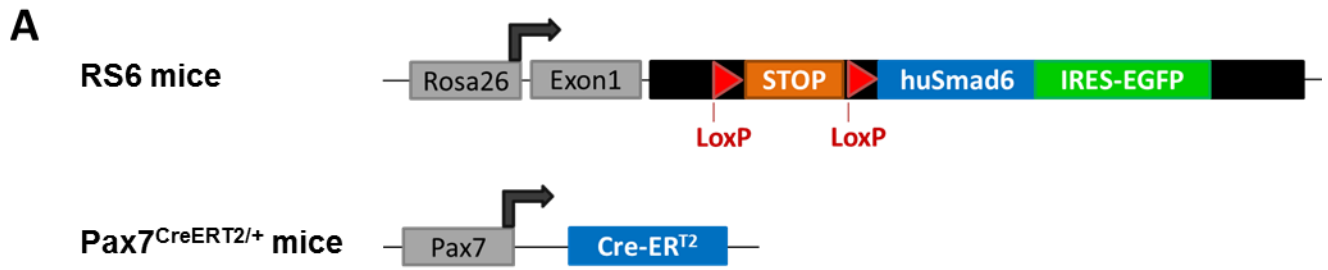
Supplementary Figure 6 – Consequences of Smad6 mediated abrogation of BMP signaling in neonatal satellite cells for muscle growth up to adulthood.

(A) Scheme of the experimental protocol: $Pax7^{CreERT2/+};RS6^{+/-}$ mice were injected with tamoxifen at P7 and P9, and sacrificed at the age of two months. Additional $Pax7^{CreERT2/+}$ control mice were sacrificed at the age of three months.

(B) Fluorescence images of immunostaining against Pax7 in red (highlighted with arrows), nuclei stained with DAPI in blue and immunostaining against laminin in green of mid-belly transverse sections of *TA* muscles from control untreated $Pax7^{CreERT2/+}$ mice compared to tamoxifen treated $Pax7^{CreERT2/+};RS6^{+/-}$ mice. Scale bar is 20 μm.

(C) Histogram presenting the distribution of *TA* muscle fiber breadth quantified on *TA* mid-belly muscle sections, in which each fiber was delineated with laminin immunostaining, from control untreated $Pax7^{CreERT2/+}$ mice (n=3, black background and white dots) compared to tamoxifen treated $Pax7^{CreERT2/+};RS6^{+/-}$ mice (n=3, white).

(D) Chart depicts the quantification of the breadth of *TA* muscle fibers, analyzed on mid-belly muscle sections following immunostaining against laminin, from control untreated $Pax7^{CreERT2/+}$ mice (n=3, black diamonds) compared to tamoxifen treated $Pax7^{CreERT2/+};RS6^{+/-}$ mice (n=3, white circles). Values are shown Whiskers-Tukey box plots together with the medians. *P* value was calculated using the nonparametric *U*-test.

(E) Diagram depicts the number of Pax7$^+$ nuclei quantified per 100 myofibers on *TA* mid-belly transverse muscle sections from control tamoxifen treated $RS6^{+/-}$ mice (n=3, black triangles), control untreated $Pax7^{CreERT2/+}$ mice (n=3, black diamonds) compared to tamoxifen treated $Pax7^{CreERT2/+};RS6^{+/-}$ mice (n=3, white circles). Values are shown as dotplots together with the median. *P* value was calculated using a *T*-test.
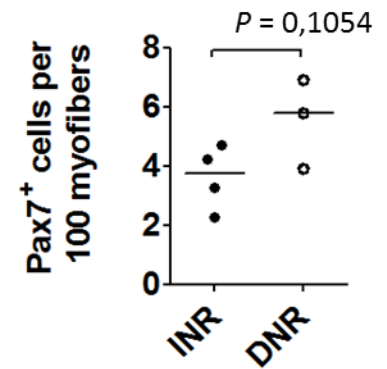
Supplementary Figure 6

A

P7   P9   2 - 3 months

Tamoxifen (ip)   analysis

◆ ▦ Pax7$^{CreERT2/+}$

○ ☐ Pax7$^{CreERT2/+}$;RS6$^{+/-}$ + TXF

B

Pax7$^{CreERT2/+}$ Pax7$^{CreERT2/+}$;RS6$^{+/-}$ + TXF

C

Fiber frequency (%)

Fiber breadth (μm)

D

Myofiber breadth (μm)

$P < 0,0001$

E

Pax7^{+} cells per 100 myofibers

$P = 0,0099$
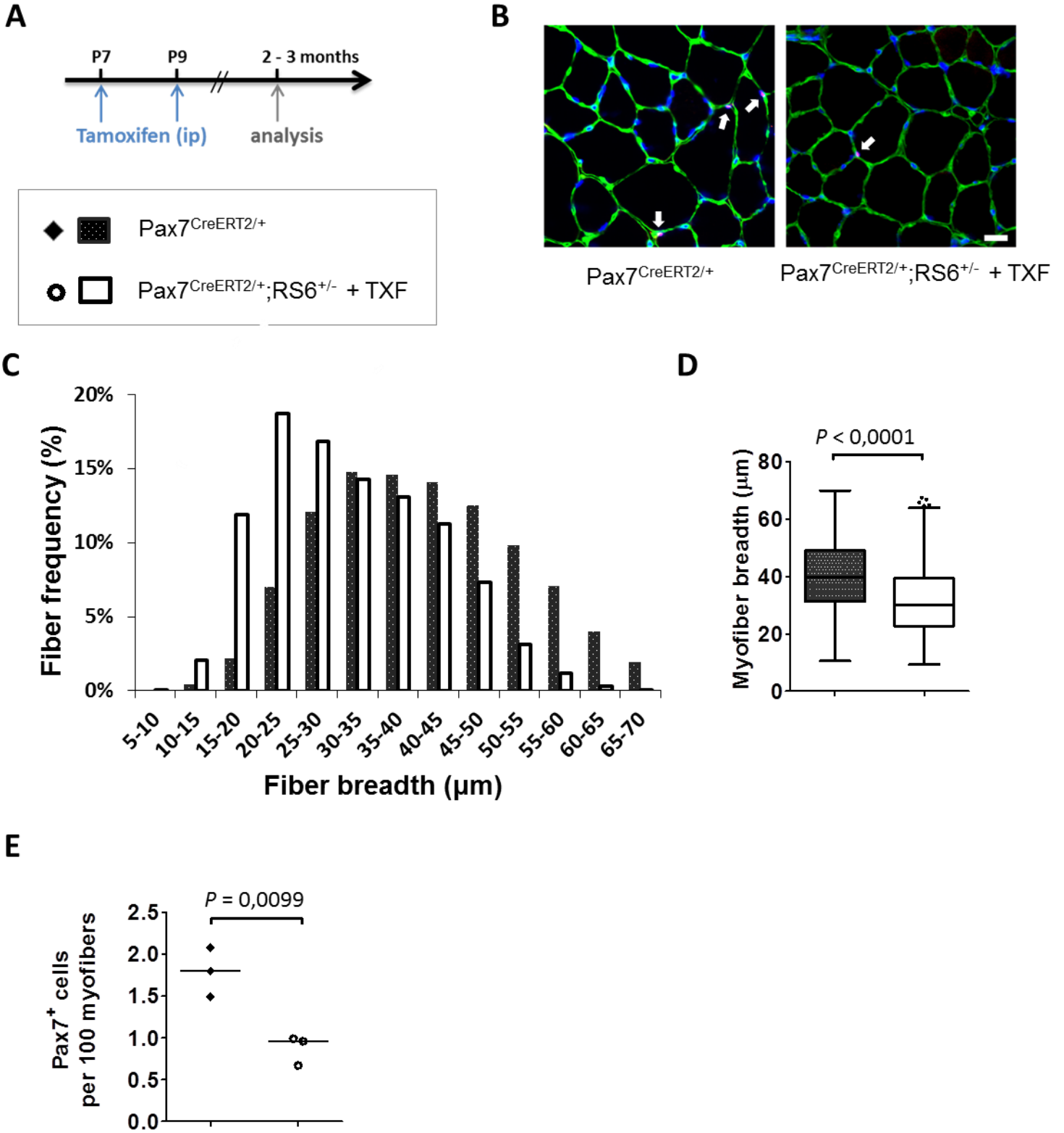
Supplementary Figure 7 - Effect of *Smad6* overexpression in terminally differentiated muscle.

(A) Scheme of *Rosa26-Lox-Stop-Lox-humanSMAD6-IRES-EGFP* and *HSA-Cre* loci of the employed transgenic mice models.

(B) Image of immunoblots showing GFP and actin bands, along with the Ponceau staining. Total proteins were extracted from the *triceps* muscle of two *HSA-Cre$^{+/-}$;RS6$^{+/-}$* mince and two *RS6$^{+/-}$* mice that were one month of age.

(C) Chart depicts the relative mRNA copy numbers per 10^6 *Gapdh* mRNA of *human SMAD6*. RNA was extracted from *gastrocnemius* muscle of one month old *RS6$^{+/-}$* mice (n=3, black dots) and *HSA-Cre$^{+/-}$;RS6$^{+/-}$* mice (n=5, white dots). Values are shown as dot plots together with the medians. *P* values were calculated using a *T*-test.

(D) Example of H&E staining on mid-belly transverse sections of *TA* muscle from control *HSA-Cre$^{+/-}$* mice compared to *HSA-Cre$^{+/-}$;RS6$^{+/-}$* mice.

(E) Example of fluorescence image following immunostaining against Pax7 in red (arrows), DAPI stained nuclei in blue and immunostaining against laminin in green of mid-belly transverse sections of *TA* muscle from control *HSA-Cre$^{+/-}$* mice compared to *HSA-Cre$^{+/-}$;RS6$^{+/-}$* mice. Scale bar is 20 μm.

(F) Chart depicting the number of Pax7$^+$ satellite cells per 100 myofibers counted on *TA* mid-belly muscle sections from one months old control *RS6$^{+/-}$* mice (n=3) compared to *HSA-Cre$^{+/-}$;RS6$^{+/-}$* mice (n=5). Values are shown as dotplots together with the medians. *P* values were calculated using a *T*-test.

(G) Chart depicting the number of Pax7$^+$ satellite cells per 100 myofibers counted on *TA* mid-belly muscle sections from two months old control *RS6$^{+/-}$* mice (n=4) compared to *HSA-Cre$^{+/-}$;RS6$^{+/-}$* mice (n=4). Values are shown as dotplots together with the medians. *P* values were calculated using the nonparametric *U*-test.

Supplementary Figure 7

A

RS6 mice

Rosa26 | Exon1 | STOP | huSmad6 | IRES-EGFP
LoxP | LoxP

HSA-Cre mice

HSA | Cre

B

HSA-Cre⁺ᐟ⁻;RS6⁺ᐟ⁻   RS6⁺ᐟ⁻

GFP

Actin

Ponceau

C

P < 0,0001

mRNA copy numbers
(per 10⁶ GAPDH mRNA copies)

huSmad6

D

RS6⁺ᐟ⁻   HSA-Cre⁺ᐟ⁻;RS6⁺ᐟ⁻

● RS6⁺ᐟ⁻
○ HSA-Cre⁺ᐟ⁻;RS6⁺ᐟ⁻

E

F

P = 0,5885

Number of Pax7⁺ nuclei
per 100 fibers

G

P = 0,3429

Number of Pax7⁺ nuclei
per 100 fibers

173
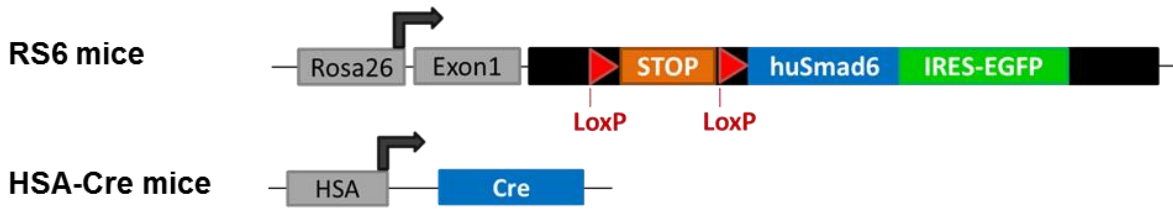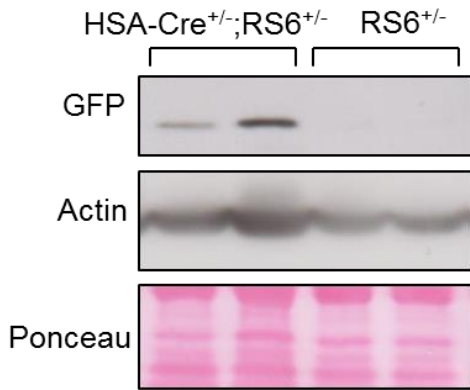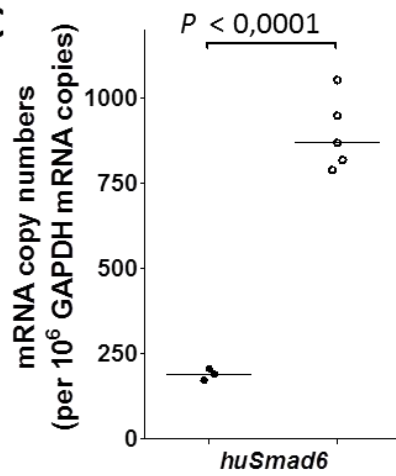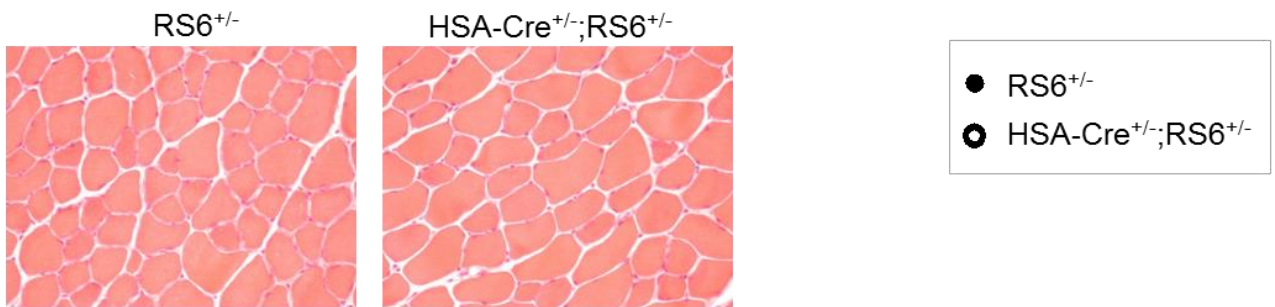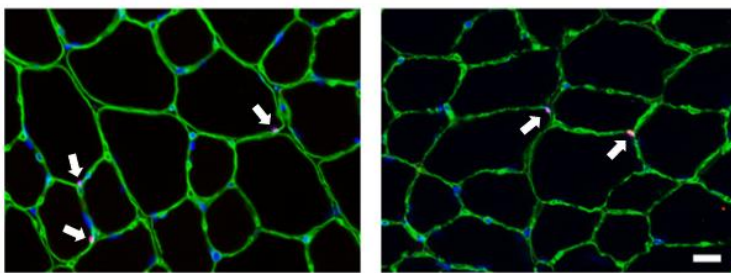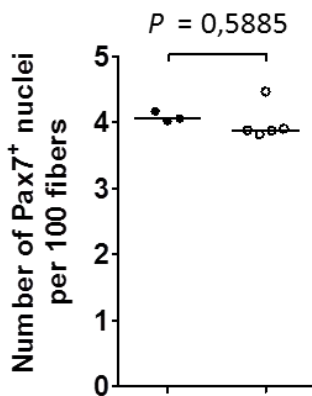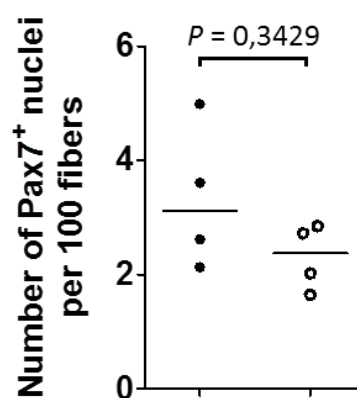
Supplementary Figure 8 – Cell imaging following abrogation of the BMP signaling pathway in satellite cell-derived primary myoblasts from *Pax7$^{CreERT2/+}$;RS6$^{+/-}$* mice.

(A) Scheme of the experimental protocol: At day 0 (D0) satellite cells from *Pax7$^{CreERT2/+}$;RS6$^{+/-}$* adult mice were isolated using FACS and cultured in low density with proliferation media; at D2-4 they were either not treated (control, CT), or treated with 1 µM hydroxytamoxifen (4-OHT) or 50 ng/mL of recombinant mouse noggin protein; at D5 cells were either fixed for immunocytochemistry or collected for RNA extraction.

(B) Representative fluorescence images of single colonies in which nuclei stained with DAPI are blue and immunostaining against MyoD, myogenin (MyoG), myosin heavy chain(MHC) or Ki67 in red (from top to bottom). Scale bar is 100 µm.

Supplementary Figure 8

A

B
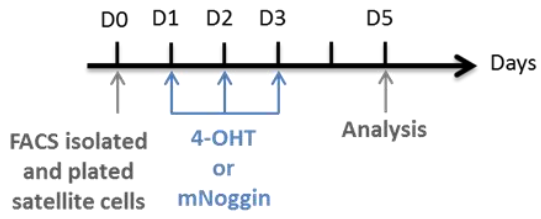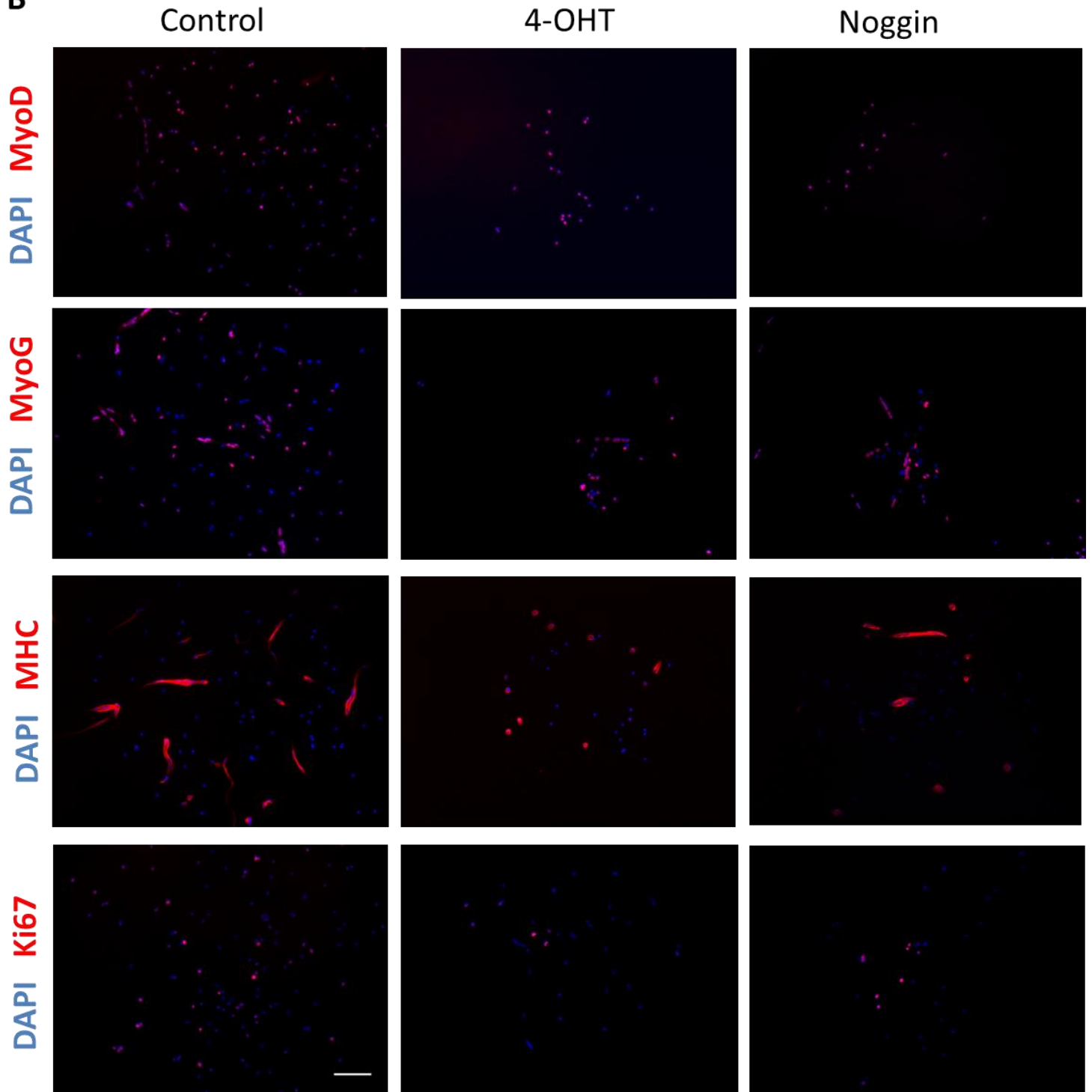
Supplementary Figure 9 - Quantitative analysis following abrogation of BMP signaling in cultured *Pax7$^{CreERT2/+}$;RS6$^{+/-}$* satellite cell-derived primary myoblasts.

Satellite cells were isolated by FACS from skeletal muscles of *Pax7$^{CreERT2/+}$;RS6$^{+/-}$* mice. The cells were cultured in low density for a proliferation assay comparing non-treated cells (control) and treated cells with either hydroxytamoxifen (4-OHT) or noggin as described in Supplementary Figure 8A.

Data is shown as cumulative rank ogives of the numbers of myoblasts expressing the protein of interest in untreated (blue), 4-OHT treated (red) and noggin treated (green) cultures. The number of cells that are positively stained for **(A)** myogenin (MyoG), **(B)** myosin heavy chain and **(C)** Ki67 is plotted on the horizontal axis. The vertical axis corresponds to the individual ranks, normalized to the rank total for each experiment to permit comparison of data sets of different sample size.

Supplementary Figure 9

A % of MyoG⁺ cells/colony

B % of MHC⁺ cells/colony

C % of Ki67⁺ cells/colony

Legend: CT, 4-OHT, Noggin
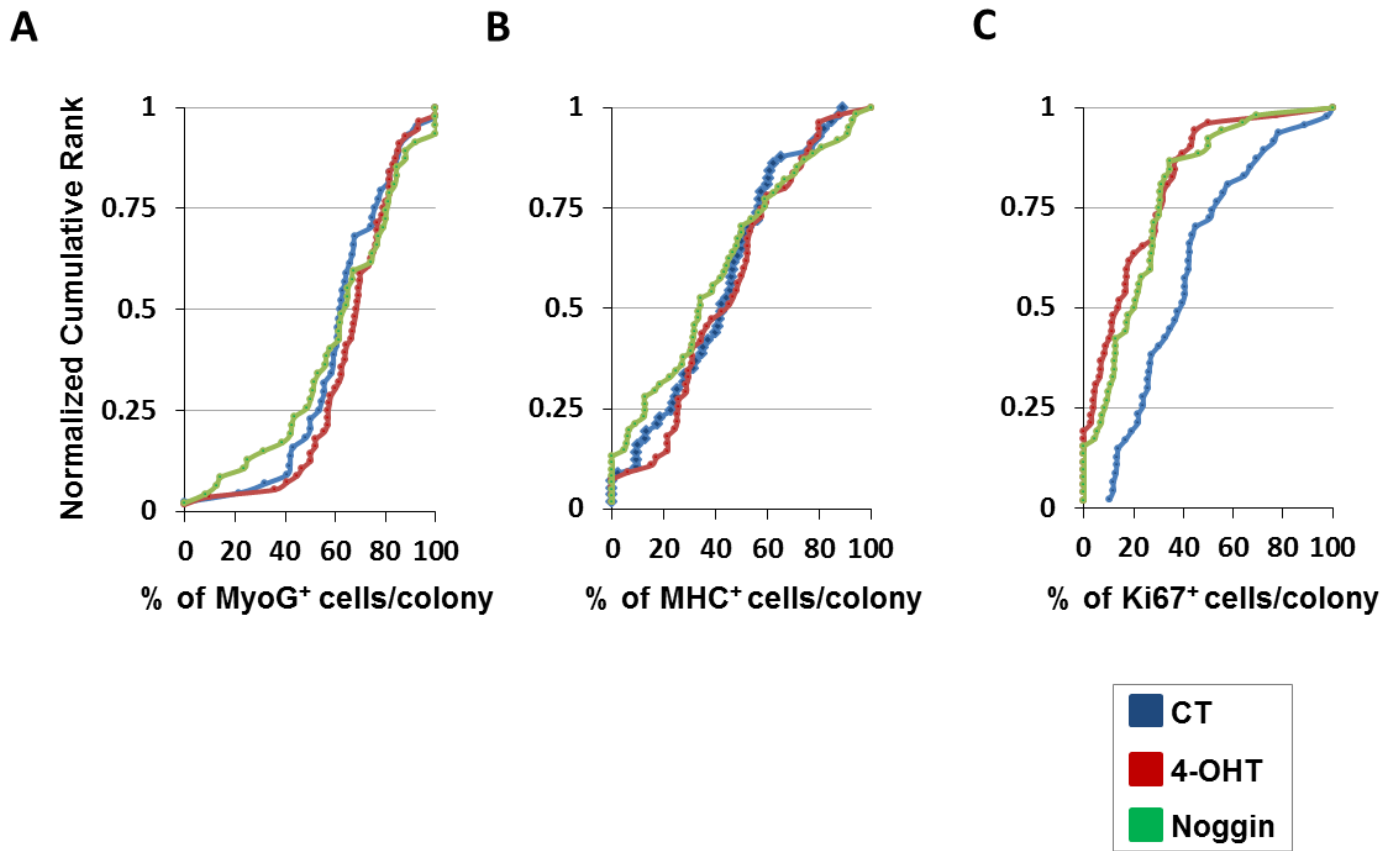
Supplementary Figure 10 – Effects of the absence of BMP6 or BMP14 on the satellite cell pool.

(A) Table describing histological parameters of *TA* and *soleus* muscles of 2 months old wild-type and *BMP6$^{-/-}$* mice. No significant differences were observed between wild-type and mutant mice.

(B) Histogram presents the distribution of myofiber breadth from anti-laminin stained cryosection of *TA* muscles from two months old wild-type and *BMP6$^{-/-}$* mice. **(C)** Diagram depicts the number of Pax7^{+} nuclei on *EDL* single myofibers. *BMP6$^{-/-}$* mice have less satellite cells than wild-type mice (n=3, *T*-test *P*<0.05).

Supplementary Figure 10

A

	Fibers		Myonuclei	
	Wild type	BMP6-null	Wild type	BMP6-null
Soleus	713	699	1623	1507
	(+/- 12)	(+/- 42)	(+/-30)	(+/- 27)
Tibialis Anterior	1794	1719	2488	2653
	(+/- 95)	(+/- 94)	(+/- 145)	(+/- 171)

B

■ Wildtype   ■ BMP6 -/-

C
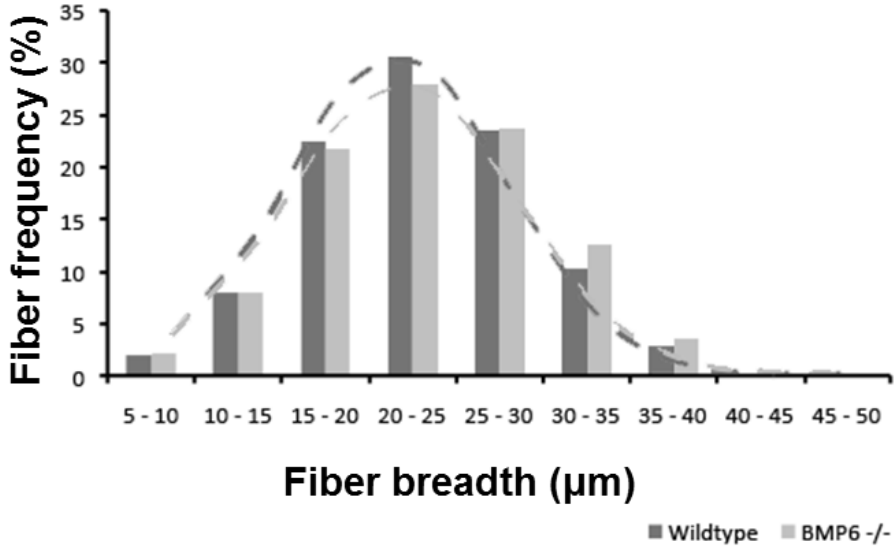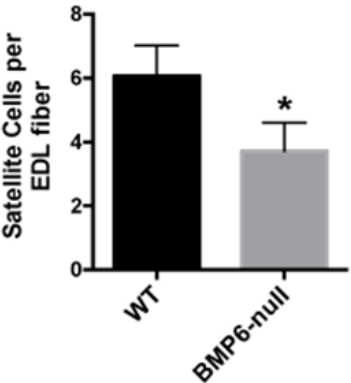
This part of my thesis has been performed in collaboration with the group of Prof. Marco Sandri (Venetian Institute of Molecular Medicine, Padova, Italy). For the contribution of our laboratory, I notably worked with my colleague, and former PhD student of our group, Dr. Elija Schirwis. The results of this project have been published:

1- Summary of the study

This study shows for the first time that BMP signaling plays a crucial role in skeletal muscle tissue homeostasis and that it is sofar the strongest hypertrophic signal for skeletal muscle cells.

Indeed, inhibition of BMP signaling, using noggin as an antagonist, causes muscle atrophy, abolishes the hypertrophy in muscles of $Mstn^{-/-}$ mice and aggravates muscle atrophy following denervation and fasting. In another experiment we investigate the gain of function of the BMP signaling pathway in muscle, through expression of a constitutive active form of receptor ALK3, which leads to muscle fiber hypertrophy. Our data demonstrate that there is a crosstalk between myostatin and BMP signaling. This study suggests a model in which BMP and myostatin pathways are in competition for the common intracellular mediator co-Smad4.

We found that skeletal muscle protects itself from severe atrophy following denervation by upregulating the BMP signaling components. Abrogation of BMP signaling in denervated muscle results in severe muscle wasting. An important factor preventing excessive muscle loss following denervation is the expression of GDF5 (BMP14), since the levels of expression of this protein is increased in denervated muscle, and its absence in $GDF5^{-/-}$ mice leads to the absence of BMP signaling activity and results in more pronounced muscle atrophy.

Furthermore, the molecular mechanism, of how BMP signaling controls muscle atrophy was elucidated. Indeed, BMP signaling negatively regulates a newly identified ubiquitin ligase required for muscle, which was named muscle ubiquitin ligase of the SCF complex in atrophy-1 (MUSA1).

Interestingly, the group of Dr. Paul Gregorevic published a parallel study on the role of BMP signaling in adult muscle, which also lead to the same conclusion that BMP signaling promotes muscle growth and inhibits muscle wasting (Winbanks et al., 2013). The latter confirmed the reproducibility of our results and conclusions.

2- My contributions to this study

For this project, I contributed in the construction of the plasmid pAAV2 containing the mutated constitutive active form of BMP receptor type I A (caALK3), which was used for the triple-transfection of HEK293 cells, method for production of adeno-associated virus AAV2/1-caALK3. I injected the latter AAV into the *TA* muscles of wild-type (*C57Bl6/J)* mice, and a non-functional control AAV-U7-c vector into the contralateral side. I analyzed the muscles 2 and 7 weeks after the injection, and performed a number of different experiments: i) muscle force was measured in collaboration with Prof. Arnaud Ferry, ii) I analyzed RNA levels of *ALK3,* iii) evaluated BMP signaling activity through P-Smad1/5/8 detection by Western blot, iv) carried out histological and morphometric analysis of muscle sections (Figure 3b, c, d and supplementary Figure 6a, b, c, d, e, f).

I also participated in experiments to determine the role of GDF5 during denervation-induced muscle atrophy in *GDF5$^{-/-}$* mice: i) I carried out histological and morphometric analysis of muscle sections, as well as ii) performed biochemical analysis of the muscles (detecting the protein levels of P-Smad1/5/8 by Western blot) (Figure 5e, f, g, h; the actual data shown in figure 5e are from our collaborator, Prof. Marco Sandri's group, who obtained similar results).

Moreover, I participated in a number of additional experiments, which involved protein extraction and immunoblotting i) for detection of P-Smad2 protein levels in AAV-Noggin or AAV-Control injected, innervated or denervated, *TA* muscles from wild-type mice (Supplementary Figure 8), and ii) for detection of P-Smad1/5/8 and Smad4 protein levels in innervated or denervated, *TA* muscles from *Mstn$^{-/-}$* mice (Supplementary Figure 13,

the actual data shown in this figure are from our collaborator, Prof. Marco Sandri's group, who obtained similar results).

In addition, I participated in the organization of an experiment in our laboratory in Paris with our collaborator, Roberta Sartori. The latter consisted in electroporating plasmids (co-transfection of *Id1-BRE* luciferase reporter along with a vector for *Renilla* luciferase for normalization of transfection efficiency) into the denervated/innervated *TA* muscles of *GDF5$^{-/-}$* mice. I provided Roberta Sartori with the harvested tissue samples for further molecular analysis (ChIP quantitative RT-PCR) (Figure 7d).

Furthermore, I maintained both *Mstn$^{-/-}$* and *GDF5$^{-/-}$* mouse lines, and genotyped the *Mstn$^{-/-}$* litters.

Finally, I participated in editing the manuscript.

3- Published article along with supplementary figures

Link to published article: http://dx.doi.org/10.1038/ng.2772

General discussion

&

Perspectives

Part I: BMP signaling is involved in regulating postnatal muscle growth.

Here we provided for the first time evidence that BMP signaling is regulating satellite cell dependent postnatal/juvenile muscle growth and the generation of the adult muscle stem cell pool. Our results shed light on how during postnatal myogenesis satellite cells shift from an active proliferative state to a quiescent state, which is reached by P21 in mice (White et al., 2010).

Previous studies have demonstrated that BMP signaling plays different roles in the stages of muscle development: i) in the early embryo it is involved in maintaining the muscle precursor population in the dermomyotome (Hirsinger et al., 1997; Pourquié et al., 1996; Reshef et al., 1998; Amthor et al., 1999; Patterson et al., 2010), ii) it is also necessary for the correct positioning of the muscle anlagen in the limbs (Amthor et al., 1998), iii) in regulating the number of muscle fibers and the number of satellite cells in fetal muscle (Wang et al., 2010), iv) in activated adult satellite cells following muscle injury (Wang et al., 2010; Friedrichs et al., 2011; Ono et al., 2011), as well as in activated cultured adult satellite cells (Friedrichs et al., 2011; Ono et al., 2011), and v) we have recently shown that it regulates muscle mass maintenance in the adult (Sartori et al., 2013) (see Results and Discussion Parts II).

With the evidence provided by our results (Results Part I) we can now stipulate that BMP signaling is required for satellite cell dependent postnatal muscle growth, and that this signaling pathway is thus playing a significant role throughout all stages of myogenesis: from embryonic development onwards to the adult muscle tissue homeostasis.

Firstly, we found the presence of P-Smad1/5/8, reflecting BMP signaling activity, in satellite cells and myonuclei throughout postnatal myogenesis: in 2-, 4-, and 8-weeks-old mice. Confirming this observation, we found transcripts of genes encoding different BMP signaling pathway components in skeletal muscle from P3, P14 and 8-weeks-old mice. Generally, the gene expression of the BMP signaling components declined from neonatal towards adulthood. Thus, since muscle growth rate correlates with BMP expression in the muscle, BMPs are most likely maintaining myogenesis. Although many BMPs are expressed in the muscle it remains unknown, i) which BMPs are involved in postnatal myogenesis, ii) which cells of the muscle tissue synthesize BMPs (myofibers, fibroblasts, endothelial cells, satellite cells, etc.), and iii) whether they act in an autocrine or paracrine manner on satellite

cells. It is likely that some BMPs have functional redundancy, such as shown for BMP2-4-7 during limb skeletal formation (Bandyopadhyay et al., 2006). With the recently developed CRISPR/Cas9 technique it will now be possible to conditionally induce mutagenesis of multiple BMPs in different cell types in the muscle (myofibers, endothelial cells, satellite cells) (Yang et al., 2013) to determine which BMPs regulate muscle growth and what is the main source of BMPs in the muscle. In the same way, conditional loss of function mutations in the different BMP specific receptors in targeted cell types could lead to an understanding of which cell types are responding to BMPs. Of note, *BMP9* and *BMP10* are not expressed in adult skeletal muscle (Sartori et al., 2013), but we have not investigated whether they are expressed during postnatal muscle growth. Interestingly both BMPs (9 and 10) are soluble BMPs found in the serum and are pivotal regulators of endothelial cells (Suzuki et al., 2010; Tillet and Bailly, 2014). One may ask whether BMP9 and BMP10 also act on satellite cells in such endocrine manner, approaching the question on complex tissue interactions such as between bone and muscle.

Secondly, we found that most BMP signaling components are expressed in satellite cells from neonatal to adult mice. Interestingly, most BMP ligands as well as receptor *ALK3* and target gene *Id1* expression levels declined between P3 and P14, a phase when satellite cells are entering quiescence, and became re-upregulated in the adult quiescent satellite cells. This re-upregulation of gene expression was surprising since by immunohistochemistry P-Smad1/5/8 seemed to be present in lower levels in adult satellite cells. We had also expected to have a decrease of gene expression between P3 and adult muscle stem cells since previous studies had found no expression of P-Smad1/5/8 or Id1 in satellite cells residing on isolated single fibers at T0 (fixation directly post isolation) (Friedrichs et al., 2011; Ono et al., 2011). As it was suggested previously that BMPs maintain satellite cells in an activated state, we initially hypothesized that BMP ligands would be downregulated in adult quiescent satellite cells. Following our finding that BMPs in fact are upregulated, we now hypothesize that BMPs in adult satellite cells have different roles depending on the context: i) during early postnatal muscle development BMPs might be required for satellite cell proliferation, ii) BMP signaling is then reduced to allow the stem cells to enter quiescence, and iii) that BMP activity might be necessary for adult satellite cell maintenance. Indeed, a previous study has shown that BMP7 maintains Pax7 expression in primary mouse satellite cells under serum-free conditions (Friedrichs et al., 2011), which reinforces our hypothesis that in the adult satellite cells BMP signaling could

be required for their maintenance. In the future it would be interesting to investigate the expression dynamics in BMP signaling components in more detail, for example at time points P3-P7-P14-P21-P28-P62, to increase the temporal resolution on what might be the role of this pathway during the switch of the satellite cell state from proliferation to quiescence. Following our hypothesis, we would expect to obtain a gradual decrease between P3 and P21, with a re-upregulation from P28 to 2 months old adult.

Interestingly, *BMP6* was most strongly expressed in adult satellite cells, and we found that mice deficient in *BMP6* have reduced numbers of satellite cells. The latter suggests that BMP6 acts on satellite cells in an autocrine manner.We next turned to investigate satellite cells in *BMP14* (*GDF5*) deficient mice. Of note, we demonstrated that *BMP14* expression was extremely stimulated following muscle denervation and upregulated more than 300 fold (Sartori et al 2013). In fact, this upregulated *BMP14* protected from exacerbated muscle fiber atrophy following denervation (see Results and Discussion Part 2). Indeed, mice deficient in *BMP14* presented profound atrophy following denervation. It was very interesting to find that *BMP14* was the only investigated ligand that we found not to be transcribed at all in satellite cells. Satellite cell number is usually maintained following denervation, however, we found that in lack of BMP14 and denervation of the muscle resulted in a substantial decrease of satellite cells. This suggests that BMP14 acts on satellite cells in a paracrine manner. Therefore, these two examples, *i.e.* the lack of *BMP14* expression and the peak of *BMP6* expression in adult satellite cells, and the consequences of their ablation, imply that BMPs have a complex function on muscle stem cells in skeletal muscle physiology and pathophysiology.

We next challenged the role of BMP signaling on postnatal muscle growth *in vivo* by abrogating BMP signaling after overexpressing noggin to antagonize BMP ligands. We found that overexpression of noggin severely impaired muscle growth: muscle fibers were smaller and the number of myonuclei per fiber was reduced as was the number of Pax7 positive satellite cells. The reduced proliferation of satellite cells was the main cellular mechanism that caused this delay of myonuclear recruitment and reduced muscle growth. We here found no evidence of precocious differentiation, which was unexpected since previous studies (Friedrichs et al., 2011; Ono et al., 2011) have shown *in vitro* that abrogating the BMP signaling pathway in proliferating satellite cells results in cell cycle exit and premature differentiation. We can only speculate on reasons why we failed to reproduce these previous observations. Possibly we injected BrDU too late during juvenile muscle

growth, indeed the time window that we looked at (AAV-noggin was injected at P3, and BrDU was injected daily between P14 and P16, muscles were analysed at P17) might not have allowed us to quantify a precocious differentiation of proliferating muscle stem cells that could have happened earlier. A possible additional experiment would be to treat juvenile mice with recombinant Noggin or soluble BMPR1A and trace the fate of satellite cells one, two and three days following the injection using mice that harbor a satellite cell reporter gene.

One major technical problem that we faced during our work was that we failed to trace *in vivo* whether satellite cells downregulated the BMP signaling pathway in response to AAV-noggin treatment or *Smad6* overexpression. For studying differentiated muscle we overexpressed reporter constructs to analyze the BMP response (Sartori 2013), however this approach is not possible for studying satellite cells. Another technical drawback was that the new lots of the P-Smad1/5/8 antibody had large non-specific staining on muscle sections that we did not observe on previous lots. However, we were able to show *in vitro* that noggin reduced almost by half the expression of the BMP target gene *Id1*. Furthermore, this experiment also reproduced the reduction of proliferation of satellite cell-derived primary myoblasts and the absence of precocious differentiation that was observed in the *in vivo* BrdU labelling experiment. Moreover, noggin might also have deprived other cell types from BMP signaling, meaning that we cannot exclude that the effect on postnatal muscle growth and muscle stem cell number was not directly due to BMP signaling inhibition in muscle cells since it could also be an indirect effect due to BMP signaling abrogation in other cell types. For example, noggin might have affected pericytes, which are known to promote postnatal muscle growth and satellite cell quiescence (Kostallari et al., 2015).

To address this point, we next tested the consequence of cell-autonomous abrogation of BMP signaling during postnatal muscle growth by overexpressing human *Smad6* (*huSmad6*), an inhibitory Smad protein of the intracellular BMP signaling cascade, directed to *Pax7* expressing satellite cells. Such time- and lineage specific expression of the *huSmad6* was obtained by crossing $Pax7^{CreERT2/+}$ mice with *Rosa26-Lox-Stop-Lox-humanSmad6-IRES-EGFP* (*RS6*) mice and tamoxifen induced expression of the transgene. In this experiment, following tamoxifen treatment, *huSmad6* was expressed under the weak, local constitutively active, Rosa26 promoter, in Pax7 positive cells. Thus, the intra-cellular BMP inhibitor Smad6 was upregulated in somewhat physiological conditions. Under the latter conditions, we obtained the same effects, although less dramatic, in the delay of muscle

growth, as observed following massive noggin upregulation. Indeed, *Smad6* upregulation in juvenile satellite cells leads to smaller *TA* and somewhat smaller *Soleus* muscles, myofiber size was also reduced in the *TA*, the number of myonuclei and of Pax7 positive cells was also decreased. Of note, one of the drawbacks of this experimental setup was that we were unable to induce recombination of floxed Stop sequence at neonatal stages, since we were unable to maintain pups injected with tamoxifen at P3 and P5. Thus, we abrogated in juvenile mice (injecting tamoxifen at P7 and P9), the resulting biological effect of *Smad6* upregulation could have been possibly stronger if it had taken place earlier. Furthermore, we have no answer regarding what is the recombination efficiency nor how fast does the recombination actually occur. Another point of discussion is that although Smad6 is commonly regarded as a BMP signaling specific inhibitor, it has recently been shown in primary hepatocytes that Smad6 inhibits a TGF-β Smad-independent non canonical pathway (Jung et al., 2013). Subsequently, it remains unknown whether our findings are exclusively due to the inhibition of the BMP canonical pathway. Similarily, noggin induced inhibition of the BMP signaling pathway might also have an effect on the Smad-independent singaling pathways.

My *in vitro* studies showed that *Smad6* upregulation, following *in vitro* hydroxytamoxifen treatment of satellite-cell derived primary myoblasts from *Pax7^CreERT2/+;RS6^+/-* mice, resulted in reduced proliferation and I found evidence of upregulation of known cell cycle exit markers known to be involved in myoblast cell cycle arrest for differentiation (Zhang et al., 1999). Indeed, expression of CDK inhibitor *p21* was slightly increased, and CDK inhibitor *p57* was upregulated, suggesting a molecular mechanism for cell cycle exit following BMP signaling abrogation. The same effect on *p21* and *p57* was observed following noggin treatment of the cells. For this experiment it would also have been interesting to try to rescue the effect of Smad6 by supplementing the proliferation media with BMP.

Like the noggin *in vivo* and *in vitro* experiment, we found no evidence of precocious differentiation following *Smad6* upregulation *in vitro* either. The main differences from the published studies (Friedrichs et al., 2011; Ono et al., 2011) showing precocious differentiation following BMP signaling abrogation were: i) the origin of the cells, we used FACS isolated satellite cells with a number of specific markers, which could include both Pax3 and Pax7 muscle stem cells, whereas the other studies used cells derived from cultured isolated single fibers or satellite cells on floating isolated fibers from one muscle, and ii) in

our *in vitro* experiment we cultured the cells in low density with proliferation medium, whereas the other studies were performed on high density cultures of expanded satellite cells from fibers with a switch to differentiation medium. Moreover, the absence of precocious differentiation in our experiments could also be explained by the fact that we only inhibited *Id1* expression levels by half. Such "low" response was sufficient to provoke reduced proliferation of the cells, however it might not have been sufficient to induce precocious differentiation by changing *Id1* mediated *MyoD* transcriptional activity. Since BMPs are known for being morphogens and leading to a concentration dependent response on cell behavior (Drossopoulou et al., 2000; Bier and De Robertis, 2015), it would thus not be surprising that a small decrease of BMP signaling activity could impinge on cell proliferation, whereas higher inhibition could also lead to a more rapid differentiation. To answer this question the same *in vitro* experiment could be done with increasing doses of noggin.

Furthermore, we have no direct evidence that satellite cell-synthesized BMPs are indeed acting on satellite cells in an autocrine fashion. To address this question a possible experiment would be to culture satellite cells and deprive them from serum, since we have seen that satellite cells express BMP ligands and receptor BMPR1A, if we observed active BMP signaling in the cells we could conclude that satellite cells can respond to BMPs in an autocrine manner.

Another important observation during this study was that when using the $Pax7^{CreERT2/+}$ mice as controls, we discovered that the number of satellite cells was also reduced in these mice due to haploinsufficiency. This observation was alarming since many laboratories in the field are using these transgenic mice for different studies (Lepper and Fan, 2010; Grand et al., 2012; Zhang et al., 2015), and it has never been described that these mice have less satellite cells due to the loss of one *Pax7* endogenous locus. However, in our study we still observed a biological effect, even in the low expression of *Smad6* under the weak promoter of Rosa26, but under these conditions it is difficult to evaluate the extent of the biological effect since it may be masked to some extent by the potential *Pax7* haploinsufficiency. Subsequently, we are convinced that for future experiments it would be more appropriate to use other *Pax7-CreERT* driver mice that are not knocked-in, such as the mice generated by the groups of Gabrielle Kardon (*Pax7iCreERT2*, Murphy et al., 2011) and Charles Keller (*Pax7CreER*, Nishijo et al., 2009), but in which an *IRES-CreERT2* cassette

would be inserted into the 3'UTR of the *Pax7* gene, thus preserving intrinsic Pax7 molecular function at a normal dosage.

Of note, in the tamoxifen treated *Pax7$^{CreERT2/+}$;RS6$^{+/-}$* mice, we observed a change in the satellite cell markers in these mice during their FACS sorting, with a loss of Sca-1^{neg} cells and the essential presence of Sca-1^{med} and Sca-1^{pos}. Satellite cells sorted from monoallelic *Pax7$^{CreERT2/+}$* tamoxifen treated adult mice did not present this difference in *Sca-1* expression. It has been previously described that satellite cells are Sca1^{neg}, which give rise to myoblasts that are heterogeneous for Sca1, which negatively regulates proliferation and differentiation of muscle cells (Mitchell et al., 2005). The latter study also reported that Sca-1^{neg} myoblasts divide rapidly in contrast to Sca-1^{pos} myoblasts, which divide slower and do not readily form myotubes. It could be of interest to further investigate the observed change in Sca1 expression levels on the membrane surface, for example by performing immunostainings of Pax7, MyoD and other myogenic markers in the different Sca1$^{neg/med/pos}$ populations. However, we also hypothesize that the result could also be due to some GFP expression that might affect the cell sorting of the Sca1 negative population, even though we were unable to detect any GFP positive cells. To elucidate the latter, it would suffice to exchange the Sca1-FITC antibody with a Sca1 antibody coupled with a different fluorochrome.

Interestingly, it has come to our attention that another method for FACS isolation of satellite cells using different markers, combining V-cam positive selection as well as negative selection of Sca1, CD45 and CD31, seems to provide much higher yields in the number of cells obtained (Cheung et al., 2012) as compared to the method we used. Thus, for future experiments on FACS-sorted satellite cells it could be interesting to establish this technique to have increased biological material for different treatments.

Finally, we concluded that BMP signaling is important throughout all stages of myogenesis. The increasing evidence of the role of BMP signaling in skeletal muscle tissue, along with many other elucidated functions of BMPs throughout the body, allow us to put into question the original name given to these signaling molecules that nowadays probably should not be called "Bone" morphogenetic proteins but better "Body" morphogenetic proteins, as suggested in the first international BMP workshop in 2009 (Wagner et al., 2010).

To advance our understanding of the role of BMP signaling involved in regulating muscle stem cells, it will be important to further elucidate the underlying molecular mechanisms. In order to identify BMP targets we will next perform RNA-Seq and ChIP-Seq experiments on satellite cells following manipulation of the BMP signaling pathway.

Part II: The BMP signaling pathway controls adult skeletal muscle mass and antagonizes the TGF-β signaling pathway.

One part of my thesis, which is devoted to elucidate the role of BMP signaling during postnatal satellite-cell dependent muscle growth in mice, is discussed in the previous chapter. The other part of my thesis was to address the question, whether BMP signaling plays a role in adult muscle mass hypertrophy and homeostasis, which has already been published and that I discuss in this chapter.

Our published work, presented in Results Part II, provides new insights into the role of BMP signaling in adult skeletal muscle mass maintenance. We here showed for the first time that the BMP signaling axis is a positive regulator of muscle mass.

The first trail for this study was the surprising observation that *Smad4* conditional muscle specific knock-out mice (in which both the canonical TGF-β and BMP signaling pathways are impaired) had a different phenotype from *Mstn*$^{-/-}$ mice (myostatin is a negative regulator of muscle mass), because *Smad4 cKO* mice did not present with hypertrophic muscles. Indeed, their muscles were actually slightly atrophic and weaker than *Smad4*$^{fl/fl}$ controls. In addition, *Smad4 cKO* mice underwent dramatically exacerbated muscle atrophy after denervation, suggesting that Smad4 is required to maintain muscle mass and prevent muscle wasting. Smad4 is a common intracellular mediator of both the myostatin and the BMP signaling pathways. Moreover, we had observed that BMP signaling is active in adult myonuclei, which expressed P-Smad1/5/8. Thus, the phenotype of the *Smad4 cKO* mice suggested that BMP signaling and myostatin might both be regulators of muscle mass, and their signaling cascades could be fine-tuned through competition for Smad4 **(Figure 29).**

Subsequently, we blocked the BMP signaling pathway in adult muscle by overexpressing noggin. This loss-of-function experiment resulted in muscle atrophy in WT mice and the reversion of the *Mstn*$^{-/-}$ hypertrophic phenotype. Furthermore, we showed that caALK3 overexpression, a gain-of-function experiment, promoted muscle hypertrophy under normal conditions and was sufficient to block muscle atrophy and even promote hypertrophy following denervation. These results demonstrated that BMP signaling is a positive regulator of muscle mass. These results also supported the hypothesis that BMP signaling operates in competition with the myostatin/TGF-β signaling pathway.
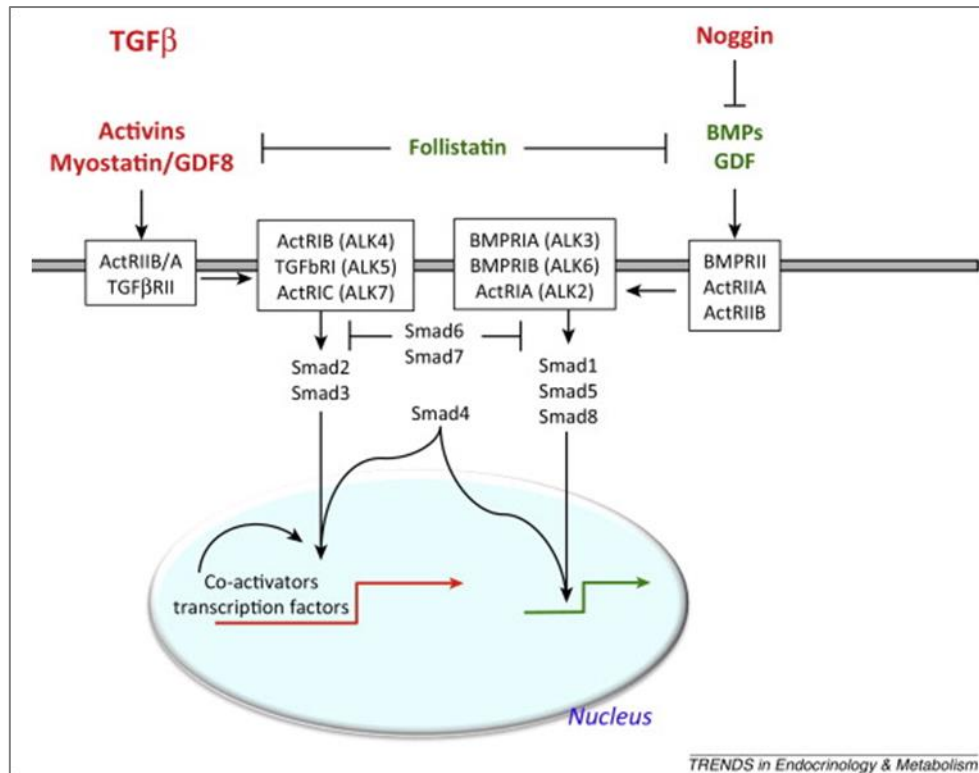
Figure 29 - Signaling and crosstalk between myostatin (GDF8)/activin/TGFβ and BMP/GDF subfamilies. Soluble factors that negatively control muscle mass are depicted in red and the factors that promote muscle growth in green. The different ligands bind to type II receptors that are partially shared by the two pathways. Type II receptors recruit different type I receptors, which activate the downstream Smad transcription factors. Myostatin (GDF8)/activin/TGFb induces Smad2/3 whereas the BMP/GDF subfamilies activate Smad1/5/8. Smad4 is a cofactor that is shared by the different Smads and is mostly required for transcriptional activity at the target genes. From Sartori et al., 2014 (Copyright clearance center license number 3658241393010).

Together with Prof. Marco Sandri's group we investigated the possibility of an interaction between the two pathways *via* Smad4 competition. We designed experimental conditions in which either one or the other pathway were activated or inhibited. We quantified the levels of either P-Smad2/3 for the myostatin signaling pathway, or P-Smad1/5/8 for the BMP signaling pathway. We performed experimental assays to evaluate the regulation of known target genes, *p21* in the case of myostatin/TGF-β pathway, or *Id1* for the BMP pathway (Korchynskyi and Dijke, 2002). Using this readout we found that in lack of myostatin (in *Mstn*^{-/-} mice) the levels of P-Smad1/5/8, as well as binding of P-Smad1/5/8 and Smad4 to the BRE (BMP Responsive Element) of *Id1*, were increased. In lack of BMP signaling (noggin treated WT mice) the binding of P-Smad1/5/8 and Smad4 to the SBE of the *Id1* promoter was abolished. However it also induced recruitment of P-Smad2/3 and Smad4 to the SBE (Smad Binding Element) of the *p21* promoter (Carlson et

240

al., 2008). In other words, as expected, the decrease of myostatin leading to less P-Smad2/3 seemed to release Smad4, which was free to bind to P-Smad1/5/8, and vice versa when BMP signaling is inhibited, Smad4 is available for binding P-Smad2/3. Therefore, our results were consistent with a model, in which the BMP and myostatin pathways are in competition for Smad4. Of note, there are other factors that contribute to the cross-regulation between the two signaling pathways, for example myostatin and BMPs/GDFs ligands compete for common type II receptors ActRIIB and ActRIIA (Moustakas and Heldin, 2009) **(Figure 29)**. Overall, our results suggest that BMPs and myostatin competition defines a signaling "balance" required for maintaining muscle mass at its correct size, and that disturbing this balance induces either hypertrophy or atrophy of the muscle.

Having identified that BMP signaling is an important regulator of muscle mass, we asked whether BMP signaling would be involved in denervation-induced muscle atrophy. We therefore compared the expression levels of BMP genes in control and denervated muscles and found that *Gdf6* (*BMP13*) and *Gdf5* (*BMP14*) were strongly induced following denervation. Of note, noggin antagonist can bind BMP13 and BMP14 (Krause et al., 2011). In line with these observations, we found that the denervation induced severe atrophy in Gdf5 null mice compared to WT mice, confirming that BMP14 is an important factor for muscle maintenance in denervation-induced atrophy. Interestingly, we also found an increase in *ALK6* (*BMPR1B*) expression levels in denervated muscles and it is known that BMP14 binds preferentially to ALK6 compared to the other type I receptors (Nishitoh, 1997).

Furthermore, we investigated the molecular mechanism by which BMP signaling maintains muscle mass in the context of denervated muscle. After performing gene expression profiling in denervated *Smad4 cKO* muscles as compared to control *Smad4$^{fl/fl}$* denervated muscles we found an upregulation of a new E3 ubiquitin ligase *Fbox30* in denervated *Smad4 cKO* muscles and we named this uncharacterized F-box protein MUSA1 (muscle ubiquitin ligase of SCD complex in atrophy-1). The latter, was also overexpressed in denervated muscle treated with noggin, which suggested that BMP signaling negatively regulates MUSA1. In addition, RNAi-mediated knock down of *MUSA1* protected denervated muscles from atrophy. Thus, our results show that BMP signaling inhibits muscle denervation induced atrophy through the regulation of *MUSA1* and subsequently the inhibition of muscle catabolism. In addition, regarding the molecular mechanism, Winbancks and colleagues have shown that inhibition of mTOR signaling prevented BMP

induced hypertrophy of skeletal muscle suggesting that BMP signaling induces hypertrophy by regulating the IGF1/Akt/mTOR pathway involved in protein synthesis and muscle size increase (Winbanks et al., 2013). The latter stands in contrast to the myostatin mediated inhibition of the IGF-1/Akt/mTOR signaling pathway (Sartori et al., 2009).

In this study there are points that remain open for discussion. For example, as it was suggested in a recent publication (Krause et al., 2011), it remains unknown if noggin can act independently of BMPs *via* binding to its own sofar unidentified receptor, like it has been shown for another BMP antagonist, gremlin, which binds to the VEGF receptor 2 (Mitola et al., 2010). Thus, it is possible that noggin may interact with unknown receptors and may have biological effects that we could not have taken into account in this study. However, this is one of the reasons why it is crucial to establish different techniques to address a biological question, which is why in our study, as an alternative approach, we inhibited the BMP signaling pathway by RNAi mediated knock down of Smad1/5 or by treatment with a synthetic pharmacological inhibitor of BMP type I receptors called LDN-193189 (Yu et al., 2008). All these interventions also induced muscle atrophy like AAV-noggin treatment. The replication of our results with these alternative approaches suggests that the biological effect observed through noggin over-expression is indeed a direct effect of inhibition of the BMP signaling and excludes the possibility of an effect due to unknown roles of noggin in this context.

Moreover, in our experiments, by over-activating the BMP signaling pathway in muscle by expressing a constitutive active form of ALK3 (BMPR-IA), we induced muscle hypertrophy. However, following transduction of AAV-caALK3 we also observed the presence of mononuclear cell infiltrates, possibly macrophages, suggesting an inflammation of the muscle. An important number of myofibers also presented with centralized myonuclei indicating that these were newly generated myofibers and that process of degeneration and regeneration had occurred in this muscle following AAV-caALK3 injection. My interpretation is that this was due to a massive and sudden hypertrophic effect that could have caused a metabolic breakdown of the myofibers, resulting in their regeneration. However, another explanation could be the effect of an immune response of the mouse injected with the human caALK3. In contrast, Dr. Gregorevic's group, who also induced muscle hypertrophy following AAV-caALK3 muscle injection, did not report any observations of degeneration or inflammation (Winbanks et al., 2013).

Furthermore, even though we observed an increase of the canonical BMP signaling pathway, since P-Smad1/5/8 levels were higher following AAV-caALK3, we cannot exclude the possibility that the non-canonical pathway was also activated, through phosphorylation of other intracellular substrates.

Although this study has focused on the role of BMP signaling in adult skeletal muscle mass homeostasis and maintenance in the context of denervation, it is interesting to note that there have been studies that indicate that BMP signaling plays a role in the establishment of the neuromuscular junction in *Drosophila* (McCabe et al., 2003; Ball et al., 2010) and some researchers speculate that BMP signaling could play a role in human neurodegenerative diseases, such as amyotrophic lateral sclerosis, spinal muscular atrophy or Huntington's disease (Bayat et al., 2011). Therefore it might be possible, that increased BMP expression levels in denervated muscle may be induced not only to prevent catabolism through MUSA1 inhibition, but also in the attempt to promote neuromuscular junction regeneration. Of note, we used denervation as a tool to study muscle atrophy but this technique does not constitute a reliable model to mimick neurodegenerative diseases. Further studies are needed to address the question whether BMP signaling is affected in such disorders.

Finally, our study, along with the results published by Winbanks and colleages, shows that further investigations allowing to better understand the negative impact of TGF-β and the positive role of BMP in regulating muscle mass could shed light on skeletal muscle mass growth and eventually be useful for the development of new therapeutic strategies for muscle-related diseases. As discussed recently by (Sartori et al., 2014), some questions that remain unanswered include: i) which are the TGF-β and BMP target genes that induce respectively atrophy and hypertrophy, ii) is Smad4 the unique limiting factor that regulates TGF-β and BMP cross-talk, iii) what is the molecular mechanism that connects myostatin and BMP signaling with the Akt/mTOR pathway.

Bibliography

Abe, M., Oda, N. and Sato, Y. (1998). Cell-associated activation of latent transforming growth factor-β by calpain. *J. Cell. Physiol.* **174**, 186–193.

Afrakhte, M., Morén, A., Jossan, S., Itoh, S., Sampath, K., Westermark, B., Heldin, C.-H., Heldin, N.-E. and Dijke, P. ten (1998). Induction of Inhibitory Smad6 and Smad7 mRNA by TGF-β Family Members. *Biochem. Biophys. Res. Commun.* **249**, 505–511.

Agbulut, O., Noirez, P., Beaumont, F. and Butler-Browne, G. (2003). Myosin heavy chain isoforms in postnatal muscle development of mice. *Biol. Cell Auspices Eur. Cell Biol. Organ.* **95**, 399–406.

Akiyama, S., Katagiri, T., Namiki, M., Yamaji, N., Yamamoto, N., Miyama, K., Shibuya, H., Ueno, N., Wozney, J. M. and Suda, T. (1997). Constitutively Active BMP Type I Receptors Transduce BMP-2 Signals without the Ligand in C2C12 Myoblasts. *Exp. Cell Res.* **235**, 362–369.

Alejandre-Alcázar, M. A., Michiels-Corsten, M., Vicencio, A. G., Reiss, I., Ryu, J., de Krijger, R. R., Haddad, G. G., Tibboel, D., Seeger, W., Eickelberg, O., et al. (2008). TGF-β signaling is dynamically regulated during the alveolarization of rodent and human lungs. *Dev. Dyn.* **237**, 259–269.

Allouh, M. Z., Yablonka-Reuveni, Z. and Rosser, B. W. C. (2008). Pax7 Reveals a Greater Frequency and Concentration of Satellite Cells at the Ends of Growing Skeletal Muscle Fibers. *J. Histochem. Cytochem.* **56**, 77–87.

Amthor, H. and M.H. Hoogaars, W. (2012). Interference with Myostatin/ActRIIB Signaling as a Therapeutic Strategy for Duchenne Muscular Dystrophy. *Curr. Gene Ther.* **12**, 245–259.

Amthor, H., Christ, B., Weil, M. and Patel, K. (1998). The importance of timing differentiation during limb muscle development. *Curr. Biol.* **8**, 642–652.

Amthor, H., Christ, B. and Patel, K. (1999). A molecular mechanism enabling continuous embryonic muscle growth - a balance between proliferation and differentiation. *Development* **126**, 1041–1053.

Amthor, H., Christ, B., Rashid-Doubell, F., Kemp, C. F., Lang, E. and Patel, K. (2002). Follistatin Regulates Bone Morphogenetic Protein-7 (BMP-7) Activity to Stimulate Embryonic Muscle Growth. *Dev. Biol.* **243**, 115–127.

Amthor, H., Nicholas, G., McKinnell, I., Kemp, C. F., Sharma, M., Kambadur, R. and Patel, K. (2004). Follistatin complexes Myostatin and antagonises Myostatin-mediated inhibition of myogenesis. *Dev. Biol.* **270**, 19–30.

Amthor, H., Otto, A., Vulin, A., Rochat, A., Dumonceaux, J., Garcia, L., Mouisel, E., Hourdé, C., Macharia, R., Friedrichs, M., et al. (2009). Muscle hypertrophy driven by myostatin blockade does not require stem/precursor-cell activity. *Proc. Natl. Acad. Sci. U. S. A.* **106**, 7479–7484.

Andriopoulos Jr, B., Corradini, E., Xia, Y., Faasse, S. A., Chen, S., Grgurevic, L., Knutson, M. D., Pietrangelo, A., Vukicevic, S., Lin, H. Y., et al. (2009). BMP6 is a key endogenous regulator of hepcidin expression and iron metabolism. *Nat. Genet.* **41**, 482–487.

Asakura, A., Rudnicki, M. A. and Komaki, M. (2001). Muscle satellite cells are multipotential stem cells that exhibit myogenic, osteogenic, and adipogenic differentiation. *Differentiation* **68**, 245–253.

Asakura, A., Seale, P., Girgis-Gabardo, A. and Rudnicki, M. A. (2002). Myogenic specification of side population cells in skeletal muscle. *J. Cell Biol.* **159**, 123–134.

Aulehla, A. and Pourquié, O. (2006). On periodicity and directionality of somitogenesis. *Anat. Embryol. (Berl.)* **211**, 3–8.

Bai, S. and Cao, X. (2002). A Nuclear Antagonistic Mechanism of Inhibitory Smads in Transforming Growth Factor-β Signaling. *J. Biol. Chem.* **277**, 4176–4182.

Bai, S., Shi, X., Yang, X. and Cao, X. (2000). Smad6 as a Transcriptional Corepressor. *J. Biol. Chem.* **275**, 8267–8270.

Ball, R. W., Warren-Paquin, M., Tsurudome, K., Liao, E. H., Elazzouzi, F., Cavanagh, C., An, B.-S., Wang, T.-T., White, J. H. and Haghighi, A. P. (2010). Retrograde BMP Signaling Controls Synaptic Growth at the NMJ by Regulating Trio Expression in Motor Neurons. *Neuron* **66**, 536–549.

Bandyopadhyay, A., Tsuji, K., Cox, K., Harfe, B. D., Rosen, V. and Tabin, C. J. (2006). Genetic analysis of the roles of BMP2, BMP4, and BMP7 in limb patterning and skeletogenesis. *PLoS Genet.* **2**, e216.

Bansal, D., Miyake, K., Vogel, S. S., Groh, S., Chen, C.-C., Williamson, R., McNeil, P. L. and Campbell, K. P. (2003). Defective membrane repair in dysferlin-deficient muscular dystrophy. *Nature* **423**, 168–172.

Bayat, V., Jaiswal, M. and Bellen, H. J. (2011). The BMP signaling pathway at the Drosophila neuromuscular junction and its links to neurodegenerative diseases. *Curr. Opin. Neurobiol.* **21**, 182–188.

Beauchamp, J. R., Heslop, L., Yu, D. S. W., Tajbakhsh, S., Kelly, R. G., Wernig, A., Buckingham, M. E., Partridge, T. A. and Zammit, P. S. (2000). Expression of Cd34 and Myf5 Defines the Majority of Quiescent Adult Skeletal Muscle Satellite Cells. *J. Cell Biol.* **151**, 1221–1234.

Benchaouir, R., Meregalli, M., Farini, A., Antona, G. D', Belicchi, M., Goyenvalle, A., Battistelli, M., Bresolin, N., Bottinelli, R., Garcia, L., et al. (2007). Restoration of Human Dystrophin Following Transplantation of Exon-Skipping-Engineered DMD Patient Stem Cells into Dystrophic Mice. *Cell Stem Cell* **1**, 646–657.

Bentzinger, C. F., Wang, Y. X. and Rudnicki, M. A. (2012). Building Muscle: Molecular Regulation of Myogenesis. *Cold Spring Harb. Perspect. Biol.* **4**, a008342.

Bhowmick, N. A., Ghiassi, M., Bakin, A., Aakre, M., Lundquist, C. A., Engel, M. E., Arteaga, C. L. and Moses, H. L. (2001a). Transforming Growth Factor-β1 Mediates Epithelial to Mesenchymal Transdifferentiation through a RhoA-dependent Mechanism. *Mol. Biol. Cell* **12**, 27–36.

Bhowmick, N. A., Zent, R., Ghiassi, M., McDonnell, M. and Moses, H. L. (2001b). Integrin β1 Signaling Is Necessary for Transforming Growth Factor-β Activation of p38MAPK and Epithelial Plasticity. *J. Biol. Chem.* **276**, 46707–46713.

Bier, E. and De Robertis, E. M. (2015). EMBRYO DEVELOPMENT. BMP gradients: A paradigm for morphogen-mediated developmental patterning. *Science* **348**, aaa5838.

Birchmeier, C. and Brohmann, H. (2000). Genes that control the development of migrating muscle precursor cells. *Curr. Opin. Cell Biol.* **12**, 725–730.

Biressi, S., Tagliafico, E., Lamorte, G., Monteverde, S., Tenedini, E., Roncaglia, E., Ferrari, S., Ferrari, S., Cusella-De Angelis, M. G., Tajbakhsh, S., et al. (2007). Intrinsic phenotypic diversity of embryonic and fetal myoblasts is revealed by genome-wide gene expression analysis on purified cells. *Dev. Biol.* **304**, 633–651.

Bischoff, R. (1986). Proliferation of muscle satellite cells on intact myofibers in culture. *Dev. Biol.* **115**, 129–139.

Bobacz, K., Gruber, R., Soleiman, A., Erlacher, L., Smolen, J. S. and Graninger, W. B. (2003). Expression of bone morphogenetic protein 6 in healthy and osteoarthritic human articular chondrocytes and stimulation of matrix synthesis in vitro. *Arthritis Rheum.* **48**, 2501–2508.

Brack, A. S., Conboy, I. M., Conboy, M. J., Shen, J. and Rando, T. A. (2008). A Temporal Switch from Notch to Wnt Signaling in Muscle Stem Cells Is Necessary for Normal Adult Myogenesis. *Cell Stem Cell* **2**, 50–59.

Brooke MH and Kaiser KK (1970). Muscle fiber types: How many and what kind? *Arch. Neurol.* **23**, 369–379.

Bruusgaard, J. C., Johansen, I. B., Egner, I. M., Rana, Z. A. and Gundersen, K. (2010). Myonuclei acquired by overload exercise precede hypertrophy and are not lost on detraining. *Proc. Natl. Acad. Sci.* **107**, 15111–15116.

Bücker, S. (2011). BMP und SMAD Signale im kardiovaskulären System.

Buckingham, M. (1992). Making muscle in mammals. *Trends Genet.* **8**, 144–149.

Buckingham, M. (2006). Myogenic progenitor cells and skeletal myogenesis in vertebrates. *Curr. Opin. Genet. Dev.* **16**, 525–532.

Buckingham, M. and Relaix, F. (2007). The Role of Pax Genes in the Development of Tissues and Organs: Pax3 and Pax7 Regulate Muscle Progenitor Cell Functions. *Annu. Rev. Cell Dev. Biol.* **23**, 645–673.

Burkin, D. J. and Kaufman, S. J. (1999). The alpha7beta1 integrin in muscle development and disease. *Cell Tissue Res.* **296**, 183–190.

Carlson, M. E., Hsu, M. and Conboy, I. M. (2008). Imbalance between pSmad3 and Notch induces CDK inhibitors in old muscle stem cells. *Nature* **454**, 528–532.

Chacko, B. M., Qin, B. Y., Tiwari, A., Shi, G., Lam, S., Hayward, L. J., de Caestecker, M. and Lin, K. (2004). Structural Basis of Heteromeric Smad Protein Assembly in TGF-β Signaling. *Mol. Cell* **15**, 813–823.

Cheek, D. B., Powell, G. K. and Scott, R. E. (1965). GROWTH OF MUSCLE MASS AND SKELETAL COLLAGEN IN THE RAT. II. THE EFFECT OF ABLATION OF PITUITARY, THYROID OR TESTES. *Bull. Johns Hopkins Hosp.* **116**, 387–395.

Chen, H., Shi, S., Acosta, L., Li, W., Lu, J., Bao, S., Chen, Z., Yang, Z., Schneider, M. D., Chien, K. R., et al. (2004). BMP10 is essential for maintaining cardiac growth during murine cardiogenesis. *Development* **131**, 2219–2231.

Chen, Q., Chen, H., Zheng, D., Kuang, C., Fang, H., Zou, B., Zhu, W., Bu, G., Jin, T., Wang, Z., et al. (2009). Smad7 Is Required for the Development and Function of the Heart. *J. Biol. Chem.* **284**, 292–300.

Cheung, T. H., Quach, N. L., Charville, G. W., Liu, L., Park, L., Edalati, A., Yoo, B., Hoang, P. and Rando, T. A. (2012). Maintenance of muscle stem-cell quiescence by microRNA-489. *Nature* **482**, 524–528.

Christov, C., Chrétien, F., Abou-Khalil, R., Bassez, G., Vallet, G., Authier, F.-J., Bassaglia, Y., Shinin, V., Tajbakhsh, S., Chazaud, B., et al. (2007). Muscle Satellite Cells and Endothelial Cells: Close Neighbors and Privileged Partners. *Mol. Biol. Cell* **18**, 1397–1409.

Ciciliot, S. and Schiaffino, S. (2010). Regeneration of Mammalian Skeletal Muscle: Basic Mechanisms and Clinical Implications. *Curr. Pharm. Des.* **16**, 906–914.

Ciciliot, S., Rossi, A. C., Dyar, K. A., Blaauw, B. and Schiaffino, S. (2013). Muscle type and fiber type specificity in muscle wasting. *Int. J. Biochem. Cell Biol.* **45**, 2191–2199.

Clever, J. L., Sakai, Y., Wang, R. A. and Schneider, D. B. (2010). Inefficient skeletal muscle repair in inhibitor of differentiation knockout mice suggests a crucial role for BMP signaling during adult muscle regeneration. *Am. J. Physiol. - Cell Physiol.* **298**, C1087–C1099.

Conboy, I. M. and Rando, T. A. (2002). The Regulation of Notch Signaling Controls Satellite Cell Activation and Cell Fate Determination in Postnatal Myogenesis. *Dev. Cell* **3**, 397–409.

Coolican, S. A., Samuel, D. S., Ewton, D. Z., McWade, F. J. and Florini, J. R. (1997). The Mitogenic and Myogenic Actions of Insulin-like Growth Factors Utilize Distinct Signaling Pathways. *J. Biol. Chem.* **272**, 6653–6662.

Cossu, G., Tajbakhsh, S. and Buckingham, M. (1996). How is myogenesis initiated in the embryo? *Trends Genet.* **12**, 218–223.

Dale, L. and Wardle, F. C. (1999). A gradient of BMP activity specifies dorsal–ventral fates in early Xenopus embryos. *Semin. Cell Dev. Biol.* **10**, 319–326.

de Castro Rodrigues, A. and Schmalbruch, H. (1995). Satellite cells and myonuclei in long-term denervated rat muscles. *Anat. Rec.* **243**, 430–437.

de Larco, J. E. and Todaro, G. J. (1978). Growth factors from murine sarcoma virus-transformed cells. *Proc. Natl. Acad. Sci. U. S. A.* **75**, 4001–4005.

Dellavalle, A., Sampaolesi, M., Tonlorenzi1, R., Tagliafico, E., Sacchetti, B., Perani, L., Innocenzi, A., Galvez, B. G., Messina, G., Morosetti, R., et al. (2007). Pericytes of human skeletal muscle are myogenic precursors distinct from satellite cells. *Nat. Cell Biol.* **9**, 255–267.

Dellavalle, A., Maroli, G., Covarello, D., Azzoni, E., Innocenzi, A., Perani, L., Antonini, S., Sambasivan, R., Brunelli, S., Tajbakhsh, S., et al. (2011). Pericytes resident in postnatal skeletal muscle differentiate into muscle fibres and generate satellite cells. *Nat. Commun.* **2**, 499.

Derynck, R. and Zhang, Y. E. (2003). Smad-dependent and Smad-independent pathways in TGF-beta family signalling. *Nature* **425**, 577–584.

de Winter, J. P., Dijke, P. ten, de Vries, C. J. M., van Achterberg, T. A. E., Sugino, H., de Waele, P., Huylebroeck, D., Verschueren, K. and van den Eijnden-van Raaij, A. J. M. (1996). Follistatins neutralize activin bioactivity by inhibition of activin binding to its type II receptors. *Mol. Cell. Endocrinol.* **116**, 105–114.

Dietrich, S., Abou-Rebyeh, F., Brohmann, H., Bladt, F., Sonnenberg-Riethmacher, E., Yamaai, T., Lumsden, A., Brand-Saberi, B. and Birchmeier, C. (1999). The role of SF/HGF and c-Met in the development of skeletal muscle. *Development* **126**, 1621–1629.

Doherty, M. J., Ashton, B. A., Walsh, S., Beresford, J. N., Grant, M. E. and Canfield, A. E. (1998). Vascular Pericytes Express Osteogenic Potential In Vitro and In Vivo. *J. Bone Miner. Res.* **13**, 828–838.

Doyle, M. J., Zhou, S., Tanaka, K. K., Pisconti, A., Farina, N. H., Sorrentino, B. P. and Olwin, B. B. (2011). Abcg2 labels multiple cell types in skeletal muscle and participates in muscle regeneration. *J. Cell Biol.* **195**, 147–163.

Drossopoulou, G., Lewis, K. E., Sanz-Ezquerro, J. J., Nikbakht, N., McMahon, A. P., Hofmann, C. and Tickle, C. (2000). A model for anteroposterior patterning of the vertebrate limb based on sequential long- and short-range Shh signalling and Bmp signalling. *Dev. Camb. Engl.* **127**, 1337–1348.

Fainsod, A., Deißler, K., Yelin, R., Marom, K., Epstein, M., Pillemer, G., Steinbeisser, H. and Blum, M. (1997). The dorsalizing and neural inducing gene follistatin is an antagonist of BMP-4. *Mech. Dev.* **63**, 39–50.

Farrington-Rock, C., Crofts, N. J., Doherty, M. J., Ashton, B. A., Griffin-Jones, C. and Canfield, A. E. (2004). Chondrogenic and Adipogenic Potential of Microvascular Pericytes. *Circulation* **110**, 2226–2232.

Feil, R., Brocard, J., Mascrez, B., LeMeur, M., Metzger, D. and Chambon, P. (1996). Ligand-activated site-specific recombination in mice. *Proc. Natl. Acad. Sci. U. S. A.* **93**, 10887–10890.

Feng, X.-H. and Derynck, R. (2005). SPECIFICITY AND VERSATILITY IN TGF-β SIGNALING THROUGH SMADS. *Annu. Rev. Cell Dev. Biol.* **21**, 659–693.

Flavell, R. A., Sanjabi, S., Wrzesinski, S. H. and Licona-Limón, P. (2010). The polarization of immune cells in the tumour environment by TGFβ. *Nat. Rev. Immunol.* **10**, 554–567.

Floss, T., Arnold, H.-H. and Braun, T. (1997). A role for FGF-6 in skeletal muscle regeneration. *Genes Dev.* **11**, 2040–2051.

Frenette, J., Cai, B. and Tidball, J. G. (2000). Complement Activation Promotes Muscle Inflammation during Modified Muscle Use. *Am. J. Pathol.* **156**, 2103–2110.

Friedrichs, M., Wirsdöerfer, F., Flohé, S. B., Schneider, S., Wuelling, M. and Vortkamp, A. (2011). BMP signaling balances proliferation and differentiation of muscle satellite cell descendants. *BMC Cell Biol.* **12**, 26.

Fukushima, K., Nakamura, A., Ueda, H., Yuasa, K., Yoshida, K., Takeda, S. and Ikeda, S. (2007). Activation and localization of matrix metalloproteinase-2 and -9 in the skeletal muscle of the muscular dystrophy dog (CXMDJ). *BMC Musculoskelet. Disord.* **8**, 54.

Galvin, K. M., Donovan, M. J., Lynch, C. A., Meyer, R. I., Paul, R. J., Lorenz, J. N., Fairchild-Huntress, V., Dixon, K. L., Dunmore, J. H., Gimbrone, M. A., et al. (2000a). A role for Smad6 in development and homeostasis of the cardiovascular system. *Nat. Genet.* **24**, 171–174.

Galvin, K. M., Donovan, M. J., Lynch, C. A., Meyer, R. I., Paul, R. J., Lorenz, J. N., Fairchild-Huntress, V., Dixon, K. L., Dunmore, J. H., Gimbrone, M. A., et al. (2000b). A role for Smad6 in development and homeostasis of the cardiovascular system. *Nat. Genet.* **24**, 171–174.

Garcia-Fernàndez, J., Aniello, S. D' and Escrivà, H. (2007). Organizing chordates with an organizer. *BioEssays* **29**, 619–624.

Gaussin, V., Putte, T. V. de, Mishina, Y., Hanks, M. C., Zwijsen, A., Huylebroeck, D., Behringer, R. R. and Schneider, M. D. (2002). Endocardial cushion and myocardial defects after cardiac myocyte-specific conditional deletion of the bone morphogenetic protein receptor ALK3. *Proc. Natl. Acad. Sci.* **99**, 2878–2883.

Ge, G. and Greenspan, D. S. (2006). BMP1 controls TGFβ1 activation via cleavage of latent TGFβ-binding protein. *J. Cell Biol.* **175**, 111–120.

Geetha-Loganathan, P., Nimmagadda, S. and Scaal, M. (2008). Wnt signaling in limb organogenesis. *Organogenesis* **4**, 109–115.

Gibson, M. C. and Schultz, E. (1982). The distribution of satellite cells and their relationship to specific fiber types in soleus and extensor digitorum longus muscles. *Anat. Rec.* **202**, 329–337.

Gokhin, D. S., Ward, S. R., Bremner, S. N. and Lieber, R. L. (2008). Quantitative analysis of neonatal skeletal muscle functional improvement in the mouse. *J. Exp. Biol.* **211**, 837–843.

Goto, K., Kamiya, Y., Imamura, T., Miyazono, K. and Miyazawa, K. (2007). Selective Inhibitory Effects of Smad6 on Bone Morphogenetic Protein Type I Receptors. *J. Biol. Chem.* **282**, 20603–20611.

Grand, F. L., Grifone, R., Mourikis, P., Houbron, C., Gigaud, C., Pujol, J., Maillet, M., Pagès, G., Rudnicki, M., Tajbakhsh, S., et al. (2012). Six1 regulates stem cell repair potential and self-renewal during skeletal muscle regeneration. *J. Cell Biol.* **198**, 815–832.

Gregory, K. E., Ono, R. N., Charbonneau, N. L., Kuo, C.-L., Keene, D. R., Bächinger, H. P. and Sakai, L. Y. (2005). The Prodomain of BMP-7 Targets the BMP-7 Complex to the Extracellular Matrix. *J. Biol. Chem.* **280**, 27970–27980.

Grifone, R., Demignon, J., Houbron, C., Souil, E., Niro, C., Seller, M. J., Hamard, G. and Maire, P. (2005). Six1 and Six4 homeoproteins are required for Pax3 and Mrf expression during myogenesis in the mouse embryo. *Development* **132**, 2235–2249.

Groppe, J., Hinck, C. S., Samavarchi-Tehrani, P., Zubieta, C., Schuermann, J. P., Taylor, A. B., Schwarz, P. M., Wrana, J. L. and Hinck, A. P. (2008). Cooperative Assembly of TGF-β Superfamily Signaling Complexes Is Mediated by Two Disparate Mechanisms and Distinct Modes of Receptor Binding. *Mol. Cell* **29**, 157–168.

Gussoni, E., Soneoka, Y., Strickland, C. D., Buzney, E. A., Khan, M. K., Flint, A. F., Kunkel, L. M. and Mulligan, R. C. (1999). Dystrophin expression in the mdx mouse restored by stem cell transplantation. *Nature* **401**, 390–394.

Hall, Z. W. and Ralston, E. (1989). Nuclear domains in muscle cells. *Cell* **59**, 771–772.

Hata, A., Lagna, G., Massagué, J. and Hemmati-Brivanlou, A. (1998). Smad6 inhibits BMP/Smad1 signaling by specifically competing with the Smad4 tumor suppressor. *Genes Dev.* **12**, 186–197.

Hemmati-Brivanlou, A. and Thomsen, G. H. (1995). Ventral mesodermal patterning in Xenopus embryos: Expression patterns and activities of BMP-2 and BMP-4. *Dev. Genet.* **17**, 78–89.

Hinck, A. P. (2012). Structural studies of the TGF-βs and their receptors – insights into evolution of the TGF-β superfamily. *FEBS Lett.* **586**, 1860–1870.

Hirsinger, E., Duprez, D., Jouve, C., Malapert, P., Cooke, J. and Pourquie, O. (1997). Noggin acts downstream of Wnt and Sonic Hedgehog to antagonize BMP4 in avian somite patterning. *Development* **124**, 4605–4614.

Howe, J. R., Bair, J. L., Sayed, M. G., Anderson, M. E., Mitros, F. A., Petersen, G. M., Velculescu, V. E., Traverso, G. and Vogelstein, B. (2001). Germline mutations of the gene encoding bone morphogenetic protein receptor 1A in juvenile polyposis. *Nat. Genet.* **28**, 184–187.

Huang, Z., Wang, D., Ihida-Stansbury, K., Jones, P. L. and Martin, J. F. (2009). Defective pulmonary vascular remodeling in Smad8 mutant mice. *Hum. Mol. Genet.* **18**, 2791–2801.

Iemura, S., Yamamoto, T. S., Takagi, C., Uchiyama, H., Natsume, T., Shimasaki, S., Sugino, H. and Ueno, N. (1998). Direct binding of follistatin to a complex of bone-morphogenetic protein and its receptor inhibits ventral and epidermal cell fates in early Xenopus embryo. *Proc. Natl. Acad. Sci.* **95**, 9337–9342.

Imamura, T., Takase, M., Nishihara, A., Oeda, E., Hanai, J., Kawabata, M. and Miyazono, K. (1997). Smad6 inhibits signalling by the TGF-β superfamily. *Nature* **389**, 622–626.

Indra, A. K., Warot, X., Brocard, J., Bornert, J.-M., Xiao, J.-H., Chambon, P. and Metzger, D. (1999). Temporally-controlled site-specific mutagenesis in the basal layer of the epidermis: comparison of the recombinase activity of the tamoxifen-inducible Cre-ERT and Cre-ERT2 recombinases. *Nucleic Acids Res.* **27**, 4324–4327.

Irintchev, A., Zeschnigk, M., Starzinski-Powitz, A. and Wernig, A. (1994). Expression pattern of M-cadherin in normal, denervated, and regenerating mouse muscles. *Dev. Dyn.* **199**, 326–337.

Ishida, W., Hamamoto, T., Kusanagi, K., Yagi, K., Kawabata, M., Takehara, K., Sampath, T. K., Kato, M. and Miyazono, K. (2000). Smad6 Is a Smad1/5-induced Smad Inhibitor CHARACTERIZATION OF BONE MORPHOGENETIC PROTEIN-RESPONSIVE ELEMENT IN THE MOUSE Smad6 PROMOTER. *J. Biol. Chem.* **275**, 6075–6079.

Ivanova, A., Signore, M., Caro, N., Greene, N. D. E., Copp, A. J. and Martinez-Barbera, J. P. (2005). In vivo genetic ablation by Cre-mediated expression of diphtheria toxin fragment A. *genesis* **43**, 129–135.

Jee, M. J., Yoon, S. M., Kim, E. J., Choi, H.-J., Kim, J.-W., Sung, R. H., Han, J. H., Chae, H. B., Park, S. M. and Youn, S. J. (2013). A Novel Germline Mutation in Exon 10 of the SMAD4 Gene in a Familial Juvenile Polyposis. *Gut Liver* **7**, 747–751.

Joubert, Y. and Tobin, C. (1995). Testosterone Treatment Results in Quiescent Satellite Cells Being Activated and Recruited into Cell Cycle in Rat Levator Ani Muscle. *Dev. Biol.* **169**, 286–294.

Jung, S. M., Lee, J.-H., Park, J., Oh, Y. S., Lee, S. K., Park, J. S., Lee, Y. S., Kim, J. H., Lee, J. Y., Bae, Y.-S., et al. (2013). Smad6 inhibits non-canonical TGF-β1 signalling by recruiting the deubiquitinase A20 to TRAF6. *Nat. Commun.* **4**,.

Kaplan, F. S., Le Merrer, M., Glaser, D. L., Pignolo, R. J., Goldsby, R. E., Kitterman, J. A., Groppe, J. and Shore, E. M. (2008). Fibrodysplasia ossificans progressiva. *Best Pract. Res. Clin. Rheumatol.* **22**, 191–205.

Kassar-Duchossoy, L., Giacone, E., Gayraud-Morel, B., Jory, A., Gomès, D. and Tajbakhsh, S. (2005). Pax3/Pax7 mark a novel population of primitive myogenic cells during development. *Genes Dev.* **19**, 1426–1431.

Katagiri, T., Yamaguchi, A., Komaki, M., Abe, E., Takahashi, N., Ikeda, T., Rosen, V., Wozney, J. M., Fujisawa-Sehara, A. and Suda, T. (1994). Bone morphogenetic protein-2 converts the differentiation pathway of C2C12 myoblasts into the osteoblast lineage. *J. Cell Biol.* **127**, 1755–1766.

Katz B (1961). The terminations of the afferent nerve fibre in the muscle spindle of the frog. *Philos Trans R Soc Lond Biol* **241**, 221–240.

Kelly, A. M. (1978). Perisynaptic satellite cells in the developing and mature rat soleus muscle. *Anat. Rec.* **190**, 891–903.

Kherif, S., Lafuma, C., Dehaupas, M., Lachkar, S., Fournier, J.-G., Verdière-Sahuqué, M., Fardeau, M. and Alameddine, H. S. (1999). Expression of Matrix Metalloproteinases 2 and 9 in Regenerating Skeletal Muscle: A Study in Experimentally Injured andmdxMuscles. *Dev. Biol.* **205**, 158–170.

Khokha, M. K., Hsu, D., Brunet, L. J., Dionne, M. S. and Harland, R. M. (2003). Gremlin is the BMP antagonist required for maintenance of Shh and Fgf signals during limb patterning. *Nat. Genet.* **34**, 303–307.

Kingsley, D. M., Bland, A. E., Grubber, J. M., Marker, P. C., Russell, L. B., Copeland, N. G. and Jenkins, N. A. (1992). The mouse short ear skeletal morphogenesis locus is associated with defects in a bone morphogenetic member of the TGFβ superfamily. *Cell* **71**, 399–410.

Kobayashi, T., Lyons, K. M., McMahon, A. P. and Kronenberg, H. M. (2005). BMP signaling stimulates cellular differentiation at multiple steps during cartilage development. *Proc. Natl. Acad. Sci. U. S. A.* **102**, 18023–18027.

Konrad, L., Scheiber, J. A., Bergmann, M., Eickelberg, O. and Hofmann, R. (2008). Identification of a new human Smad6 splice variant. *Andrologia* **40**, 358–363.

Korchynskyi, O. and Dijke, P. ten (2002). Identification and Functional Characterization of Distinct Critically Important Bone Morphogenetic Protein-specific Response Elements in the Id1 Promoter. *J. Biol. Chem.* **277**, 4883–4891.

Kostallari, E., Baba-Amer, Y., Alonso-Martin, S., Ngoh, P., Relaix, F., Lafuste, P. and Gherardi, R. K. (2015). Pericytes in the myovascular niche promote post-natal myofiber growth and satellite cell quiescence. *Development* **142**, 1242–1253.

Krause, C., Guzman, A. and Knaus, P. (2011). Noggin. *Int. J. Biochem. Cell Biol.* **43**, 478–481.

Kretzschmar, M., Liu, F., Hata, A., Doody, J. and Massagué, J. (1997). The TGF-beta family mediator Smad1 is phosphorylated directly and activated functionally by the BMP receptor kinase. *Genes Dev.* **11**, 984–995.

Kuang, S., Chargé, S. B., Seale, P., Huh, M. and Rudnicki, M. A. (2006). Distinct roles for Pax7 and Pax3 in adult regenerative myogenesis. *J. Cell Biol.* **172**, 103–113.

Kuang, S., Kuroda, K., Le Grand, F. and Rudnicki, M. A. (2007). Asymmetric Self-Renewal and Commitment of Satellite Stem Cells in Muscle. *Cell* **129**, 999–1010.

Kuschel, R., Yablonka-Reuveni, Z. and Bornemann, A. (1999). Satellite Cells on Isolated Myofibers from Normal and Denervated Adult Rat Muscle. *J. Histochem. Cytochem.* **47**, 1375–1383.

Lafyatis, R. (2014). Transforming growth factor β—at the centre of systemic sclerosis. *Nat. Rev. Rheumatol.* **10**, 706–719.

Langley, B., Thomas, M., Bishop, A., Sharma, M., Gilmour, S. and Kambadur, R. (2002). Myostatin inhibits myoblast differentiation by down-regulating MyoD expression. *J. Biol. Chem.* **277**, 49831–49840.

Lee, S.-J. and McPherron, A. C. (2001). Regulation of myostatin activity and muscle growth. *Proc. Natl. Acad. Sci.* **98**, 9306–9311.

Le Goff, C., Mahaut, C., Abhyankar, A., Le Goff, W., Serre, V., Afenjar, A., Destrée, A., di Rocco, M., Héron, D., Jacquemont, S., et al. (2012). Mutations at a single codon in Mad homology 2 domain of SMAD4 cause Myhre syndrome. *Nat. Genet.* **44**, 85–88.

Lepper, C. and Fan, C.-M. (2010). Inducible lineage tracing of Pax7-descendant cells reveals embryonic origin of adult satellite cells. *Genes. N. Y. N 2000* **48**, 424–436.

Lepper, C., Conway, S. J. and Fan, C.-M. (2009). Adult satellite cells and embryonic muscle progenitors have distinct genetic requirements. *Nature* **460**, 627–631.

Lepper, C., Partridge, T. A. and Fan, C.-M. (2011). An absolute requirement for Pax7-positive satellite cells in acute injury-induced skeletal muscle regeneration. *Development* **138**, 3639–3646.

Lin, X., Liang, Y.-Y., Sun, B., Liang, M., Shi, Y., Brunicardi, F. C., Shi, Y. and Feng, X.-H. (2003). Smad6 Recruits Transcription Corepressor CtBP To Repress Bone Morphogenetic Protein-Induced Transcription. *Mol. Cell. Biol.* **23**, 9081–9093.

Liu, W., Selever, J., Wang, D., Lu, M.-F., Moses, K. A., Schwartz, R. J. and Martin, J. F. (2004). Bmp4 signaling is required for outflow-tract septation and branchial-arch artery remodeling. *Proc. Natl. Acad. Sci. U. S. A.* **101**, 4489–4494.

López-Rovira, T., Chalaux, E., Massagué, J., Rosa, J. L. and Ventura, F. (2002). Direct Binding of Smad1 and Smad4 to Two Distinct Motifs Mediates Bone Morphogenetic Protein-specific Transcriptional Activation ofId1 Gene. *J. Biol. Chem.* **277**, 3176–3185.

Lounev, V. Y., Ramachandran, R., Wosczyna, M. N., Yamamoto, M., Maidment, A. D. A., Shore, E. M., Glaser, D. L., Goldhamer, D. J. and Kaplan, F. S. (2009). Identification of Progenitor Cells That Contribute to Heterotopic Skeletogenesis. *J. Bone Jt. Surg.* **91**, 652–663.

Luyten, F. P., Cunningham, N. S., Ma, S., Muthukumaran, N., Hammonds, R. G., Nevins, W. B., Woods, W. I. and Reddi, A. H. (1989). Purification and partial amino acid sequence of osteogenin, a protein initiating bone differentiation. *J. Biol. Chem.* **264**, 13377–13380.

Luz, M. a. M., Marques, M. J. and Santo Neto, H. (2002). Impaired regeneration of dystrophin-deficient muscle fibers is caused by exhaustion of myogenic cells. *Braz. J. Med. Biol. Res.* **35**, 691–695.

Macias, M. J., Martin-Malpartida, P. and Massagué, J. (2015). Structural determinants of Smad function in TGF-β signaling. *Trends Biochem. Sci.* **40**, 296–308.

Mansouri, A., Stoykova, A., Torres, M. and Gruss, P. (1996). Dysgenesis of cephalic neural crest derivatives in Pax7−/− mutant mice. *Development* **122**, 831–838.

Massagué, J. (1998). TGF-β SIGNAL TRANSDUCTION. *Annu. Rev. Biochem.* **67**, 753–791.

Massagué, J., Seoane, J. and Wotton, D. (2005). Smad transcription factors. *Genes Dev.* **19**, 2783–2810.

Massari, M. E. and Murre, C. (2000). Helix-Loop-Helix Proteins: Regulators of Transcription in Eucaryotic Organisms. *Mol. Cell. Biol.* **20**, 429–440.

Mauro, A. (1961). SATELLITE CELL OF SKELETAL MUSCLE FIBERS. *J. Biophys. Biochem. Cytol.* **9**, 493–495.

McCabe, B. D., Marqués, G., Haghighi, A. P., Fetter, R. D., Crotty, M. L., Haerry, T. E., Goodman, C. S. and O'Connor, M. B. (2003). The BMP Homolog Gbb Provides a Retrograde Signal that Regulates Synaptic Growth at the Drosophila Neuromuscular Junction. *Neuron* **39**, 241–254.

McCarthy, J. J., Mula, J., Miyazaki, M., Erfani, R., Garrison, K., Farooqui, A. B., Srikuea, R., Lawson, B. A., Grimes, B., Keller, C., et al. (2011). Effective fiber hypertrophy in satellite cell-depleted skeletal muscle. *Development* **138**, 3657–3666.

McCroskery, S., Thomas, M., Maxwell, L., Sharma, M. and Kambadur, R. (2003). Myostatin negatively regulates satellite cell activation and self-renewal. *J. Cell Biol.* **162**, 1135–1147.

McCroskery, S., Thomas, M., Platt, L., Hennebry, A., Nishimura, T., McLeay, L., Sharma, M. and Kambadur, R. (2005). Improved muscle healing through enhanced regeneration and reduced fibrosis in myostatin-null mice. *J. Cell Sci.* **118**, 3531–3541.

McPherron, A. C. and Lee, S.-J. (1997). Double muscling in cattle due to mutations in the myostatin gene. *Proc. Natl. Acad. Sci.* **94**, 12457–12461.

McPherron, A. C., Lawler, A. M. and Lee, S.-J. (1997). Regulation of skeletal muscle mass in mice by a new TGF-p superfamily member. *Nature* **387**, 83–90.

Mikić, B., Van Der Meulen, M. C. H., Kingsley, D. M. and Carter, D. R. (1995). Long bone geometry and strength in adult BMP-5 deficient mice. *Bone* **16**, 445–454.

Miller, K. J., Thaloor, D., Matteson, S. and Pavlath, G. K. (2000). Hepatocyte growth factor affects satellite cell activation and differentiation in regenerating skeletal muscle. *Am. J. Physiol. - Cell Physiol.* **278**, C174–C181.

Miniou, P., Tiziano, D., Frugier, T., Roblot, N., Meur, M. L. and Melki, J. (1999). Gene targeting restricted to mouse striated muscle lineage. *Nucleic Acids Res.* **27**, e27–e30.

Mitchell, P. O., Mills, T., O'Connor, R. S., Graubert, T., Dzierzak, E. and Pavlath, G. K. (2005). Sca-1 negatively regulates proliferation and differentiation of muscle cells. *Dev. Biol.* **283**, 240–252.

Mitchell, K. J., Pannérec, A., Cadot, B., Parlakian, A., Besson, V., Gomes, E. R., Marazzi, G. and Sassoon, D. A. (2010). Identification and characterization of a non-satellite cell muscle resident progenitor during postnatal development. *Nat. Cell Biol.* **12**, 257–266.

Mitola, S., Ravelli, C., Moroni, E., Salvi, V., Leali, D., Ballmer-Hofer, K., Zammataro, L. and Presta, M. (2010). Gremlin is a novel agonist of the major proangiogenic receptor VEGFR2. *Blood* **116**, 3677–3680.

Miyazona K, D. R. *TGF-β and the TGF-β family*. Cold Spring Harbor Press.

Miyazono, K. and Miyazawa, K. (2002). Id: a target of BMP signaling. *Sci. STKE Signal Transduct. Knowl. Environ.* **2002**, pe40.

Moses, H. L., Branum, E. L., Proper, J. A. and Robinson, R. A. (1981). Transforming Growth Factor Production by Chemically Transformed Cells. *Cancer Res.* **41**, 2842–2848.

Mosher, D. S., Quignon, P., Bustamante, C. D., Sutter, N. B., Mellersh, C. S., Parker, H. G. and Ostrander, E. A. (2007). A Mutation in the Myostatin Gene Increases Muscle Mass and Enhances Racing Performance in Heterozygote Dogs. *PLoS Genet* **3**, e79.

Mosler, S., Relizani, K., Mouisel, E., Amthor, H. and Diel, P. (2014). Combinatory effects of siRNA-induced myostatin inhibition and exercise on skeletal muscle homeostasis and body composition. *Physiol. Rep.* **2**, e00262.

Mouisel, E., Relizani, K., Mille-Hamard, L., Denis, R., Hourdé, C., Agbulut, O., Patel, K., Arandel, L., Morales-Gonzalez, S., Vignaud, A., et al. (2014). Myostatin is a key mediator between energy metabolism and endurance capacity of skeletal muscle. *Am. J. Physiol. - Regul. Integr. Comp. Physiol.* **307**, R444–R454.

Mourikis, P., Sambasivan, R., Castel, D., Rocheteau, P., Bizzarro, V. and Tajbakhsh, S. (2012). A Critical Requirement for Notch Signaling in Maintenance of the Quiescent Skeletal Muscle Stem Cell State. *STEM CELLS* **30**, 243–252.

Moustakas, A. and Heldin, C.-H. (2005). Non-Smad TGF-β signals. *J. Cell Sci.* **118**, 3573–3584.

Moustakas, A. and Heldin, C.-H. (2009). The regulation of TGFβ signal transduction. *Development* **136**, 3699–3714.

Munger, J. S., Huang, X., Kawakatsu, H., Griffiths, M. J., Dalton, S. L., Wu, J., Pittet, J. F., Kaminski, N., Garat, C., Matthay, M. A., et al. (1999). The integrin alpha v beta 6 binds and activates latent TGF beta 1: a mechanism for regulating pulmonary inflammation and fibrosis. *Cell* **96**, 319–328.

Murakami, G., Watabe, T., Takaoka, K., Miyazono, K. and Imamura, T. (2003). Cooperative Inhibition of Bone Morphogenetic Protein Signaling by Smurf1 and Inhibitory Smads. *Mol. Biol. Cell* **14**, 2809–2817.

Murphy, M. M., Lawson, J. A., Mathew, S. J., Hutcheson, D. A. and Kardon, G. (2011). Satellite cells, connective tissue fibroblasts and their interactions are crucial for muscle regeneration. *Development* **138**, 3625–3637.

Musarò, A. and Rosenthal, N. (1999). Maturation of the Myogenic Program Is Induced by Postmitotic Expression of Insulin-Like Growth Factor I. *Mol. Cell. Biol.* **19**, 3115–3124.

Myhre, S. A., Ruvalcaba, R. H. and Graham, C. B. (1981). A new growth deficiency syndrome. *Clin. Genet.* **20**, 1–5.

Nakamura, T., Takio, K., Eto, Y., Shibai, H., Titani, K. and Sugino, H. (1990). Activin-binding protein from rat ovary is follistatin. *Science* **247**, 836–838.

Narusawa, M., Fitzsimons, R. B., Izumo, S., Nadal-Ginard, B., Rubinstein, N. A. and Kelly, A. M. (1987). Slow myosin in developing rat skeletal muscle. *J. Cell Biol.* **104**, 447–459.

Nishijo, K., Hosoyama, T., Bjornson, C. R. R., Schaffer, B. S., Prajapati, S. I., Bahadur, A. N., Hansen, M. S., Blandford, M. C., McCleish, A. T., Rubin, B. P., et al. (2009). Biomarker system for studying muscle, stem cells, and cancer in vivo. *FASEB J.* **23**, 2681–2690.

Nishitoh, H. (1997). [Identification of receptors for bone morphogenetic proteins]. *Kōkūbyō Gakkai Zasshi J. Stomatol. Soc. Jpn.* **64**, 24–37.

Ono, Y., Calhabeu, F., Morgan, J. E., Katagiri, T., Amthor, H. and Zammit, P. S. (2011). BMP signalling permits population expansion by preventing premature myogenic differentiation in muscle satellite cells. *Cell Death Differ.* **18**, 222–234.

Ontell, M., Feng, K. C., Klueber, K., Dunn, R. F. and Taylor, F. (1984). Myosatellite cells, growth, and regeneration in murine dystrophic muscle: A quantitative study. *Anat. Rec.* **208**, 159–174.

Otto, A., Schmidt, C., Luke, G., Allen, S., Valasek, P., Muntoni, F., Lawrence-Watt, D. and Patel, K. (2008). Canonical Wnt signalling induces satellite-cell proliferation during adult skeletal muscle regeneration. *J. Cell Sci.* **121**, 2939–2950.

Oustanina, S., Hause, G. and Braun, T. (2004). Pax7 directs postnatal renewal and propagation of myogenic satellite cells but not their specification. *EMBO J.* **23**, 3430–3439.

Pallafacchina, G., François, S., Regnault, B., Czarny, B., Dive, V., Cumano, A., Montarras, D. and Buckingham, M. (2010). An adult tissue-specific stem cell in its niche: A gene profiling analysis of in vivo quiescent and activated muscle satellite cells. *Stem Cell Res.* **4**, 77–91.

Pannérec, A., Marazzi, G. and Sassoon, D. (2012). Stem cells in the hood: the skeletal muscle niche. *Trends Mol. Med.* **18**, 599–606.

Parr, B. A., Shea, M. J., Vassileva, G. and McMahon, A. P. (1993). Mouse Wnt genes exhibit discrete domains of expression in the early embryonic CNS and limb buds. *Development* **119**, 247–261.

Patel, K. and Amthor, H. (2005). The function of Myostatin and strategies of Myostatin blockade—new hope for therapies aimed at promoting growth of skeletal muscle. *Neuromuscul. Disord.* **15**, 117–126.

Patterson, S. E., Bird, N. C. and Devoto, S. H. (2010). BMP regulation of myogenesis in zebrafish. *Dev. Dyn.* **239**, 806–817.

Pavlath, G. K., Rich, K., Webster, S. G. and Blau, H. M. (1989). Localization of muscle gene products in nuclear domains. *Nature* **337**, 570–573.

Peluso, C. E., Umulis, D., Kim, Y.-J., O'Connor, M. B. and Serpe, M. (2011). Shaping BMP Morphogen Gradients through Enzyme-Substrate Interactions. *Dev. Cell* **21**, 375–383.

Perez-Ruiz, A., Ono, Y., Gnocchi, V. F. and Zammit, P. S. (2008). β-catenin promotes self-renewal of skeletal-muscle satellite cells. *J. Cell Sci.* **121**, 1373–1382.

Pfaffl, M. W. (2001). A new mathematical model for relative quantification in real-time RT–PCR. *Nucleic Acids Res.* **29**, e45–e45.

Polinkovsky, A., Robin, N. H., Thomas, J. T., Irons, M., Lynn, A., Goodman, F. R., Reardon, W., Kant, S. G., Brunner, H. G., van der Burgt, I., et al. (1997). Mutations in CDMP1 cause autosomal dominant brachydactyly type C. *Nat. Genet.* **17**, 18–19.

Pourquié, O., Coltey, M., Bréant, C. and Le Douarin, N. M. (1995). Control of somite patterning by signals from the lateral plate. *Proc. Natl. Acad. Sci. U. S. A.* **92**, 3219–3223.

Pourquié, O., Fan, C.-M., Coltey, M., Hirsinger, E., Watanabe, Y., Bréant, C., Francis-West, P., Brickell, P., Tessier-Lavigne, M. and Le Douarin, N. M. (1996). Lateral and Axial Signals Involved in Avian Somite Patterning: A Role for BMP4. *Cell* **84**, 461–471.

Qin, B. Y., Chacko, B. M., Lam, S. S., de Caestecker, M. P., Correia, J. J. and Lin, K. (2001). Structural Basis of Smad1 Activation by Receptor Kinase Phosphorylation. *Mol. Cell* **8**, 1303–1312.

Radley, H. G. and Grounds, M. D. (2006). Cromolyn administration (to block mast cell degranulation) reduces necrosis of dystrophic muscle in mdx mice. *Neurobiol. Dis.* **23**, 387–397.

Rebbapragada, A., Benchabane, H., Wrana, J. L., Celeste, A. J. and Attisano, L. (2003). Myostatin Signals through a Transforming Growth Factor β-Like Signaling Pathway To Block Adipogenesis. *Mol. Cell. Biol.* **23**, 7230–7242.

Relaix, F. and Marcelle, C. (2009). Muscle stem cells. *Curr. Opin. Cell Biol.* **21**, 748–753.

Relaix, F. and Zammit, P. S. (2012). Satellite cells are essential for skeletal muscle regeneration: the cell on the edge returns centre stage. *Development* **139**, 2845–2856.

Relaix, F., Rocancourt, D., Mansouri, A. and Buckingham, M. (2005). A Pax3/Pax7-dependent population of skeletal muscle progenitor cells. *Nature* **435**, 948–953.

Relaix, F., Montarras, D., Zaffran, S., Gayraud-Morel, B., Rocancourt, D., Tajbakhsh, S., Mansouri, A., Cumano, A. and Buckingham, M. (2006). Pax3 and Pax7 have distinct and overlapping functions in adult muscle progenitor cells. *J. Cell Biol.* **172**, 91–102.

Relizani, K., Mouisel, E., Giannesini, B., Hourdé, C., Patel, K., Morales Gonzalez, S., Jülich, K., Vignaud, A., Piétri-Rouxel, F., Fortin, D., et al. (2014). Blockade of ActRIIB Signaling Triggers Muscle Fatigability and Metabolic Myopathy. *Mol. Ther.* **22**, 1423–1433.

Reshef, R., Maroto, M. and Lassar, A. B. (1998). Regulation of dorsal somitic cell fates: BMPs and Noggin control the timing and pattern of myogenic regulator expression. *Genes Dev.* **12**, 290–303.

Rios, A. C., Serralbo, O., Salgado, D. and Marcelle, C. (2011). Neural crest regulates myogenesis through the transient activation of NOTCH. *Nature* **473**, 532–535.

Roberts, A. B., Anzano, M. A., Lamb, L. C., Smith, J. M. and Sporn, M. B. (1981). New class of transforming growth factors potentiated by epidermal growth factor: isolation from non-neoplastic tissues. *Proc. Natl. Acad. Sci. U. S. A.* **78**, 5339–5343.

Rudnicki, M. A. and Jaenisch, R. (1995). The MyoD family of transcription factors and skeletal myogenesis. *BioEssays* **17**, 203–209.

Sacco, A., Doyonnas, R., Kraft, P., Vitorovic, S. and Blau, H. M. (2008). Self-renewal and expansion of single transplanted muscle stem cells. *Nature* **456**, 502–506.

Sadeh, M., Czyzewski, K. and Stern, L. Z. (1985). Chronic myopathy induced by repeated bupivacaine injections. *J. Neurol. Sci.* **67**, 229–238.

Sampaolesi, M., Torrente, Y., Innocenzi, A., Tonlorenzi, R., Antona, G. D', Pellegrino, M. A., Barresi, R., Bresolin, N., Angelis, M. G. C. D., Campbell, K. P., et al. (2003). Cell Therapy of α-Sarcoglycan Null Dystrophic Mice Through Intra-Arterial Delivery of Mesoangioblasts. *Science* **301**, 487–492.

Sandri, M. (2008). Signaling in Muscle Atrophy and Hypertrophy. *Physiology* **23**, 160–170.

Sartori, R., Milan, G., Patron, M., Mammucari, C., Blaauw, B., Abraham, R. and Sandri, M. (2009). Smad2 and 3 transcription factors control muscle mass in adulthood. *Am. J. Physiol. - Cell Physiol.* **296**, C1248–C1257.

Sartori, R., Schirwis, E., Blaauw, B., Bortolanza, S., Zhao, J., Enzo, E., Stantzou, A., Mouisel, E., Toniolo, L., Ferry, A., et al. (2013). BMP signaling controls muscle mass. *Nat. Genet.* **45**, 1309–1318.

Sartori, R., Gregorevic, P. and Sandri, M. (2014). TGFβ and BMP signaling in skeletal muscle: potential significance for muscle-related disease. *Trends Endocrinol. Metab.* **25**, 464–471.

Sassoon, D., Lyons, G., Wright, W. E., Lin, V., Lassar, A., Weintraub, H. and Buckingham, M. (1989). Expression of two myogenic regulatory factors myogenin and MyoD1 during mouse embryogenesis. *Nature* **341**, 303–307.

Sauer, B. (1987). Functional expression of the cre-lox site-specific recombination system in the yeast Saccharomyces cerevisiae. *Mol. Cell. Biol.* **7**, 2087–2096.

Sauer, B. and Henderson, N. (1988). Site-specific DNA recombination in mammalian cells by the Cre recombinase of bacteriophage P1. *Proc. Natl. Acad. Sci. U. S. A.* **85**, 5166–5170.

Schiaffino, S. (2010). Fibre types in skeletal muscle: a personal account. *Acta Physiol.* **199**, 451–463.

Schiaffino, S. and Reggiani, C. (1996). Molecular diversity of myofibrillar proteins: gene regulation and functional significance. *Physiol. Rev.* **76**, 371–423.

Schiaffino, S., Gorza, L., Sartore, S., Saggin, L., Ausoni, S., Vianello, M., Gundersen, K. and LØmo, T. (1989). Three myosin heavy chain isoforms in type 2 skeletal muscle fibres. *J. Muscle Res. Cell Motil.* **10**, 197–205.

Schiaffino, S., Dyar, K. A., Ciciliot, S., Blaauw, B. and Sandri, M. (2013). Mechanisms regulating skeletal muscle growth and atrophy. *FEBS J.* **280**, 4294–4314.

Schmalbruch, H. and Lewis, D. m. (2000). Dynamics of nuclei of muscle fibers and connective tissue cells in normal and denervated rat muscles. *Muscle Nerve* **23**, 617–626.

Schmierer, B. and Hill, C. S. (2007). TGFβ–SMAD signal transduction: molecular specificity and functional flexibility. *Nat. Rev. Mol. Cell Biol.* **8**, 970–982.

Scholzen, T. and Gerdes, J. (2000). The Ki-67 protein: from the known and the unknown. *J. Cell. Physiol.* **182**, 311–322.

Schuelke, M., Wagner, K. R., Stolz, L. E., Hübner, C., Riebel, T., Kömen, W., Braun, T., Tobin, J. F. and Lee, S.-J. (2004). Myostatin Mutation Associated with Gross Muscle Hypertrophy in a Child. *N. Engl. J. Med.* **350**, 2682–2688.

Schultz, E. (1996). Satellite Cell Proliferative Compartments in Growing Skeletal Muscles. *Dev. Biol.* **175**, 84–94.

Schultz, E., Jaryszak, D. L. and Valliere, C. R. (1985). Response of satellite cells to focal skeletal muscle injury. *Muscle Nerve* **8**, 217–222.

Schultz-Cherry, S. and Murphy-Ullrich, J. E. (1993). Thrombospondin causes activation of latent transforming growth factor-beta secreted by endothelial cells by a novel mechanism. *J. Cell Biol.* **122**, 923–932.

Schuster-Gossler, K., Cordes, R. and Gossler, A. (2007). Premature myogenic differentiation and depletion of progenitor cells cause severe muscle hypotrophy in Delta1 mutants. *Proc. Natl. Acad. Sci.* **104**, 537–542.

Seale, P., Sabourin, L. A., Girgis-Gabardo, A., Mansouri, A., Gruss, P. and Rudnicki, M. A. (2000). Pax7 Is Required for the Specification of Myogenic Satellite Cells. *Cell* **102**, 777–786.

Sémonin, O., Fontaine, K., Daviaud, C., Ayuso, C. and Lucotte, G. (2001). Identification of three novel mutations of the noggin gene in patients with fibrodysplasia ossificans progressiva. *Am. J. Med. Genet.* **102**, 314–317.

Sharma, M., Kambadur, R., Matthews, K. G., Somers, W. G., Devlin, G. P., Conaglen, J. V., Fowke, P. J. and Bass, J. J. (1999). Myostatin, a transforming growth factor-β superfamily member, is expressed in heart muscle and is upregulated in cardiomyocytes after infarct. *J. Cell. Physiol.* **180**, 1–9.

Sinha-Hikim, I., Roth, S. M., Lee, M. I. and Bhasin, S. (2003). Testosterone-induced muscle hypertrophy is associated with an increase in satellite cell number in healthy, young men. *Am. J. Physiol. - Endocrinol. Metab.* **285**, E197–E205.

Smith, W. C. and Harland, R. M. (1992). Expression cloning of noggin, a new dorsalizing factor localized to the Spemann organizer in Xenopus embryos. *Cell* **70**, 829–840.

Steinhardt, R. A., Bi, G. and Alderton, J. M. (1994). Cell membrane resealing by a vesicular mechanism similar to neurotransmitter release. *Science* **263**, 390–393.

Stopa, M., Anhuf, D., Terstegen, L., Gatsios, P., Gressner, A. M. and Dooley, S. (2000). Participation of Smad2, Smad3, and Smad4 in Transforming Growth Factor β (TGF-β)-induced Activation of Smad7 THE TGF-β RESPONSE ELEMENT OF THE PROMOTER REQUIRES FUNCTIONAL Smad BINDING ELEMENT AND E-BOX SEQUENCES FOR TRANSCRIPTIONAL REGULATION. *J. Biol. Chem.* **275**, 29308–29317.

Storm, E. E., Huynh, T. V., Copeland, N. G., Jenkins, N. A., Kingsley, D. M. and Lee, S.-J. (1994). Limb alterations in brachypodism mice due to mutations in a new member of the TGFβ-superfamily. *Nature* **368**, 639–643.

Suzuki, K., Wilkes, M. C., Garamszegi, N., Edens, M. and Leof, E. B. (2007). Transforming Growth Factor β Signaling via Ras in Mesenchymal Cells Requires p21-Activated Kinase 2 for Extracellular Signal-Regulated Kinase-Dependent Transcriptional Responses. *Cancer Res.* **67**, 3673–3682.

Suzuki, Y., Ohga, N., Morishita, Y., Hida, K., Miyazono, K. and Watabe, T. (2010). BMP-9 induces proliferation of multiple types of endothelial cells in vitro and in vivo. *J. Cell Sci.* **123**, 1684–1692.

Taipale, J., Lohi, J., Saarinen, J., Kovanen, P. T. and Keski-Oja, J. (1995). Human Mast Cell Chymase and Leukocyte Elastase Release Latent Transforming Growth Factor-β1 from the Extracellular Matrix of Cultured Human Epithelial and Endothelial Cells. *J. Biol. Chem.* **270**, 4689–4696.

Thomas, M., Langley, B., Berry, C., Sharma, M., Kirk, S., Bass, J. and Kambadur, R. (2000). Myostatin, a Negative Regulator of Muscle Growth, Functions by Inhibiting Myoblast Proliferation. *J. Biol. Chem.* **275**, 40235–40243.

Thompson, T. B., Lerch, T. F., Cook, R. W., Woodruff, T. K. and Jardetzky, T. S. (2005). The Structure of the Follistatin:Activin Complex Reveals Antagonism of Both Type I and Type II Receptor Binding. *Dev. Cell* **9**, 535–543.

Tidball, D. J. G. and Daniel, T. L. (1986). Myotendinous junctions of tonic muscle cells: structure and loading. *Cell Tissue Res.* **245**, 315–322.

Tillet, E. and Bailly, S. (2014). Emerging roles of BMP9 and BMP10 in hereditary hemorrhagic telangiectasia. *Front. Genet.* **5**, 456.

Trendelenburg, A. U., Meyer, A., Rohner, D., Boyle, J., Hatakeyama, S. and Glass, D. J. (2009). Myostatin reduces Akt/TORC1/p70S6K signaling, inhibiting myoblast differentiation and myotube size. *Am. J. Physiol. - Cell Physiol.* **296**, C1258–C1270.

Tsuji, K., Bandyopadhyay, A., Harfe, B. D., Cox, K., Kakar, S., Gerstenfeld, L., Einhorn, T., Tabin, C. J. and Rosen, V. (2006). BMP2 activity, although dispensable for bone formation, is required for the initiation of fracture healing. *Nat. Genet.* **38**, 1424–1429.

Tylzanowski, P., Mebis, L. and Luyten, F. P. (2006). The Noggin null mouse phenotype is strain dependent and haploinsufficiency leads to skeletal defects. *Dev. Dyn.* **235**, 1599–1607.

Urist, M. R. (1965). Bone: formation by autoinduction. *Science* **150**, 893–899.

Urist, M. R. (2002). Bone: formation by autoinduction. 1965. *Clin. Orthop.* 4–10.

van Amerongen, R. and Nusse, R. (2009). Towards an integrated view of Wnt signaling in. *Development* **136**, 3205–3214.

Vargesson, N. and Laufer, E. (2009). Negative Smad Expression and Regulation in the Developing Chick Limb. *PLoS ONE* **4**,.

Vasyutina, E. and Birchmeier, C. (2006). The development of migrating muscle precursor cells. *Anat. Embryol. (Berl.)* **211**, 37–41.

Vasyutina, E., Lenhard, D. C., Wende, H., Erdmann, B., Epstein, J. A. and Birchmeier, C. (2007). RBP-J (Rbpsuh) is essential to maintain muscle progenitor cells and to generate satellite cells. *Proc. Natl. Acad. Sci.* **104**, 4443–4448.

Wagner, D. O., Sieber, C., Bhushan, R., Börgermann, J. H., Graf, D. and Knaus, P. (2010). BMPs: From Bone to Body Morphogenetic Proteins. *Sci. Signal.* **3**, mr1–mr1.

Wang, Q. and McPherron, A. C. (2012). Myostatin inhibition induces muscle fibre hypertrophy prior to satellite cell activation. *J. Physiol.* **590**, 2151–2165.

Wang, H., Noulet, F., Edom-Vovard, F., Le Grand, F. and Duprez, D. (2010). Bmp Signaling at the Tips of Skeletal Muscles Regulates the Number of Fetal Muscle Progenitors and Satellite Cells during Development. *Dev. Cell* **18**, 643–654.

Wang, R. N., Green, J., Wang, Z., Deng, Y., Qiao, M., Peabody, M., Zhang, Q., Ye, J., Yan, Z., Denduluri, S., et al. (2014). Bone Morphogenetic Protein (BMP) signaling in development and human diseases. *Genes Dis.* **1**, 87–105.

Watt, D. J., Morgan, J. E., Clifford, M. A. and Partridge, T. A. (1987). The movement of muscle precursor cells between adjacent regenerating muscles in the mouse. *Anat. Embryol. (Berl.)* **175**, 527–536.

Weintraub, H., Davis, R., Tapscott, S., Thayer, M., Krause, M., Benezra, R., Blackwell, T. K., Turner, D., Rupp, R. and Hollenberg, S. (1991). The myoD gene family: nodal point during specification of the muscle cell lineage. *Science* **251**, 761–766.

Wheater, Burkitt, P. ., H. . (1987). *Functional histology: a text and colour atlas.* Churchull Livingstone.

White, R. B., Biérinx, A.-S., Gnocchi, V. F. and Zammit, P. S. (2010). Dynamics of muscle fibre growth during postnatal mouse development. *BMC Dev. Biol.* **10**, 21.

Winbanks, C. E., Chen, J. L., Qian, H., Liu, Y., Bernardo, B. C., Beyer, C., Watt, K. I., Thomson, R. E., Connor, T., Turner, B. J., et al. (2013). The bone morphogenetic protein axis is a positive regulator of skeletal muscle mass. *J. Cell Biol.* **203**, 345–357.

Wozney, J. M. (1992). The bone morphogenetic protein family and osteogenesis. *Mol. Reprod. Dev.* **32**, 160–167.

Wozney, J. M., Rosen, V., Celeste, A. J., Mitsock, L. M., Whitters, M. J., Kriz, R. W., Hewick, R. M. and Wang, E. A. (1988). Novel regulators of bone formation: molecular clones and activities. *Science* **242**, 1528–1534.

Wrana, J. L., Attisano, L., Cárcamo, J., Zentella, A., Doody, J., Laiho, M., Wang, X.-F. and Massague, J. (1992). TGFβ signals through a heteromeric protein kinase receptor complex. *Cell* **71**, 1003–1014.

Wu, M. Y. and Hill, C. S. (2009). TGF-β Superfamily Signaling in Embryonic Development and Homeostasis. *Dev. Cell* **16**, 329–343.

Wu, S., Wu, Y. and Capecchi, M. R. (2006). Motoneurons and oligodendrocytes are sequentially generated from neural stem cells but do not appear to share common lineage-restricted progenitors in vivo. *Development* **133**, 581–590.

Yaffe, D. and Saxel, O. (1977). Serial passaging and differentiation of myogenic cells isolated from dystrophic mouse muscle. *Nature* **270**, 725–727.

Yang, H., Wang, H., Shivalila, C. S., Cheng, A. W., Shi, L. and Jaenisch, R. (2013). One-Step Generation of Mice Carrying Reporter and Conditional Alleles by CRISPR/Cas-Mediated Genome Engineering. *Cell* **154**, 1370–1379.

Yin, H., Price, F. and Rudnicki, M. A. (2013). Satellite Cells and the Muscle Stem Cell Niche. *Physiol. Rev.* **93**, 23–67.

Yu, P. B., Deng, D. Y., Lai, C. S., Hong, C. C., Cuny, G. D., Bouxsein, M. L., Hong, D. W., McManus, P. M., Katagiri, T., Sachidanandan, C., et al. (2008). BMP type I receptor inhibition reduces heterotopic ossification. *Nat. Med.* **14**, 1363–1369.

Zawel, L., Le Dai, J., Buckhaults, P., Zhou, S., Kinzler, K. W., Vogelstein, B. and Kern, S. E. (1998). Human Smad3 and Smad4 Are Sequence-Specific Transcription Activators. *Mol. Cell* **1**, 611–617.

Zhang, Y. E. (2009). Non-Smad pathways in TGF-β signaling. *Cell Res.* **19**, 128–139.

Zhang, H. and Bradley, A. (1996). Mice deficient for BMP2 are nonviable and have defects in amnion/chorion and cardiac. *Development* **122**, 2977–2986.

Zhang, P., Wong, C., Liu, D., Finegold, M., Harper, J. W. and Elledge, S. J. (1999). p21(CIP1) and p57(KIP2) control muscle differentiation at the myogenin step. *Genes Dev.* **13**, 213–224.

Zhang, T., Günther, S., Looso, M., Künne, C., Krüger, M., Kim, J., Zhou, Y. and Braun, T. (2015). Prmt5 is a regulator of muscle stem cell expansion in adult mice. *Nat. Commun.* **6**,.

Zhu, X., Topouzis, S., Liang, L. and Stotish, R. L. (2004). Myostatin signaling through Smad2, Smad3 and Smad4 is regulated by the inhibitory Smad7 by a negative feedback mechanism. *Cytokine* **26**, 262–272.

Zimmers, T. A., Davies, M. V., Koniaris, L. G., Haynes, P., Esquela, A. F., Tomkinson, K. N., McPherron, A. C., Wolfman, N. M. and Lee, S.-J. (2002). Induction of Cachexia in Mice by Systemically Administered Myostatin. *Science* **296**, 1486–1488.

Zou, H. and Niswander, L. (1996). Requirement for BMP signaling in interdigital apoptosis and scale formation. *Science* **272**, 738–741.